2-Methoxy-4-chromanone ligated transition metal complexes: A novel class of effectual bioactive compounds

Thesis submitted to

Cochin University of Science and Technology

in partial fulfillment of the requirements
for the award of the degree of

Doctor of Philosophy

In

Chemistry

In the Faculty of Science

by

Sneha Jose E.
(Reg. No: 4421)

Department of Applied Chemistry
Cochin University of Science and Technology
Kochi – 22, Kerala, India

September 2018

2-Methoxy-4-chromanone ligated transition metal complexes: A novel class of effectual bioactive compounds

Ph.D. Thesis in the Faculty of Science

By

Sneha Jose E.
Research Fellow
Department of Applied Chemistry
Cochin University of Science and Technology
Kochi, India 682 022
Email: josesneha7@gmail.com,snehaabinesh@cusat.ac.in

Research Advisor

Dr. P. V. Mohanan
Associate Professor
Department of Applied Chemistry
Cochin University of Science and Technology
Kochi 682 022
India
Email: mohan@cusat.ac.in

Department of Applied Chemistry
Cochin University of Science and Technology
Kochi 682 022
India

September 2018

Front cover:

Back cover:

The lord is my shepherd. . . I shall not be in want...

Psalms 23:1

…. For my dearest Pappa & Mummy

DEPARTMENT OF APPLIED CHEMISTRY
COCHIN UNIVERSITY OF SCIENCE AND TECHNOLOGY
KOCHI – 22, KERALA, INDIA

Dr. P. V. Mohanan
Associate Professor

Ph: 0484-2575804
Fax: 0484-2577595
Email:pvmohanan@gmail.com
mohan@cusat.ac.in

Certificate

This is to certify that the thesis entitled **2-Methoxy-4-chromanone ligated transition metal complexes: A novel class of effectual bioactive compounds** submitted by **Ms. Sneha Jose E.,** in partial fulfillment of the requirements for the degree of Doctor of Philosophy, to the Cochin University of Science and Technology, Kochi-22, is an authentic record of the original research work carried out by her under my guidance and supervision. The results embodied in this thesis, in full or in part, have not been submitted for the award of any other degree. All the relevant corrections and modifications suggested by the audience and recommended by the doctoral committee of the candidate during the presynopsis seminar have been incorporated in the thesis.

Kochi-22
13/09/2018

P. V. Mohanan
(Supervising Guide)

Declaration

I hereby declare that the work presented in this thesis entitled **2-Methoxy-4-chromanone ligated transition metal complexes: A novel class of effectual bioactive compounds** is entirely original and was carried out independently under the supervision of **Dr. P. V. Mohanan**, Department of Applied Chemistry, Cochin University of Science and Technology and has not been included in any other thesis submitted previously for the award of any other degree.

Kochi-22 **Sneha Jose E.**

13/09/2018

Acknowledgement

First and foremost, I thank God Almighty for the blessings He has bestowed upon me and for giving me the strength and wisdom to achieve this dream. I thank Holy Mother Mary and all saints for solacing me when I was depressed and frustrated during the course of my studies. It is to their intercession I attribute my success.

It's a boundless pleasure and a great privilege to be thankful to those who have come across our lives and have made an impact on me by being what they are and without having our own knowledge. But as an important and significant period of both my personal life and research life, I have to be feel indebted to all those who had been of much help during my research sting over here at CUSAT.

The person to whom I am extremely grateful and committed is my research supervisor Dr. P. V. Mohanan sir who gave me all the freedom and flexibilities with my own space during my research work. His constant encouragement, fruitful discussions and valuable suggestions at different stages were really a great inspiration. Always I feel it as my luck to be the part of a stressfree lab.

I extend my sincere thanks to my doctoral committee member, Dr. P. A. Unnikrishnan sir for the timely suggestions.

I would like to express my deep gratitude and heartfelt thanks to Prof. Dr. K. Girish Kumar, Head, Department of Applied Chemistry for providing the necessary advice and facilities for carrying out my research. I also thank all other faculty members of the department including the former heads of the Department Prof. Dr. M. R. Prathapachandra Kurup sir, Prof. Dr. K. Sreekumar sir and Dr. N. Manoj sir for their immense help during the different stages of my research. I express my gratitude to them, and for allowing me to use the facilities of this department. Non-teaching staff of the department deserve special mention with whom the thesis submission would not have been speeded up. I sincerely appreciate Thahira ma'am who joined me during the M. Sc. practical hours.

I express my sincere thanks to Prof. M. V. Rajasekharan, School of Chemistry, University of Hyderabad who introduced me the world of metal complexes and crystallography. I always fondly remember my research days at MVR lab at School of Chemistry. I thank Dr. Toms Joseph and Dr. C. G. Joshi, Scientists, ICAR-CIFT Cochin for helping me to do antimicrobial studies of synthesized ligands and complexes.

I am indebted to all the staff of SAIF-Stic, Cochin and IIT Bombay for the services rendered for sample analyses. I am thankful to the University Grants Commission, New Delhi, India for the financial assistance for carrying out the research work.

Room No. 47, the last lab at the end of the second floor of department, bioinorganic chemistry lab, was one of my favorite places and was like a second home for me. Looking back through this span of five years, in all the cheerful moments I cherish, there is the face of at least one of my lab mates. My heartfelt thanks to my seniors - Dr. Priya Rajan S. who recommended me for joining the lab and Dr. Navya Antony.

Dr. Shanty was the only familiar face when I joined the lab. Since then, Shantychechi was always there for me with timely advices and motivation with sisterly affection whenever I was in difficult situation. Chechi, thank you so much for being so enthusiastic and inspirational. Thanks a ton to Jesicca for such a great support and help during the research work and academic discussions. Divyachechi, I missed you during the later years of my research period. Binduchechi, you will be always in my heart for being so kind and lovely. Thank you, Mariyachechi for your love and care and also the delicious treat. Geetha, you were such a wonderful junior, will be always remembered with bundle of sweet memories. Savitha, you were simply awesome. Thank you so much for making the lab so comfortable and cordial. The travel freak Anjali, there is always heartful of prayers and wishes so that all your dreams come true. All the very best for the new face Dhanya.

I gratefully remember all my friends of other labs in the department who helped and encouraged me throughout my research life. Polymer lab friends,

Smithachechi, Jibychechi, Anjalichechi, Jishachechi, Soumyachechi, Sinijachechi, Kunjanjali, Shaibuna, Letsy, Shebithatha, Hiba, Avadi, Manikandan, Priyachechi and Unni deserve a special mention for making my CUSAT days so memorable, especially for the long lunches and lots of sniggers.

I like to express my deep hearted thanks to the teacher, Ambili aunty, Jomol aunty and Mani aunty of CUSAT day care for taking care of my girls so considerately and lovingly.

To acknowledge my family, I am so running out of words. And I know, it will be so formal if I thank my Pappa and Mummy. Amidst of all odd health circumstances, it was my dearest Pappa and Mummy who were the invariable spring of encouragement and hope. They always infused the packets of confidence and strength when I am down and were my paradigm role models for hard work. It is your unconditional love, prayers, dreams and incitation that moulded me as I am today. I also fondly remember the love and support extended by my sister Smitha and her family.

I wish to express my deep sense of gratitude to my in laws, Pappa and Amma for their extended serenity and being considerate during my extensive work without whom I would ever have travelled through the far-reaching path. Their constant support and motivation was my power boosters which helped to move forward the road with ease. Thanks a lot to my sis in law, Ambily and her family for support and care rendered for me.

Thanks from the heart and soul to apple of my eyes, Elsa and Sarah, who are the cutest part of my doctoral life. It will not be a worth less if the dedication of the thesis is also to their credit as they are my research buddies and coauthors both before and after their birth.

Above all, to my soulmate Abiyettan, my solid rock, my pillar and my roof, no words to express my gratitude, love and warmth for you. Having you by my side makes me feels like anything is possible. Thank you so much for the being my best half.

I am extremely grateful to all those who inspired and motivated me directly or indirectly for accomplishing this achievement and I personally apologize for not mentioning all of them one by one.

Once again, I am kneeling before the supreme power God Almighty who was there with me in spite of my all flaws.

With all good wishes, love and prayers

Sneha

Preface

Antimicrobial resistance is considered as a global crisis which threatens the health benefits that were acquired through the wide range of antibiotics. Novel and improved class of antibiotics that can meet the problem is always a hot topic of research in the field of medicinal and pharmaceutical chemistry. Inorganic metal complexes with functionalized organic ligands that are consistently exploited are a promising source of drug model systems that can better manage or treat the diseases. Chromone ring system which is the core fragment of several naturally occurring compounds like flavonoids, coumarins, chalcones etc. are always considered as a privileged scaffold for the designing of drug library. Chemical reactivity and pharmaceutical properties have aroused the interest of using 3-formylchromone and its derivatives for the synthesis of higher heterocycles. So in the present study, we choose 3-formylchromones for the synthesis of ligands that can easily form metal complexes with good biological properties.

Our efforts to investigate the reactions of 3-formylchromone with aminopyridines and to synthesis its metal complexes along with its biological properties are embodied in the thesis entititled "2-**Methoxy-4-chromanone ligated transition metal complexes: A novel class of effectual bioactive compounds".** The work was carried out by the author in Department of Applied Chemistry, CUSAT, Kochi, during the period of 2013-2018. There are eight chapters in the thesis. Chapter 1 deals with the introduction to 3-formylchromones along with the details regarding the biological properties. Objectives of the work and also analytical techniques used are also included in the first chapter. Chapter 2 gives the synthesis and characterization of 2-methoxy-4-chromanones from 3-formylchromones and aminopyridines. Synthesis and characterization of metal complexes incorporating these ligands are explained in Chapter 3. Chapter 4-7 gives the evaluation of biological properties like DNA binding, alpha-amylase and alpha-glucosidase inhibition, antimicrobial and cytotoxicity of these synthesised ligands and complexes. Chapter 8 gives the summary of the whole work and also the future perspectives. The pursued work can be considered as a potential connecting link for the future research.

Contents

Chapter 1

Introduction

Contents

1.1 Chromones

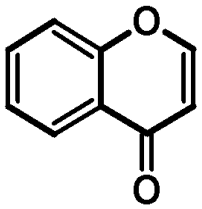

Chromones (4H-chromen-4-one, 4H-1-benzopyran-4-one) are benzoannulated γ-pyrone heterocycles that are widely distributed in nature. They contain γ-pyrone nucleus fused to benzene ring at the 5- and 6-position. It was from the Greek word 'chroma', the word 'chromone' derived and it means color [1]. Chromones and their derivatives occur in plant life, mostly in leaves and flowers in the form of pigments from algae to conifers. Several plant cycle reactions like oxidation of indole acetic acid, oxygen uptake in plant tissues etc. involve chromone derivatives as their active compounds [2]. Generally chromones exhibit low toxicity along with a wide spectrum of useful properties. They are well-known by their diversity of pharmacological

properties and have been used since ancient times in traditional medicine [3]. They are important for the synthesis of many oxygen heterocycles, xanthones as well as transition metal chelates [4]. Chromone ring system is the core fragment of several flavonoids (such as flavones, isoflavones), coumarins and chalcones (Fig 1.1).

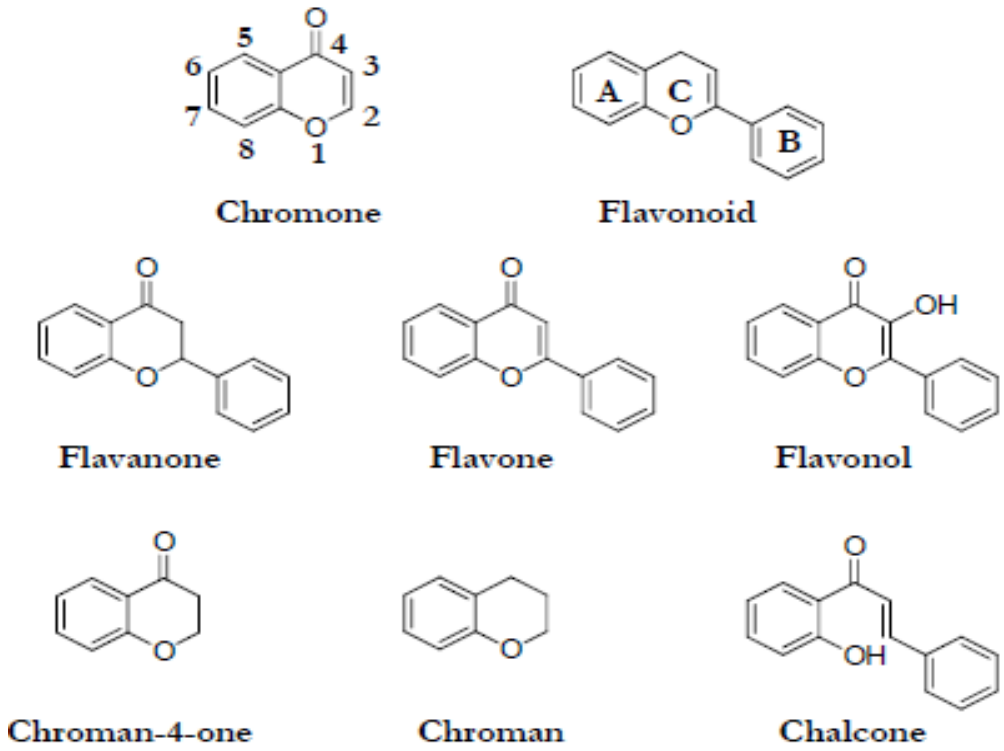

Fig. 1.1: Compounds with chromone ring as core fragment

Due to plant origin chromones constitute a crucial part of human diet. These compounds are reported to have low cytotoxicity in mammalian cells. Chromone derivatives have wide range of pharmacological activities [5-11]. Chromone derivatives are active on lipoxygenase and cyclooxygenase, at photoinduced reactions due to the excellent photoactive nature and on benzodiazepine receptors [12-14]. Excellent antimutagenic properties of

chromone derivatives are reported [15]. The ability of chromone derivatives to inhibit electron transport through inhibition of the activity of NADH: ubiquinone oxidoreductase and phorbolester-induced ornithine decarboxylase is also assayed [16, 17]. Chromones activate the transmembrane conductance regulator of cystic fibrosis and hence is a potent candidate in the treatment of cystic fibrosis [18].

There are several chromone derivatives which are used as therapeutic agents like Cromolyn or cromoglicate, Nedocromil (Alocril) (prevent wheezing, shortness of breath, and other breathing problems caused by asthma), Apigenin (4,5,7-trihydroxyflavone)(potent inhibitor of Cytochrome P450 2C9 (CYP2C9)), Diosmin (chronic venous insufficiency (CVI) and hemorrhoidal disease (HD), in acute or chronic haemorrhoids), Flavoxate (2-(1-piperidyl)ethyl-3-methyl-4-oxo-2-phenylchromene-8-carboxylate) (anticholinergic with antimuscarinic effects). Chromone compound like Khellin is a smooth muscle relaxant in the cure of angina pectoris and asthma. Because of all these properties, this rigid bicyclic chromone fragment system is often considered as a valuable scaffold for medicinal chemistry [19].

Metal complexes incorporating chromone moiety enjoy various biological activities and there are cases comparable with cisplatin, the celebrated anticancer drug. These metal complexes are also used in various fields due to its reported biological activities including antimycobacterial, antifungal [20], anticonvulsant [21], antimicrobial and mushroom tyrosinase inhibition activities of chromone derivatives. These derivatives can be used as intermediates to many products of fine chemical industries such as pharmaceuticals, agrochemicals and dyestuffs [22]. Chromone derivatives and their metal complexes also act as good fluorescent compounds. Designing and synthesizing brightly emissive molecules with a heterocyclic backbone and allowing for

alterations in emission properties is a hot topic of current research in order to exploit their potential applications as chemo sensors, fluorescent probes, hydrogen bonding sensors, fluorophores, optoelectronic devices etc. They can find applications in apopstosis, protein labeling and DNA binding affinity studies [23-25].

1.1.1 Synthesis of chromones

Heywang and Kostanecki introduced one of the earliest methods for the synthesis of chromones which involved the decarboxylation of chromone-2-carboxylic acid. Since then, several other higher yield routes and mild experimental conditions have been developed [26].

One of the most general methods involves formation of an aryl ester by acylation of an o-hydroxyacetophenone with an aromatic acid chloride. This aryl ester is then rearranged by a base (Baker-Venkataraman rearrangement) to a 1, 3-diaryl 1, 3-diketone, later compound gives a 2-arylchromone on cyclocondensation. This is typically a catalyzed reaction and it has been carried out in different media. Some reaction conditions utilized for the reaction were the use of excess of sulfuric acid in glacial acetic acid, cationic exchange resins in isopropanol, glacial acetic acid-anhydrous sodium acetate or aqueous potassium carbonate. Greener procedures have been recently described, using $CuCl_2$ in ethanol, ionic liquid under microwave irradiation, heteropolyacids, and ortho-fluorobenzoyl chloride in condensation with a 1, 3- keto ester the fluoride is displaced in an intramolecular sense by enolate oxygen, and the chromone obtained directly [27].

1.2 3-Formylchromone

3-Formylchromone (4-oxo-4H-1-benzopyran-3-carboxaldehyde, chromone -3-carboxaldehyde) which is generally prepared by the Vilsmeier- Haack synthesis has been frequently used in the formation of various heterocyclic systems. Chromone-3-carboxaldehyde is a neutral molecule without charge and the examination of the structure disclose that it is well suited to derivatization. Derivatives of 3-formylchromone are useful synthetic building block in an organic and medicinal chemistry [28].

1.2.1 Synthesis of 3-formylchromone

First synthesized in 1973 by Nohara *et al.* by Vilsmeir–Hack reaction (Scheme 1.1) [29]

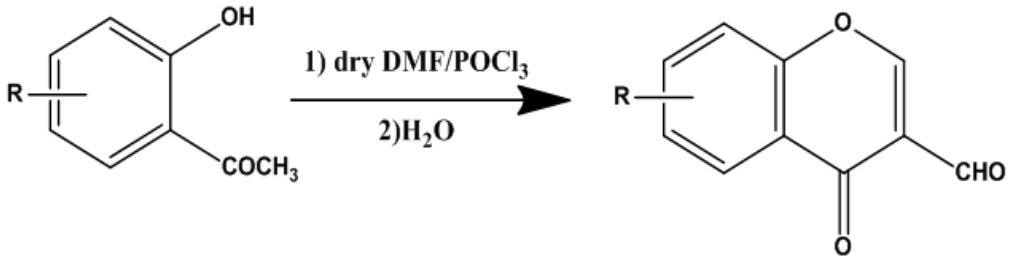

o-hydroxyacetophenones 3-formylchromone

Scheme: 1.1

The reaction of o-hydroxyacetophenones with substituted amide, typically anhydrous N, N-dimethyl formamide (DMF) with phosphorous oxy chloride ($POCl_3$) below 5°C leads to the formation 3-formylchromones via, Vilsmeier-Haack reaction. The active agent in the reaction is the substituted chloroiminium ion formed by the reaction of DMF and $POCl_3$. This chloroiminium ion then attacks the electron rich arene to give the corresponding aromatic ketone or aldehyde [30].

3-Formylchromones are relevant for two reasons:

- They are carrying significant biological activity and they are attractive synthetic intermediates. 4-Oxo-4H-1-benzopyran-3-carboxaldehyde is a highly reactive and well examined compound.

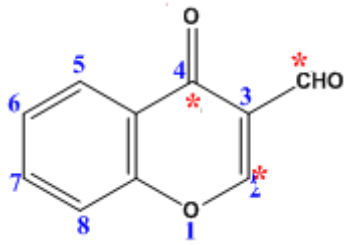

Fig. 1.2 3-Formylchromone

- Three electrophilic centres: unsaturated keto function, a conjugated second carbonyl group at C3 and a very reactive electrophilic centre at C2 are present in the structure of this compound. Out of three electron deficient centres, the carbon at position 4 of δ -pyrone ring is having obviously the least electrophilicity compared to that at the other two centres.

  For these reasons, 4-oxo-4H-1-benzopyran-3-carboxaldehyde is often used as a starting material for the syntheses of different heterocycles [31, 32].

1.2.2 Chemical reactivity of 3-formylchromone

According to literature, the reaction of 4-oxo-4H-1-benzopyran-3-carboxaldehyde and primary aromatic amines allows to obtain various types of products. Generally, three types of products of these reactions were observed.

i. Schiff bases: Schiff bases or imines (X= NAr) were formed in aprotic solvents, enamines in protic solvents (water, alcohols, thiols and amines).

ii. 4-Chromanone derivatives: They are formed by the condensation of 3-formylchromone with primary aromatic amines followed by another nucleophilic attack.

iii. Higher heterocycles: Opening of δ-pyrone ring may lead to the formation of new derivatives such as quinolines [33].

Depending upon the reaction environment, more complicated products may be formed due to the multiple nucleophilic attacks. Sometimes both types of products or very complicated structures consisting from two nucleophile components were observed. Hence, experimental conditions and the nature of the amine used are the major parameters that determine the type of products of reaction between 4-oxo-4H-1-benzopyran-3-carboxaldehyde and amines

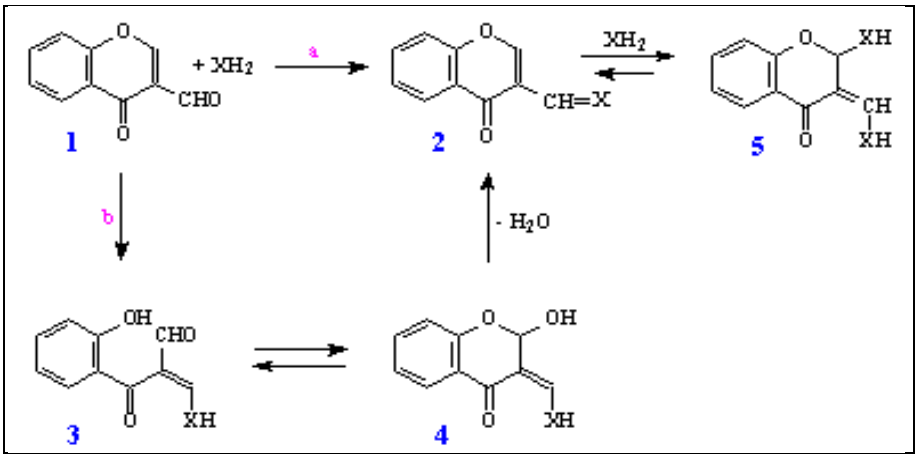

Scheme 1.2: Reaction of 3-formylchromone with primary aromatic amine

Scheme 1.2 will give an overall idea about the reactivity of 3-formylchromone with primary aromatic amines. It is known that the reaction of 3-formylchromone **1** with any nucleophile such as an amine, XH_2, gives

initially the condensation product **2** via a straightforward 1, 2-addition of the nucleophile to the carbonyl group of aldehyde function (Scheme 1.2, path a). An alternative route by 1, 4-addition of the nucleophile with concomitant opening of the δ - pyrone ring and subsequent recyclisation of the intermediate **3** via **4** (Scheme 1.2, path b) may also lead to the formation of **2**. It is very difficult to find whether the nucleophile is undergoing 1, 2- or 1, 4-addition to 4-oxochromene-3-carboxaldehyde due to the "symmetry" acquired after opening pyrone ring [34].

H. Stangkovicova *et al.* reported that PM3 semiemperical computations specify the formation of several isomers for 3-(acylamio methylene)chroman-4-ones (Fig. 1.3). A isomers were calculated to be more stable than the B isomers for all computed compounds, even though there is only low energy difference between the two isomeric forms. It is also reported that heating the reaction mixture causes isomerisation of enamines to the isomer with geometry favourable for the elimination of alcohol molecule [35].

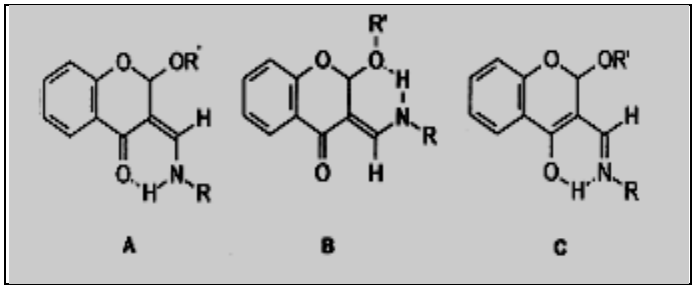

Fig. 1.3: Isomers for 2-substitute3-(acylamio methylene)chroman-4-ones

A. O. Fitton and his coworkers reported that equimolar quantities of 3-formylchromone and a primary aromatic amine in benzene leads to a mixture of the 3-(aryliminomethyl)chromone and 2-arylamino-3-(arylaminomethylene) chroman-4-one, and the isolation of pure compounds is found to be difficult. The motive for this quite unusual ring addition of a second aromatic amine

molecule to the imine is the formation of the stable ketoamine hydrogen bond (Fig. 1.4) [36]. Alcohols, thiols and amines are reportedly sufficiently nucleophilic to add to 3-(aryliminomethyl) chromones.

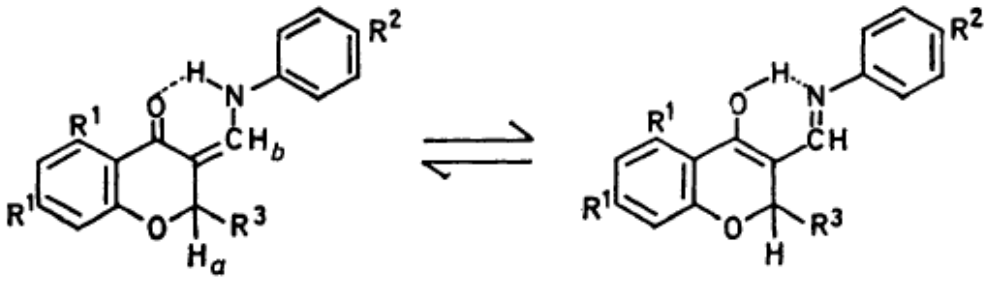

Fig.1.4: Keto-amine bond formation

The reactions between the amines and the anils are found to be evidently reversible. The differences in amine behaviour can be explicated in terms of amine nucleophilicity, which have an effect on the addition step, and amine basicity, which directs the elimination step. Thus, its main stabilizing feature is lost, if the base is sufficiently strong to remove the hydrogen-bonded proton in the adduct and the amine is eliminated (or the ring is cleaved).

Aromatic primary amines are suitably nucleophilic to add to the anil, but not sufficiently basic to deprotonate adduct and begin the elimination. Aromatic secondary amines cannot add to the anil due to their reduced nucleophilicity and also the typical steric reasons. Alternatively, aliphatic amines are sufficiently nucleophilic for adduct formation but too basic to hold a protonated adduct, and the equilibrium favours amine and anil more willingly than adduct. The argument is supported by the instant decomposition of the stable aromatic amine adducts of n-propylamine.

Alcohols are also sufficiently nucleophilic to add to 3-(aryliminomethyl) chromones**.** Primary and secondary alcohols gave crystalline adducts, although t-

butyl alcohol furnished an unstable compound providing additional confirmation that the course of addition is prone to steric influences. Simply heating the alcohol adducts above their melting-points under vacuum also causes elimination of the alcohol giving an additional route to the pure anil. A much improved yield of 3-(aryliminomethyl)chromones can be obtained from the condensation of reactants in the presence of 4-toluenesulfonic acid [37]. Primary aromatic amines having a nucleophilic functionality at their ortho position react with 3-formylchromones giving fused seven-membered heterocycles [38], 3-(aryliminomethyl)chromones or dihydrotetraaza[1]anulenes [39].

1.3 4-Chromanones

4-Chromanone (2,3-dihydro-1-benzopyran-4-one) is composed a benzene nucleus fused to 2, 3-dihydro-γ-pyranone ring and constitute a major class of six-membered heterocyclic compounds [40]. 4-Chromanone is distinct from chromone by reduced C2-C3 double bond. This small difference in the structure of 4-chromanones and chromones often lead to the big differences in their chemistry and bioactivity.

4-Chromanone scaffold is a privileged structure in drug discovery and development. There are several 4-chromanone derivatives such as 5-deoxyflavanone, (2S)-5-hydroxy-2-(4-hydroxyphenyl)-7-methoxy-2,3-dihydro -4H-chromen-4-one, 4′-hydroxyflavanone, and (2S, 3S)-trans-dihydroquercetin which are currently under experimental or clinical development, and hesperetin has been approved as a cholesterol-lowering agent [41]. The synthesis of 4-chromanone derivatives and their chemistry have aroused great attention in the field of organic and medicinal chemistry. The 4-chromanone scaffold is proved to be an important intermediate and interesting building block in organic synthesis and design of new lead compounds in drug design and discovery.

Derivatives of chromanones mainly 4-chromanone are essentially significant flavonoid skeletal structures, which are found in a wide variety of natural products and pharmaceutically active molecules. Such compounds have been identified as having antifungal [42], antibacterial [43], antiviral [44], anti-inflammatory [45], anticancer, antidepressive, antihypertensive, antidiabetic [46, 47] and antioxidant activities [48]. The classical methods for preparing 4-chromanones involve the condensation cyclization of carbonyl compounds with *o*-hydroxyacetophenone[49]. Some chromanone derivatives have been screened for *in vitro* antiviral activities against human immunodeficiency virus (HIV) and Simian immunodeficiency virus (SIV) [50]. They have also been asserted to be active in photosynthesis and have hereditary bleaching effect (similar to antibiotics) on the plastid system of Euglena gracilis [51] and for the treatment of bronchial asthma [52].

1.4 Aminopyridines

Aminopyridines are the heterocyclic compounds containing the monovalent chemical group -NH_2 attached to a pyridine ring. A free electron pair is contributed to the proton of an acid by nitrogen atom in amino functional group. There are three positional isomers. In 1894 the three isomeric aminopyridines were obtained using the Hoffman procedure (treatment of the amides of pyridine monocarboxylic acids by alkaline hypobromites). The six possible diaminopyridines were synthesized later. In 1915, 2-aminopyridine was synthesised by T. Chitchibabine by heating pyridine with sodamide. 2-Aminopyridine derivatives have attracted considerable interest recently because of their applications in various fields especially in pharmaceutical research. For example, the use of 2-aminopyridines has been reported as selective inhibitors of neuronal nitric oxide synthase [55] or glucokinase activators [56]. The most straight forward

methods reported for the synthesis of 2-aminopyridine derivatives includes the reaction of 2-halopyridines with substituted or unsubstituted amines using a transition metal catalyst *e.g.* palladium, or at elevated pressure. Another commonly used method for the synthesis of 2-aminopyridine derivatives is via nitration of (un)substituted aminopyridines or oxidative amination of nitropyridines. Recently, microwave assisted solvent free amination of halo pyridine without transition metal catalysts have been reported [57].

3-Aminopyidine has proved to be a strong convulsive agent. Local application of 3-AP in concentrations of 15–20 mM resulted in typical paroxysmal alterations of neuronal activity such as (a) enhancement of background firing, (b) depression of IPSPs, (c) augmentation of EPSPs and (d) single and serial paroxysmal depolarization shifts (PDSs). Serial PDSs were reflected by large synchronous waves in the surface EcoG [58].

Substituted or unsubstituted aminopyridines are also valuable precursors for the synthesis of a various heterocyclic compounds possessing medicinal value [59]. For example, 2-(methylamino)nicotinonitrile or 2-amino-3-nitropyridine was used as a synthetic precursor of 1H, 3H-pyrido[2,3-*d*]pyrimidine-2,4-dione or pyrido[2,3-*b*]pyrazines and imidazo[4,5-b]pyridines respectively [60]. Aminopyridines serve as very useful chelating ligands in a variety of inorganic and organometallic compounds [61]. In most cases aminopyridines and their derivatives act as monodentate ligands which coordinate the metal ions through the ring nitrogen [62]. But there are several works on 2-aminopyridine complexes in which the amino group also participates in coordination [63]. The high rate of pharmacological activity among heteroaromatic amines has also stimulated many research efforts to prepare compounds of this structural type [64].

1.5 Transition metal complexes incorporating 3-formylchromone derivatives:

Coordination chemistry always exploits the interaction of organic molecules with the metals. Coordination of small molecules with metals will cause the dramatic alteration of the reactivity. Simple metal complexes involving biologically active ligands are considered as relevant models for studying more complex biological systems. So the quest of a coordination chemist will be directed to acquire a wider and deeper understanding and designing of more competent model for biological systems. Metal complexes enjoy the ability to coordinate ligands in a three-dimensional configuration, thus allowing functionalization of groups that can be shaped to defined molecular targets [65].

Transition metal complexes often possess unique and vibrant properties such as

- Charge variation: depending on the existing coordination environment
- Structure and bonding: wide range of coordination geometries that give those unique shapes, bond length, bond angle and coordination site depending on the metal and its oxidation state.
- Metal–ligand interaction: usually lead to the formation of complexes that are unique from those of individual ligands or metals.
- Lewis acidity of metals: most metal ions can easily polarize groups that are coordinated to them, thus facilitating their hydrolysis.
- Partially filled d shell: influences the electronic and magnetic properties of metal complexes.
- Redox activity: key feature for the design of the coordination compound [66].

Chromone derivatives incorporated metal complexes constitute a major and valuable class of pharmaceutically important compounds. Large volumes of work have been reported regarding the structural and functional aspects of these metal complexes. Interest in the field has rapidly grown in recent years as illustrated by the increasing number of cited publications reported since 1992.

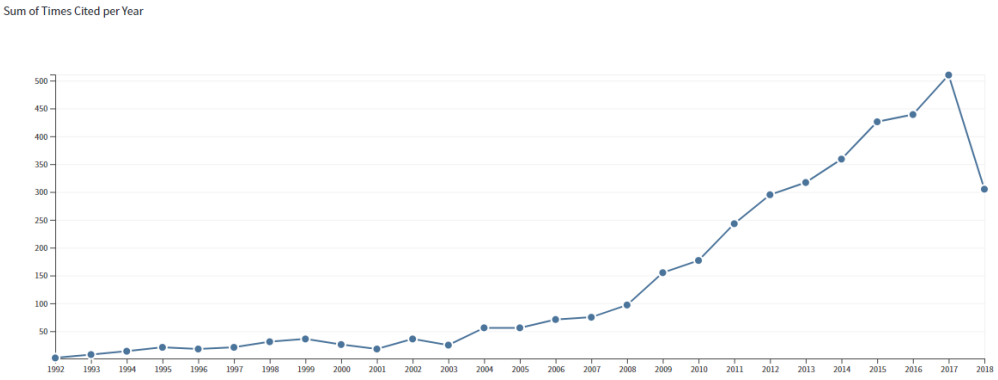

Fig. 1.5 Chromone metal complexes sum of times cited per year from Web of Science From 1992 to 2018

Synthesis of ligands from 3-formylchromone derivatives and its complexes has received much attention due to its prominent biological profiles. Recently, a series of 5-(4-oxo-4H-chromen-3-yl)-4,5-dihydro-1,3,4-thiadiazole-2-carboxamide and Cu(II), Co(II) and Ni(II) complexes of their tautomers 2-oxo-2-(arylamino)-(2*E*)-2-[(4-hydroxy-2-oxo-2H-1-benzopyran-3-yl)methyledene]ethanethioic acid hydrazides have been synthesized by Myannik and his coworkers. Copper complex was structurally elucidated using single crystal XRD and it reveals that copper (II) ions in complex molecule are coordinated by aldimine nitrogen atom, thiolate sulfur atom and the oxygen atom the pyrone ring keto-group as well as two bridged chloride anions in distorted triangular bipyramidal geometry [67].

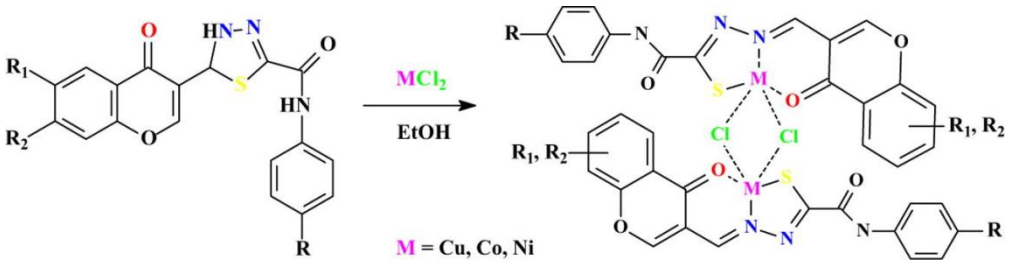

Scheme 1.6: Synthesis of metal complex incorporating 3-formylchromone derivative

Synthesis and structural characterization of Co(II), Ni(II), Cu(II), Zn(II) and Pd(II) complexes of 3-(((1H-1,2,4-triazol-3-yl)imino)methyl)-4H-chromen-4-one was reported. Tetrahedral and square pyramidal geometry was proposed for the complexes [68].

1.6 Biological applications of 3-formylchromone derivatives and its metal complexes

1.6.1 DNA: Function and structure

Deoxyribonucleic acid is often referred to as the molecule of life. DNA is described as a chemical storehouse for the complete genetic information of a living organism. The total DNA content of the cell is called as genome, governs every characteristic of every living species on earth. It seems that DNA is a simple biopolymer with four distinct building blocks, which is capable to store, to retrieve and to process massive amounts of genetic information rapidly and competently upon cellular demand.

As per Watson and Crick proposed model, DNA has two oppositely running strands which make DNA as a double helical structure [69]. DNA contains two nearly planar purine bases and two planar pyrimidine bases. A nucleoside is formed when these bases are covalently attached to a pentose, 2-deoxy-ribose. Nucleoside attached to a phosphate group gives a nucleotide.

The nucleotides are joined together covalently through phosphate group bridges in which the 5′ phosphate group of one nucleotide is joined to the 3′-OH group of the adjacent nucleotide forming a phosphodiester bond. The strands of DNA are complementary so that bases on one strand will decide the ones on the other strand [70].

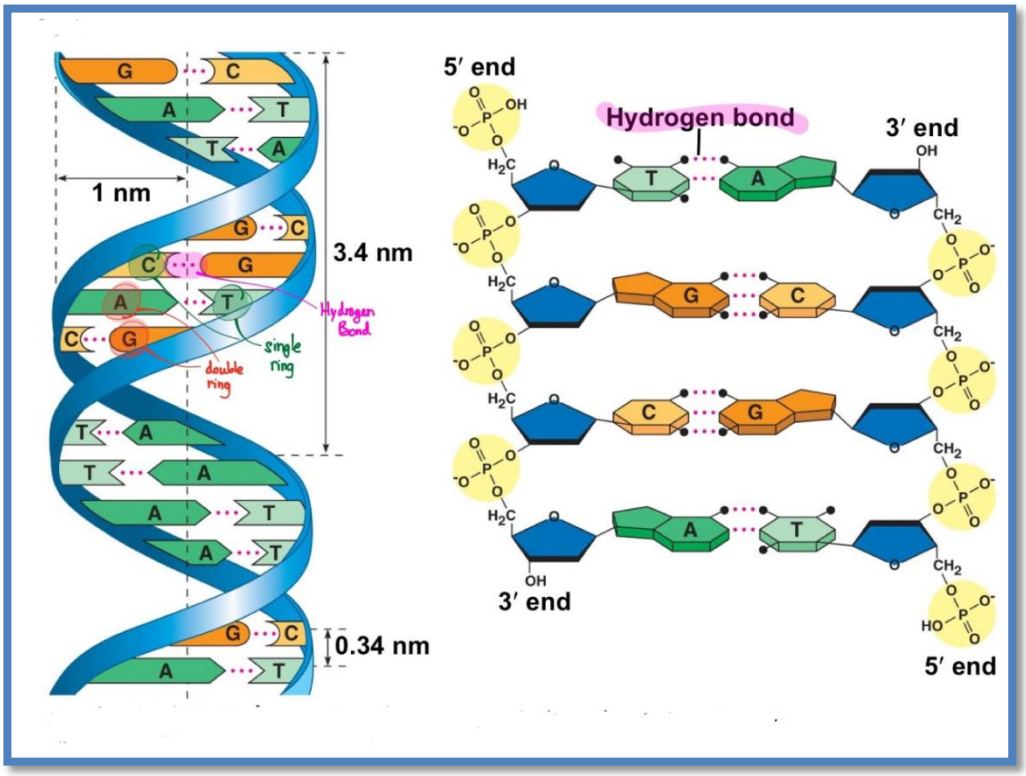

Fig. 1.6: Structure of DNA

Purines and pyramidines in DNA stack together through base stacking hydrophobic interactions which help to stabilize the three dimensional structure of DNA. Functional groups in purines and pyrimidines; ring nitrogens, carbonyl groups and amino groups are also involved in hydrogen bonding. Three hydrogen bonds are formed between guanine and cytocine and two hydrogen bonds between adenine thymine pairs in the DNA helical structure.

Forms of DNA - A, B, C, D and Z have been identified, with form B being the most prominent. These conformations are distinguished by distance between consecutive bases, the handedness of the helix, their pitch (the distance between base and the base obtained after a full 360° turn) and the number of nucleotides within one pitch [71]. A-DNA and B-DNA forms are right-handed while Z-DNA form is left-handed. However, DNA double strands are able to take up the A-conformation in some protein-DNA complexes and under dehydrated conditions. Both B-helix and A-form helix have two grooves, the major and the minor grooves. In B form, two grooves are equally deep but differ in their width. In contrast, the A-form helix possesses a small deep major groove, which is accessible only to water and metal ions. The term Z-DNA stems from the zigzag conformation of the phosphate backbone of a left-handed helix taken up by alternating purine-pyrimidine DNA sequences (GC repeats) under high salt conditions. The distance amid consecutive base-pairs and the degree of rotation of the helix per residue results from the alterations in the sugar pucker from a C3′-endo to C2′-endo. Base pair sequence, relative humidity, and the presence of DNA-binding compounds influence the sugar puckering and conformation of DNA Additionally, other forms of DNA are triplex (H-DNA), tetraplex (G-quadruplex DNA) and i-motif due to atypical (Hoogsteen) base pairs [72].

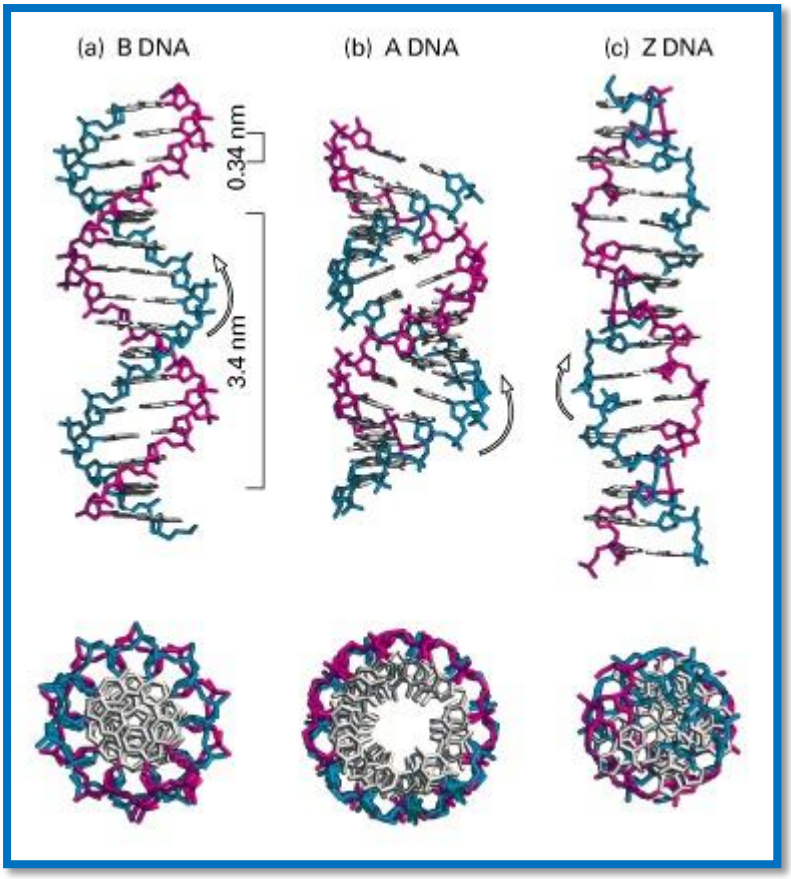

Fig.1.7 Different forms of DNA

1.6.1.1 DNA Binding Modes

DNA can bind with small molecules either covalently or non-covalently.

a) Covalent mode of binding

Covalent binding is an irreversible method of DNA interaction which causes complete inhibition of DNA functions and subsequent cell death [73]. A major advantage of covalent binders is its irreversible nature and high binding strength. Three modes of covalent binding to DNA are: inter and intra-strand crosslinking, replacement of nitrogenous bases, and alkylation of

nitrogenous bases. Cisplatin is the most clinically successful DNA covalent binder that and makes an intra/interstrand cross-link through the chloro groups with the nitrogen on the DNA bases although it reacts with a various range of other biomolecules [74]. Such binding causes the unwinding of the double helix and subsequent inhibition of transcription, thereby resulting in subsequent cell death by the disruption of protein complex recruitment [75].

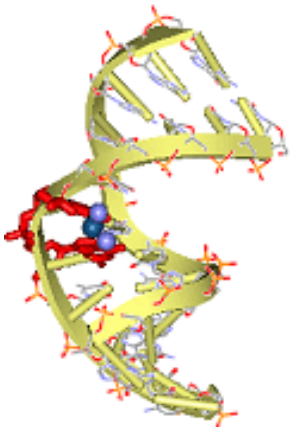

Fig. 1.8 DNA covalently bound to cisplatin

b) Non covalent mode of binding: Non covalent mode of binding can be of three types

   i. Intercalation: Due to the small molecule insertion between the base pairs of DNA, intercalative mode of binding is resulted. Nucleobases – molecule π interactions from either major or minor groove seems to stabilize this type of interactions. This type of interactions will increase the separation between the nucleobases which in turn causes the reduced helical twist and increased DNA structure distortion [76]. DNA helix will partially unwind to cop up this deformation.

   ii. Groove binding: Major and minor groves of DNA can also interact with small molecules and metal complexes. There are several factors

which steer the selection of the groove and also the ability of the complex to react with DNA. The size, shape, charge and hydrogen bonding potential are some of them. [77].

iii. Outside edge / electrostatic interaction: Electrostatic attraction between the metal complexes and the DNA backbone.

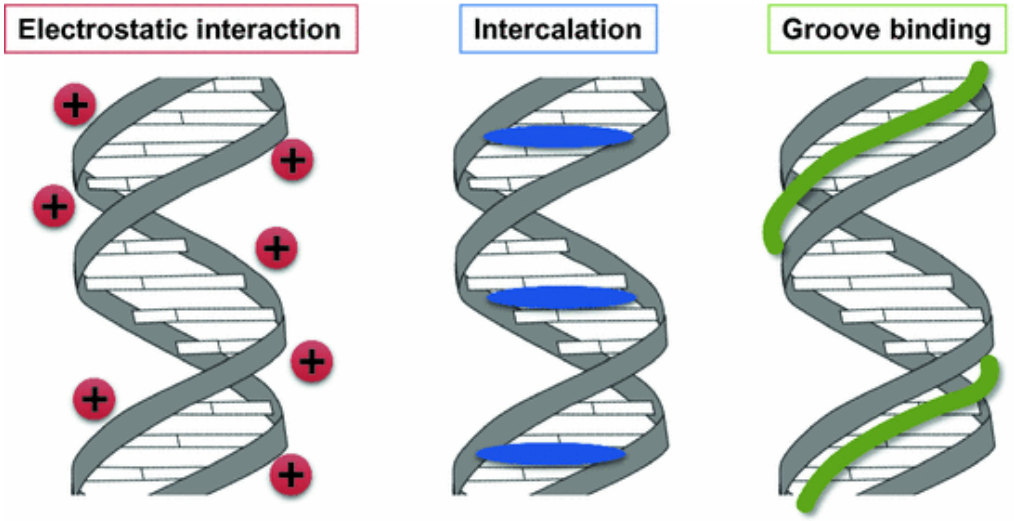

Fig. 1.9: Non covalent binding modes in DNA

Intercalative mode of binding can cause more conformational changes in DNA that happen with groove binding. Groove binders are generally crescent-shaped molecules that can block DNA protein interactions through binding to the minor groove of DNA [78]. Planarity of compounds, nature of donor atom and ligand coordination can influence the binding efficiency of the molecule [79].

UV-visible spectrophotometry utilizes the interaction between chromophore groups with DNA, and this interaction can be observed as variations in the absorption spectra in the absence and presence of the small molecule. It leads to the alterations in the intensity and also change in the maximum wavelength. Hypochromicity points to the compaction of DNA due

to then electrostatic interaction [80]. Decrease in the intensity of absorption spectra is due to lengthening of the DNA helix .Intercalation causes DNA base pairs separation in order to lodge the small molecule inserting itself. Viscosity studies can also be used to determine mode of binding as viscosity is sensitive to DNA length. This makes this method very sensitive for intercalators. Groove binders and non-classical or partial intercalators reduce the length of DNA. Electrostatic binding will not make any alterations in viscosity [81].

Pharmacological evaluation pertaining to chemotherapy revolves round interaction of DNA molecules. Therefore, any studies towards the development of metallonucleases focus primarily on the interaction of nucleic acids with molecules. Among the so far known drugs, cis-platin and its derivatives are the most widely used metal based drugs for cancer therapy. However their use is restricted because of its serious side effects, general toxicity and acquired drug resistance. These are the challenges that drive the inorganic chemists to design more effective, economically viable, less toxic and site specific anticancer drugs.

1.6.2 Enzymes

Enzymes are protein molecules that can catalyze thousands of biochemical reactions that are essential to sustain life without undergoing any alterations to them. They provide alternative reaction pathway by reducing the activation energy (E_a) necessary to initiate the reaction and thereby increasing the rate of the reaction. Enzymes are characterized by the following properties when compared to classical chemical catalysts: (1) higher reaction rates (2) ability to be regulated either by reaction rate control, by catalyst concentration or by specific small molecules (3) greater reaction specificity in terms of the reactants, products, and the absence of undesirable side reactions and (4)

effectiveness under milder reaction conditions in terms of temperature, pressure, and pH [82].

Enzymes are high molecular weight compounds which are made of chains of amino acids linked together with peptide bonds. The protein part of enzyme is known as apoenzyme. Co factor is the non-protein part required for proteins biological activity. Holoenzyme is the active enzyme composed of apoenzyme and a co-factor. Coenzyme is a non–protein compound or substance that is required for an enzyme to initiate the function of the enzyme. Prosthetic group is either a coenzyme or metal ion that is very tightly or even covalently bound to the protein component of the enzyme. Enzymes have a high degree of specificity for their substrates and are the most remarkable and highly specialized proteins [83]. Enzymes are classified to six major classes based on their reactions they catalyze.

- Hydrolases: Catalyse hydrolytic cleavage. Eg.: Esteraces, lipases, proteinases
- Oxidoreductases: In redox reactions: Eg.: reductases, oxidases
- Transferaces: Transfer of various group from one molecule to another. Eg.: transacylases, transaminases
- Lyases: Bond cleavage, Eg.: C-C lyases, C-O lyases, C-N lyases, C-S lyases
- Isomerases: In isomerisation reactions, Eg.: Racemases, cis- trans isomerases
- Ligases: Single bond formation using ATP. Eg.: C-O bonds, C-S bonds, C-N bonds, C-C bonds

There are many factors that affect the activity of enzyme such as concentration of enzyme, concentration of substrate, temperature, pH, product concentration, activators, time, light radiations etc.

1.6.2.1 Mechanism of action

Enzyme action begins with the binding of the substrate (or substrates) to the active site on the enzyme. The active site is characterized as a cleft or a pocket on the specific region of the enzyme which combines with the substrate. The active site will have a unique geometric shape that is complementary to the geometric shape of a substrate molecule, similar to the fit of puzzle pieces. This means that enzymes specifically react with only one or a very few similar compounds. Substrate- metal ion activator interaction proceeds through several polar, nonpolar interactions, hydrogen bonding, coordinate bonding and covalent bonding. Substrate binding to the enzyme results in the formation of enzyme substrate complex which leads to electron cloud modification and ultimately forming the products. The products are then released from the enzyme surface to regenerate the enzyme for another reaction cycle (Fig 1.10) [84].

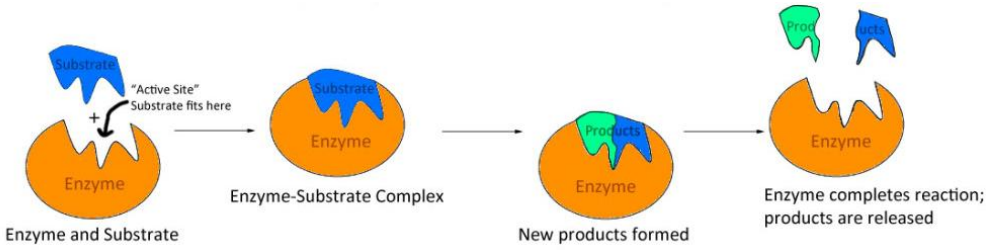

Fig. 1.10: Mechanism of enzyme action

The mechanism of enzyme action is comparable in principle to other types of chemical catalysis. Enzyme reduces the energy required to reach the highest energy transition state of the reaction by providing an alternative

reaction route. The reduction of activation energy (E_a) increases the amount of reactant molecules that achieve an adequate level of energy, such that they pass the activation energy barrier to form the product. As like other chemical catalysts, the enzyme is not consumed during the reaction (as a substrate is) but is recycled such that a single enzyme performs many rounds of catalysis [85].

1.6.2.3 Factors affecting reaction rate

- Temperature: Reaction rate rises with temperature to a maximum level, and then suddenly declines with further increase of temperature. In most cases optimal temperatures of most animal enzymes hardly ever exceed 50°C.
- pH: Optimum pH for almost intracellular enzymes is in the range of 5 to 9. Relation between activities to hydrogen ion concentration reflects enzyme denaturation and effects on the charged state of the enzyme, the substrates, or both.
- Enzyme concentration: Rate of the reaction and enzyme concentration is directly proportional upto saturation point. After that there will not be any effect on the rate for the enzyme concentration.
- Substrate concentration: Reaction follow first order kinetics at the higher concentrations of substrate, the active sites on most of the enzyme molecules are continuously filled. But further increase of concentration at saturation point will causes leveling off the reaction rate [86].

1.6.2.4 Michaelis-Menten kinetics

The Michaelis-Menten kinetics describes the relationship between the rate of an enzyme-catalyzed reaction v, the concentration of substrate [S] and two constants, V_{max} and K_m.

The Michaelis-Menten equation:

$$\mathbf{v = \frac{V_{max}\,[S]}{K_m + [S]}}$$

Where V_{max} is the maximum initial velocity and Michaelis constant (K_m) is the substrate concentration at half maximum velocity of a steady state reaction. [87]

The dependence of initial reaction velocity on substrate concentration and K_m may be illustrated by evaluating the Michaelis-Menten equation under three conditions.

1) When [S] <<< K_m, then K_m + [S] ≈ K_m. V_{max} is proportionate to K[S]. The initial reaction velocity therefore is directly proportionate to [S].
2) When [S] >>> K_m, then K_m + [S] ≈ [S]. Then reaction velocity is maximal to (V_{max}) and no effect for further increases in substrate concentration.
3) When [S] = K_m, a constant. [88].

Double reciprocal plots or Lineweaver-Burk plots are obtained by plotting the reciprocal values of the initial velocity of the enzymatic reaction (1/v) versus the reciprocal values of substrate concentration (1/[S]), in the absence and presence of different fixed concentrations of the inhibitor [89].

Michaelis Menten equation is modified as

$$\frac{1}{V} = \frac{K_M}{V_{max}}\ \frac{1}{[S]} + \frac{1}{V_{max}}$$

A plot of 1/v Vs 1/[S] gives straight line whose y intercept is 1/ V_{max} and slope is K_m /V_{max}

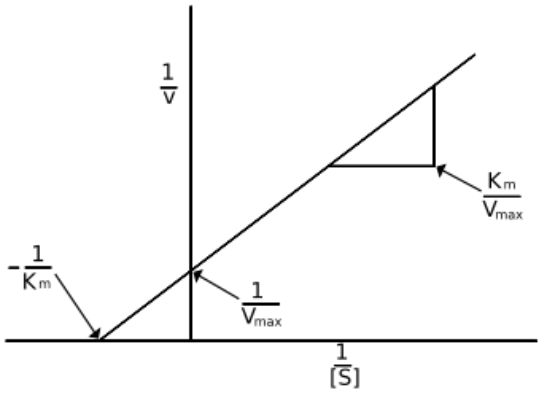

Fig.1.11: Line weaver–Burk plot

1.6.2.5 Enzyme inhibition

Enzyme inhibition is the process by which molecules lower the enzyme action by binding with the enzymes. Such molecules that can bind to active sites of enzymes and lower their action are called enzyme inhibitors. The ability of enzyme inhibitors to retard the enzyme activity is the chemistry behind action of several drugs. Therefore, innovations in the area of enzyme inhibitors are a promising and active area of research in biochemistry and pharmacology. There are enzyme activators that bind to enzymes and elevate their enzymatic activity [90].

Inhibitor binding can be either reversible or irreversible. Generally, irreversible inhibitors change the substrate chemically on reacting with the enzyme. Reversible inhibitors bind non-covalently to produce different types of inhibition, depending on whether these inhibitors bind the enzyme, the enzyme-substrate complex, or both. The inhibition constant (K_i) is an indication for the degree of enzyme inhibition [91].

Reversible inhibition can be of several types: competitive, non-competitive and uncompetitive. At times a mixed type also arises. Michaelis Menten plots can be used to differentiate the type of inhibition (Fig.1.12).

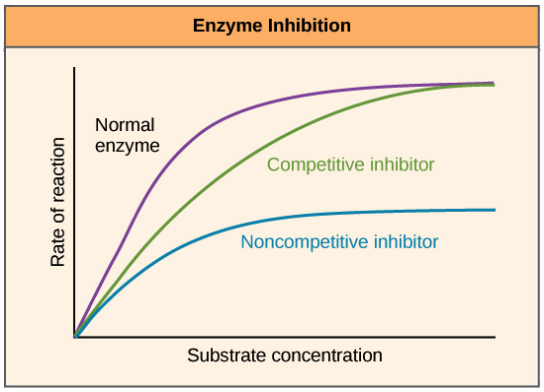

Fig.1.12 Michaelis –Menten curves for enzyme with and without inhibitor

In competitive inhibition, inhibitor will block the active site so that substrate cannot bind to the enzyme at the same time. It can be surmounted by sufficiently high concentrations of substrate, so that there is higher chance of enzyme and substrate binding. Competitive inhibitors are often similar in structure to the real substrate. In competitive inhibition, LB plots give the intersection at same point on the vertical axis. The competitive inhibitors do not alter V_{max} and increase K_m (Fig. 1.13)

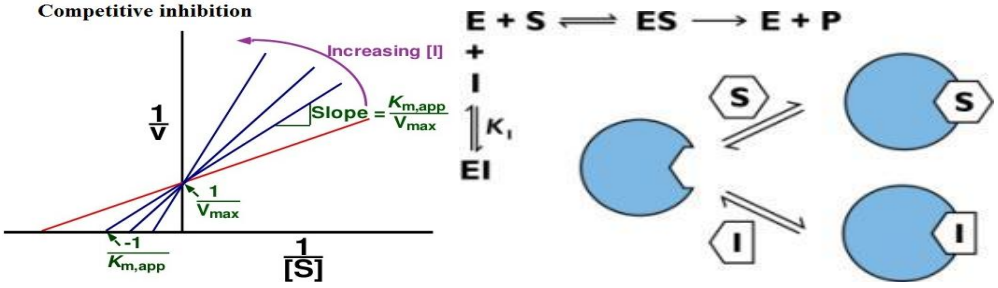

Fig. 1.13: Lineweaver-Burk plot and equation for competitive inhibition

Non-competitive inhibition is a type of inhibition in which the inhibitor reduces the enzyme activity by binding to it. Inhibitor has no effect on substrate binding. As a result an enzyme-substrate-inhibitor complex will be formed which cannot lead to the formation of product. It can only be converted back to the enzyme-substrate complex or the enzyme-inhibitor complex. Non-competitive

inhibitors have an equal affinity for the enzyme and the enzyme-substrate complex and it is the major difference from general mixed inhibition. For non-competitive type, LB plot gives intersection at same point in x axis. Non-competitive inhibitors do not alter K_m value and decrease V_{max} (Fig. 1.14). This type of inhibition cannot be prohibited by adding excess substrate. In case of mixed type of inhibition, the intersection of lines is between the two axes and it is a type of non-competitive inhibition [92].

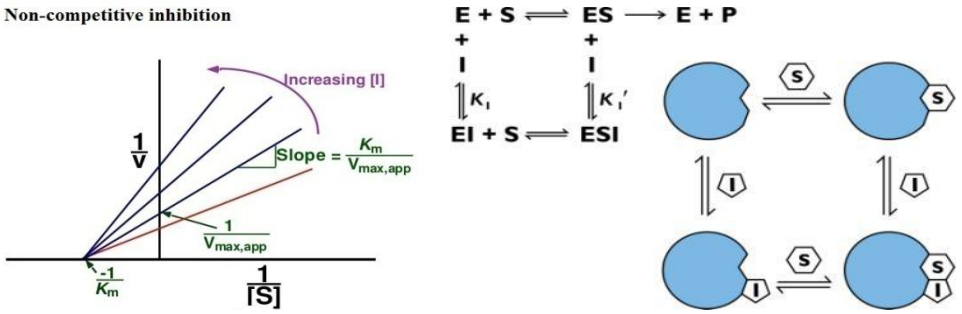

Fig. 1.14: Lineweaver-Burk plot and equation for noncompetitive inhibition

Uncompetitive inhibition, also known as anti-competitive inhibition, occurs when an inhibitor binds only to the E-S complex. That means inhibitor binds to enzyme only after the enzyme-substrate complex is formed. This will reduce the concentration of enzyme substrate complex which increases the apparent affinity for the substrate. As a result there is a decrease in the maximum enzyme activity V_{max} because substrate or product takes longer time to leave the active site (Fig. 1.15). Uncompetitive inhibition typically takes place in reactions with two or more substrates or products. This type of inhibition works when the substrate concentration is high and does not need the resemblance between the active site and substrate [93].

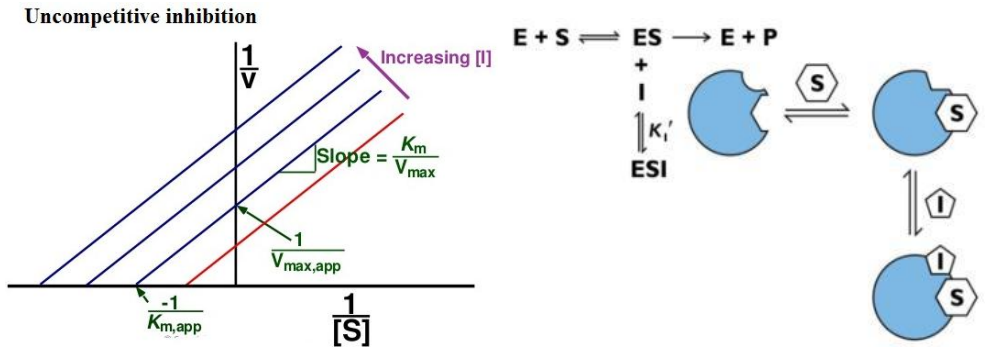

Fig. 1.15: Lineweaver-Burk plot and equation for uncompetitive inhibition

1.6.2.6 Determination of IC_{50} values

The half maximal inhibitory concentration (IC_{50}) evaluates the ability of a substance to inhibit a specific biological or biochemical function. IC_{50} is another important parameter that is determined during enzyme inhibition studies. According to the FDA, IC_{50} is the concentration of a drug that is required for 50% inhibition *in vitro*. This parameter quantitatively indicates how much of a particular drug or other substance (inhibitor) is needed to inhibit a given biological process (or component of a process, i.e. an enzyme, cell, cell receptor or microorganism) by half. The values are typically expressed as molar concentration [94].

1.6.3 Antimicrobial screening

Diversity of microorganisms was elucidated to cause infectious diseases in the latter half of the 19th century. Antimicrobial drugs made dramatic advances, resulting in the overly optimistic view that infectious diseases would be conquered in the near future. However, in reaction to the progress of antimicrobial agents, microorganisms that have acquired resistance to drugs through a range of mechanisms have emerged and keep on plaguing human beings. In current

scenario, infectious diseases caused by drug-resistant bacteria are one of the most vital problems in daily clinical practice. Options for treatment with antimicrobial agents are limited in the existing situation, where multidrug-resistant bacteria have spread widely and the number of brand novel drugs placed on the market is decreasing. Since drug-resistant bacteria have been chosen by the use of antimicrobial drugs, the proper use of currently accessible antimicrobial drugs, as well as efforts to minimize the transmission and spread of resistant bacteria through appropriate infection control would be the first step in resolving the issue of resistant organisms [95].

As per WHO, antimicrobial resistance (AMR) make threats to the effective prevention and treatment of an ever-increasing range of infections caused by several microbes like bacteria, parasites, viruses and fungi and requires coordinated action across all government sectors and society. The health care cost for patients with resistant infections is higher than for patients with non-resistant infections due to longer time of illness, additional tests and use of more expensive drugs. In 2016, about 4, 90,000 people developed multi-drug resistant TB globally, and drug resistance is starting to complicate the fight against HIV and malaria, as well. Superior innovation and investment are obligatory in research and development of new antimicrobial medicines, vaccines, and diagnostic tools [96].

1.6.3.1 Classifications of antimicrobials

Antimicrobials are classified on several ways including spectrum of activity, effect on bacteria, and mode of action.

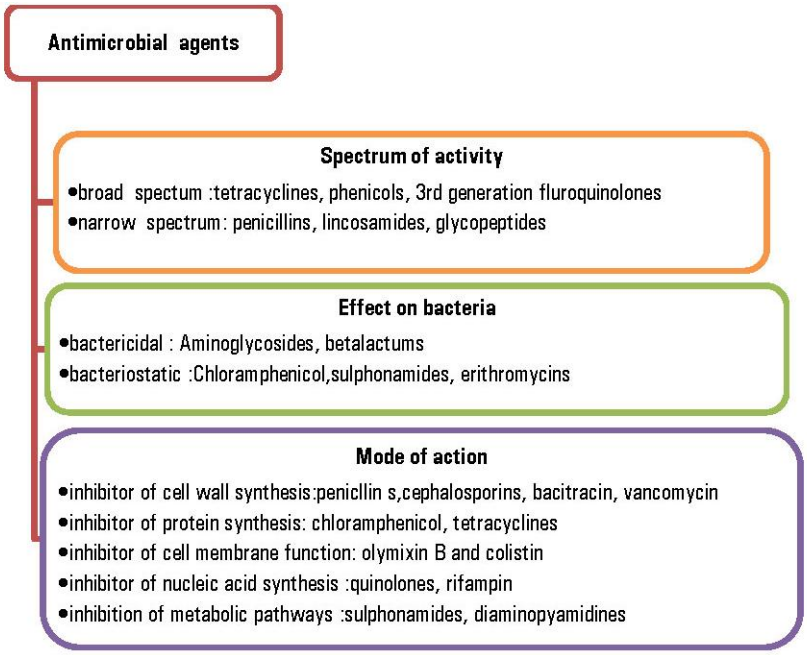

Fig. 1.16: Classification of antimicrobials

In the search of new antimicrobial agents, there are numerous studies regarding new metal-based complexes active against bacteria and fungus. The mechanisms of action are different depending on the metals and the ligands present in the complex. They can be active against the microorganism by the occupation of surface sites, which would usually be utilized in the initiation of the infection of the host cell preventing the first step in the infection. On the other hand, the compound may break through the cell wall, disturbing different molecule targets [97, 98].

The strategy of using molecules and ions coordinated to metal ions was used in several areas of the pharmacology to develop new pharmacologically active molecules. In spite of the fact that metal-based drugs correspond to a comparatively small fraction of total drugs, they accomplish imperative roles in medicine. Just consider the cisplatin (platinum-containing anti-cancer drug), the aurothioglucose (chrysotherapy for the treatment of rheumatoid arthritis)

and the Ag-sulfadiazine (silver complex with antibacterial activity used in burns) to comprehend the importance of this field [99].

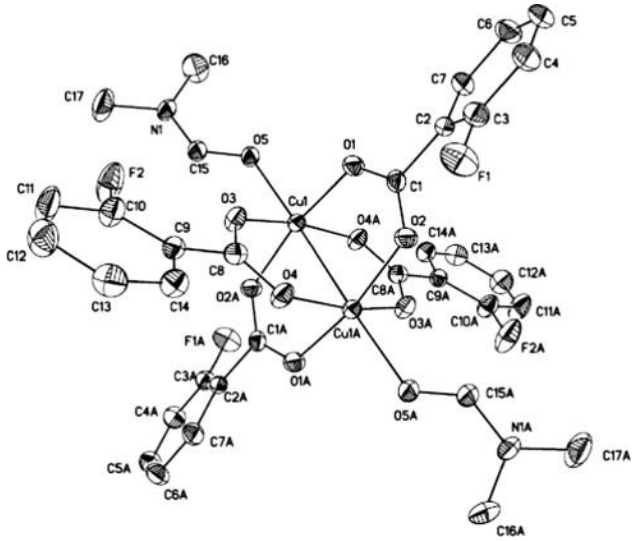

Fig.1.17: Crystal structure of the complex [Cu2 $(L3)_4(DMF)_2$] [100]

H. Liu *et al* reported a Cu (II) complex with 2-fluorobenzoate $[Cu_2(L3)_4(DMF)_2]$ which is having strong antimicrobial ability due to the increased lipophilic character due to the presence of metal ion.

1.6.3.2 Methods for determining antimicrobial activity

An array of laboratory methods can be used to appraise or screen the in vitro antimicrobial activity of an extract or a pure compound. The most acknowledged and basic methods are the disc-diffusion and broth or agar dilution methods. Further methods are employed especially for antifungal testing, such as poisoned food technique. Other recommended tests to further study the antimicrobial effect of an agent in depth are time-kill test and flow cytofluorometric methods which provide information on the nature of the inhibitory effect (bactericidal or bacteriostatic) (time-dependent or concentration-

dependent) and the cell damage inflicted to the test microorganism. Some techniques used for evaluation of antimicrobial activity are diffusion methods [101-106], dilution methods [110-113], TLC bioautography [107-109], time kill tests [114], ATP bioluminescence assay [115] and cytoflourometry[116-117]. Fig. 1.18 gives the different methods for the determination of antimicrobial activity.

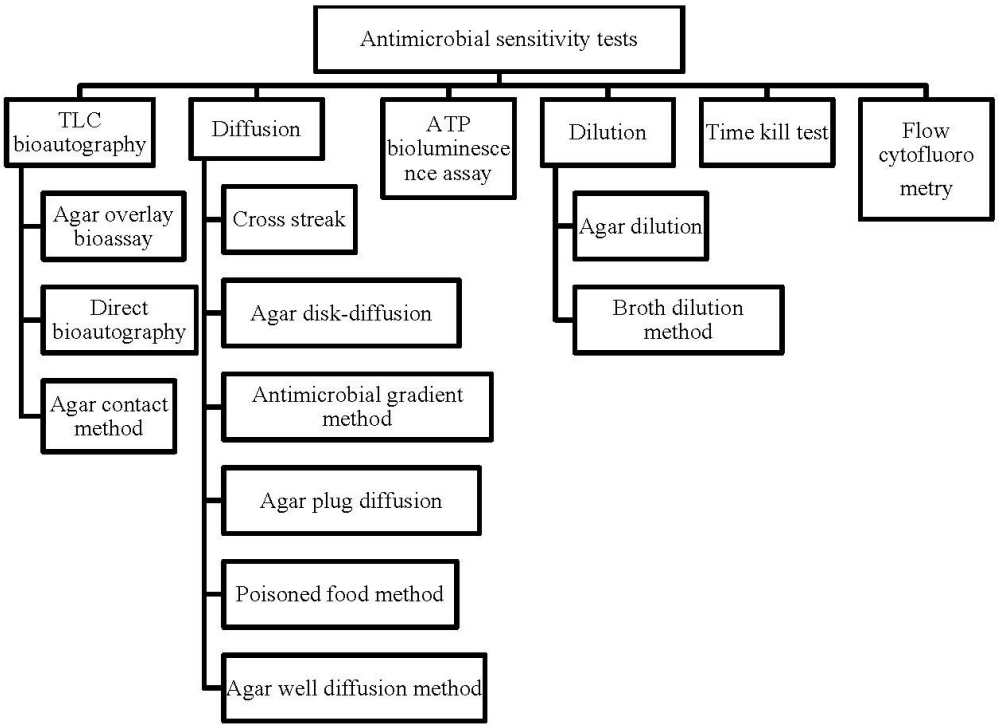

Fig. 1.18: Different antimicrobial sensitivity tests

1.6.4 Cytotoxicity tests

Cytotoxicity assays are designed to evaluate the ability of a compound to kill the cells intrinsically. The major factors that decide the toxicology of an entity is the dosage, the duration of exposure to a compound and the compound's mechanism of toxicity [118]. *In vitro* toxicity can be manifested in several ways like diminished cellular adhesion, dramatic morphological

changes and a decrease in replication rate or a reduction in overall viability in cellular level. Various different assays have been developed to resolve *in vitro* toxicity such as cell enumeration by total protein content and enumerating viable cells, quantifying cell death/survival by assessing plasma membrane integrity through evaluating certain vital functions [119].

Most accepted assays that are extensively used are

1.6.4.1 Total cellular protein assay (sulfo-rhodamine B)

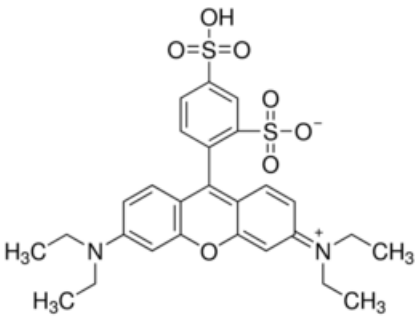

Fig. 1.19: sulphorhodamine B

This method is based on the property of SRB, to bind stoichiometrically to proteins under mild acidic condition and then to be extracted using basic conditions [120,121].

1.6.4.2 Neutral-red uptake assay

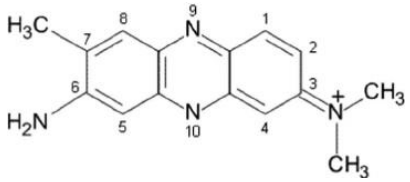

Fig. 1.20: Neutral red dye

This assay, one of the most used cytotoxicity tests with many biomedical and environmental applications, provides a quantitative estimation of the number

of viable cells in a culture. Assay is based on the ability of viable cells to incorporate and bind the supravital dye neutral red in the lysosomes[122].

1.6.4.3 LDH leakage assay

Lactate dehydrogenase (LDH), present in most eukaryotic cells is a soluble cytosolic enzyme, releases into culture medium upon cell death due to damage of plasma membrane. The hydrolysis of lactate to pyruvate is catalyzed by the LDH released from cells in the culture supernatant. This reaction is accompanied by the stoichiometrical reduction of Nicotinamide Adenine Dinucleotide(NAD+)in NADH. The latter is used as a limiting reagent in a second reaction catalyzed by the diaphorase. A tetrazolium salt: INT (2-(4-iodophenyl)-3-(4-nitrophenyl)-5-phenyl-2H-tertrazolium) is transformed to red formazan whose formation can be spectrophotometrically quantified at 490nm and amount of formazan formed is proportional to that of LDH present in the medium [123].

1.6.4.4 MTT assays

The MTT (3-(4, 5-dimethylthiazol-2-yl)-2, 5-diphenyltetrazolium bromide) tetrazolium colorimetric assay is a recognized method of evaluating viable cell number in cell proliferation and cytotoxicity studies. This assay is based on the cleavage of the yellow tetrazolium salt, MTT, to form a soluble blue formazan product by mitochondrial enzymes. The amount of formazan produced is directly proportional to the number of living cells, present during MTT exposure. Since the MTT assay is economical, rapid and convenient it has become a much admired technique for quantification of viable cells in culture. However, various parameters have been identified that can affect cellular metabolism and other factors, which significantly modify MTT-specific activity and can result in calculated false high or false low cell counts.

Therefore, it is critical to create assay parameters with the suitable controls for each cell line and/or drug treatment in order to optimize assay conditions and minimize confounding effects. These parameters should comprise determining appropriate cell densities, culture medium, optimal concentrations and exposure times for MTT, fresh culture medium at the time of assay to avoid nutrient depletion, and controlling for drug treatment effects that may influence cellular metabolism. By calculating these important parameters, the MTT colorimetric assay provides precise and unswerving quantification of viable cell number [124, 125].

1.7 Objectives and scope of present study

Synthesis and characterization of biologically important ligands and metal complexes are always considered as a hot topic of research in the field of inorganic and medicinal chemistry. Chromones and its derivatives are good candidates as valid scaffold for drug library due to the peculiar properties and low toxic nature. The chemical reactivity of 3-substituted chromones is widely different depending on the nature of the functional group present at the position 3 and the reaction conditions. The prevailing ambiguity regarding the reaction between 3-formylchromone and primary aromatic amines aroused our interest to investigate the reaction between substituted 3-formylchromone and aminopyridines. 4-Chromanone scaffold is an important intermediate and interesting building block in heterocyclic synthesis and design of new lead compounds in drug discovery.

The objectives set for the study are:

a. To investigate the reaction between 3-formylchromone/3-formyl-6-methylchromone with different aminopyridines in methanolic media and to characterize the products using different spectral and analytical techniques.

b. To synthesis Ni (II), Cu (II) and Zn (II) complexes using these ligands.

c. To study the alpha amylase and alpha glucosidase inhibitory properties of these synthesized ligands and complexes and to study the inhibitory kinetics.

d. To investigate DNA binding abilities of these synthesized compounds.

e. To evaluate antimicrobial efficacy of these compounds.

f. To evaluate the cytotoxic behavior of the synthesized ligands and complexes.

1.8 Physical techniques used for the study

1.8.1 Elemental analysis

Elemental analysis is a method where a sample is analyzed to obtain its elemental and sometimes isotopic composition. Elemental analysis can be qualitative and quantitative. This information is important to help determine the structure of an unknown compound, as well as to help ascertain the structure and purity of a synthesized compound. Carbon, hydrogen and nitrogen analyses of all synthesized compounds were carried out using a Vario EL III CHNS analyzer at Sophisticated Test and Instrumentation Centre (SAIF), Cochin University of Science and Technology, Kochi, India. The metal content of the complexes were determined by AAS after digestion with concentrated nitric acid. The analysis were done using Thermo Electron Corporation, M series Atomic Absorption Spectrophotometer.

1.8.2 Mass spectrometry

Mass spectrometry is one of the precise methods for illustrating the molecular mass of a compound and its elemental composition. In this

technique molecules are ionized and broken up into many fragments by bombarding with highly energetic electrons. Each kind of ion possess a particular mass to charge ratio (m/z) which is the identity of a compound and help us to establish molecular mass and molecular formula for a new compound. Mass spectra of the synthesized ligands were recorded using Waters 3100 Mass Detector using ESI technique designed for routine LC-MS analysis at Department of Applied Chemistry, Cochin University of Science and Technology, Kochi, India.

1.8.3 Ultraviolet–visible spectroscopy

Refers to absorption spectroscopy or reflectance spectroscopy in the ultraviolet-visible spectral region in which the molecules undergo electronic transitions from the ground state to the excited state. This spectroscopy is regularly used in analytical chemistry for the quantitative determination of different analytes including high molecular weight proteins and macromolecules. This technique can be used to correlate wavelengths of absorption peaks with the types of bonds in a given molecule. Several factors such as geometry of complex, nature of the ligands, and oxidation state of central metal atom can decide the energy gap in these transitions. There can be intraligand transition bands, metal to ligand charge transfer bands, ligand to metal transition bands and *d-d* bands. Uv-visible absorption studies gives clear evidence for complexation by shift in position and intensity of these transition bands.

Uv-vis spectrum was measured using Thermo Scientific Evolution 201 Uv-vis spectrophotometer (200-900 nm range) in DMSO solutions of ligands and complexes. Quatrz cuvette of 1 cm path length was used for recording the spectra.

1.8.4 FT -IR spectroscopy

Infrared spectrum gives different vibrational frequencies of the different type of bonds that are present in the system. Formation of new peaks and shift in the vibrational frequencies of the ligand metal systems clearly indicate the complexation. Presence of functional groups and mode of coordination can be easily understood from IR spectra which help to structurally elucidate the molecule. IR spectra for the ligands and complexes was recorded on a JASCO FT-IR-5300 Spectrometer using KBr pellets in the range 4000–400 cm^{-1}.

1.8.5 Conductivity measurements

Conductivity measurements help to understand and ionic or non ionic nature of the coordination compounds. These measurements are frequently used to identify the degree of ionization of the complexes and also the molecular ions that a complex liberates in solution (in case of presence anions outside the coordination sphere). Molar conductivities of the complexes in DMSO solutions (10^{-3} M) at room temperature were measured using a Systronic model 303 direct reading conductivity meter.

1.8.6 Magnetic susceptibility measurements

The magnetic susceptibility measurements were recorded on a Magway MSB Mk 1 Magnetic Susceptibility Balance at room temperature [126].

1.8.7 TG-DTG Analysis

Thermal analysis determines the change in the chemical and physical properties as the function of temperature which gives clear idea about the relative mass loss. The changes in mass of the compound are due to the rupture or formation of chemical bonds at elevated temperatures and loss of some volatile products. TGA is useful in determining the moisture content, oxidation reduction process, physical process such as desorption, volatilization

and sublimation. TG -DTG analysis of the complexes were carried out under air and nitrogen at a heating rate of 10°C min^{-1} using a Perkin Elmer Pyris Diamond TG analyzer in the temperature range of 0-800°C at Sophisticated Test and Instrumentation Centre (SAIF), Cochin University of Science and Technology, Kochi, India.

1.8.8 EPR spectroscopy

EPR spectroscopy works in microwave region of electromagnetic spectrum so as to elucidate the electronic structure of paramagnetic molecules. The EPR spectra of a complex give idea about the metal ligand bonding, unpaired electron distribution and spatial disposition of ligands around the central metal ion [128]. The principal g tensor values provide valuable information regarding the geometry as well as the nature of bonding in the complexes. *If* $g_{||} > g_{\perp} > g_e$, then the ground state is $d_{x^2-y^2}$ and geometry of the complex can be elongated octahedron, square pyramid or square planar. If $g_{\perp} > g_{||} > g_e$, then the ground state becomes d_{z^2} and geometry may be compressed octahedron or trigonal bipyramid. The coordination geometry is identified by the overall spectral shape such as the relative position of the peaks with respect to the given magnetic field strength and the splitting between two adjacent peaks [129]. The EPR spectra of the complexes in the solid state at polycrystalline state at 298 K and in frozen DMF at 77 K were recorded on a Varian E-112 spectrometer using TCNE as the standard with 100 kHz modulation frequency, 2G modulation amplitude and 9.1 GHz microwave frequency at the SAIF, IIT Bombay, India. Some of the EPR spectra are simulated using EasySpin.

1.8.9 ^{1}H NMR spectroscopy

Proton NMR spectroscopy is one of the most reliable techniques that can be used for the structural elucidation of organic compounds. Chemical shifts ranging from +14 to -4 ppm, spin-spin coupling between protons and

integration curves will give clear picture regarding the intensity of individual proton type. Chemical shift values reflect the molecular structure and the solvent, temperature, magnetic field in which the spectrum being recorded and other neighboring functional groups [130]. ^{1}H NMR spectra of ligands and zinc complexes were recorded using Bruker Advance III, 400MHz FT-NMR spectrometer using TMS as internal standard. $CDCl_3$ and DMSO were used as the solvents at Sophisticated Test and Instrumentation Centre (SAIF), Cochin University of Science and Technology, Kochi, India.

1.8.10 ^{13}C NMR spectroscopy

^{13}C NMR is a vital tool in chemical structure elucidation in organic chemistry. ^{13}C NMR detects only the ^{13}C carbon isotope, whose natural abundance is only 1.1%, because the main carbon isotope, ^{12} C, having zero net spin is not detectable by NMR .^{13}C nucleus is about 400 times less sensitive than proton nucleus and common range of energy absorption for ^{13}C is wide 0 – 200 ppm relative to TMS. ^{13}C NMR spectroscopy is analogous to proton NMR in that the number of the peaks in the spectrum normally corresponds to the number of different carbon environments and the chemical shifts of carbon signals provide some hints of nature of each environment. Number and splitting of signals give idea about different types of carbons present and number of hydrogen attached to each carbon. Chemical shift values indicate the electronic environment and hybridization of each carbon in the system [130]. NMR spectra of ligands were recorded using Bruker Advance III, 400MHz FT-NMR spectrometer using TMS as internal standard. $CDCl_3$ and DMSO were used as the solvents at Sophisticated Test and Instrumentation Centre (SAIF), Cochin University of Science and Technology, Kochi, India.

References

[1] J. D. Hepworth; A. J. Boulton; A. McKillop; Comprehensive Heterocyclic Chemistry 3; Pergamon Press; Oxford; **1984**, 835.

[2] G. Singh; L. Singh; M. P. S. Ishar; Tetrahedron **2002,** 58, 7883.

[3] A. A. Abu-Hashem; M. M. Youssef; Molecules **2011**, 16, 1956.

[4] A. Gaspar; M. J. Matos; J. Garrido; E. Uriarte; F. Borges, Chem. Rev. **2014**, 114, 4960.

[5] B. N. Ruhs; K. C. H. Julia; P. H. William; S. P. Tor; HOLZFORSCHUNG **2008**, 62, 264.

[6] N. S. Parmer; M. Tariq; A. M. Ageel; Res. Commun. Chem. Pathol. Pharmacol. **1987**, 58, 15.

[7] M. Gabor; Prog. Clin. Biol. Res. **1986**, 213, 471.

[8] T. Zhou; Q. Shi; K. H. Lee; Tetrahedron Lett. **2010**, 51, 4382.

[9] S. Maho; K. Yoshiyuki; Phytomedicine **2010,** 17, 820.

[10] M. G. Amira; D. C. Pierre; T. Marguerite; T. N. Bonaventure; T. Pierre; T. Hirata; J. Biosci. **2007**, 62, 331.

[11] D. C. Pierre; G. Donatien; T. Marguerite; N. T. Bonaventure; P. Pierre; A. A. Ahmed, G. M. Amira; A. I. Godwin; T. Hirata; M. J. Tom; Nat. Prod. Commun. **2006**, 1, 961.

[12] R. Kumar; M. Yusuf; ARKIVOC, **2006,** 9, 239.

[13] Marder; H. Viola; J. A. Bacigaluppo; M. I. Colombo; C. Wasowski; C. Wolfman; J. H. Medina; E. A. Ruveda; A.C. Paladini; Biochem. Biophy. Res. **1998**, 249, 481.

[14] D. F. Ortwine. PCT Int. Appl. PIXXD2 WO 2004014880 A1 20040219 CAN 140: 175192, **2004**, 138.

[15] S. Sogawa; Y. Nihro; H. Ueda; Akihiro Izumi; T. Miki, H. Matsumoto; T. Satoh; Med. Chem. **1993,** 36, 3904.

[16] N. Fang, J. E. Casida; Proc. Natl. Acad. Sci, **1998**, 95, 3380.

[17] L. Luyengi; I. Lee; W. Mar; H. H. S. Fong; J. M. Pezzuto; A. DouglasKinghorn; Phytochemistry, **1994**, 36, 1523.

[18] L. J. V. Galietta; M. F. Springsteel; M. Eda; E. J. Niedzinski; K. By; M. J. Haddadin; M. J. Kurth; M. H. Nantz; A. S. VerKMan; J. Biol. Chem. **2001**, 276, 19723.

[19] V. A. Kostyuk; A. I. Potapovich; E. N. Vladykovskaya; L. G. Korkina; I. B. Afanas'ev; Arch. Biochem. Biophys. **2001**, 385, 129.

[20] M. A. Somra; C. T. Supuran; J. Enz Inhib. Med. Chem. **2006**, 21, 173.

[21] F. A Ragab; M. M Hussein; M. M .Hanna; G. S. Hassan; S. A Kenawy; Pharmazie. **1993**, 48, 808.

[22] K. M. Khan; N. Ambreen; S. Hussain; S. Perveen; M. I. Choudhary; Bioorg. Med. Chem. **2009**, 17, 2983.

[23] C. Dyrager; A. Friberg; K. Dahlén; M. Fridén-Saxin; K. Börjesson; L. M. Wilhelmsson; M. Smedh; M. Grøtli; K. Luthman; Chem. Eur. J. **2009**, 15, 9417.

[24] M. Kawase; T. Tanaka; H. Kan; S. Tani; H. I. Nakashima; H. Sakagam; Iiar. J. **2007**, 21, 829.

[25] P. Kavitha; K. L. Reddy; Arabian J. Chem. **2013**, doi.org/10.1016/ j.arabjc. 2013.06.018.

[26] H. A. Tawfik; E. F. Ewies; W. S. El-Hamouly; IJRPC. **2014**, 4, 1046.

[27] S. Keri; S. Budagumpi; R. K. Pai; R. G. Balakrishna; Eur. J. Med. Chem. **2014**, 78, 340.

[28] A. D. Kułaczkowska; L. Mazur; J. Mol. Str. **2011**, 985, 233.

[29] A. Nohara; T. Umetani; Y. Sanno, Tetraedron Lett. **1973**, 22, 1995.

[30] R. Tapia; M. Sitges; Brain Res. **1982,** 250, 291.

[31] V. Y. Sasnovskikh; R. A. Irgashev, Tetrahedron Lett. **2007**, 48, 74.

[32] M. A. Terzidis; J. Stephanidou-Stephanatou; C. A. Tsoleridis, Tetrahedron Lett. **2009,** 50, 1196.

[33] J. Quiroga; A. Rengifo; B. Insuasty; R. Abonia; M. Nogueras; A. Sanchez, Tetrahedron Lett. **2003,** 43, 9061.

[34] H. Stankovicova; M. Lacova; A. Gaplovsky, J. Chovancova; N. Pronayova, 32nd International Electronic Conference on Synthetic Organic Chemistry (ECSOC-2), http://www.mdpi.org/ecsoc/, September 1-30, **1998.**

[35] H. Stankovicova; M. Lacova; A. Gaplovsky; J. Chavanova; N. Paranayova, Tetrahedron **2001,** 57, 3455.

[36] G. O. Dudek, J. Am. Chem. Soc. **1963**, 85, 694.

[37] A. O. Fitton; J. R. Frost, P. G. Houghton; H. Suschitzky, J. Chem. Soc. Perkin Trans. **1979**, 2**,** 1691.

[38] C. K. Ghosh; S. Khan, Synthesis **1980**, 701.

[39] G. Rihs; I. Sigg; G. Haas; T. Winkler, Helv. Chim. Acta, **1985**, 68, 1933.

[40] S. T. Saengchantara; T. W. Wallace; Nat. Prod. Rep. **1986**, 3, 465.

[41] Drug Bank, http://www.drugbank.ca/drugs

[42] T. A. Nakib; V. Bezjak; M. J .Meegan; R. Chandy; Eur. J. Med. Chem. **1990**, 25, 455.

[43] G. Toker; E. Kuepeli, M. Memisoglu; Yesilada, E. J. Ethnopharmacol. **2004,** 95, 393.

[44] D. Tasdemir; M. Kaiser; R. Brun; V. Yardley; T. J. Schmidt; F. Tosun; P. Ruedi, Antimicrob. Agents Chemother. **2006,** 50, 1352.

[45] S. S. Costa; A. Jossang; B. Bodo; M. I. Souza; V. G. Moraes; J. Nat. Prod. **1994**, 57, 1503.

[46] H. Matsuda; T. Morikawa; M. Yoshikawa; Pure Appl. Chem. **2002**, 74, 1301.

[47] A. P. Jorge; H. Horst; E. de Sousa; M. G. Pizzolatti; F. R. M. B. Silva, Chem.-Biol. Interact. **2004**, 149, 89.

[48] R. Mestre; D. Escande; I. Cavero; Eur. J. Pharmacol. **1990**, 183, 1239.

[49] Chopra; M. Kaur; Navpreet; Divneet; Lalit; Jour. Harmo. Res. pharm. **2015**, 4, 162.

[50] H. Stankovičova; M. Lácová; A. Gáplovský; J. Chovancová; N. Prónayová; Tetrahedron. **2011**, 57, 3455.

[51] Y. Zhong; D. T. Boruta; D. R. Gauthier; D. Askin; Tetrahedron Lett. **2011**, 52, 4824.

[52] V. V. Shynkar; A. S. Klymchenko; E. Piémont; A. P. Demchenko; Y. Mély; J. Phys. Chem. **2004**, 108, 8151.

[53] Y. Araki; A. Andoh; Y. Fujiyama; K. Hata; J. Makino; T. Okuno; F.Nakanura; T. Bamba; J. Chromatogr. **2001**,753, 209.

[54] P. Lechat; S.Thesleef; W.C. Bowmann; Adv. Biosci**. 1981**, 35, 3.

[55] G. R. Lawton; H. R. Ranaivo; L. K .Chico; H. Ji; F. Xue; P. Martásek; L. J. Roman; D. M. Watterson; R. B. Silverman, Bioorg. Med. Chem. **2009**, 17, 2371.

[56] T. D. Aicher; S. A. Boyd; M. J. Chicarelli; K. R. Condroski; R. J. Hinklin; A. Singh; US Pat. 20090156603, **2007.**

[57] A. Kodimuthali; A. Mungara; P. L. Prasunamba; M. Pal; J. Braz. Chem. Soc. **2010**, 21,103.

[58] A. Baranyi; O. Fehér; EEG. Clin. Neurol. **1979**, 47, 745.

[59] F. Canssens; J. Torremans; M. Janssen; R. A. Stokbroekx; M. Luyckx; P. A. J. Janssen; J. Med. Chem. **1985**, 28, 1943.

[60] I. K. Khanna; R. M. Weier; K. T. Lentz; L. Swenton; D. C. Lakin; J. Org. Chem. **1995**, 60, 960.

[61] H. Fuhrmann; S. Brenner; P. Arndt; Inorg. Chem. **1996**, 35, 6742.

[62] W. R. McWhinnie; J. Chem. Soc. **1964,** 2959.

[63] A. Garcia-Raso; J. J. Fiol; A. Lopez-Zafra; A. Cabrero; I. Mata; E. Molins; Polyhedron **1999**, 18, 871.

[64] S. Lechat; Tesleff; W. C. Bownan; Aminopyridines and Similarly Acting Drugs, Pergamon, Oxford, **1982.**

[65] M. Frezza, S. Hindo, D. Chen, Curr. Pharm. Des. **2010**, 16, 1813.

[66] U. Ndagi; N. Mhlongo; M. E. Soliman; Drug Des. Develop. Ther. **2017**, 11, 599.

[67] K. A. Myannik; V. N. Yarovenko; E. K. Beloglazkina; A. A. Moiseeva; M. M. Krayushkin ; Polyhedron, **2018**, 139, 208.

[68] M. Bheemarasetti; K. Palakuri; S. R. Prakash; S. Durgaiah; G. N. Reddy; L. R. Kotha; J. Iranian. Chem. Soc., https://doi.org/10. 1007/s13738-018-1338-7

[69] J. D. Watson; F. H. C. Crick, Nature, **1953**, 171, 737.

[70] C. Ban; B. Ramakrishnan; M. Sundaralingam; J. Mol. Biol. **1994**, 236, 275.

[71] R. E. Dickerson; Methods Enzymol. **1992**, 211, 67.

[72] A. Bacolla; R. D. Wells; Int. J. Biol. Chem. **2004**, 279, 47411.

[73] Q. Lu; J. Med. Chem. **2007**, 50, 2601.

[74] K. Suntharalingam; O. Mendoza; A. A. Duarte; D. J. Mann; R. Vilar; Metallomics. **2013,** 5, 514.

[75] V. Cepeda; M. A. Fuertes; J. Castilla; C. Alonso; C. Quevedo; J. M. Perez; Med. Chem. **2007**, 7, 3.

[76] H. H. Li; J. Aubrecht; A. J. Fornace; Mutat. Res. **2007,** 623, 98.

[77] M. Mariappan; M. Suenaga; A. Mukhopadhyay; P. Raghavaiah; B. G. Maiya; Inorg. Chim. Acta **2011,** 376, 340.

[78] C. A. Hawkins; C. Watson; Y. Yan; B. Gong; D. E. Wemmer; Nucleic Acids Res. **2001,** 29, 936.

[79] H. Xu; K.-C. Zheng; Y. Chen; Y.-Z. Li; L.-J. Lin; H. Li; P.-X. Zhang; L.-N. Ji; Dalton Trans. **2003,** 33, 34.

[80] R. Hajian; T. Guan Huat; J. Spectrosc. **2013,** 2013, 8.

[81] M. Sirajuddin; A. Haider; S. Ali; Int. J. Adv. Res. **2013,** 1, 499.

[82] T. P. Bennett; E. Frieden; Modern Topics in Biochemistry, Macmillan, London, **1969**, 43.

[83] J. Holum; Elements of General and Biological Chemistry, 2nd, ed. Wiley, New York, **2000.**

[84] M. F. Chaplin; C. Bucke; Enzyme Technology, Science Cambridge University press, Cambridge, **1990**.

[85] D. B. Živadin; B. Jovana; P. Biljana; H. Stephanie; V. E. Rudi; Dalton Trans. **2012**, 41, 12329.

[86] W. W. Cleland; CRC Crit. Rev. Biochem. **1982,** 13, 385.

[87] "Substrate Concentration (Introduction to Enzymes)". www. worthington-biochem.com

[88] A. L. Lehninger; D. L. Nelson; M. M. Cox; Lehninger principles of biochemistry. New York: W.H. Freeman. **2005**, ISBN 978-0-7167-4339-2.

[89] R. Martinek; J. Am. Med. Tech. **1969**, 31, 162.

[90] I. H. Segel; Biochemical calculations: how to solve mathematical problems in general biochemistry. (2^{nd} edition), Wiley Publications, **1976**, NewYork.

[91] R. J. Leatherbarrow; Trend. Biochem. Sci. **1990,** 15, 455.

[92] R. Walsh; E. Martin; S. Darvesh; Integr. Biol. **2011**, 3, 1197.

[93] W. W. Cleland; Biochim. Biophys. Acta. **1963,** 67,173.

[94] Y. Cheng, W. H. Prusoff; Biochem. Pharmacol. **1973,** 22 (23), 3099.

[95] T. Saga; K. Yamaguchi, JMAJ **2009,** 52, 103.

[96] http://www.who.int/news-room/fact-sheets/detail/antimicrobial-resistance.

[97] N. Hughes; The Inorganic Chemistry of Biological Processes. Chichester: John Wiley & Sons, **1981**, 300.

[98] M. J. Clarke; P. J. Sadler; Metallopharmaceuticals II: Diagnosis and Therapy (Topics in biological inorganic chemistry) Vol. 2 Springer- Verlag, **1999,** Berlin.

[99] N. Farrell (Ed.) Uses of Inorganic Chemistry in Medicine. The Royal Society of Chemistry, **1999**, Cambridge.

[100] H. Liu; W. Yang; W. Zhou; Y. Xu; J. Xie ; M. Li; Inorg. Chim. Acta. **2013**, 405, 387.

[101] CLSI, Performance Standards for Antimicrobial Disk Susceptibility Tests, Approved Standard, 7th ed., CLSI document M02-A11. Clinical and Laboratory Standards Institute, 950 West Valley Road, Suite 2500, Wayne, Pennsylvania 19087, USA**, 2012.**

[102] J. Hausdorfer; E. Sompek; F. Allerberger; Int. J. Tuberc. LungDis. **1998**, 2751.

[103] S. Magaldi; S. Mata-Essayag; C. HartungdeCapriles; Int. J. Infect. Dis. **2004**, 839.

[104] A. E. Jiménez-Esquilín; T. M. Roane; J. Ind. Micro- biol. Biotechnol. **2005**, 32, 378.

[105] M. Lertcanawanichakul; S. Sawangnop; J.Sci. Tech. **2008**, 5161.

[106] M. S. Ali-Shtayeh; S. I. AbuGhdeib; Mycoses **1999**, 42, 665.

[107] A. Marston; J. Chromatogr. A. **2011**, 1218, 2676.

[108] M. Suleiman; L. McGaw; V. Naidoo; Afr. J. Tradit. Complement. Altern. Med. **2010**, 764.

[109] M. Balouiri; S. Bouhdid; E. Harki; Asian J. Pham. Clin. Res. **2015,** 8, 213.

[110] CLSI, Methods for Dilution Antimicrobial Susceptibility Tests for Bacteria that Grow Aerobically, Approved Standard, 9th ed., CLSI document M07-A9. Clinical and Laboratory Standards Institute, 950 West Valley Road, Suite 2500, Wayne, Pennsylvania 19087, USA, **2012**.

[111] D. M. Kuhn; M. Balkis; J. Chandra; J. Clin. Microbiol. **2003**, 41, 506.

[112] R. S. Reis; I. Neves; S. L. S. Lourenço; J. Clin. Microbiol. **2004**, 42, 2247.

[113] CLSI, Methods for Antimicrobial Dilution and Disk Susceptibility of Infre- quently Isolated or Fastidious Bacteria, Approved Guideline, 2nd. ed., CLSI document M45-A2. Clinical and Laboratory Standards Institute, 950 West Valley Roadn Suite 2500, Wayne, Pennsylvania 19087, USA, **2010**.

[114] M. A. Pfaller; D. J. Sheehan; H. Rex; Clin. Microbiol. Rev. **2004**, 17, 268.

[115] L. Vojtek; P. Dobes; E. Buyukguzel; Eur. J. Entomol. **2014**, 111, 335.

[116] A. Paparella; L. Taccogna; I. Aguzzi; C. Chaves-López; A. Serio; F. Marsilio; G. Suzzi; Food Contr. **2008**, 19, 1174.

[117] Y.W. Tang, C.W. Stratton, Advanced Techniques in Diagnostic Microbiology, 2nd Ed., Springer, New York Heidelberg Dordrecht, London, **2013**. 937

[118] M. Ferro; A. Doyle; Cell Biol Toxicol. **2001**, 17, 205.

[119] T. L. Riss; R. A. Moravec; Drug Dev. Technol. **2004**, 2, 51.

[120] V. Vichai; K. Kirtikara; Nat. Protoc. **2006**, 1, 1112.

[121] A. L. Kasinski; K. Kelnar; C. Stahlhut; E. Orellana; J. Zhao; E. Shimer; S. Dysart; X. Chen; A.G. Bade; F. J. Slack; Oncogene. **2015**, 34, 3547.

[122] G. Repetto; A. del Peso; J. L. Zurita; Nat. Protoc. **2008**, 3, 1125.

[123] F. Valérie; F. Agathe; D. Boudard; M. Cottier; P. Grosseau; J. Pourchez, Langmuir **2015**, 31, 12.

[124] P. W. Sylvester; Methods Mol Biol. **2011**, 716, 157.

[125] T. Mosmann; J. Immunol. Methods **1983,** 65**,** 55.

[126] B. N. Figgis; J. Lewis; Modern Coordination Chemistry, ed., J. Lewis and R. G. Wilkins, Interscience, New York, **1960**, 400.

[127] B. N. Figgis; J. Lewis; Progress in Inorganic Chemistry, ed. F. A. Cotton, Interscience, New York, **1964,** 6, 37.

[128] J. Peisach; Blumberg; Arch. Biochem. Biophys. **1974**, 165, 691.

[129] E. Garribba; G. Micera; J. Chem. Educ. **2006**, 83, 1229.

[130] R. M. Silverstein; G. C. Bassler; T. C. Morrill, Spectrometric Identification of Organic Compounds, 5th Ed., Wiley, **1991**.

******

Chapter 2

Synthesis and spectral characterizations of 2-methoxy-4-chromanones

Contents

Abstract

3-Formylchromone have always attained special attention due to its peculiar chemical reactivity. Presence of three electron deficient centres in the system makes it open to different type of reactions. So we were curious to investigate the reaction between 3-formylchromones and different aminopyridines using methanol as the solvent. 2-methoxy-4-chromanones were obtained as the products instead of the expected Schiff bases. Products were characterized using different analytical and physical techniques including elemental analysis, IR spectral analysis, Uv-visible spectra, mass spectra, ^{1}H & ^{13}C NMR analysis. These compounds are expected to have excellent chelating ability and profound biological properties.

2.1 Introduction

Benzopyran ring chemistry has been extensively studied during past decades especially for exploring its structural diversities and biological applications. 4H-1-benzopyran-4-one derivatives, also known as 4H-chromen-4-ones or chromone, constitute an important class of natural oxygen-containing heterocycles that are widely distributed among many plants. 3-Formylchromone always occupy a unique position due to excellent chemical reactivity and hence find valuable use as synthetic precursors in the preparation of pharmacologically significant products and new heterocyclic systems [1]. Due to the outstanding physiological and pharmaceutical activities of these compounds, as well as their important position in synthetic chemistry, the advancing aspirations of scientists and interest in new routes to construct benzopyran and benzopyrone rings systems further stimulates studies in this area [2].

3-Formylchromone reacts with primary amine to give various products based on the reaction media. Basicity and nucleophilicity of amine and the reaction media will steer the category of products formed. One of them is those which have imine bond –C═N (Schiff bases) [3]. Another type of products of condensation of 3-formylchromone with primary aromatic amines are 4-chromanone derivatives [4]. The third type of products of reactions of 3-formylchromone with primary amines are compounds in which δ-pyrone ring is broken and new derivatives are formed (for example quinolines).The type of products of reaction between 4-oxo-4H-1-benzopyran-3-carboxaldehyde and amines depends on nature of used amine and/or experimental conditions[5].

M. Jacubek *et al.* has reported water-soluble chromone Schiff base derivatives bearing polyhydroxylated moiety from 3-formylchromone and 1-

amino-1-deoxy-glucitol [6]. Ammar *et al*. has recently reported tridentate Schiff's base ligand, 3-hydroxypyridin-2-yliminomethyl-4H-chromen-4-one which are highly promising bactericides and fungicides [7]. M. Rashidha *et al.* has reported a series of 2-alkoxy-(sulphonylarilaminomethylene)-chroman-4-ones which are potent selective inhibitors of ectonucleotidases. 2-alkoxy side chain was modified by changing the reaction media from methanol to ethanol, isopropanol and n-butanol [8]. The same group has reported that when 3-formylchromones reacted with aminobenzenesulfonamides using ethanol as the reaction solvent, an enamine product containing a 2-ethoxy side chain is obtained. And these 2-ethoxy-3-(sulfonylarylaminomethylene)-chroman-4-ones were reported as potent and selective inhibitors of alkaline phosphatase [9].

These facts prompted us to find out the reaction products of 3-formylchromone and 2-aminopyridine derivatives in methanolic media. Thus, we ended up with eight new 2-methoxy-4-chromanones by reacting 3-formylchromone/6-methyl-3-formylchromone and 2-aminopyridine/2-amino-5-bromopyridine/2-amino-5-nitropyridine/2-amino-5-methylpyridine/3-aminopyridine in methanol. This chapter deals with synthesis and spectral characterization of these eight chromanone derivatives. The compounds are expected to have excellent chelating behavior to form metal complexes. The newly synthesized ligand systems are given below.

1) ***2-Methoxy-3-(pyridin-2-ylamino)methylenechroman-4-one(L1)***
2) ***2-Methoxy-3-(((5-nitropyridin-2-yl)amino)methylene)chroman-4-one(L2)***
3) ***2-Methoxy-3-(((5-methylpyridin-2-yl)amino)methylene)chroman-4-one(L3)***
4) ***2-Methoxy-3-((pyridin-2-ylamino)methylene)chroman-4-one(L4)***
5) ***2-Methoxy-6-methyl-3-((pyridin-2-ylamino)methylene)chroman-4-one(L5)***

6) ***3-(((5-Bromopyridin-2-yl)amino)methylene)-2-methoxy-6-methylchroman-4-one(L6)***

7) ***2-Methoxy-6-methyl-3-(((5-methylpyridin-2-yl)amino)methylene)chroman-4-one(L7)***

8) ***2-Methoxy-6-methyl-3-((pyridin-3-ylamino)methylene)chroman-4-one(L8).***

These ligands were characterized using elemental analysis, mass spectra, IR spectra, Uv-vis spectra, proton NMR and ^{13}C NMR analysis.

2.2 Experimental

2.2.1 Materials used:

3-Formylchromone (Sigma Aldrich), 6-methyl-3-formylchromone (Sigma Aldrich), 2-aminopyridine (Sigma Aldrich), 2-amino-5-nitropyridine (Sigma Aldrich), 2-amino-5-bromopyridine (Sigma Aldrich), 2-amino-5-methylpyriridine (Sigma Aldrich), 3-aminopyridine (Sigma Aldrich) were analar grade and were used as such without further purification. Methanol (Merck), diethyl ether (Merck), hexane (Merck) were analytical grade and used as such.

2.2.2 Procedure for synthesis of ligands:

2.2.2.1 *2-Methoxy-3-((pyridin-2-ylamino)methylenechroman-4-one)*(L1):

Equimolar mixture of 3-formylchromone (0.174 g) and 2-aminopyridine (0.094 g) is dissolved in 25 ml of methanol. Then the mixture was refluxed for five hours with stirring at room temperature. Light yellow precipitate obtained was filtered off, washed with methanol, ether, hexane and dried. Yield and melting point noted. (Scheme: 2.1).

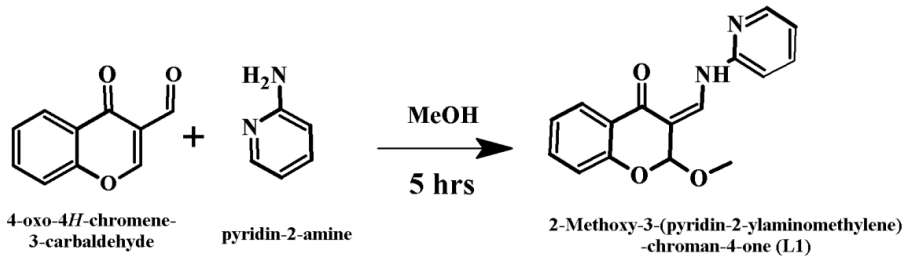

Scheme: 2.1

Light yellow powder, Yield: 0.210 g (75%), Anal. Calcd. For $C_{16}H_{14}N_2O_3$ (281) C% 68.07, H% 5.00, N% 9.96. Found: C% 67.97, H%4.86, N%9.91

2.2.2.2 *2-Methoxy-3-(((5-nitropyridin-2-yl)amino)methylene)chroman-4-one*(L2):

3-Formylchromone (0.174 g) and 2-amino-5-nitropyridine (0.139 g) was taken in the ratio 1:1 and dissolved in 25 ml of methanol. Then the mixture was stirred for five hours at room temperature. Dark yellow precipitate obtained was filtered off, washed with methanol, ether, hexane and dried. (Scheme: 2.2)

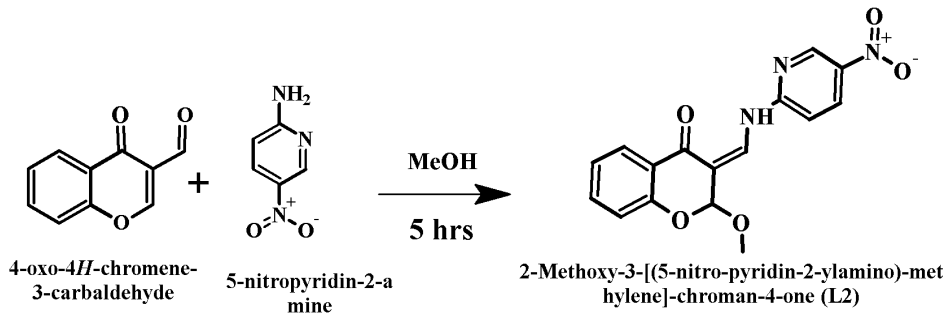

Scheme: 2.2

Dark yellow powder; Yield: 0.206 g (63%), Anal. Calcd. For$C_{16}H_{13}N_3O_5$ (327), C%58.72, H% 4.00, N% 12.84. Found: C% 58.95, H% 3.85, N% 12.82

2.2.2.3 *2-Methoxy-3-(((5-methylpyridin-2-yl)amino)methylene)chroman-4-one)*(L3):

To the methanolic solution of 3-formylchromone (0.174 g), 2-amino-5-methyl-pyridine (0.1081 g) dissolved in minimum amount of methanol was added slowly. Resultant mixture was stirred for 5 hours at room temperature. On keeping, yellow colored solid precipitated out which was filtered off, washed thoroughly with diethyl ether, hexane and dried. Yield and melting point was determined. (Scheme: 2.3)

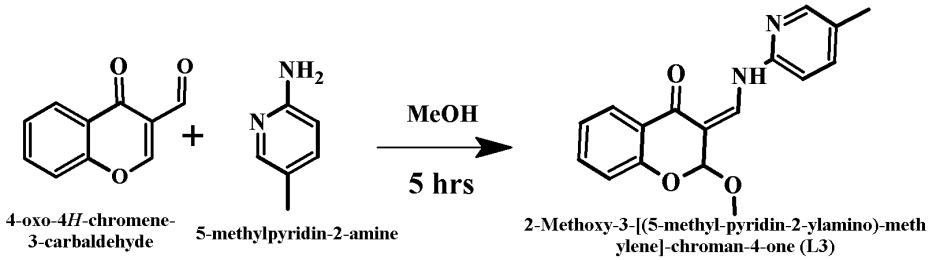

Scheme: 2.3

Yellow powder; Yield: (0.2 g) 68%, Anal. Calcd. For $C_{17}H_{16}N_2O_3$ (296.21) C% 68.91, H% 5.44, N% 9.45. Found: C% 68.81, H% 5.16, N% 9.11

2.2.2.4 *2-Methoxy-3-((pyridin-2-ylamino)methylene)chroman-4-one(L4):*

Methanolic solution of 3-formylchromone (0.174 g) was added to methanolic solution of 3-aminopyridine (0.094 g) (1:1 ratio). Then the mixture was stirred at room temperature for 18 hours. Yellow precipitate obtained on evaporation of solvent was filtered, washed with methanol, diethyl ether, hexane and dried. Yield and melting point noted. (Scheme: 2.4)

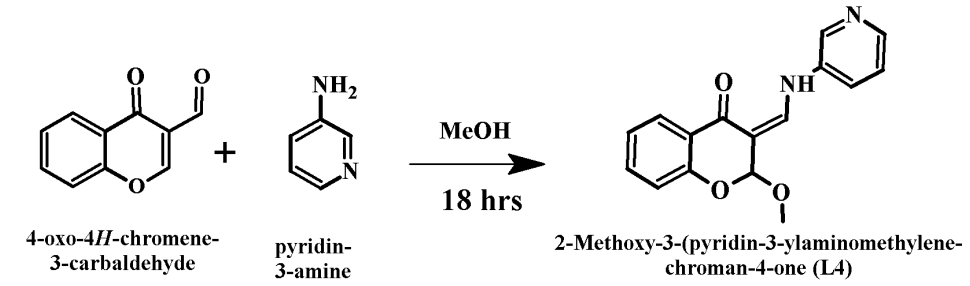

Scheme: 2.4

Light yellow powder; Yield: (0.210 g) 75%. Anal. Calcd. For $C_{16}H_{14}N_2O_3$ (282.1) C% 68.07, H% 5.00, N% 9.96. Found: C% 67.97, H% 4.96, and N% 9.71.

2.2.2.5 *2-Methoxy-6-methyl-3-((pyridin-2-ylamino)methylene)chroman-4-one)*(L5)*:*

Equimolar mixture of 3-formyl-6-methylchromone (0.188 g) and 2-aminopyridine (0.094 g) is dissolved in 25 ml of methanol. Then the mixture was refluxed for five hours with stirring at room temperature. Yellow precipitate obtained was filtered off, washed with methanol, diethyl ether, hexane and dried. Yield and melting point determined (Scheme: 2.5)

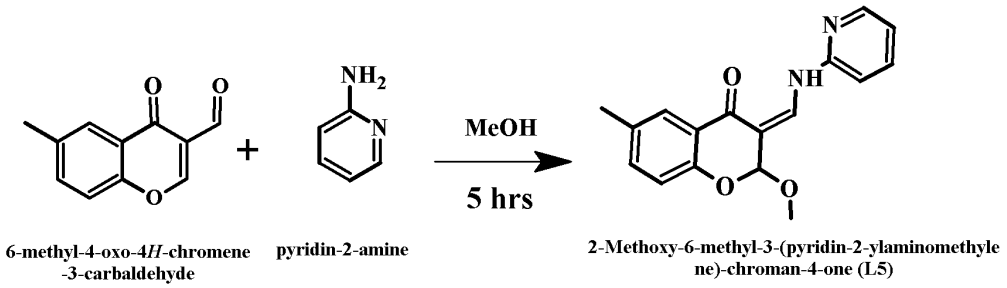

Scheme: 2.5

Yellow powder; Yield: (0.213 g) 72%; Anal. calcd. for $C_{17}H_{16}N_2O_3$ C% 68.91, H% 5.44, N% 9.45. Found: C% 68.00, H% 5.65, N% 9.47

2.2.2.6 *3-(((5-Bromopyridin-2-yl)amino)methylene)-2-methoxy-6-methylchroman-one*(L6)*:*

3-Formyl-6-methylchromone (0.188 g) dissolved in minimum quantity of methanol and methanolic solution of 2-amino-5-bromopyridine (0.173 g) was mixed slowly. Then the mixture was magnetically stirred for five hours at room temperature. Yellow precipitate obtained was filtered off, washed with methanol, diethyl ether, hexane and dried. Yield and melting point noted. (Scheme: 2.6)

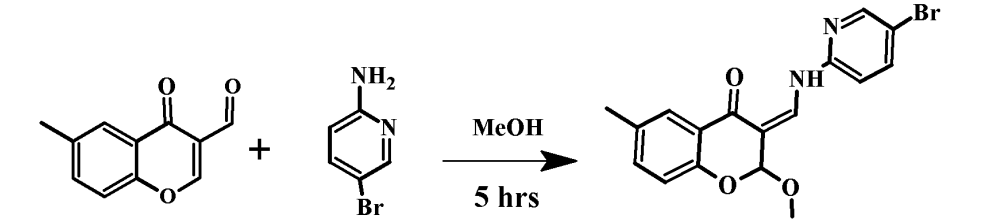

Scheme: 2.6

Lemon yellow powder, Yield: (0.285 g) 76% Anal. Calcd. For $C_{17}H_{15}BrN_3O_5$ (375.1) C% 54.42, H% 4.03, N% 7.43. Found: C% 54.30, H% 3.97, N% 7.47

2.2.2.7 2-*Methoxy-6-methyl-3-(((5-methylpyridin-2-yl)amino)methylene) chroman-4-one*(L7)**:**

3-Formyl-6-methylchromone (0.188 g) and 2-amino-5-methylpyridine (0.108 g) are dissolved in 25 ml of methanol. Then the mixture was stirred for five hours at room temperature. Yellow precipitate obtained was filtered off, washed with diethyl ether and hexane. It was then dried. Yield and melting point noted. (Scheme: 2.7)

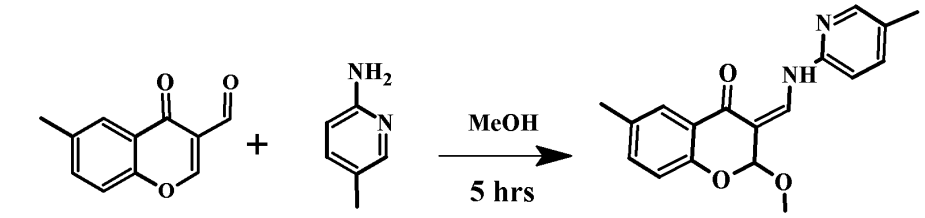

6-methyl-4-oxo-4*H*-chromene -3-carbaldehyde + 5-methylpyridin -2-amine → 2-Methoxy-6-methyl-3-[(6-methyl-pyridin-3 -ylamino)-methylene]-chroman-4-one (L7)

Scheme: 2.7

Light yellow powder, Yield: (0.2g) 65% Anal. Calcd. For $C_{18}H_{18}N_2O_3$ (310.2) C% 69.66, H% 5.85, N% 9.03. Found: C% 69.05, H% 5.16, N% 8.89

2.2.2.8 *2-Methoxy-6-methyl-3-((pyridin-3-ylamino)methylene) chroman-4-one (L8):*

A methanolic solution of 3-formyl-6-methylchromone and 3-aminopyridine was mixed and the mixture was stirred at room temperature for 18 hours. Yellow precipitate obtained on evaporation of solvent was filtered off, washed with methanol, diethyl ether, hexane and dried. Yield and melting point noted. (Scheme: 2.8)

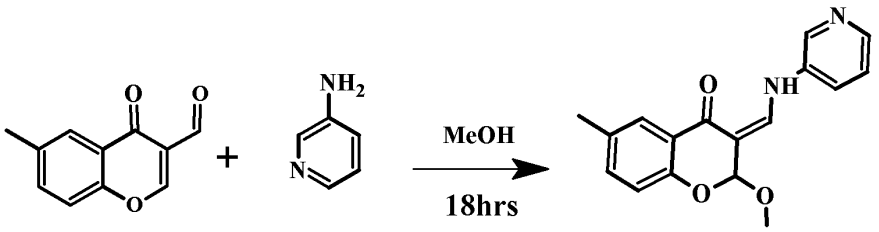

6-methyl-4-oxo-4*H*-chromene -3-carbaldehyde + pyridin-3-amine → 2-Methoxy-6-methyl-3-(pyridin-3-ylamino methylene)-chroman-4-one (L8)

Scheme: 2.8

Yellowish white powder Yield: (0.210g) 75%, Anal. Calcd. For $C_{17}H_{16}N_2O_3$ (282.2) C% 68.91, H% 5.44, N% 9.45. Found: C% 68.37, H% 5.16, N% 9.11

2.3 Results and discussion

3-Formylchromone is often considered as an efficient precursor for the synthesis of higher heterocycles with much expected biological potentialities. Competition between the three electron deficient centre in 3-formylchromone to react with strong nucleophiles results in variety of products [10]. Addition of a primary aromatic amine may form diverse products depending on the nucleophilicity of amine used and environmental conditions. Initially, aryliminomethylchromone, also known as anils, can be formed by direct 1, 2 addition of amine to aldehyde function of 3-formylchromone. Presence of iminomethyl moiety at C3 carbon will trigger nucleophilic addition at C2 carbon. Enamines may be formed by a fast 1, 4 addition of a nucleophile to the iminomethylmoeity or as intermediates which arise due to ring opening caused by 1,4 addition of the amine followed by recyclisation. Stability of these enamines formed is determined by the hydrogen bond between pyranone carbonyl carbon and NH group. Nucleophilicity of amine will affect addition step and basicity of amine will govern elimination step. If the amine is too basic, it will abstract the proton and it will result in the loss of the main stabilizing hydrogen bond [11].

In this study, 3-formylchromone is made to react with substituted 2-aminopyridines in methanolic media. Instead of expected Schiff bases, 2-methoxy-4-chromanones were the products. During the formation of chromanone, amine is added to formyl carbonyl carbon by straight forward 1, 2 additions to the aldehyde functional group [12]. Formation of intramolecular hydrogen bond between pyranone oxygen and NH will facilitate the attack of nucleophilic methoxide ion from the solvent at C2. Consequently, lose of hydroxyl group causes electron shift resulting in the formation of stable chromanones. Methoxide ions from the solvent are sufficiently nucleophilic

and not too basic to form hydrogen bonded protonated adduct. Stability is due to the formation of intramolecular hydrogen bond [13].

All the ligand structures were elucidated by elemental analysis, FT-IR, Uv-visible, NMR and mass spectral analysis. A plausible mechanism for the formation of ligands can be depicted as below (fig. 2. 1):

Fig.2.1: Plausible mechanism for the formation of ligands

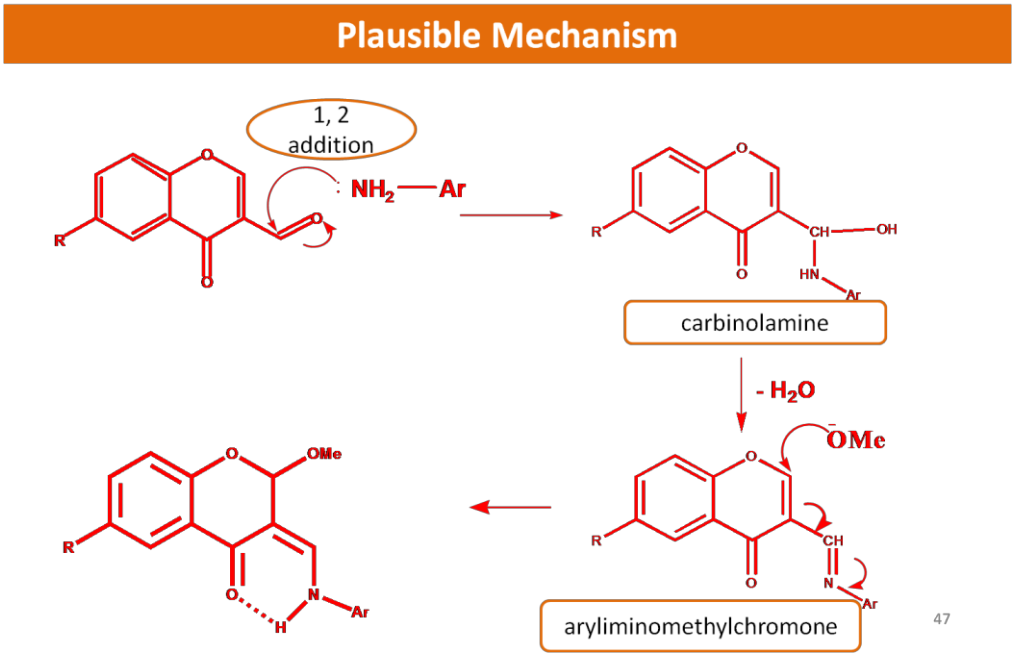

Here the reaction begins with the 1, 2 addition of amine to the formyl group leading to the formation of carbinolamine. This step is followed by the dehydration leading to the formation of an aryliminomethylchromone. Presence of aryliminomethyl group at C3 will cause the attack of methoxide ion at C2 leading to the formation of stable product. Methoxide ion from the solution is sufficiently nucleophilic to attack at C2 and not too basic so that it can abstract the proton which may destabilize the system.

2.3.1 Elemental analysis

CHN analysis data of the synthesized 2-methoxy-4-chromanones are given in section 2.2 which indicate that synthesized compounds are analytically pure and are in good agreement with the proposed chemical formula.

2.3.2 Mass spectra

Mass spectrometry (MS) is a dominant analytical technique which is usedto identify unknown compounds and to elucidate the structure of molecules. The electro spray ionization (ESI) technique was used to measure the m/z ratio of charged particles. MS works by ionizing the compound to generate charged molecules or fragments and measuring their mass to charge ratios. Mass spectrum is a plot of m/z of positive ion fragments versus their relative abundance. Synthesized chromanones are unstable at higher temperatures and have relatively high boiling points but are stable at room temperature. Therefore GC-MS is not easy to apply for mass analysis due to this physical nature. Hence, LC-MS has been used to analyze these derivatives [14].

In the present study, molecular ion $[M-1]^+$ peak of synthesized chromanones are evident from their respective mass spectra (Fig 2.2.(a-h)). Molecular mass of the compounds as indicated from their mass spectra is given in Table 2.1

Fig. 2.2(a-h): Mass spectra of L1, L2, L3, L4, L5, L6, L7 and L8

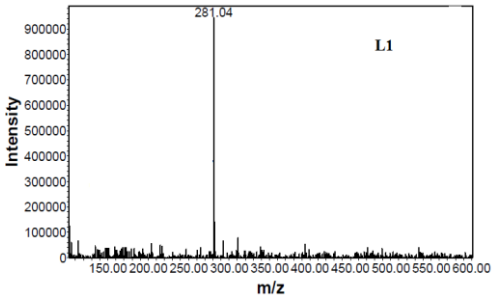

Fig. 2.2(a): LC-MS spectra of L1

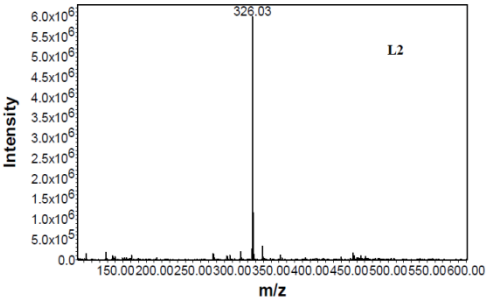

Fig. 2.2(b): LC-MS spectra of L2

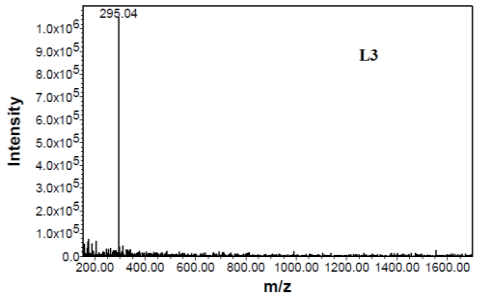

Fig. 2.2(c): LC-MS spectra of L3

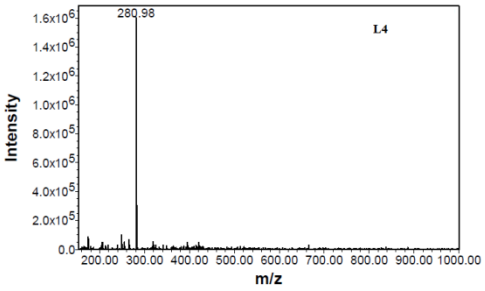

Fig. 2.2(d): LC-MS spectra of L4

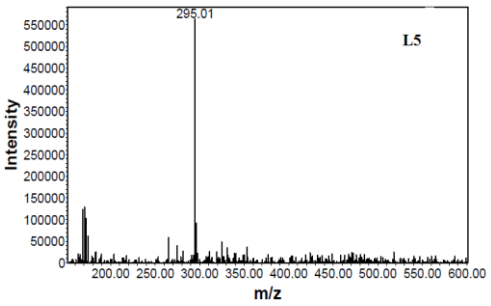

Fig. 2.2(e): LC-MS spectra of L5

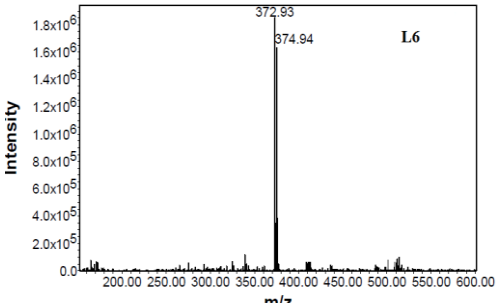

Fig. 2.2(f): LC-MS spectra of L6

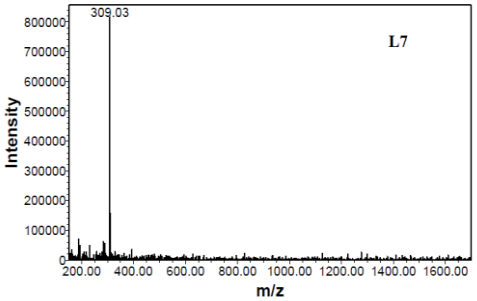

Fig. 2.2(g): LC-MS spectra of L7

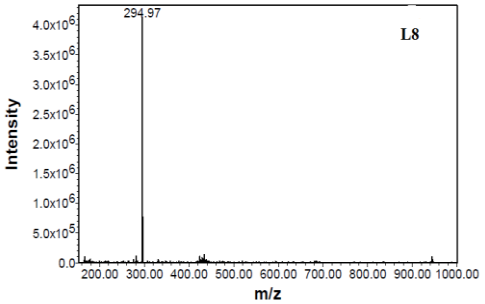

Fig. 2.2(h): LC-MS spectra of L8

Table 2.1 Formula weight of ligands

Ligands	Formula weight
L1	282.0
L2	327.3
L3	296.3
L4	282.3
L5	296.3
L6	375.1
L7	310.2
L8	282.0

2.3.3 IR spectral analysis

Infrared spectra of the 2-methoxy-4-chromanones were recorded on a JASCO FT-IR-5300 spectrometer in the 4000-400 cm^{-1} range using KBr pellets (Fig. 2.3.(a-h)). The important bands observed in the IR spectra of the ligands along with their functional group assignments as per the literature data of similar compounds and are presented in the Table 2.2 The strong band observed in the spectrum of 3-formylchromone at 1700 cm^{-1} has been assigned to the C=O stretching in –CHO group [15]. This band disappears in the FT-IR spectra of 2-methoxy-4-chromanones. The disappearance of ν (C=O) bands of the aldehyde group confirms their condensation with molecules of amines. The disappearance of the band of ν (NH_2) in spectrum of ligands also indicates that the condensation takes place via NH_2 group of amino pyridines. The ligands showed strong absorption bands around 1650 cm^{-1} of C=O stretching of pyrone ring [16].The asymmetric and symmetric stretching bands of methoxy group are observed at 2922 and 2823 cm^{-1}, respectively. For this group, peaks at 1468 and 1368 cm^{-1} were registered, respectively for asymmetric and symmetric deformation bands in plane. Strong band around 1215 and 1020 cm^{-1} is due to Ar-O-C stretching. The very strong band at 1384, 1284 and

1204 cm^{-1} in the spectrum of ligands was attributed to the ν(C–N). In the spectrum of 2-methoxychroman-4-one, the strong and medium bands in the range of 1604–1468 cm^{-1} are due to the skeletal C-C stretching modes in benzene ring [17].

Table 2.2: IR spectral band assignments of ligands

Ligands	Frequency(cm^{-1})		
	ν(C=O)	ν(C-N)	ν(Ar-O-C)
L1	1660	1273	1017
L2	1647	1276	1016
L3	1649	1279	1025
L4	1638	1277	1063
L5	1647	1271	1066
L6	1648	1273	1050
L7	1649	1278	1055
L8	1652	1281	1050

Fig. 2.3 (a-h): IR spectra of L1, L2, L3, L4, L5, L6, L7and L8

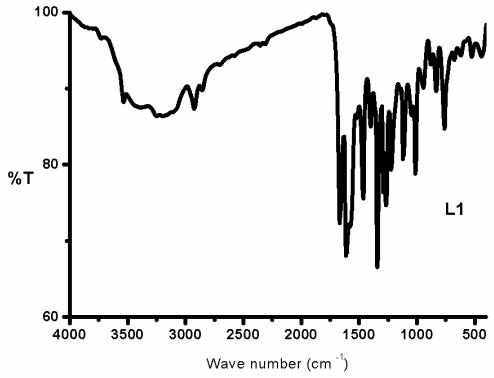

Fig. 2.3(a): IR spectra of L1

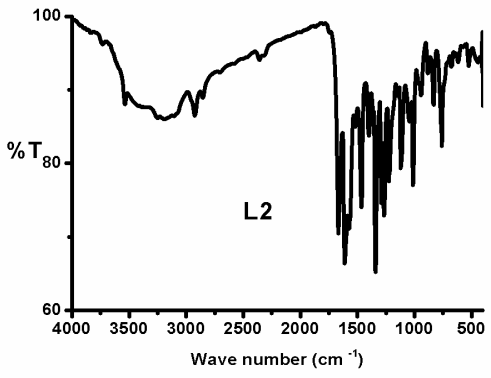

Fig. 2.3(b): IR spectra of L2

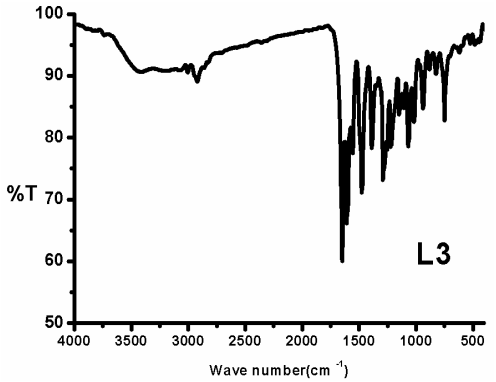

Fig. 2.3(c): IR spectra of L3

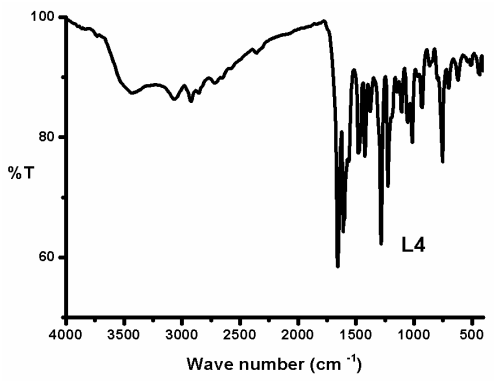

Fig. 2.3(d): IR spectra of L4

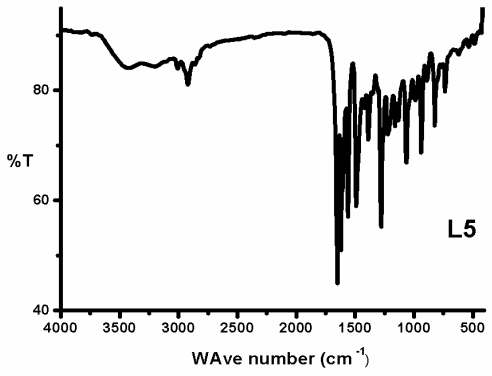

Fig. 2.3(e): IR spectra of L5

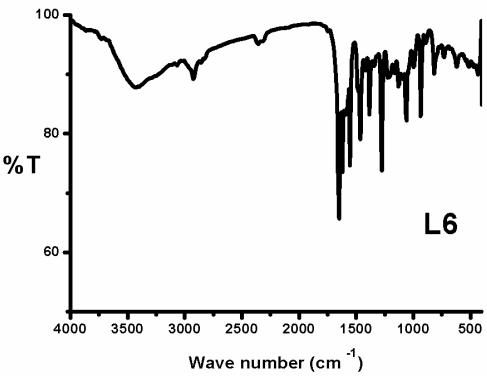

Fig. 2.3(f): IR spectra of L6

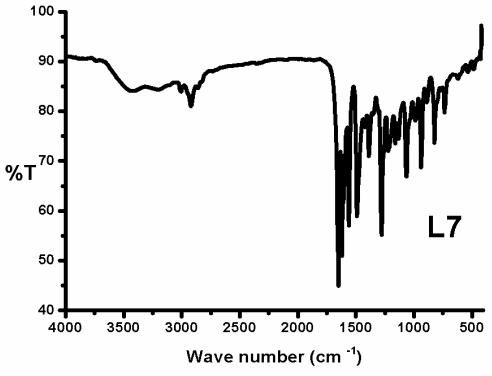

Fig. 2.3(g): IR spectra of L7

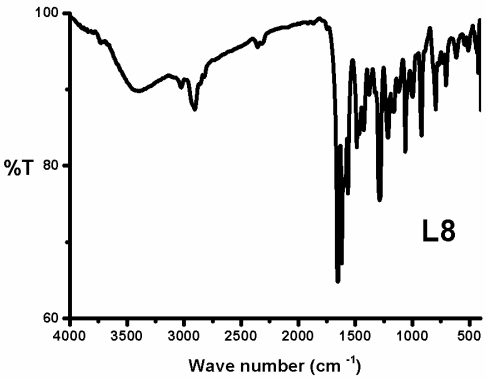

Fig. 2.3(h): IR spectra of L8

2.3.4 Electronic spectra of ligands:

In electronic spectroscopy, wavelengths of absorption peaks can be correlated with the types of bonds in a given molecule and are valuable in

determining the functional groups within molecule. The electronic spectral investigations were performed in 10^{-5} M DMSO solutions of ligands in the range of 200-800 nm. The spectral assignments for electronic transitions in ligands are given in table 2.3. Uv-visible spectra of the compounds are shown in the fig.2.4.(a-h). Spectrum gave two absorption maxima corresponding to two intraligand transitions: a weak peak and a strong peak at 250-290nm and 380-390 nm respectively. Low energy band is due to n→π* on =CH-NH- group which is characteristic of chromanones [18]. The high energy band can be attributed to the π→π* transitions on pyridine and benzene aromatic rings [19].

Table 2.3 Uv-visible spectral data of ligands

Ligands	λ_{max} nm(cm^{-1})	log ε ($L\ mol^{-1}cm^{-1}$)	Band assignments
L1	259(39866) 296(33585) 373(26896)	4.32 3.87 4.88	Intraligand transitions
L2	250(39840) 395(25856)	3.78 4.85	Intraligand transitions
L3	261(38522) 379(26379)	4.07 4.68	Intraligand transitions
L4	263(38487) 300(33485) 379(26379)	4.77 4.68 4.69	Intraligand transitions
L5	258(38487) 304(32832) 379(26379)	4.60 4.39 4.9	Intraligand transitions
L6	266(38878) 379(26375)	4.03 4.56	Intraligand transitions
L7	262(38829) 384(26178)	4.42 4.93	Intraligand transitions
L8	263(37870) 382(26275)	4.29 4.79	Intraligand transitions

Fig. 2.4 (a-h) Uv-visible spectra of L1, L2, L3, L4, L5, L6, L7and L8

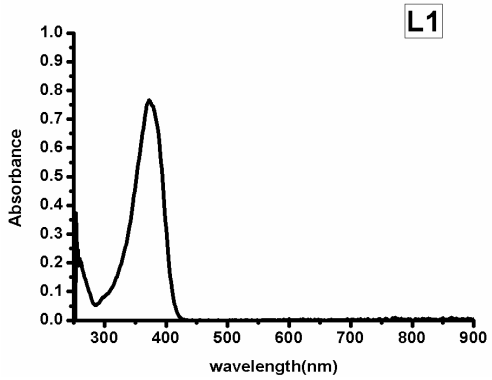

Fig. 2.4(a): Uv-vis spectra of L1

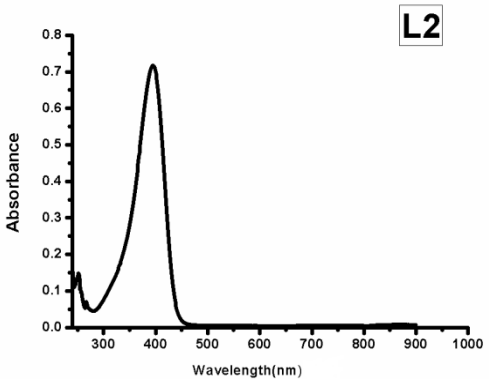

Fig. 2.4(b): Uv-vis spectra of L2

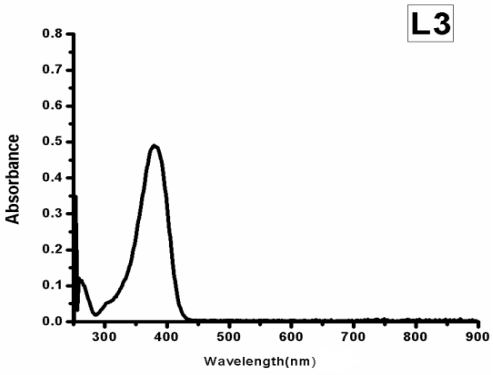

Fig. 2.4(c): Uv-vis spectra of L3

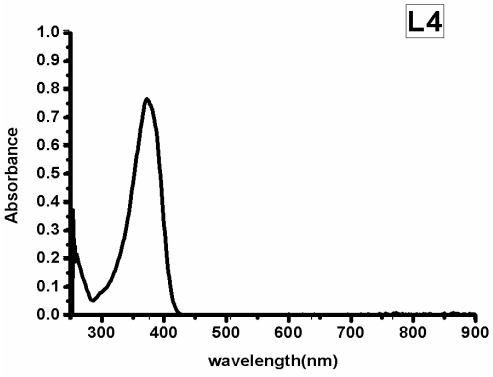

Fig. 2.4(d): Uv-vis spectra of L4

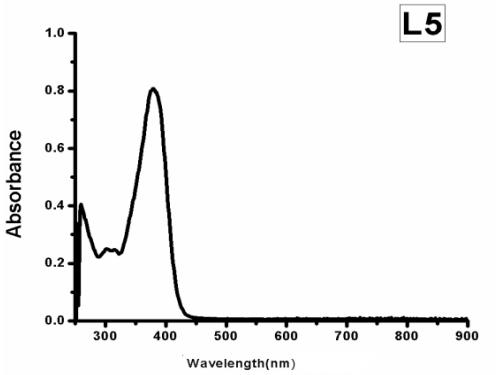

Fig. 2.4(e): Uv-vis spectra of L5

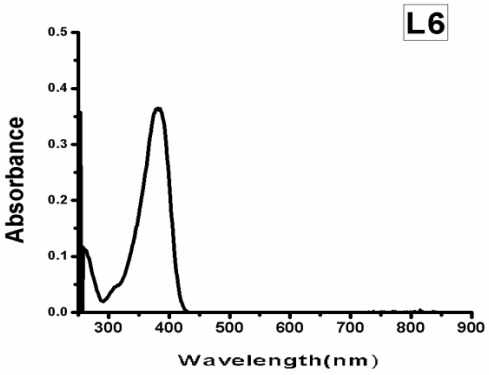

Fig. 2.4(f): Uv-vis spectra of L6

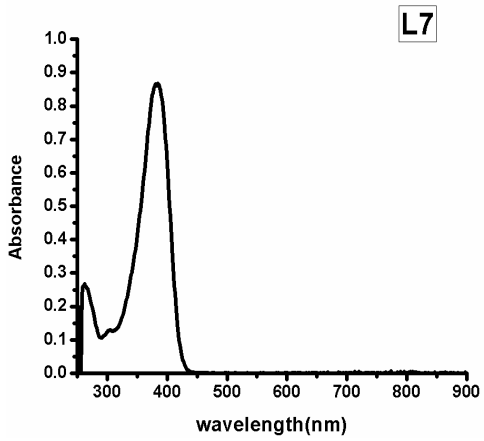

Fig. 2.4(g): Uv-vis spectra of L7

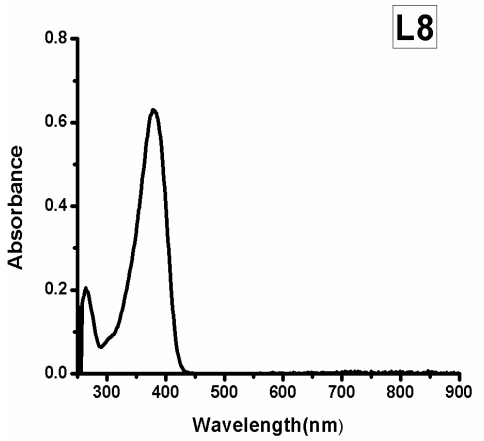

Fig. 2.4(h): Uv-vis spectra of L8

2.3.5 NMR spectral studies of ligands:

2.3.5.1 ^{1}H NMR spectral studies:

The ^{1}H NMR spectrum of the synthesized chromanones were recorded with DMSO-d^{6} as solvent on a Bruker AMX 400 spectrometer and TMS as standard. ^{1}H NMR spectrum of the ligands is given in fig. 2.5(a-h) and the spectral assignments are summarized in table 2.4.Singlet in the region of 2.2-2.4 ppm is due to the presence of methyl protons. Presence of singlet at 3.4 ppm is caused due to the presence of methoxy group at C2 carbon. Singlet, around 5.5 ppm attribute to the proton at C2 carbon. Another downfield doublet discernible at around δ 12.09 was allotted to NH proton. The fairly higher downfield effect on NH proton owed to strong intramolecular H-bonding in its Z-configuration [20]. The remaining protons of chromanone and protons of pyridine moieties were present in the form of multiplets at δ 6.84–7.66 [21].

Table 2.4: ^{1}H NMR spectral data of ligands

Ligands	Chemical shift δ(ppm)	assignments
L1	3.59	OC**H**$_3$,3H,s
	5.71	O-C**H**-O,1H,s
	6.8-8.3	Aromatic protons,8H,m
	7.9	C**H**,1H,d
	12.09	N**H**,1H,d
L2	3.83	OC**H**$_3$, 3H, s
	5.73	O-C**H**-O,1H, s
	6.8 - 9.1	Aromatic protons,7H, m
	8.28	C**H**,1H, d
	12.11	N**H**, 1H, d
L3	2.29	C**H**$_3$, 3H, s
	3.44	OC**H**$_3$,3H, s
	5.58	O-C**H**-O, 1H, s
	6.8 - 8 .3	Aromatic protons 7H, m
	7.9	C**H** ,1H,d
	12.01	N**H**, 1H, d
L4	3.44	OC**H**$_3$,3H,s
	5.63	O-C**H**-O,1H,s
	6.8- 8.3	Aromatic protons, 8H,m
	7.9	C**H**,1H,d
	12.09	N**H**,1H,d
L5	2.34	CH$_3$, 3H, $_S$
	3.48	OC**H**$_3$,3H, s
	5.67	O-C**H**-O, 1H, s
	6.8-8.3	Aromatic protons 7H, m
	7.76	C**H** ,1H,d
	12.09	N**H**, 1H, d
L6	2.35	C**H**$_3$, 3H, $_S$
	3.49	OC**H**$_3$,3H, s
	5.67	O-C**H**-O, 1H, s
	6.8-8.3,	Aromatic protons 6H, m
	8.20	C**H** ,1H,d
	12.09	N**H**, 1H, d
L7	2.319,	C**H**$_3$, 3H,s,
	2.379	C**H**$_3$, 3H,s
	3.512,	OC**H**$_3$,3H, s
	5.704	O-C**H**-O, 1H, s
	6.7-8.3	Aromatic protons 6H, m
	7.9	C**H** ,1H,d
	12.44	N**H**, 1H, d
L8	2.29	C**H**$_3$, 3H,s
	3.44	OC**H**$_3$,3H, s
	5.58	O-C**H**-O, 1H, s
	6.8-8.3	Aromatic protons 7H, m
	7.9	C**H** ,1H,d
	12.01	N**H**, 1H, d

Fig. 2.5 (a-h): ^{1}H NMR spectra of L1, L2, L3, L4, L5, L6, L7and L8

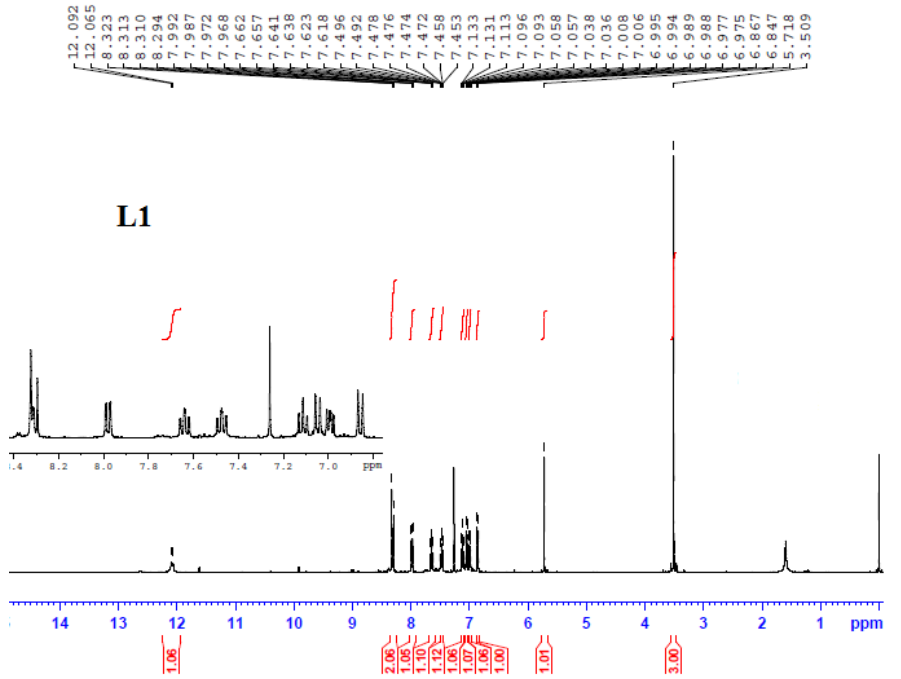

Fig. 2.5(a): ^{1}H NMR spectra of L1

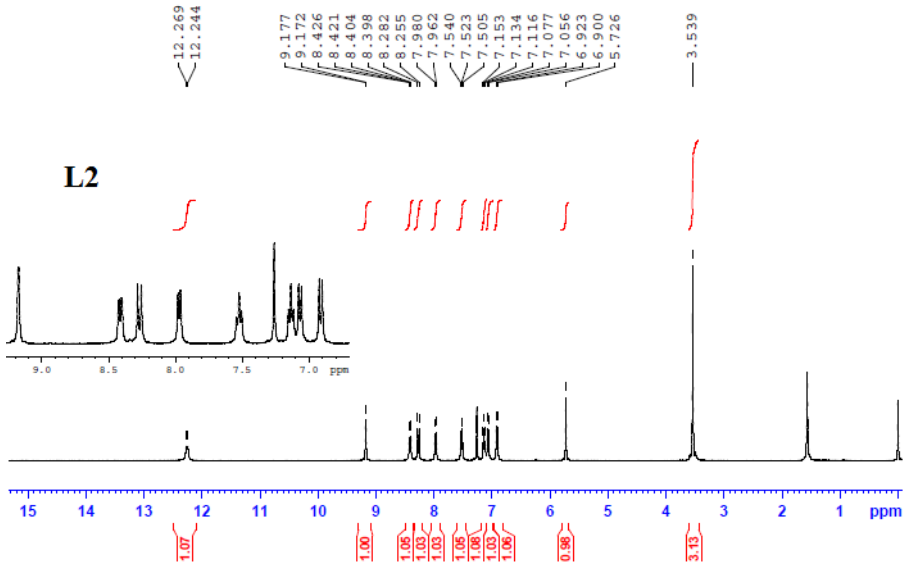

Fig. 2.5(b): ^{1}H NMR spectra of L2

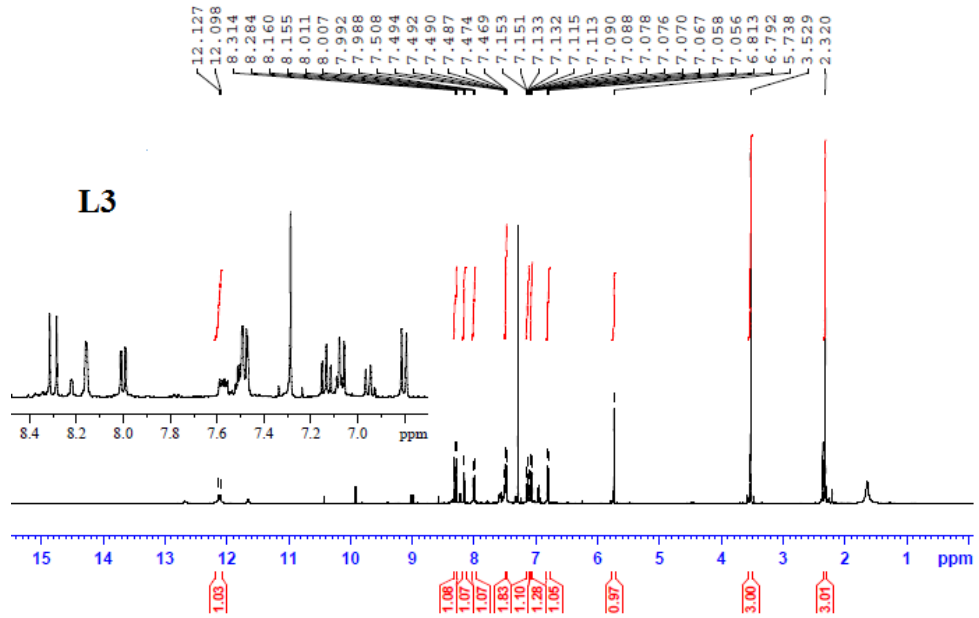

Fig. 2.5(c): ^{1}H NMR spectra of L3

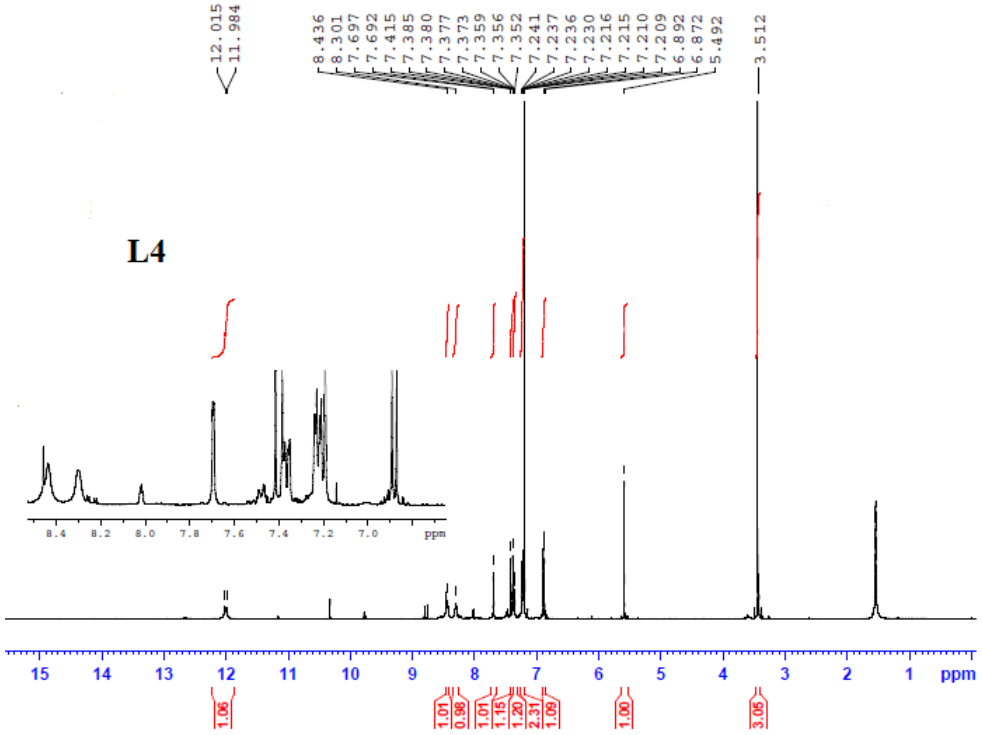

Fig. 2.5(d): ^{1}H NMR spectra of L4

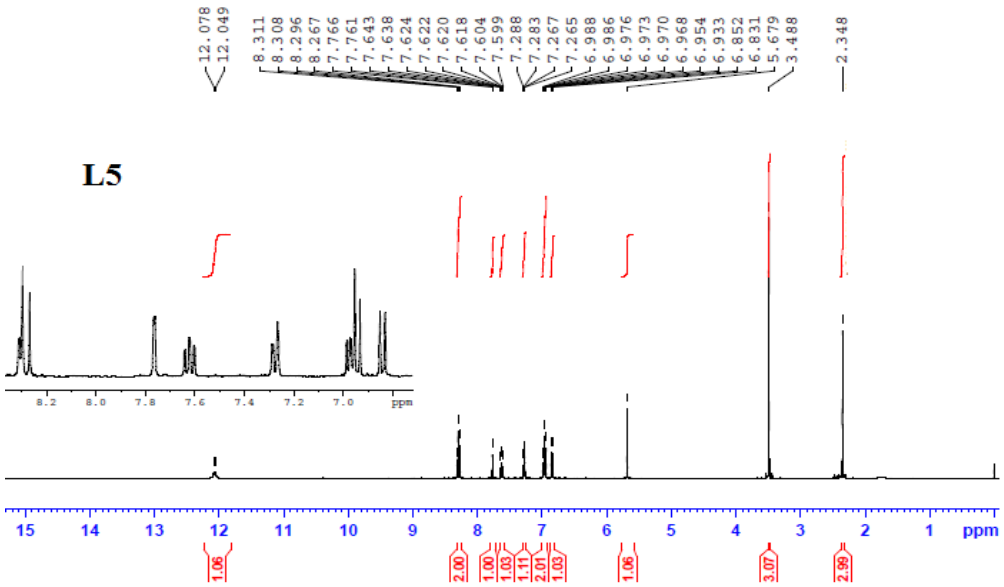

Fig. 2.5(e): ^{1}H NMR spectra of L5

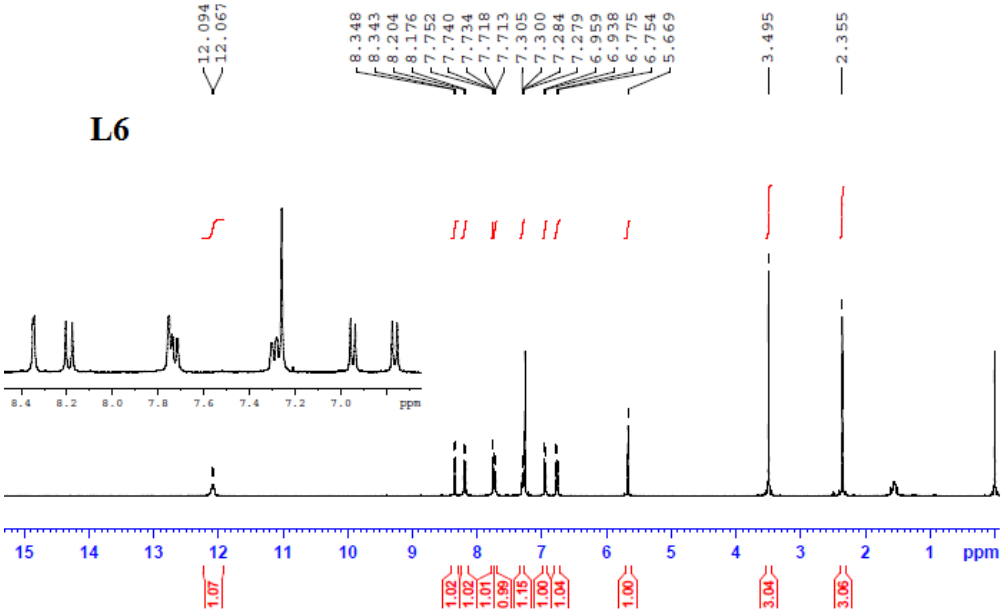

Fig. 2.5(f): ^{1}H NMR spectra of L6

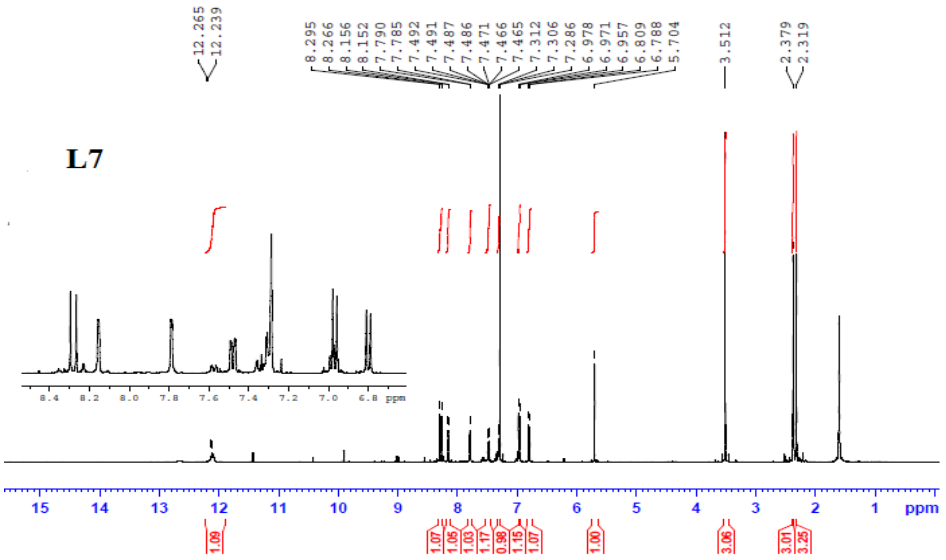

Fig. 2.5(g): ^{1}H NM R spectra of L7

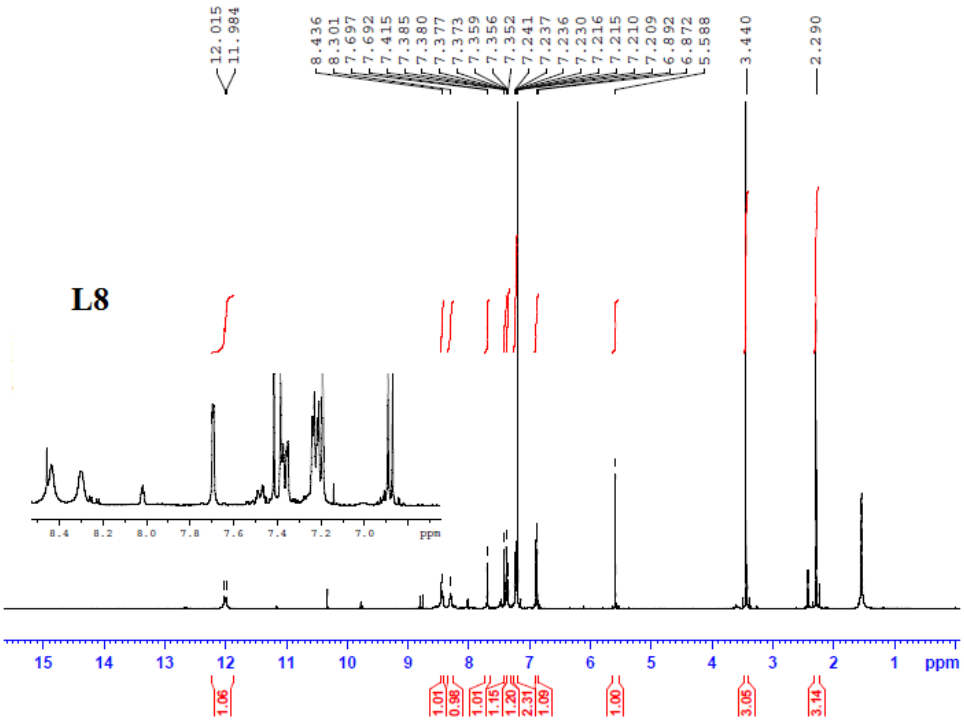

Fig. 2.5(h): ^{1}H NMR spectra of L8

2.3.5.2 ^{13}C NMR spectral studies:

The proton decoupled ^{13}C NMR spectrum provides direct information about the carbon skeleton of the molecule.^{13}C NMR spectra were recorded using DMSO-d^{6} as the solvent and TMS was used as the internal standard. ^{13}C NMR values are in agreement with proton NMR avlues.^{13}C NMR spectra of the synthesized ligands are shown the fig. 2.6. (a-h) and assignments for the signals are given in table 2.5. Signal around 180-182 ppm corresponds to carbonyl carbon of pyrone ring. Aromatic carbons resonate between 100-150 ppm. High value near 160 ppm is due to the presence of electronegative atom [22]. Carbon attached to NH resonates at 140-145 ppm. C2 resonates at high value of 102 ppm because of the attached oxygen atoms. Methoxy carbon resonates at 55 ppm. Methyl group in chromone resonates at 20 ppm and methyl group attached to pyridine ring in L3 and L7 resonates at 17 ppm [23].

Table 2.5:^{13}C NMR spectral data of ligands

Ligands	δ(ppm)						
	Pyrone C=O	Chromone carbons	Pyridine carbons	=CH-NH-	O-CH-O	O-CH_3	CH_3
L1	182	156,134, 126,122,121,119,112	151,148,138,118,105	142	102	55	-
L2	183	156,139,126,121,121, 118,111	155,145,135,134,108	145	101	55	-
L3	181	155,131,126,122,121, 117,111	149,148,139,123,104	145	102	55	18
L4	183	161,135,126,121,121, 120,114	140,138,136,134,127,	145	102	55	-
L5	182	154,138,131,126,122, 119,112	151,148,135,117,105	142	102	55	20
L6	183	154,135,131,126,122, 117,114	150,149,141,113,105	140	101	55	20
L7	182	153,39,131,124,122,117,11 1	149,148,137,126,109	142	102	55	20, 17
L8	182	153,140,131,124,121, 121,117	140,138,136,134,127	145	102	55	20

Fig. 2.6 (a-h): 13 C NMR spectra of L1, L2, L3, L4, L5, L6, L7and L8

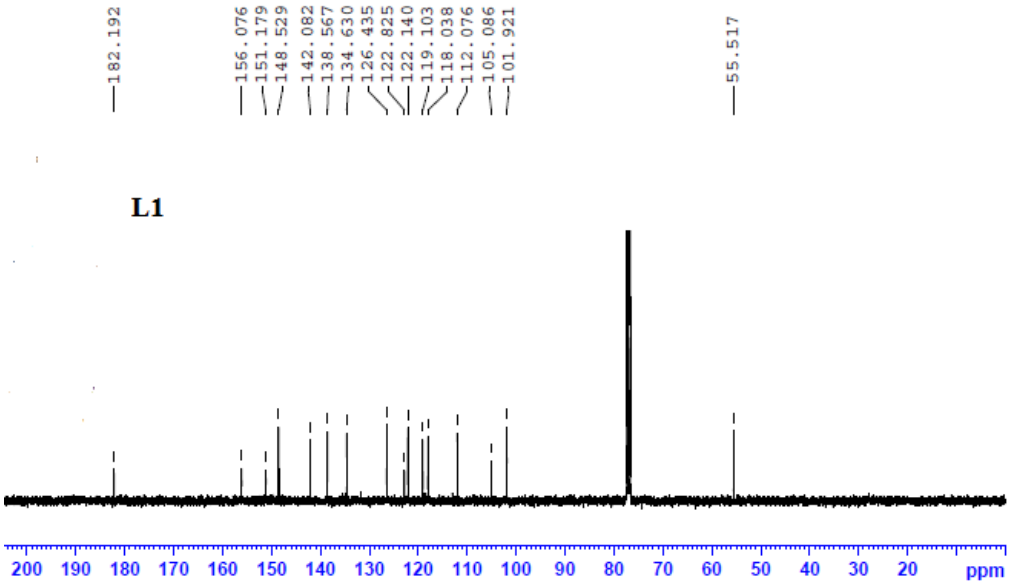

Fig. 2.6(a):^{13}C NMR spectra of L1

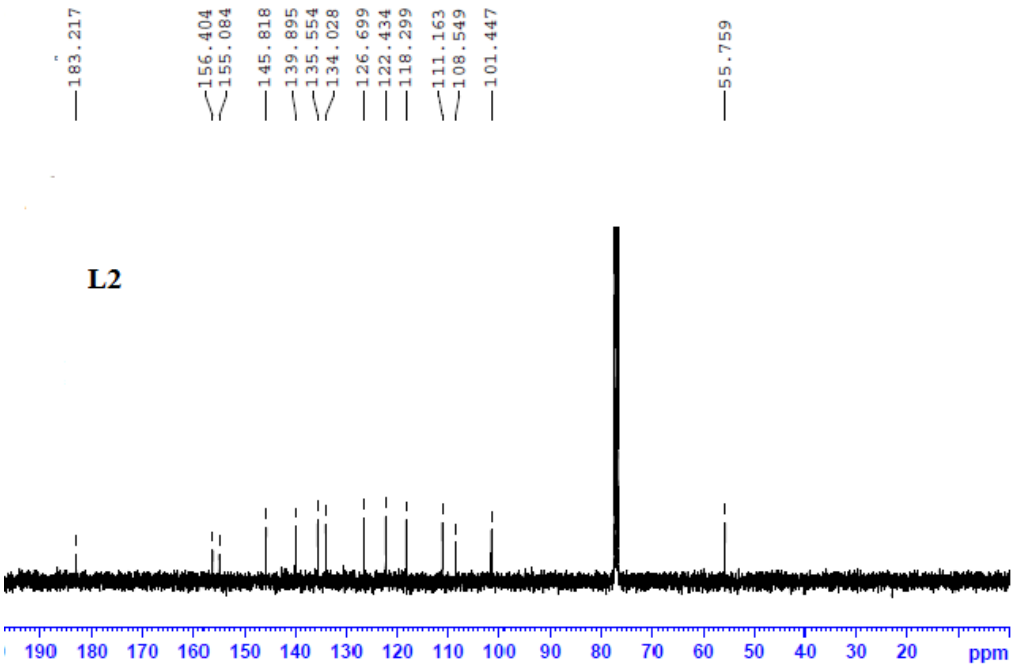

Fig. 2.6(b):^{13}C NMR spectra of L2

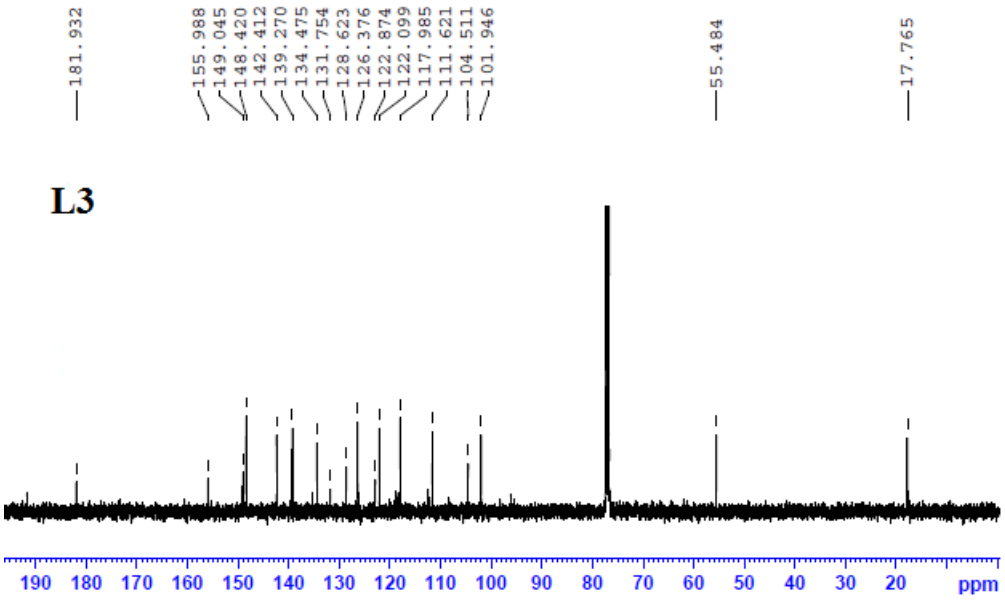

Fig. 2.6(c):^{13}C NMR spectra of L3

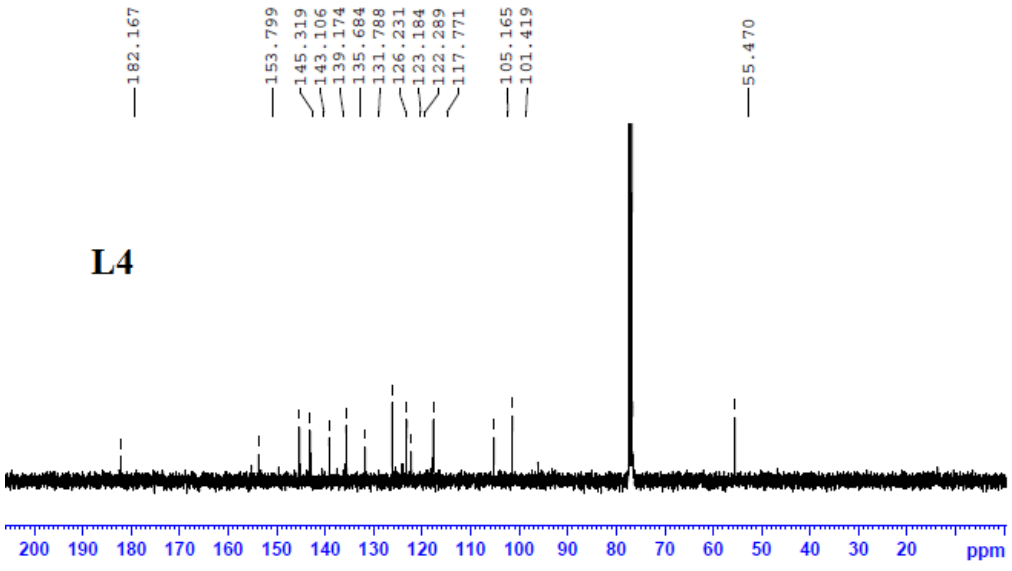

Fig. 2.6(d):^{13}C NMR spectra of L4

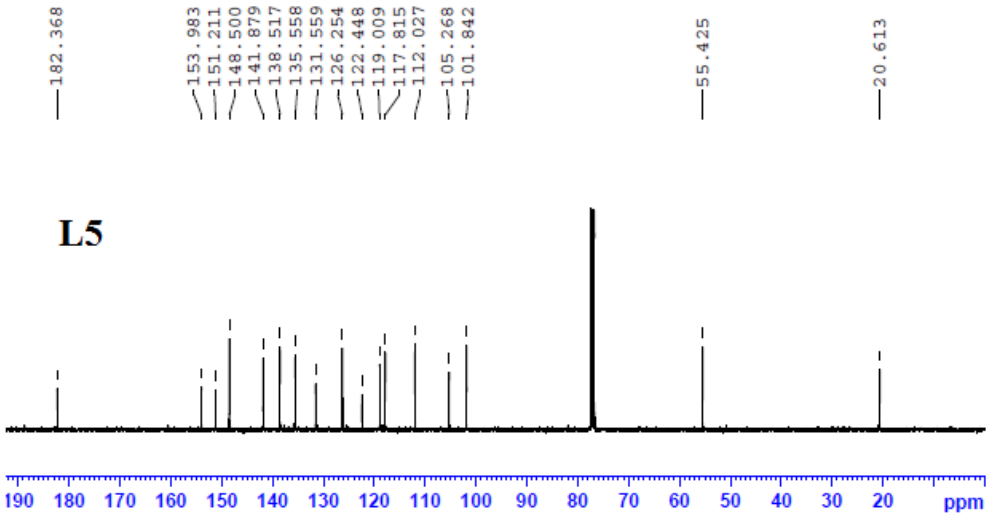

Fig. 2.6(e):^{13}C NMR spectra of L5

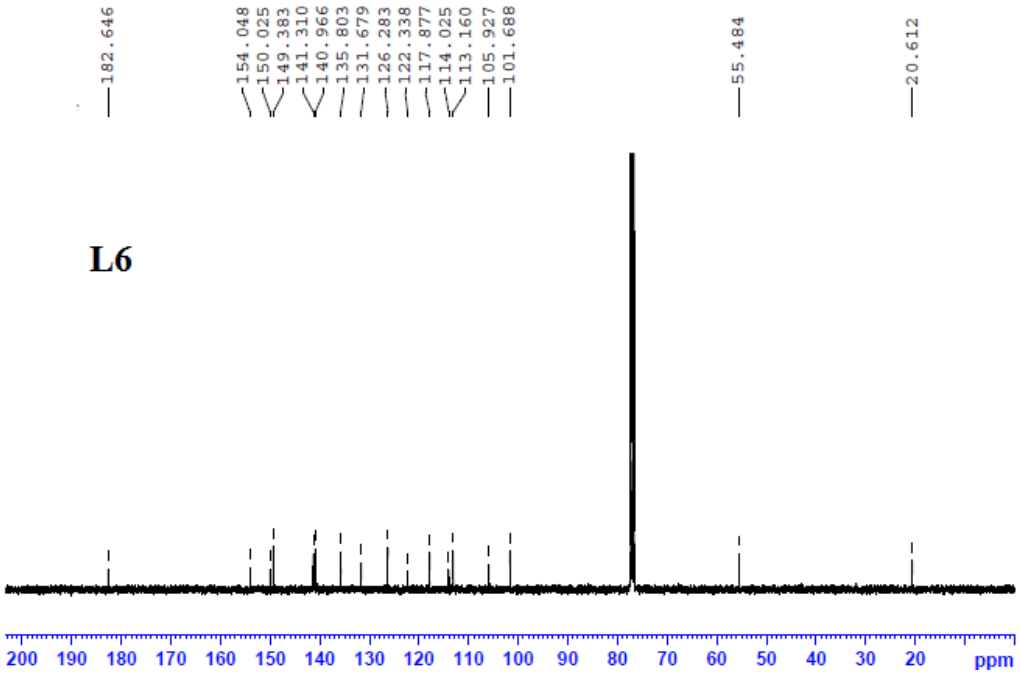

Fig. 2.6(f):^{13}C NMR spectra of L6

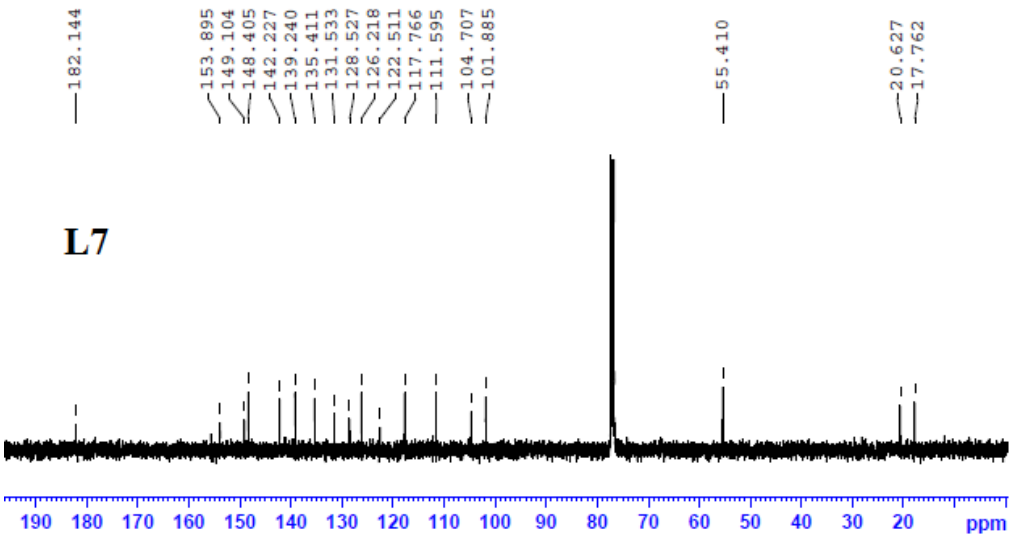

Fig. 2.6(g):^{13}C NMR spectra of L7

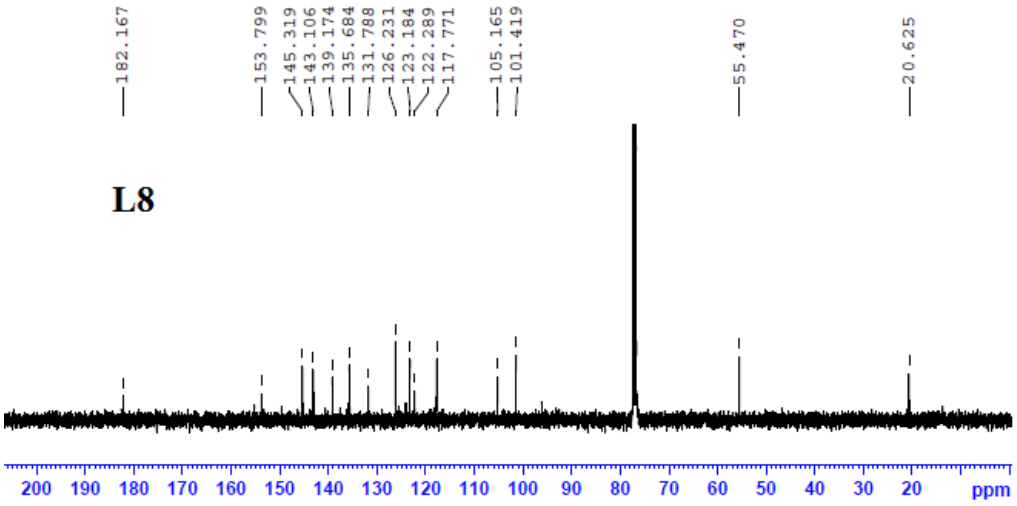

Fig. 2.6(h):^{13}C NMR spectra of L8

2.3.6 Proposed strucuture of ligands

By interpreting and analysing data obtained from elemental analysis, mass spectra, IR spectra, Uv-vis spectra and NMR spectral studies, following structures are proposed for the synthesized ligands.

2.3.6.1 L1: 2-methoxy-3-((pyridin-2-ylamino)methylene)chroman-4-one

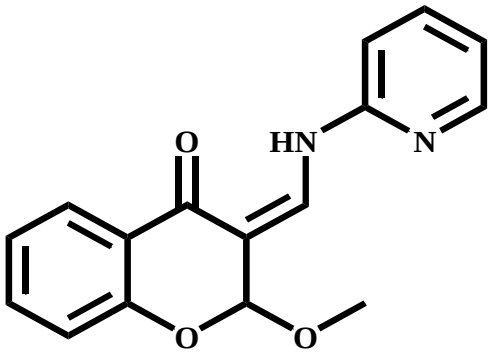

2.3.6.2 L2: 2-methoxy-3-(((5-nitropyridin-2-yl)amino)methylene)chroman-4-one

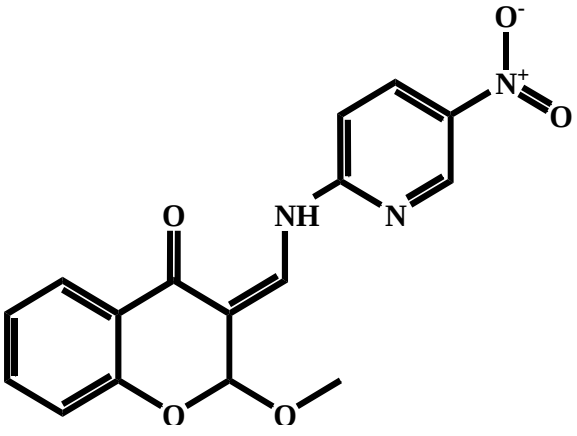

2.3.6.3 L3: 2-methoxy-3-(((5-methylpyridin-2-yl)amino)methylene)chroman-4-one

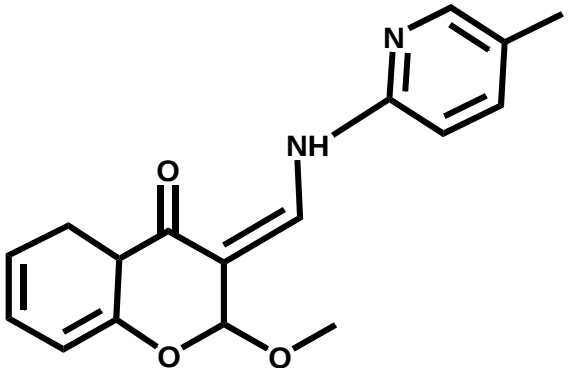

2.3.6.4 L4: 2-methoxy-3-((pyridin-2-ylamino)methylene)chroman-4-one

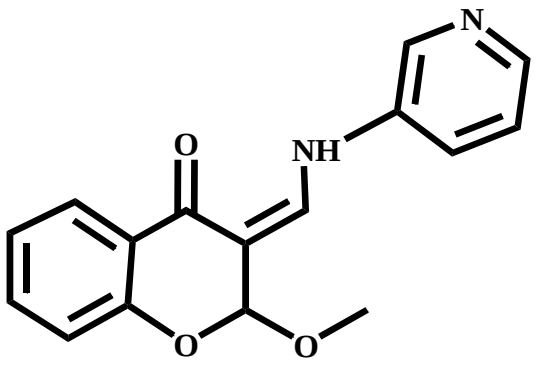

2.3.6.5 L5: 2-methoxy-6-methyl-3-((pyridin-2-ylamino) methylene) chroman-4-one:

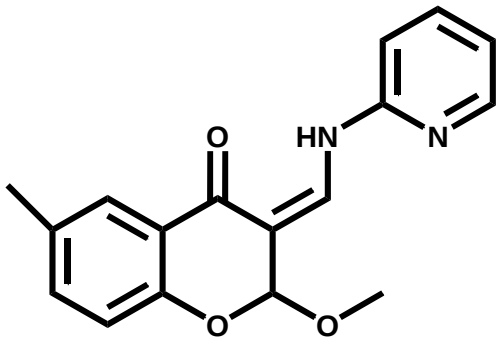

2.3.6.6 L6: 3-(((5-bromopyridin-2-yl)amino)methylene)-2-methoxy-6-methylchroman -4-one:

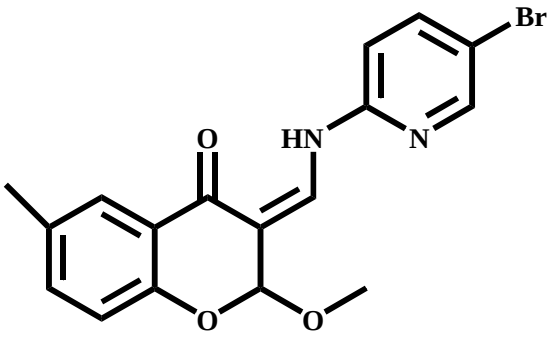

2.3.6.7 L7: 2-methoxy-6-methyl-3-(((5-methylpyridin-2-yl)amino)methylene) chroman-4-one

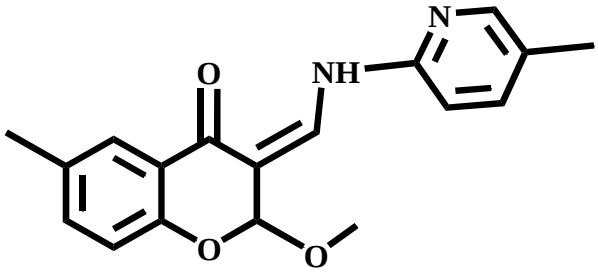

2.3.6.8 L8:2-methoxy-6-methyl-3-((pyridin-3-ylamino)methylene)chroman-4-one

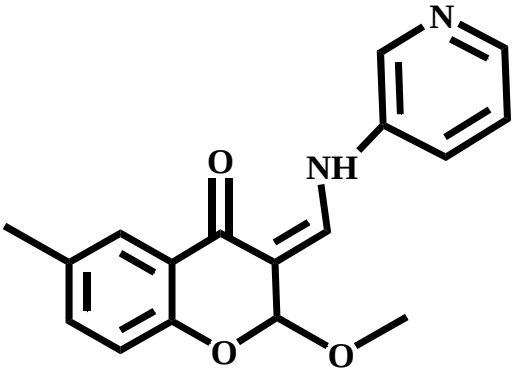

2.4 Conclusion

3-Formylchromone ring chemistry is always interesting due to the presence of electron deficient centres. This chapter discusses the reaction between 3-formylchromone/6-methyl-3-formylchromone and substituted 2-aminopyridines

in methanolic media and analysis of the products obtained using different characterization techniques such as elemental analysis, mass spectrometry, IR spectroscopy, Uv-vis spectroscopy, ^{1}H NMR and ^{13}C NMR spectral studies. Spectral studies reveal that eight new 2-methoxy-4-chromanones namely, L1, L2, L3, L4, L5, L6, L7 and L8 were obtained instead of the expected Schiff bases. Presence of methoxy group at C2 carbon is confirmed from NMR and IR data. Intramolecular hydrogen bond which is the stabilizing feature for ligands was evident from proton NMR spectra. These ligands were expected to have excellent chelating abilities and profound biological activities.

References:

[1] A. Chopra; M. Kaur; P. Navpreet; A. Divneet; M. Lalit; Jour. Harmo. Res. pharm. **2015**, 4, 162.

[2] G. Singh; L. Singh; M. P. S. Ishar, Tetrahedron **2002**, 58, 7883.

[3] B. D. Wang; Z.Y. Yang; D. D. Qin; Z. N. Chen, J. Photochem. Photobiol. A: Chem. **2008**, 194, 49.

[4] H. Stankovicova; M. Lacova; A. Gaplovsky; J. Chavanova; N. Paranayova, Tetrahedron **2001**, 57, 3455.

[5] J. Quiroga; A. Rengifo; B. Insuasty; R. Abonia; M. Nogueras; A. Sanchez, Tetrahedron Lett. **2003**, 43, 9061.

[6] M. Jakubek; Z. Kejí;, V. Parchaňský; R. Kaplánek; L. Vasina; P. Martásek; Vladimír Král Supramol. Chem. **2017**, 29, 1.

[7] R. A. Ammar; A. M. A. Alaghaz; M. E. Zayed; L. A. Al-Bedair; J. Mol. Struc. **2017**, 1141, 368.

[8] M. al-Rashida; G. Batool; A. Sattar; S. A. Ejaz; S. Khan; J. Lecka; J. Sevigny; A. Hameed; J. Iqbal; Eur. J. Med. Chem. **2016**, 115 , 484.

[9] M. al-Rashida; M. Ashraf; B. Hussain; S. A. Nagra; G. Abbas; Bioorg. Med. Chem. **2011**, 19, 3367.

[10] R. S. Keri; S. Budagumpi; R. K. Pai; R. G. Balakrishna; Eur. J. Med. Chem. **2014**, 78, 340.

[11] A. Y. Barkov; V. Y. Korotaev; I. B. Kutyashev; V. Y. Sosnovskikh; Tetrahedron **2016,** 72, 2026.

[12] A. O. Fitton; J. R. Frost; H. Suschitzky; Tetrahedron Lett. **1975**, 25, 2099.

[13] A. O. Fitton; J. R. Frost; P. G. Houghton; H. Suschitzky; J. Chem. Soc., Perkin Trans. **1979**, 1, 1691.

[14] a) A. Yasuhara; Y. Tanaka; M. Makishima; S. Suzuki; T. Shibamoto; J. Chromatograph. Separat. Techniq. **2011**, 2, 1. b) D. Strazic; T. Benkovic; D. Gembarovski; D. Kontrec; N. Galic; Int. J. Mass Spectrom. **2014**, 371, 54.

[15] K. Nakamoto, Infrared and Raman Spectra of Inorganic and Coordination Compounds, Wiley, Toronto, **1997**.

[16] A. Dziewulska-Kułaczkowska; L. Mazur; J. Mol. Struc. **2011,** 985, 233.

[17] T. Rosu; E. Pahontu; C. Maxim; R. Georgescu; N. Stanica; Polyhedron **2011,** 30, 154.

[18] A. D. Kułaczkowska; A. Bartyzel; J. Mol. Struc. **2011**, 997, 1, 87.

[19] P. R. Chetana; B. S. Srinath; M. N. Somashekar; R. S. Policegoudra; J. Mol. Struct. **2016**, 1106, 352.

[20] Y. Pourshojaei; A. Gouranourimi; S. Hekmat; A. Asadipour; S. R. Nezhad; Alireza Moradi; H. Nadri; F. H. Moghadam; S. Emami; A. Foroumadi; A. Shafiee; Eur. J. Med. Chem. **2015**, 97, 181.

[21] M. al-Rashida; R. Raza, G. Abbas; M. S. Shah; G. E. Kostakis; J. Lecka; J. Sévigny; M. Muddassar; C. Papatriantafyllopoulou; J. Iqbal ; Eur. J. Med. Chem. **2013**, 66, 438.

[22] S. K. Roy; N. Kumari ; S. Gupta; S. Pahwa; H. Nandanwar; S. M. Jachak; Eur. J. Med. Chem. **2013**, 66, 499.

[23] M. F. en-Saxin; T. Seifert; M. Malo; K. da Silva Andersson; N. Pemberton; C. Dyrager; A. Friberg;, K. Dahl; E. A. A. Wallen ; M. Grotli; K. Luthman; Eur. J. Med. Chem. **2016**, 114, 59.

******

Chapter 3

Synthesis and spectral characterization of Ni (II), Cu (II), Zn (II) complexes incorporating 2-methoxy-4-chromanones

Contents

Abstract

Transition metal complexes always constitute a very productive group of compounds due to its recognition in interdisciplinary areas like bioorganic chemistry, organometallic chemistry, biomimetic chemistry etc. A major advantage is the versatility in its stereochemistry and geometry of the complexes aided by the custom tailored organic ligands. This chapter discusses the synthesis and characterization of twenty one new coordination complexes prepared using 2-methoxy-4-chromanones and Ni (II), Cu (II), Zn (II) metals. Characterization techniques used for structural elucidation include elemental analysis, molar conductivity, magnetic susceptibility, IR spectra, Uv-visible spectra, TG/DTG and NMR analysis. Complexes are proposed to have square pyramidal geometries or distorted octahedral geometry. These complexes are considered as a novel class which is expected to have vibrant pharmaceutical properties.

3.1 Introduction

It is well proved that organic life relies on inorganic elements for carrying out many vital processes. Metal ions play a crucial role in the human body and small deviations from normal levels of concentration are recognized as symptoms of malfunctions or diseases. Metal complexes play important and diversified roles in biological systems. The role of chlorophyll, hemoglobin, enzymes, vitamins etc. indicates the intimate linkage of metals with biosystems [1]. The sustained attention and pursuit in the chemistry of transition metal complexes of bioactive ligands have significantly enhanced mainly due to their use as models for the more intricate naturally occurring primary bioinorganic systems. Implication of synthetic analogies for these metals containing biological systems makes use of the basic chemical behavior of theses metal ions. It will make better understanding of the system more precisely and easily. Large numbers of bioactive ligands and their metal complexes have been synthesized and extensively studied for the understanding of underlying mechanism of the biological reactions. These studies enable the use of novel bioactive ligands and their complexes as new vehicles of various drugs in pharmaceutical industry [2].

Copper (Cu) is classified as a trace element and is the third most abundant transition metal in biology, after iron and zinc. Copper ions are present as cofactor in more than 30 enzymes in humans and animals which are inevitable for different cellular activities and metabolic process. Copper ions can form various coordination complexes with ligands with different geometries and stereochemistry. There are several unique properties for copper such as exhibition of various stereo chemistries in complexes [3], redox reactions due to variable oxidation state [4] and ability to bind to ligands especially of oxygen and nitrogen donor types [5]. $Cu^{2+/+}$redox chemistry is a significant feature required for many

biological reactions. Though it is useful, it causes harm if it is not taken care properly by the cell as it leads to the formation of reactive oxygen species. Due to the prevailing reducing conditions in the cell, Cu^{+} may also present along with Cu^{2+}. Soft character makes Cu^{+} unique among the biological metal ions, so it has potential to be selected based on ligand donor groups. Due to d^{10} ion configuration of Cu^{+} it form flexible geometries like tetragonal, trigonal, or even linear geometries that are disfavored by other metals. Due to d^{9} configuration of Cu^{2+}, there is a nonspherical symmetry for the cation which leads to the distortions in the geometries. Jahn-Teller effect plays a dominant role in deciding the shape and geometry of the molecule [6].

Zinc metal is the second most common metallic element found in biological system, iron being the first. 2.3 g of zinc is present in an average 70 kg adult human [7]. It is the only one known to be essential for functions of enzymes and has important roles in enzymatic activity and other functional regulations of over 300 enzymes like carbonic anhydrase and alcohol dehydrogenase. Zn ion is unique due to its strong Lewis acidity, fast ligand exchange ability and decreased redox character under normal conditions [8]. Zn^{2+} is also a d^{10} ion, but is a hard acid than Cu^{+}, so can be minimized as an interfering species based on ligand donor choice. Zn (II) ion is reported to have strong affinity towards oxygen, nitrogen and sulphur donor ligands and easily form stable complexes with the same. Due to the absence of crystal field stabilization, the geometry of Zn (II) complexes is clearly defined by the polarizing power of this ion. There are different stable chelates of Zn (II) with coordination numbers ranging from two to six due to its versatility and flexibility [9].

Nickel (II) redox chemistry is of special interest to bioinorganic chemists due to its presence in several enzymes, like carbon monoxide dehydrogenase, superoxide dismutase and methyl coenzyme-M-reductase. Nickel ion can easily form complexes with organic ligands and coordination

number of Ni (II) complexes range from -1 to +4 and most common being Ni (II) state. They can form paramagnetic octahedral, trigonal bipyramidal, quadratic-pyramidal and tetrahedral complexes whereas their quadratic-planar complexes are found to be diamagnetic. Due to its borderline metal ion character, it binds to both hard and soft ligands albeit rarely, to both in the same complex [10]. Diamagnetic square planar complexes are usually formed from the d^8 configuration, predominantly with strong field ligands or where steric hindrances hamper higher coordination numbers [11].

Metal complexes incorporating chromone derivatives are always an interesting area in the field of pharmaceutical chemistry due to the extensive medicinal and biological properties. G. Kalairasi *et al* and coworkers have reported two water soluble nontoxic Cu (II) complexes containing 7-hydroxy-4-oxo-4[H]-chromene derived ONO pincer ligands with potent DNA binding and antimicrobial activities [12]. Chromone and benzyldithiocarbazate based ligand was reported recently which can complex with Cu^{2+}exhibiting instant color change from colorless to yellow. This property can be exploited for its use as an excellent sensitive and selective colorimetric detection of Cu^{2+} in aqueous medium [13]. A series of chromone Schiff base complexes which activate tumor suppressor p53 in cancer cells was synthesized and characterized by M. M. E. Shalkdofa and his coworkers [14]. Enantiomeric specificity of chiral Zn (II) and Cu (II) chromone complexes towards DNA was studied in detail by Arjmand and his coworkers. Studies revealed a higher propensity of Cu (II) complexes for guanosine-5′-monophosphate disodium salt, whereas Zn (II) complexes preferentially bind to thymidine-5′-monophosphate disodium salt [15]. Two new chromone Schiff bases and their transition metal complexes were synthesized and characterized and have been investigated as functional models for catechol oxidase (catecholase) activity by employing 3,5-di-*tert*-butylcatechol as a model substrate [16]. Agnieszka Dziewulska-Kułaczkowska has reported thermal and

spectral investigations of Mn (II), Co (II), Ni (II), Cu (II) and Zn (II) complexes with 3-(anilinomethylene)-2-methoxychroman-4-one. They have reported that the coordination is through nitrogen atom from ligand and oxygen atom present in 4-position of γ-pyrone to the metal ion to form octahedral complexes [17].

This chapter describes the preparation and characterization of twenty one new metal complexes incorporating the synthesized ligands. Elemental analysis, infrared spectra, Uv-visible spectra, magnetic susceptibility measurements, conductivity studies, TG-DTG studies and proton NMR analysis were done to characterize these complexes.

3.2 Experimental

3.2.1 Materials used

3-Formylchromone, 6-methyl-3-formylchromone, 2-aminopyridine, 2-amino-5-nitropyridine, 2-amino-5-bromopyridine, 2-amino-5-methylpyridine, 3-aminopyridine were purchased from Aldrich and were used as such without further purification. Acetates of the metal ions Cu $(CH_3COO)_2$. H_2O, Zn $(CH_3COO)_2.2H_2O$, $Ni(CH_3COO)_2.4H_2O$ were purchased from Sigma Aldrich and was used as received. Methanol (Merck), DMF (Merck), diethyl ether (Merck), hexane (Merck) were analytical grade and used as such.

3.2.2 Synthesis of ligands

The procedure for synthesis and characterization of ligands are explained in Chapter 2.

3.2.3 General procedure for the synthesis of metal complexes

The metal acetate (1mmol) in methanol (20 mL) was added drop wise to ligand (1mmol) dissolved in minimum quantity of DMF. The resultant solution was stirred at room temperature for 18-24 hours. The solution was

evaporated slowly and the precipitated complexes were filtered, washed thoroughly with hot methanol, diethyl ether and hexane. Dried in vacuum. Yield was noted.

3.3 Results and discussion

3.3.1 Physical and analytical properties of complexes

All the complexes were prepared stoichiometrically by the direct reaction of ligands and the metal acetates at room temperature in 1:1 ratio. Products were obtained in moderate to good yield. All the complexes were colored and air stable. They were insoluble in water and most of the organic solvents but soluble in Lewis bases such as DMF and DMSO. The conductivity measurements were made in DMSO (10^{-3} M) at room temperature and values were between 10-50 Ω^{-1} cm^2 mol^{-1} indicating non electrolytic nature of the prepared complexes [18]. Elemental analyses obtained were in good agreement with the assigned chemical formula of the proposed structure of the complexes. Percentage of metal character was determined after digesting the sample with concentrated nitric acid. All the complexes were formed in 1:1 ratio of ligand and metal. Efforts to obtain single crystals of required quality of the complexes were not successful. Numerous attempts were made by changing reaction conditions but none were fruitful. Table 3.1 gives physical and analytical properties of NiL1, NiL2, NiL3, NiL5, NiL6 and NiL7. Table 3.2 gives physical and analytical properties of the CuL1, CuL2, CuL3, CuL4, CuL5, CuL6 and CuL7. Table 3.3 gives physical and analytical properties of ZnL1, ZnL2, ZnL3, ZnL4, ZnL5, ZnL6, ZnL7 and ZnL8.

Table 3.1: Physical and analytical properties of NiL1, NiL2, NiL3, NiL5, NiL6 and NiL7

Compound	Yield (%) & colour	Elemental Analysis calc. (found)				Λ_M (Ω^{-1} cm^2mol^{-1})	Formula weight
		C (%)	H (%)	N (%)	M (%)		
NiL1[NiL1(OAc)(H_2O)$_2$]. H_2O	69, yellow solid	47.52 (47.5)	4.89 (4.75)	6.18 (6.20)	12.81 (12.84)	19.6	453.3
NiL2[NiL2(OAc)(H_2O)$_2$]. H_2O	75, green powder	44.56 (44.51)	4.53 (4.65)	8.21 (8.23)	11.46 (11.36)	29.6	512.3
NiL3[NiL3(OAc)(H_2O)].0.5H_2O	66,green powder	49.79 (49.82)	6.06 (6.12)	4.73 (5.06)	12.33 (12.81)	21.5	458.6
NiL5[NiL5(OAc)(H_2O)]. H_2O	69, green solid	50.68 (50.61)	4.94 (4.79)	6.24 (6.26)	13.17 (13.07)	17.6	449
NiL6[NiL6(OAc)(H_2O)$_2$]. H_2O	74, green powder	41.79 (41.51)	3.84 (4.02)	5.12 (5. 23)	10.73 (10.75)	39.6	546
NiL7[NiL7(OAc)(H_2O)$_2$]. H_2O	74, green powder	50.06 (50.15)	6.07 (6.02)	5.57 (5. 23)	12.98 (12.94)	45.2	503

Table 3.2: Physical and analytical properties of the CuL1, CuL2, CuL3, CuL4, CuL5, CuL6 and CuL7

Compound	Yield (%) & colour	Elemental Analysis calc. (found)				Λ_M (Ω^{-1} cm^2mol^{-1})	Formula weight
		C (%)	H (%)	N (%)	M (%)		
CuL1[CuL1(OAc)(H_2O)$_2$]. ½DMF	72, dark green solid	49.14 (49.15)	5.45 (5.95)	7.31 (7.35)	14.31 (14.39)	18.6	475.5
CuL2[CuL2(OAc)(H_2O].DMF. ½H_2O	78, olive green solid	44.4 (44.42)	4.09 (3.99)	9.88 (9.90)	13.91 (13.99)	24.6	567.2
CuL3[CuL3(OAc)(H_2O)$_2$].½H_2O	81, green powder	49.3 (49.14)	4.99 (5.01)	6.10 (6.05)	13.72 (13.79)	21	463.0
CuL4[CuL4(OAc)(H_2O)$_2$].½H_2O	75,dark green powder	48.2 (48.16)	4.8 (4.78)	6.21 (6.24)	14.99 (15.03)	32.5	449
CuL5[CuL5(OAc)(H_2O)$_2$]	75, olive green solid	50.27 (50.27)	4.89 (4.90)	6.17 (6.14)	14.00 (14.049)	13.6	454.5
CuL6[CuL6(OAc)(H_2O)$_2$]. H_2O	78, green solid	41.46 (41.42)	2.84 (2.81)	5.01 (5.02)	11.53 (11.59)	24.6	550
CuL7[CuL7(OAc)(H_2O)]. H_2O	73, green solid	51.25 (51.33)	5.32 (5.17)	5.92 (5.88)	13.58 (13.59)	24.6	468

Table 3.3: Physical and analytical properties of ZnL1, ZnL2, ZnL3, ZnL4, ZnL5, ZnL6, ZnL7 and ZnL8

Compound	Yield (%) & colour	Elemental Analysis calc. (found)				$\Lambda_M(\Omega^{-1}$ $cm^2mol^{-1})$	Formula weight
		C (%)	H (%)	N (%)	M (%)		
ZnL1[ZnL1(OAc)$(H_2O)_2$]. H_2O	79, yellow solid	47.02 (47.09)	5.14 (5.46)	6.09 (6.11)	15.13 (15.13)	34.6	459.7
ZnL2[ZnL2(OAc)$(H_2O)_2$].H_2O. MeOH	80, yellow powder	41.52 (41.7)	5.81 (5.02)	7.33 (7.34)	11.42 (11.52)	31.6	554.8
ZnL3[ZnL3(OAc)$(H_2O)_2$].½H_2O	78, greenish yellow powder	49.1 (48.9)	4.99 (5.88)	6.03 (6.01)	14.07 (13.99)	33.6	463.9
ZnL4 [ZnL4(OAc)$(H_2O)_2$]	68,light yellow powder	48.1 (48.9)	4.56 (4.12)	6.34 (6.32)	14.81 (14.56)	30.21	441.7
ZnL5[ZnL5(OAc)(H_2O)]. H_2O	71, bright yellow solid	50.09 (50.07)	4.63 (4.89)	6.15 (6.17)	14.36 (14.33)	26.6	456.7
ZnL6[ZnL6(OAc)$(H_2O)_2$]. H_2O	80, yellow powder	41.06 (41.29)	4.12 (4.19)	5.06 (5.12)	11.42 (11.34)	31.6	552.8
ZnL7[ZnL7(OAc)$(H_2O)_2$]. H_2O	79, yellow powder	49.24 (49.5)	4.32 (4.5)	5.73 (5.74)	13.12 (13.34)	31.6	588
ZnL8[ZnL8(OAc)(H_2O)]. H_2O	79, yellow powder	49.95 (49.5)	4.82 (4.65)	6.16 (6.15)	14.35 (14.55)	30.0	454

3.3.2 IR spectral analysis of complexes

IR spectra of the complexes were recorded in the range of 4000-400 cm^{-1} using KBr pellets. Strong absorption bands around 1660-1635 cm^{-1} of C=O stretching of pyrone ring in IR spectra of ligands were shifted to around 1620cm^{-1} on complexation which clearly indicate coordination through carbonyl oxygen in the pyrone ring. The very strong band around 1270 cm^{-1} in the spectrum of ligands attributed to the ν(C–N) stretching shifts to 1240-1190 cm^{-1} in complexes indicates the coordination of metal ion with nitrogen atom [19]. A new broad peak is present between 3650-3400 cm^{-1} in the spectra of all

complexes which indicates the presence of water molecules in the complexes [20]. Presence of acetate ligand in the complexes was confirmed by appearance of new bands near 1450-1420 $cm^{-1}$and 1350-1330 cm^{-1} for $\nu(OAc)_{asym}$ and $\nu(OAc)_{sym}$ respectively. Separation of bands, $\Delta\nu \sim 120$ cm^{-1}, which is less than for standard sodium mandalate, suggests bidendate coordination. Formation of new bands in the range 520-430 cm^{-1} and 620-520 cm^{-1} indicates the participation of nitrogen and oxygen through M-N and M-O bonds respectively in complex formation. Thus from IR spectra, it can be concluded that ligands coordinate bidentatively through NO donor sites to the metal during complex formation [21, 22].

Fig. 3.1(a-f): IR spectra of NiL1, NiL2, NiL3, NiL5, NiL6 and NiL7

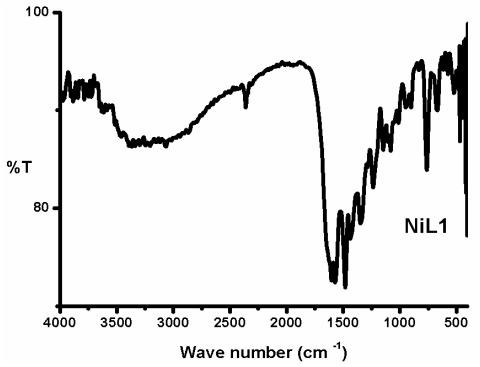

Fig. 3.1(a): IR spectra of NiL1

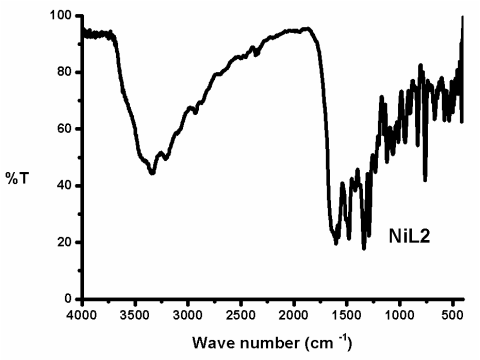

Fig. 3.1(b): IR spectra of NiL2

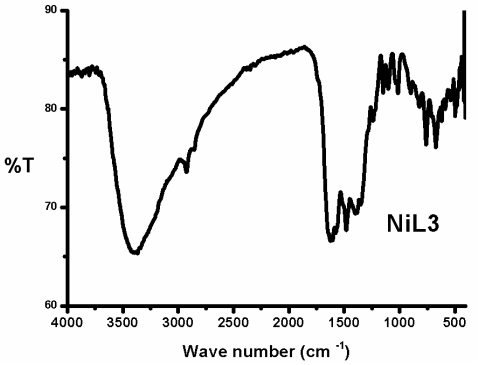

Fig. 3.1(c): IR spectra of NiL3

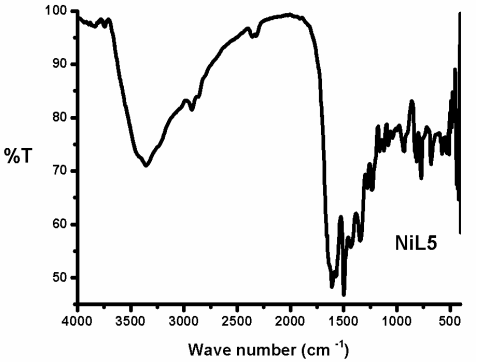

Fig. 3.1(d): IR spectra of NiL5

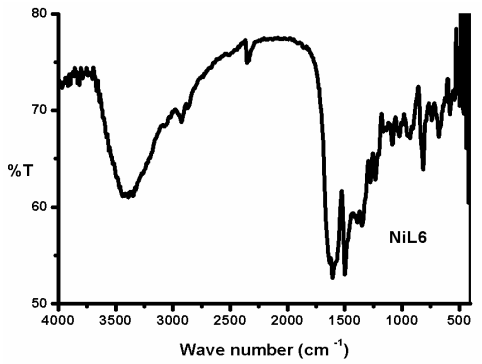

Fig. 3.1(e): IR spectra of NiL6

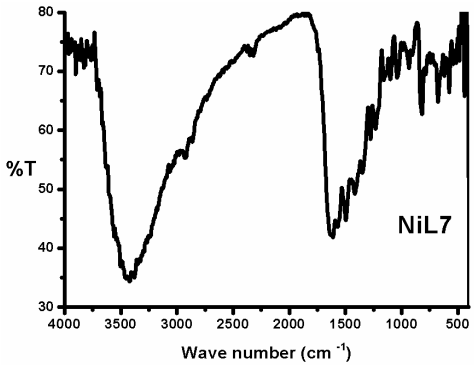

Fig. 3.1(f): IR spectra of NiL7

Table 3.4: IR spectral data of Ni (II) complexes

Compound	Frequency(cm^{-1})					
	ν(O-H)	ν(C=O)	ν(C-N)	ν(M-O)	ν(M-N)	$\nu(OAc)_{asym}$,$\nu(OAc)_{sym}$
NiL1	3343	1614	1227	455	537	1445,1336, bidendate
NiL2	3340	1627	1223	488	534	1439,1338, bidendate
NiL3	3366	1623	1239	498	587	1420,1337,bidendate
NiL5	3350	1614	1244	464	537	1438,1348, bidendate
NiL6	3406	1627	1223	476	573	1439,1348, bidendate
NiL7	3408	1620	1230	448	568	1436,1338, bidendate

Fig. 3.2(a-g): IR spectra of CuL1, CuL2, CuL3, CuL4, CuL5, CuL6 and CuL7.

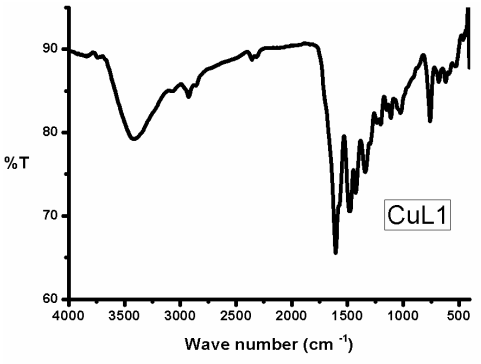

Fig. 3.2(a): IR spectra of CuL1

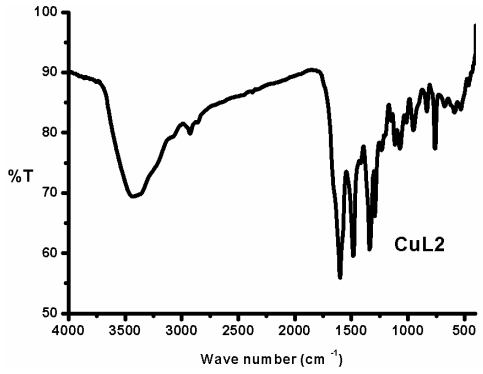

Fig. 3.2(b): IR spectra of CuL2

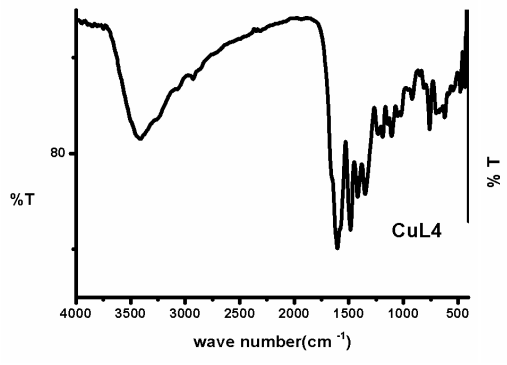

Fig. 3.2(c): IR spectra of CuL3

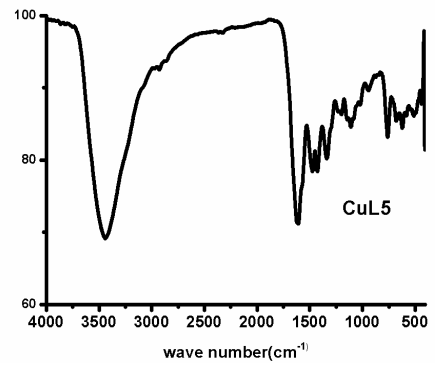

Fig. 3.2(d): IR spectra of CuL4

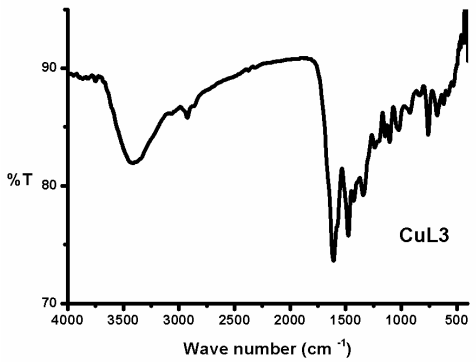

Fig. 3.2(e): IR spectra of CuL5

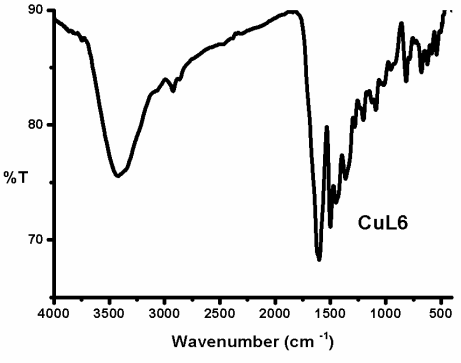

Fig. 3.2(f): IR spectra of CuL6

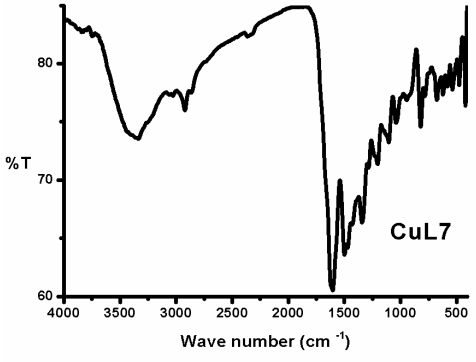

Fig. 3.2(g): IR spectra of CuL7

Table 3.5: IR spectral data of Cu (II) complexes

Compound	Frequency(cm^{-1})					
	ν(O-H)	ν(C=O)	ν(C-N)	ν(Cu-O)	ν(Cu-N)	$\nu(OAc)_{asym}$,$\nu(OAc)_{sym}$
CuL1	3404	1614	1215	526	583	1420,1336,bidendate
CuL2	3430	1619	1225	440	542	1449,1344,bidendate
CuL3	3415	1620	1239	441	533	1476,1343,bidendate
CuL4	3407	1615	1233	479	621	1482,1349,bidendate
CuL5	3443	1619	1225	499	554	1416,1333,bidendate
CuL6	3419	1619	1235	420	543	1449,1363,bidendate
CuL7	3419	1619	1213	420	547	1449,1363,bidendate

Fig. 3.3(a-h): IR spectra of ZnL1, ZnL2, ZnL3, ZnL4, ZnL5, ZnL6, ZnL7 and ZnL8.

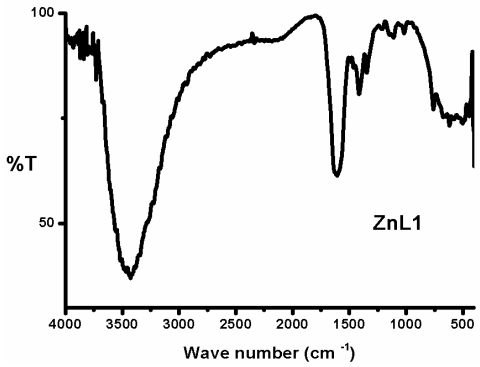

Fig. 3.3(a): IR spectra of ZnL1

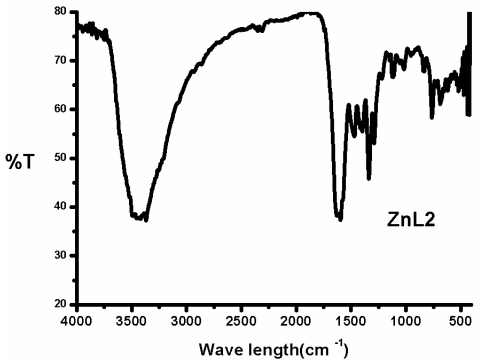

Fig. 3.3(b): IR spectra of ZnL2

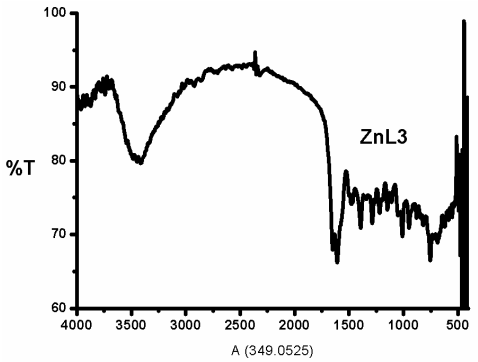

Fig. 3.3(c): IR spectra of ZnL3

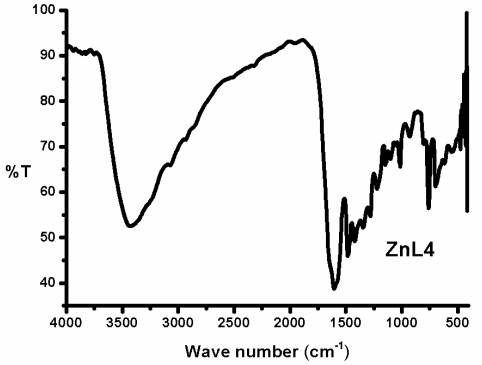

Fig. 3.3(d): IR spectra of ZnL4

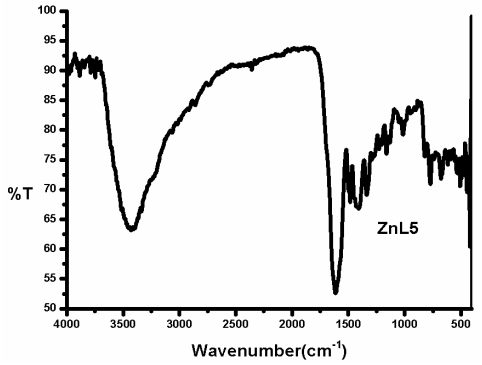

Fig. 3.3(e): IR spectra of ZnL5

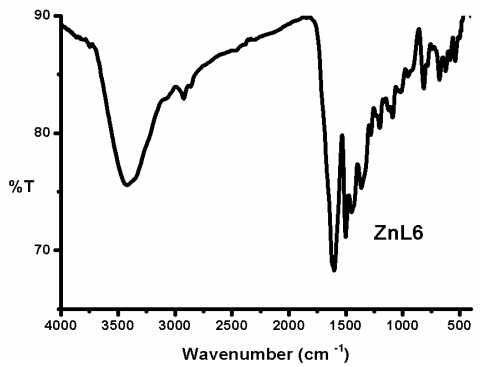

Fig. 3.3(f): IR spectra of ZnL6

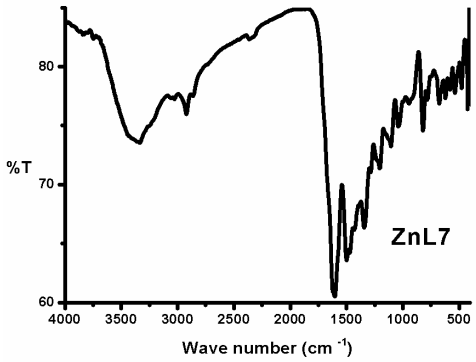

Fig. 3.3(g): IR spectra of ZnL7

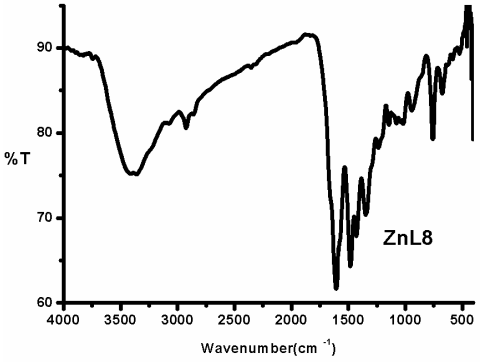

Fig. 3.3(h): IR spectra of ZnL8

Table 3.6: IR spectral data of Zn (II) complexes

Compound	Frequency (cm^{-1})					
	ν(O-H)	ν(C=O)	ν(C-N)	ν(Zn-O)	ν(Zn-N)	$\nu(OAc)_{asym}$, $\nu(OAc)_{sym}$
ZnL1	3343	1613	1226	462	539	1425,1358, bidendate
ZnL2	3361	1638	1225	460	520	1447,1366, bidendate
ZnL3	3389	1616	1233	478	521	1420,1336, bidendate
ZnL4	3347	1624	1229	431	539	1420,1336, bidendate
ZnL5	3418	1615	1235	451	539	1430,1339, bidendate
ZnL6	3361	1638	1225	460	520	1447,1366, bidendate
ZnL7	3436	1613	1233	458	592	1425,1344,bidendate
ZnL8	3426	1613	1215	467	526	1400,1337,bidendate

3.3.3 Magnetic susceptibility measurements

The magnetic susceptibility measurements of complexes were done using simple Gouy type balance at room temperature. In this method, interaction between unpaired electron and magnetic field is used. A diamagnetic material gets repelled by a magnetic field whereas a paramagnetic material gets attracted into it. $Hg[CO(NCS)_2]$ was used as the calibrant. Finely powdered sample is tightly packed in the previously weighed sample holder. Sample length is noted as L. The packed sample tube is placed in the tube guide of the balance and the reading is noted.

Evans method which measures attraction of sample to magnetic field was used to determine molar magnetic susceptibility (χ_M). χ_M was calculated using the following equation:

$$\chi_m = \frac{C \times L \times (R - R_0) \times MW}{(m - m_0) \times 10^9}$$

C is a constant for the balance, m is the mass of sample with holder, m_0 is the mass of empty holder, MW is the sample molecular weight, L is the sample length, and (R-Ro) is the balance reading (with minus without sample in holder).

Diamagnetic corrections were applied using Pascal constants for various atoms and structural units to obtain corrected molar magnetic susceptibility, χ_A. Effective magnetic moment, μ_{eff} is calculated from corrected molar magnetic susceptibility using the following equation,

$\mu_{eff} = 2.84\sqrt{(T \times \chi_A)}$, Where, T is the absolute temperature.

μ_{eff} of copper and nickel complexes at 298 K is tabulated in the given table 3.7:

Table 3.7: Effective magnetic moment of Cu (II) and Ni (II) complexes

compound	μ_{eff} (BM)	compound	μ_{eff} (BM)
CuL1	1.99	NiL1	3.18
CuL2	1.89	NiL2	3.21
CuL3	1.72	NiL3	3.00
CuL4	1.76	NiL5	3.45
CuL5	1.93	NiL6	3.21
CuL6	1.94	NiL7	3.14
CuL7	1.82		

The magnetic moment value observed for Cu (II) complexes lies slightly different from the spin-only value 1.73 BM for a d^9 copper monomeric system [23, 24].This also offers possibility of distorted octahedral geometry around the Cu (II) ion in line with the electronic spectral studies. The magnetic moments of the copper (II) complexes were treated by Boudreaux. According to Boudreaux, in complexes having a square pyramidal configuration, the five-fold degenerate 3d level of Cu (II) is split by a ligand field of C_{4v} symmetry into four components. The $d_{x^2-y^2}$, $d_{x^2}$and d_{xy} levels are nondegenerate, while (d_{xz}, d_{yz}) levels are four-fold degenerate, including spin. The spin-orbit interaction splits this level into two components, each of which is further split into two sublevels by the external magnetic field. Boudreaux calculated theoretically the magnetic moment of square- pyramidal copper (II) complexes to be 2.11–2.2 BM at room temperature. These values are slightly higher than those obtained during the experimental measurements (1.8μB) [25]. Room temperature magnetic moment value of CuL2 and CuL7 is 1.89 and 1.82 BM respectively, thus proposing the square pyramidal environment of Cu (II) for the complex [26]. Effective magnetic moment of zinc complexes are found to be zero as these complexes are diamagnetic.

For nickel complexes, μ_{eff} (2.9-3.2BM) is higher than spin only value (2.83BM) corresponding to two unpaired electrons. The deviation is due to the orbital contribution and the observed values lies well within the range of octahedral geometry [27].

3.3.4 Electronic spectral measurements

The electronic absorption studies are often very supportive in the assessment of results furnished by other methods of structural analysis. The electronic spectral measurements were used to assign the stereochemistries of the metal ions in the complexes based on the positions and number of d-d transition peaks.

3.3.4.1 Uv-visible spectral studies of nickel complexes:

Electronic spectra of NiL1, NiL2, NiL3, NiL5, NiL6, and NiL7 were recorded in 10^{-3} M DMSO solution (Fig 3.4 (a-f)) and data is tabulated in Table 3.4.

Table 3.8: Uv-vis spectral data of Ni (II) complexes

Compound	Electronic spectral bands (nm)	log ε ($L\ mol^{-1}cm^{-1}$)	Band assignments
NiL1	260	4.82	Intraligand transitions
	301	3.87	Intraligand transitions
	377	4.63	Intraligand transitions
	519	2.30	CT
	598	1.66	$^3A_{2g}(F)\rightarrow{}^3T_{1g}(P)$
	742	1.46	$^3A_{2g}(F)\rightarrow{}^3T_{1g}(F)$
NiL2	358	4.77	Intraligand transitions
	308	3.98	Intraligand transitions
	260	3.84	Intraligand transitions
	451	2.44	CT
	682	1.47	$^3A_{2g}(P)\rightarrow{}^3T_{1g}(P)$
	769	1.44	$^3A_{2g}(F)\rightarrow{}^3T_{1g}(F)$
	867	1.41	$^3A_{2g}\rightarrow{}^3T_{2g}$

NiL3	256	4.47	Intraligand transitions
	310	4.41	Intraligand transitions
	353	4.33	Intraligand transitions
	601	1.79	CT
	693	0.847	$^3A_{2g}(F)\rightarrow{}^3T_{1g(}P)$
	796	0.602	$^3A_{2g}(F)\rightarrow{}^3T_{1g}(F)$
NiL5	265	4.28	Intraligand transitions
	310	3.78	Intraligand transitions
	386	4.36	Intraligand transitions
	519	3.10	CT
	598	2.20	$^3A_{2g}(F)\rightarrow{}^3T_{1g(}P)$
	687	1.46	$^3A_{2g}(F)\rightarrow{}^3T_{1g}(F)$
NiL6	316	4.77	Intraligand transitions
	369	3.98	Intraligand transitions
	260	3.84	Intraligand transitions
	457	3.44	CT
	541	1.69	CT
	658	1.04	$^3A_{2g}(P)\rightarrow{}^3T_{1g}(P)$
	763	0.845	$^3A_{2g}(F)\rightarrow{}^3T_{1g}(F)$
	845	0.698	$^3A_{2g}\rightarrow{}^3T_{2g}$
NiL7	255	4.56	Intraligand transitions
	310	4.85	Intraligand transitions
	360	4.66	Intraligand transitions
	660	1.69	$^3A_{2g}(P)\rightarrow{}^3T_{1g}(P)$
	762	1.23	$^3A_{2g}(F)\rightarrow{}^3T_{1g}(F)$
	825	1.17	$^3A_{2g}\rightarrow{}^3T_{2g}$

The electronic spectrum of Ni (II) complexes, along with the intraligand transition bands of the free ligand, displays three bands, at 820-840 nm, 750-760 nm, 650-650 nm corresponding to $^3A_{2g}\rightarrow{}^3T_{2g}$, $^3A_{2g}(F) \rightarrow {}^3T_{1g}(F)$, $^3A_{2g}(P)\rightarrow{}^3T_{1g}(P)$ respectively confirming the octahedral configuration for the Ni(II) complexes [31, 32].

Fig.3.4 (a-f): Uv-visible spectra of NiL1, NiL2, NiL3, NiL5, NiL6, NiL7. Inset graph gives the d-d spectra taken in 10^{-3} M sample solution in DMSO

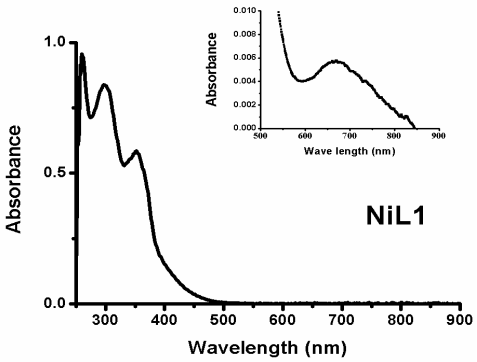

Fig. 3.4 (a): Uv-visible spectra of NiL1

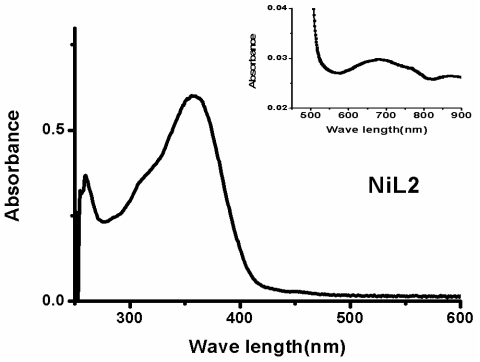

Fig. 3.4 (b): Uv-visible spectra of NiL2

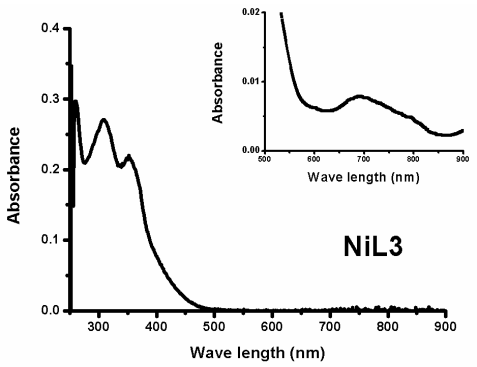

Fig. 3.4 (c) Uv-visible spectra of NiL3

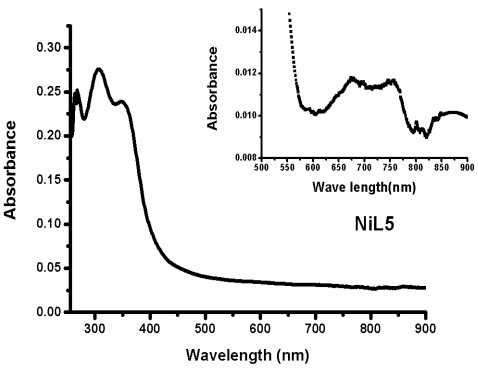

Fig. 3.4 (d): Uv-visible spectra of NiL5

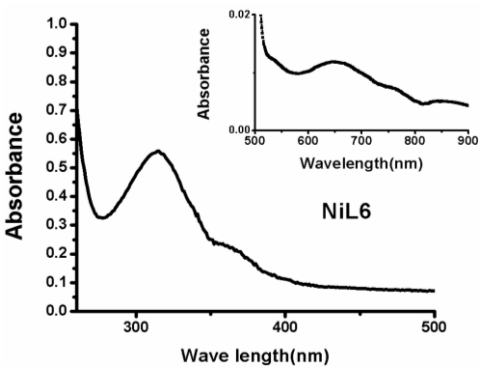

Fig. 3.4 (e): Uv-visible spectra of NiL6

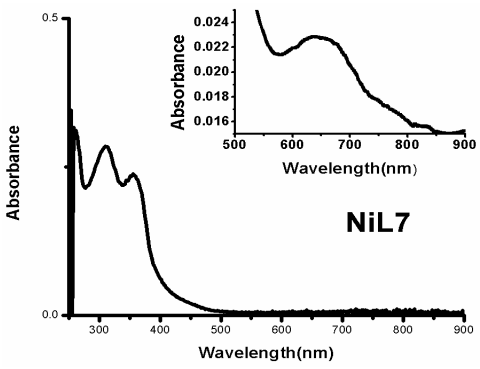

Fig. 3.4 (f): Uv-visible spectra of NiL7.

3.3.4.2 Uv-vis spectral studies of copper complexes:

Electronic spectra of the CuL1, CuL2, CuL3, CuL4, CuL5, CuL6, and CuL7 were recorded in 10^{-3} M DMSO solution (Fig.3.5 (a-g)) and data is tabulated in Table 3.9

Table 3.9: Uv-vis spectral data of copper complexes

Compound	Electronic spectral bands(nm)	log ε ($L\ mol^{-1}cm^{-1}$)	Band assignments
CuL1	260	4.38	Intraligand transitions
	308	4.39	Intraligand transitions
	360	3.12	Intraligand transitions
	454	3.67	CT
	728	1.14	$^2B_{1g}\rightarrow{}^2A_{1g}$
CuL2	265	4.71	Intraligand transitions
	310	4.70	Intraligand transitions
	360	4.98	Intraligand transitions
	753	1.92	$^2B_{1g}\rightarrow{}^2A_{1g}$
CuL3	257	4.90	Intraligand transitions
	311	4.86	Intraligand transitions
	359	4.81	Intraligand transitions
	722	1.92	$^2B_{1g}\rightarrow{}^2A_{1g}$
CuL4	261	4.69	Intraligand transitions
	303	4.58	Intraligand transitions
	348	4.53	Intraligand transitions
	701	1.92	$^2B_{1g}\rightarrow{}^2A_{1g}$
CuL5	260	4.38	Intraligand transitions
	308	4.39	Intraligand transitions
	360	3.12	Intraligand transitions
	454	2.67	CT
	728	1.14	$^2B_{1g}\rightarrow{}^2A_{1g}$ $(d_{x^2-y^2}\rightarrow d_{z^2})$
CuL6	307	4.98	Intraligand transitions
	384	4.70	Intraligand transitions
	449	4.71	Intraligand transitions
	735	2.92	$^2B_{1g}\rightarrow{}^2A_{1g}$ $(d_{x^2-y^2}\rightarrow d_{z^2})$

CuL7	265	4.56	Intraligand transitions
	312	4.49	Intraligand transitions
	347	4.43	Intraligand transitions
	458	2.97	CT
	706	1.68	$^2B_{1g}\rightarrow{}^2A_{1g}$

Three spin allowed transitions may be anticipated in the visible region, suggesting D_{4h} or C_{4v} symmetry, and the E_g & T_{2g} levels of ^2D free ion will split into B_{1g}, A_{1g}, B_{2g} and E_g levels, respectively. The Cu(II) complexes with d^9 configuration is likely to experience Jahn-Teller distortion which lead to further splitting of the ^2E_g and $^2T_{2g}$ levels and give rise to three spin allowed transitions viz. $^2B_{1g}\rightarrow{}^2A_{1g}$ ($d_{x^2-y^2}\rightarrow d_{z^2}$), $^2B_{1g}\rightarrow{}^2B_{2g}$ ($d_{x^2-y^2}\rightarrow d_{xy}$), $^2B_{1g}\rightarrow{}^2E_g$ ($d_{x^2-y^2}\rightarrow dx_z,d_{yz}$) which occur in the ranges 850-550, 850-640 and 580-500 nm respectively [28]. But often these theoretical expectations are unobserved in practice and these bands generally seen overlapped and become hard to resolve into separate bands due to the insignificant energy difference between the d levels. The presence of a broad band in all Cu(II) complexes in the range 650-750 nm can be assigned to the envelope of $^2B_{1g}\rightarrow{}^2A_{1g}$($d_{x^2-y^2}\rightarrow d_{z^2}$), $^2B_{1g}\rightarrow{}^2B_{2g}$ ($d_{x^2-y^2}\rightarrow d_{xy}$), $^2B_{1g}\rightarrow{}^2E_g$ ($d_{x^2-y^2}\rightarrow dx_z,d_{yz}$) transitions[29]. For copper complexes, presence of these transitions indicates distorted octahedral geometry [30] around Cu (II) ion.

Fig. 3.5(a-g) Uv-vis spectra of CuL1, CuL2, CuL3, CuL4, CuL5, CuL6, and CuL7. Inset graph gives the d-d spectra taken in 10^{-3} M sample solution in DMSO.

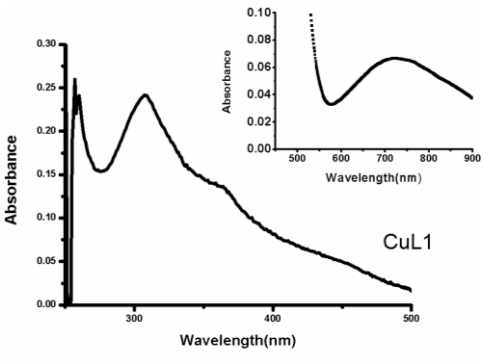

Fig. 3.5(a) Uv-vis spectra of CuL1

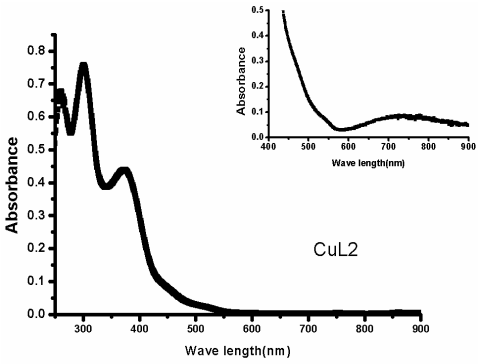

Fig. 3.5(b) Uv-vis spectra of CuL2

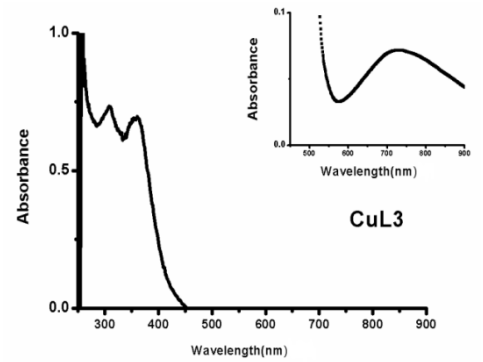

Fig. 3.5(c) Uv-vis spectra of CuL3

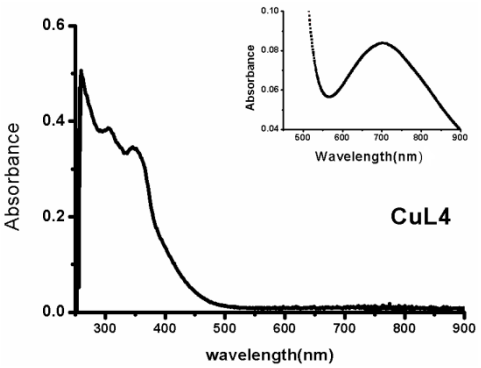

Fig. 3.5(d) Uv-vis spectra of CuL4

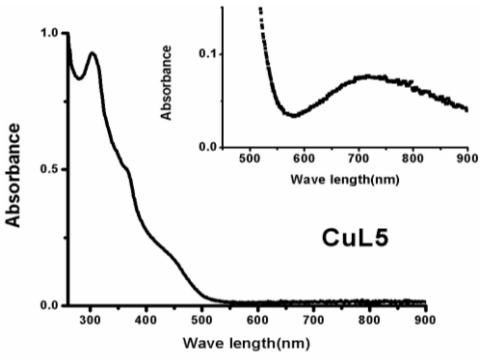

Fig. 3.5(e) Uv-vis spectra of CuL5

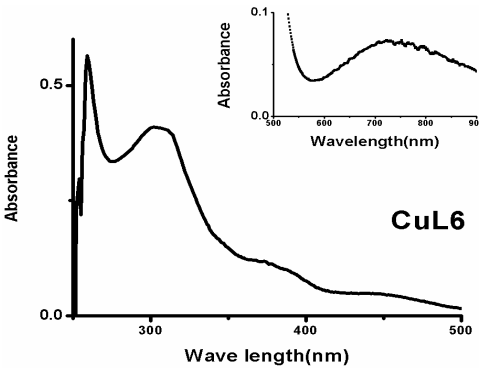

Fig. 3.5(f) Uv-vis spectra of CuL6

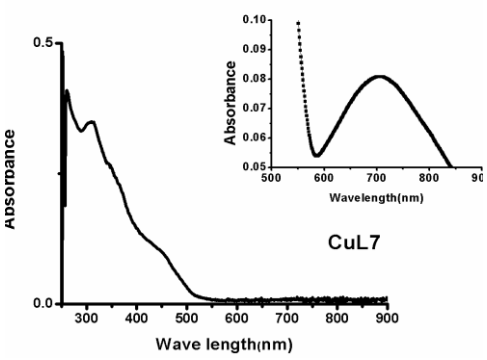

Fig. 3.5(g) Uv-vis spectra of CuL7

3.3.4.3 Uv-vis spectral studies of zinc complexes

Electronic spectra of ZnL1, ZnL2, ZnL3, ZnL4, ZnL5, ZnL6, ZnL7 and ZnL8 were recorded in 10^{-3} M DMSO solution (Fig.3.6 (a-h)) and data is tabulated in Table 3.10.

Table 3.10: Uv-visible spectra of zinc complexes

Compound	Electronic spectral bands(nm)	log ε ($L\ mol^{-1}cm^{-1}$)	Band assignments
ZnL1	264	4.379	Intraligand transitions
	307	4.40	Intraligand transitions
	359	4.35	Intraligand transitions
ZnL2	362	4.38	Intraligand transitions
	312	4.15	Intraligand transitions
	266	4.01	Intraligand transitions
	518	3.22	CT
ZnL3	263	4.98	Intraligand transitions
	304	4.86	Intraligand transitions
	362	4.81	Intraligand transitions
	448	3.55	CT
ZnL4	260	4.69	Intraligand transitions
	305	4.58	Intraligand transitions
	363	4.53	Intraligand transitions
	453	3.92	CT

ZnL5	260	4.38	Intraligand transitions
	307	4.39	Intraligand transitions
	382	3.12	Intraligand transitions
ZnL6	269	4.98	Intraligand transitions
	309	4.70	Intraligand transitions
	371	4.71	Intraligand transitions
	506	2.92	CT
ZnL7	261	4.56	Intraligand transitions
	307	4.49	Intraligand transitions
	366	4.43	Intraligand transitions
	503	2.97	CT
ZnL8	259	4.96	Intraligand transitions
	311	4.86	Intraligand transitions
	368	4.22	Intraligand transitions
	459	3.12	CT

Absence of d-d bands confirmed diamagnetic nature of zinc complexes. There were peaks in UV region of electronic spectrum due to intraligand transitions.

Fig. 3.6 (a-h): Uv-visible spectra of ZnL1, ZnL2, ZnL3, ZnL4, ZnL5, ZnL6, ZnL7 and ZnL8.

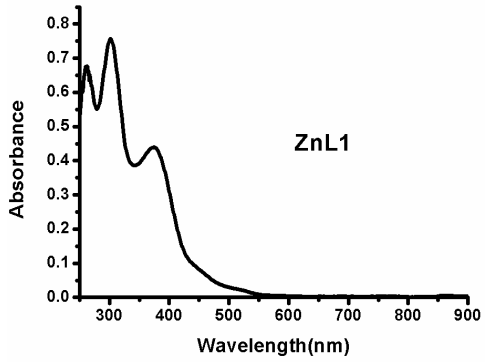

Fig. 3.6 (a): Uv-vis spectra of ZnL1

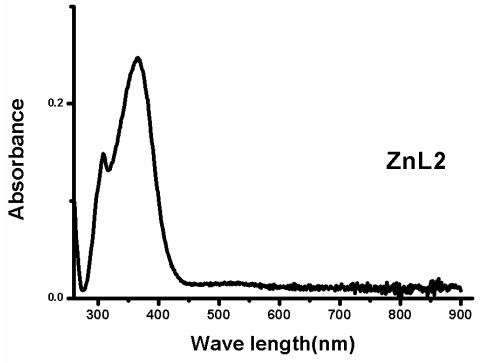

Fig. 3.6 (b): Uv-vis spectra of ZnL2

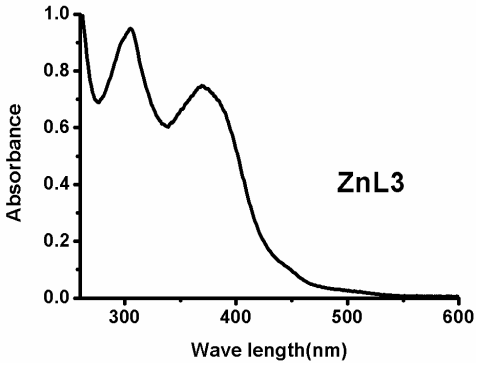

Fig. 3.6 (c): Uv-vis spectra of ZnL3

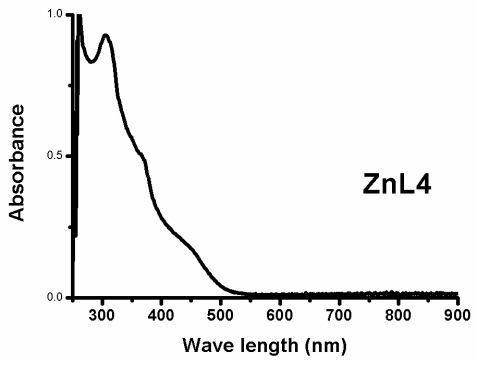

Fig. 3.6 (d): Uv-vis spectra of ZnL4

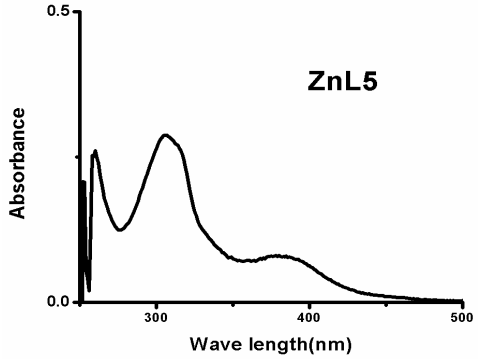

Fig. 3.6 (e): Uv-vis spectra of ZnL5

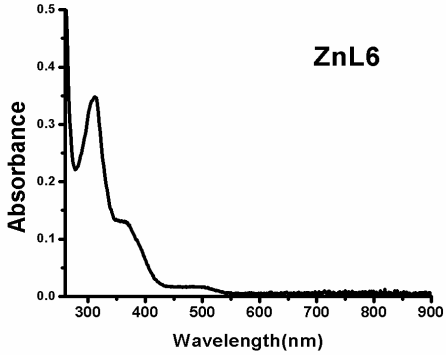

Fig. 3.6 (f): Uv-vis spectra of ZnL6

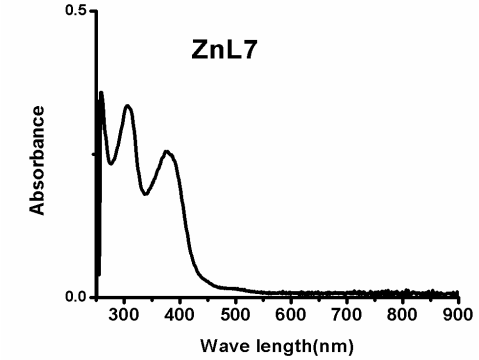

Fig. 3.6 (g): Uv-vis spectra of ZnL7

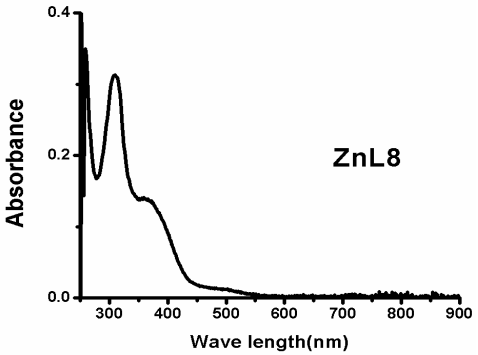

Fig. 3.6 (h): Uv-vis spectra of ZnL8

3.3.5 Electron paramagnetic resonance spectral analysis of copper complexes

The spectra in the polycrystalline state provide a good deal of information regarding the coordination environment around the copper (II) ion in these complexes. EPR magnetic measurements are related to complex structure, the number of ligands, and effect of bonding and spatial arrangements of the ligands around the central metal ion.

In the absence of magnetic field, copper(II) ion (d^9) has an effective spin of S = 1/2 and is associated with a spin angular momentum, $m_s = \pm 1/2$, leading to a doubly degenerate spin state. In presence of a magnetic field the degeneracy is splitted between these states and the energy difference between them is given by $\Delta E = h\nu = g\beta B$, where h is Planck's constant, ν is the microwave frequency for transition from $m_s = +½$ to $m_s = -½$, g is the Lande splitting factor equal to 2.0023 for a free electron, β is the Bohr magneton and B is the magnetic field.

EPR spectra can be mainly of three types

a) Isotropic spectrum: Single g value shows a cubic coordination environment. Enhanced spin lattice relaxation and dipolar interaction may cause broadening of signal.

b) Axial spectrum: At least three fold axis of symmetry in which $g_{\parallel}$ is obtained when the axis is aligned parallel to z axis. Signal due to $g_{\perp}$ is obtained when the axis is aligned perpendicular to z axis.

c) Rhombic spectrum: No axis of symmetry and hence three different g values are obtained[33].

In addition to these, hyperfine and super hyperfine lines which arise due to interaction with ^{14}N can also be used to interpret characteristic features about the coordination environment. The ^{14}N super hyperfine structure though not typically evidently seen in the parallel region is very clear in the perpendicular region. Theoretically, three peaks (triplet, with line intensities 1:1:1), five peaks (quintet, with line intensities 1:2:3:2:1), seven peaks (septet, with line intensities 1: 3:6:7:6:3:1) and nine peaks (nonet, with line intensities 1:4:10:16:19:16:10:4:1) can be solved for one, two, three and four equivalent nitrogen in super hyperfine multiplets respectively. However the circumstance is more convoluted in the experimental conditions. Explicit interpretation of this super hyperfine multiplet is not easy, because of the number of physical contributions to this region of the spectra. Also clarity in resolution of peaks may be absent, due to poor signal-to-noise ratio [34].

The geometric parameter G, which is a measure of the exchange interaction between the copper centers in the polycrystalline state is calculated using the equation,

for axial spectra $G = \frac{g_{||} - 2.0023}{g_{\perp} - 2.0023}$.

For rhombic spectra, $G = \frac{g3 - 2.0023}{g_{\perp} - 2.0023}$ where $g_{\perp} = \frac{(g_1 + g_2)}{2}$

If G > 4.4, exchange interaction is negligible and if G < 4.4 considerable exchange interaction is indicated in the solid state [35]. The EPR parameters $g_{||}$, $g_{\perp}$, $A_{||}$, $A_{\perp}$ and energies of d-d transitions were used to calculate the bonding parameters α^2, $\beta^2$and γ^2, which may be regarded as a measure of covalency of the in-plane σ bonds, in-plane π bonds and out-of-plane π bonds, respectively

The value of in-plane σ bonding parameter α^2 was estimated from the expression [36].

$$\alpha^2 = \frac{A}{0.036} + (g_{\parallel} - 2.0023) + \frac{3}{7}(g_{\perp} - 2.0023) + 0.04$$

β^2 and γ^2 were calculated using the equation

$$K_{\parallel} = \alpha^2\beta^2 \quad \text{and} \quad K_{\perp} = \alpha^2\gamma^2$$

The orbital reduction factors, $K_{\parallel}$ and $K_{\perp}$ were calculated using the given expressions

$$K_{\parallel}{}^2 = \frac{(g_{\parallel} - 2.0023)E_{d-d}}{8\lambda_0}$$

$$K_{\perp}{}^2 = \frac{(g_{\perp} - 2.0023)E_{d-d}}{2\lambda_0}$$

$E_{d\text{-}d}$ represents energy of d-d transition in cm^{-1}. λo represents the one electron spin orbit coupling constant which equals -828 cm^{-1}.

Hathaway has pointed out that, for pure sigma bonding, $K_{\parallel} \approx K_{\perp} \approx 0.77$ and for in plane σ -bonding, $K_{\parallel} < K_{\perp}$, while for out-of-plane σ -bonding $K_{\perp} < K_{\parallel}$. In all the synthesized copper complexes it is seen that $K_{\parallel} > K_{\perp}$, which indicate that complexes have strong out of -plane π-bonding. The α^2 values for the complexes were calculated and since the obtained values lie in between 0.5 and 1.0, it is inferred that the metal-ligand bonds in the complexes are partially ionic and partially covalent in nature. The values of bonding parameters α^2, β^2, γ^2 which is less than unity due to the extended delocalization of metal electrons due to metal ligand bonding, confirm the covalent nature of complexes [37].

The empirical factor $f = g_{\parallel}/A_{\parallel}$ is an index of tetragonal distortion and the value depends on the nature of coordinated atom. All the Cu (II)

complexes have medium distortion as their f values are between 105-130cm indicating tetragonal distortions for geometry [38].

The EPR spectra of the polycrystalline copper samples at 298K, DMF solution at 298 and 77 K were recorded in the X-band, using 100 kHz modulaton; g factors were quoted relative to the standard marker TCNE (g = 2.00277).The EPR spectra are simulated using EasySpin package [39] and the experimental (red) and simulated (blue) best fits are included.

Table 3.11 EPR data of CuL1, CuL2, CuL3, CuL4, CuL5, CuL6 and CuL7 at 298 K

Polycrystalline state at 298 K							
	CuL1	CuL2	CuL3	CuL4	CuL5	CuL6	CuL7
g_{iso}	2.123		2.122	2.132			2.11
$g\|\|/g_3$	-	2.282	-	-	2.26	2.281	-
$g\perp/g_1$, g_2	-	2.103	-	-	2.045, 2.07	2.09	-
g_{av}	-	2.34	-	-	2.120	2.156	-
G/R	-	2.77	-	-	0.204	3.17	-

Table 3.11 gives the EPR parameters of copper complexes at 298 K and the spectra are given in fig.3.7 (a-g). In polycrystalline state at 298 K, complexes CuL1, CuL3, CuL4 and CuL7 gave one broad isotropic signal with one g_{iso} values which is due to extensive exchange coupling through misalignment of the local molecular axes between molecules in the unit cell (dipolar broadening) and better spin lattice relaxation. No much information is obtained about the electronic ground state of complex from this kind of spectra. CuL2 and CuL6 gave axial spectra with well-defined $g_{\|}$ and $g_{\perp}$ values. Spectrum is broad due to fast spin lattice relaxation and exchange coupling. Hyperfine splitting was not clear both in parallel and perpendicular regions even if axial features are displayed due to magnetic concentrated sample. G value of 2.7 and 3.1 for CuL2 and CuL6 respectively corresponds to strong exchange interaction with $d_{x^2-y^2}$ ground state.

EPR spectra of complex CuL5 recorded in polycrystalline state gave three g different values which are in accordance with rhombic distortion geometry.

Fig 3.7(a-g): EPR spetra of CuL1, CuL2, CuL3, CuL4, CuL5, CuL6 and CuL7 at 298 K

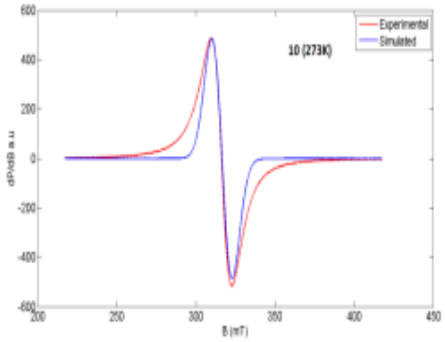

Fig. 3.7(a): EPR spectrum of CuL1 at 298K

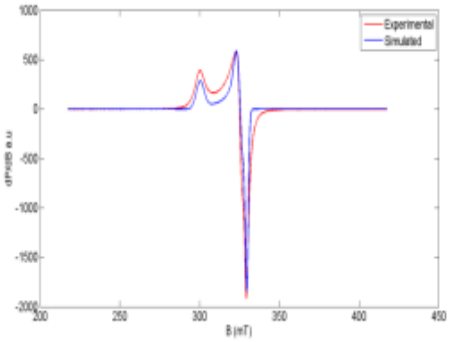

Fig. 3.7(b): EPR spectrum of CuL2 at 298K

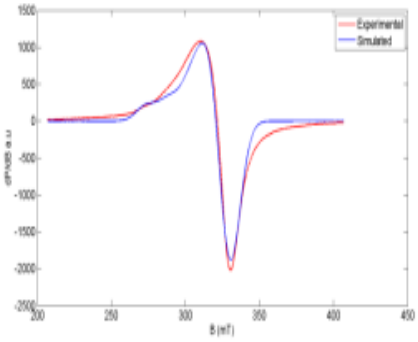

Fig. 3.7(c): EPR spectrum of CuL3 at 298K

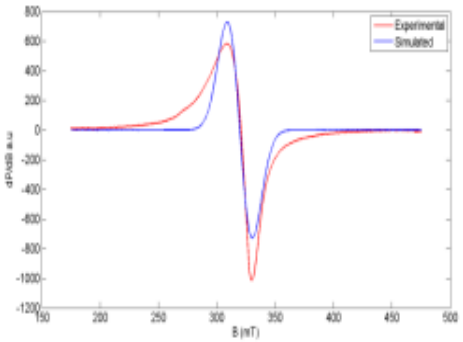

Fig. 3.7(d): EPR spectrum of CuL4 at 298K

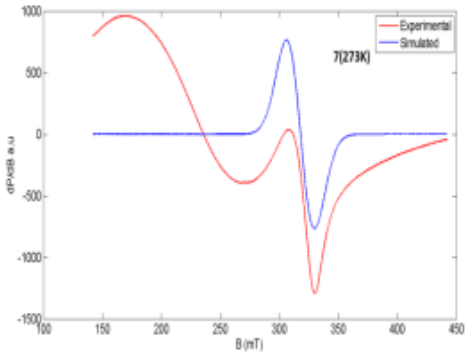

Fig. 3.7(e): EPR spectrum of CuL5 at 298K

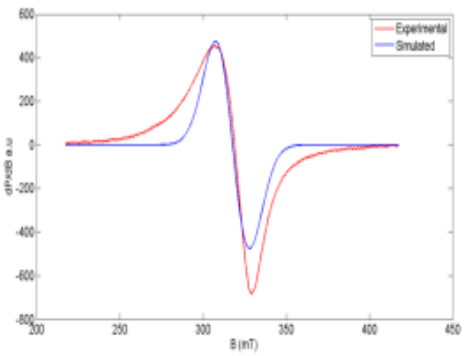

Fig. 3.7(f): EPR spectrum of CuL6 at 298K

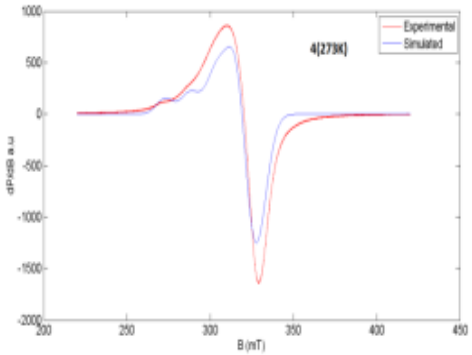

Fig. 3.7(g): EPR spectrum of CuL7 at 298K

Table 3.12 EPR data of CuL1, CuL2, CuL3, CuL4, CuL5, CuL6 and CuL7 at 77K

	Solution state at 77 K						
	CuL1	**CuL2**	**CuL3**	**CuL4**	**CuL5**	**CuL6**	**CuL7**
$g\|\|/g_3$	2.290	2.221	2.283	2.23	2.246	2.283	2.282
$g\perp/g_1, g_2$	2.07	2.036	2.064	2.06	2.04, 2.076	2.064	2.064
G/R	4.33	6.489	4.54	4.54	0.1739	3.19	4.54
$A\|\|(cm^{-1})^a$	198.6	177.0	192.6	194.7	189	192.6	197.3
$A\perp(cm^{-1})^a$	-	14	-	-	15	-	-
α^2	0.909	0.764	0.889	0.87	0.798	0.882	0.895
β^2	0.849	0.827	0.853	0.875	0.892	0.864	0.865
$\gamma 2$	0.835	0.683	0.800	0.82	0.853	0.810	0.812
K||	0.762	0.667	0.757	0.707	0.712	0.712	0.674
K⊥	0.719	0.5237	0.715	0.628	0.681	0.684	0.527
f(cm)	115	125	117	118	125	118	115

[a]A values in 10^{-4} cm^{-1}

Table 3.12 gives EPR parameters in frozen state at 77K. Fig.3.8 (a-g) gives EPR spectra of CuL1, CuL2, CuL3, CuL4, CuL5, CuL6 and CuL7 at 77K. The EPR spectra of the complexes recorded in frozen state at 77 K gives more information on the geometry of the complexes. All complexes except CuL5 display well-resolved axial anisotropy with hyperfine splitting in the parallel region resulting from coupling of the electron spin with ^{63}Cu nucleus

spin (I = 3/2).The tendency of g values g|| >g⊥> 2.0023 observed for the complexes indicates that the unpaired electron most likely resides in the $d_{x^2-y^2}$ orbital which propose distorted octahedral geometry. CuL5 displays a rhombic spectrum in frozen state with three distinct g values. Since it is a hexacoordinated complex, the lowest g > 2.04 indicates copper (II) in elongated rhombic octahedral symmetry.

The possibility of the formation of dimer is ruled out as there is no signal in the half field spectrum. Magnetic moment values (1.59-1.9 B.M) also confirms the mononuclearity of the complexes [40].

Kievelson and Nieman reported that $g_{\|}$ value less than 2.3 indicate considerable covalent character to M-L bond. Here for all complexes $g_{\|} < 2.3$ indicate considerable covalent character for M-L bond. Geometrical parameter G for axial spectra value for CuL6 is less than 4 which indicate strong exchange interactions. For all other complexes $g_{\|} > 2.3$ which indicate negligible exchange coupling. For pentacoordinated complexes CuL2 and CuL7, g values are in the order $g_{\|} > g\perp > 2.0023$. This indicates square pyramidal geometry which is supported by magnetic moment data and rules out the possibility of a trigonal bipyramidal structure which would be expected to have $g\perp > g_{\|}$.

For all Cu (II) it is observed that orbital reduction factors, $K_{\|} > K\perp$ which indicate that complexes have strong out of plane π-bonding. The bonding parameters α^2, β^2 and γ^2 can calculated and they can be considered as measures of covalency of the in-plane σ bonds, in-plane π bonds and out-of plane π bonds respectively. Since calculated α^2 values lie in between 0.5 and 1.0, it can be inferred that the metal-ligand bonds in the complexes are partially ionic and partially covalent in nature. The values of bonding parameters α^2, β^2, γ^2 which is less than unity due to the extended delocalization of metal electrons due to metal ligand bonding, confirm the covalent nature of complexes [41]. The empirical factor $f = g_{\|}/A_{\|}$ is an index of

tetragonal distortion and the value depends on the nature of coordinated atom. All the Cu (II) complexes have medium distortion as their f values are between 105-130 cm indicating medium tetragonal distortions for geometry [42].

Fig 3.8(a-g): EPR spectra of CuL1, CuL2, CuL3, CuL4, CuL5, CuL6 and CuL7 at 77 K

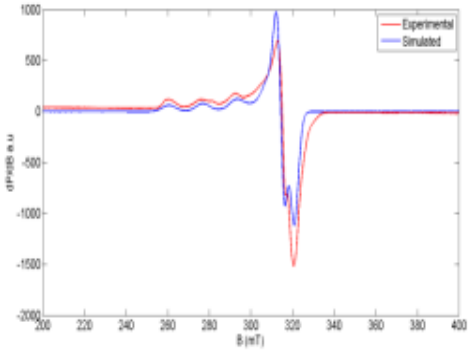

Fig 3.8(a): EPR spectra of CuL1 at 77K

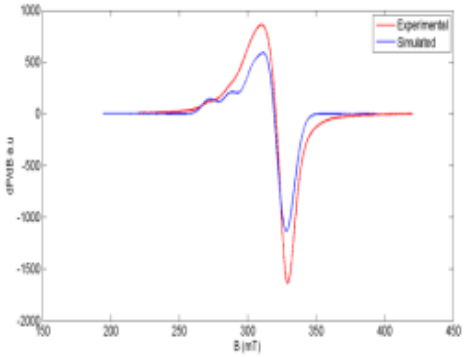

Fig 3.8(b): EPR spectra of CuL2 at 77K

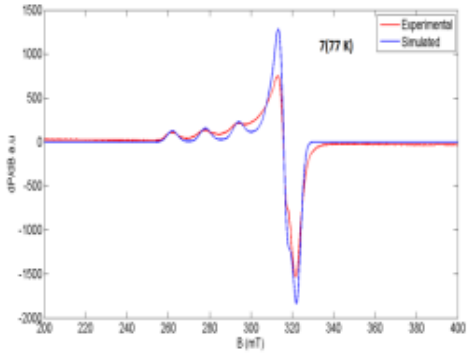

Fig 3.8(c): EPR spectra of CuL3 at 77K

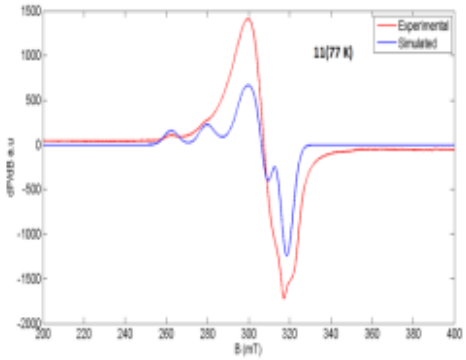

Fig 3.8(d): EPR spectra of CuL4 at 77K

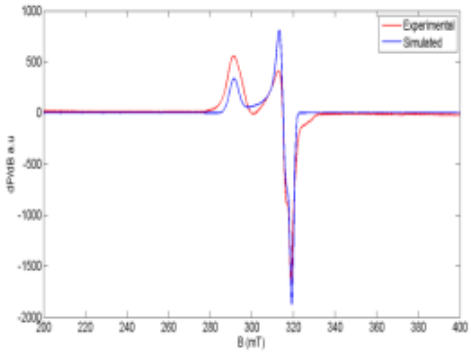

Fig 3.8(e): EPR spectra of CuL5 at 77K

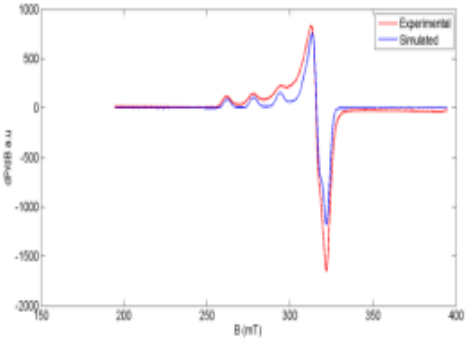

Fig 3.8(f): EPR spectra of CuL6 at 77K

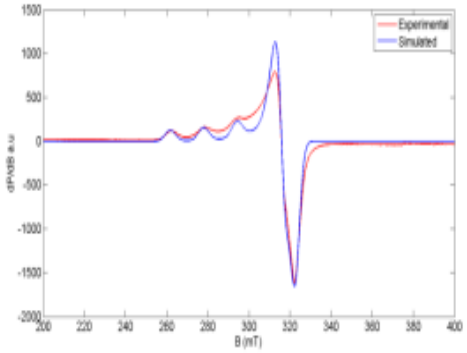

Fig 3.8(g): EPR spectra of CuL7 at 77K

3.3.6 Thermogravimetric analysis of complexes

TG-DTG analyses of the complexes were carried out under nitrogen at a heating rate of 10 °C min^{-1} in the 50-800 °C range. Thermo gravimetric analysis give useful insight into nature of water or solvent molecule in the inner or outer coordination sphere of metal complexes.TG-DTG also help us to detect oxidation, decomposition and physical process like vaporization, sublimation and desorption. It helps us to distinguish between the coordinated water and lattice water molecule. According to the literature reports, weight loss for lattice water is between 50-120 °C and coordinated water is between 130-250 °C [43]. All the complexes have similar thermo grams.

3.3.6.1 TG/DTG analysis of nickel complexes

Table 3.13 gives the thermo gravimetric data of Ni (II) complexes and fig. 3.9(a-f) gives the TG/DTG of Ni (II) complexes. Among Ni (II) complexes NiL2 and NiL5 left metal oxide residue after complete decomposition. All other complexes showed incomplete decomposition owing to their higher thermal stability. For all complexes, 60-120 °C, there is the loss of lattice water. Between 120 – 400 °C there is the loss, coordinated water, acetate group and methoxy group of the ligand moiety. After 400 ° C organic part of the complex is lost in multiple steps.

Table 3.13 Thermo gravimetric data of NIL1, NiL2, NiL3, NiL5, NiL6, and NiL7

Compound	Temperature (°C)	Fragment lost	Weight %loss Found (calc.)
NiL1[$NiL_1(OAc)(H_2O)_2$].H_2O	60-120	H_2O	3.9(4.1)
	120-250	$2H_2O$+ OMe	14.73(14.33)
	240-330	OAc	12.3(11.9)
	350-550	$C_6H_5N_2$	24.7(24.6)
NiL2[$NiL_2(OAc)(H_2O)_2$].H_2O	90-105	H_2O	3.2(3.4)
	120-300	$2H_2O$ +OAc	20.7(20.6)
	320-650	$C_{16}H_{14}N_2O_3$	61.42(61.9)
NiL3[$NiL_3(OAc)(H_2O)$].0.5 H_2O	90-105	0.5 H2O	1.7(1.94)
	110-235	$2H_2O$+ OMe	13.9(14.5)
	250-330	OAc	11.8(12.02)
	330-565	$C_9H_8N_2O$	34.2(34.5)
NiL5[$NiL_5(OAc)(H_2O)$]. H_2O	80-120	H_2O	4.2(4.0)
	120-300	H_2O +OAc	16.2(16.2)
	310-615	$C_{17}H_{16}N_2O_2$	61.4(61.3)
NiL6[$NiL_6(OAc)(H_2O)_2$]. H_2O	80-205	$3H_2O$+ OMe	15.9(15.7)
	120-315	OAc	10.80(10.99)
	310-500	C_5H_3BrN	29.8(29.3)
NiL7[$NiL_7(OAc)(H_2O)_2$]. H_2O	40-110	H_2O	3.6(3.6)
	125-316	$2H_2O$+OMe +OAc	24.73(25.03)
	310-585	$C_9H_8N_2O$	31.4(31.2)

Fig.3.9 (a-f): TG /DTG of NiL1, NiL2, NiL3, NiL5, NiL6, NiL7

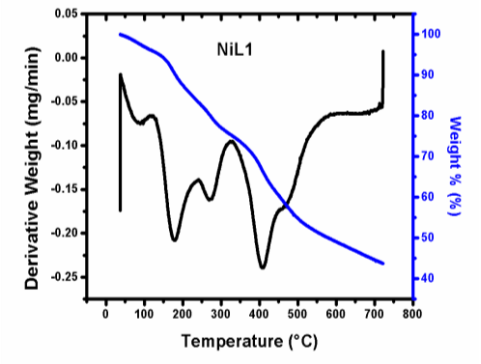

Fig. 3.9 (a): TG /DTG of NiL1

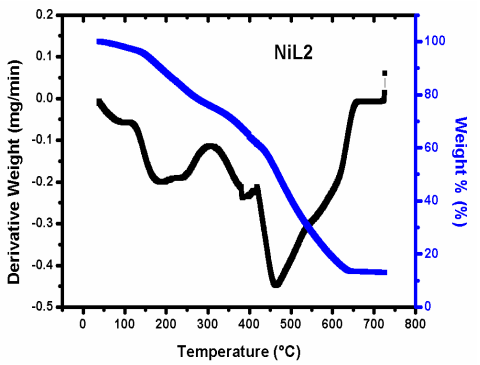

Fig. 3.9 (b):TG /DTG of NiL2

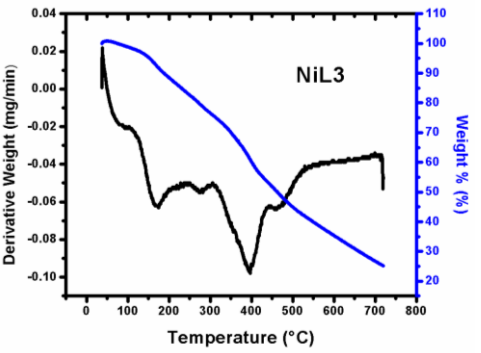

Fig. 3.9 (c): TG /DTG of NiL3

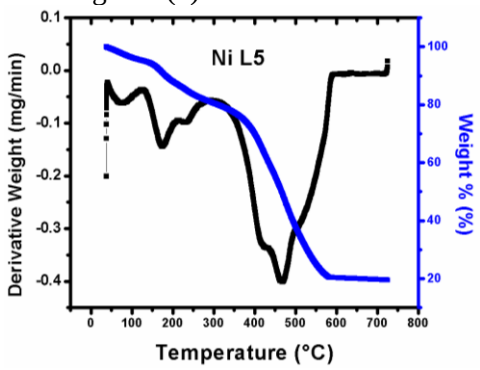

Fig. 3.9 (d):TG /DTG of NiL5

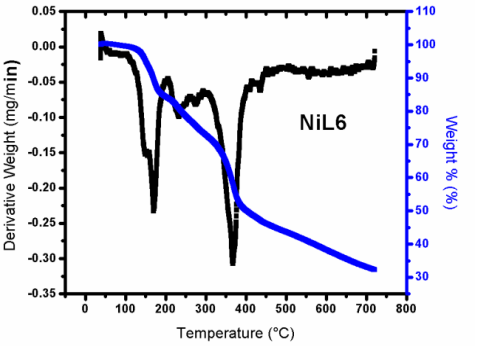

Fig. 3.9 (e):TG /DTG of NiL6

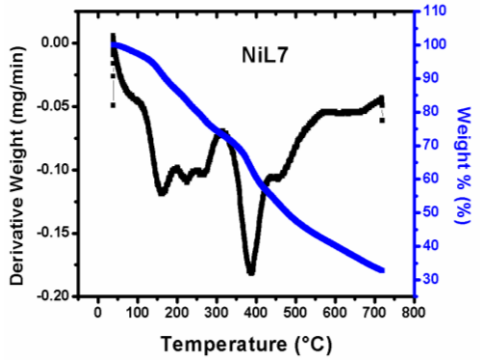

Fig. 3.9 (f):TG /DTG of NiL7

3.3.6.2 TG/DTG analysis of copper complexes

Among Cu (II) complexes, only for CuL7 decomposition is complete, leaving behind metal oxide residue. All other complexes decompose above

700°C gradually to form metal oxides. For all complexes upto 400°C there is the loss of lattice water, coordinated water, acetate group and methoxy group of the ligand moiety. After 400° C organic part of the complex is lost in multiple steps. Table 3.14 gives the thermogravimetric analytical data of copper complexes. Fig. 3.10(a-g) gives TG/DTG of copper complexes.

Table 3.14: TG/DTG data of CuL1, CuL2, CuL3, CuL4, CuL5, CuL6 and CuL7

Compound	Temperature (°C)	Fragment lost	Weight %loss Found(calc.)
CuL1[$CuL_1(OAc)(H_2O)_2$].½DMF	30-120	0.5 DMF	7.46(7.66)
	120-219	$2H_2O$+OAc	20.5(20.9)
	219-290	OCH_3	7.2(7.36)
	320-500	$C_7H_8N_2O$	36.3(36.6)
CuL2[$CuL_2(OAc)(H_2O)$].DMF. ½H_2O	100-280	$2.5H_2O$+DMF	21.2(22)
	300-460	OMe+OAc	19.3(19.2)
CuL3[$CuL_3(OAc)(H_2O)_2$].½H_2O	50-110	0.5 H_2O	1.85(1.9)
	110-210	$2H_2O$ +OCH_3	14.38(14.65)
	215-483	OAc+ $C_7H_7N_2$	38.13(37.9)
CuL4[$CuL_4(OAc)(H_2O)_2$].½H_2O	60-105	0.5 H_2O	1.9(1.99)
	110-200	$2H_2O$ +OCH_3	11.0(10.9)
	220-297	OAc	14.18(13.66)
	300-445	$C_6H_5N_2$	24.66(24.5)
	450-690	C_3HO_2	15.84(15.4)
CuL5[$CuL_5(OAc)(H_2O)_2$]	110-190	$2H_2O$ +OCH_3	15.1(14.7)
	200-275	OAc	12.2(12.9)
	280-450	C_9H_4O	29.1(29.2)
CuL6[$CuL_6(OAc)(H_2O)_2$]. H_2O	60-110	H_2O	3.1(3.2)
	110-225	$2H_2O$+OMe	11.7(12.30
	250-350	OAc	9.7(10.1)
	280-450	C_7H_6O	19.1(19.5)
	450-715	C_3H_5BrN	24.2(24.1)
CuL7[$CuL_7(OAc)(H_2O)$]. H_2O	40-120	H_2O	3.5(3.8)
	125-320	H_2O+OAc+OMe	24.5(25.2)
	375-650	$C_{17}H_{12}N_2O$	60.3(60.1)

Fig. 3.10(a-g): TG/DTG of CuL1, CuL2, CuL3, CuL4, CuL5, CuL6 and CuL7

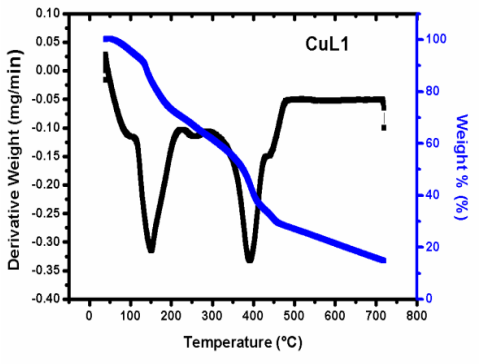

Fig.3.10 (a): TG /DTG of CuL1

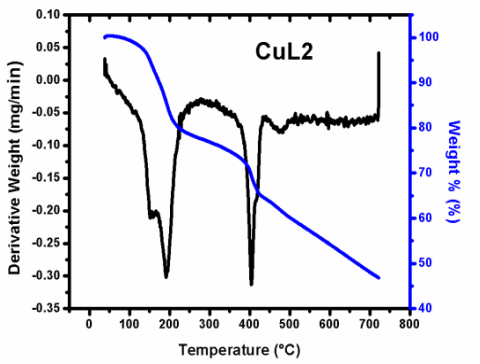

Fig. 3.10(b):TG /DTG of CuL2

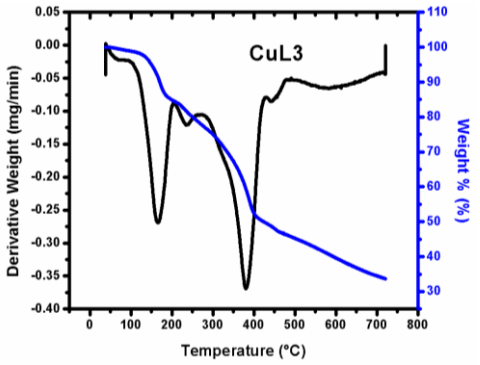

Fig.3.10(c):TG /DTG of CuL3

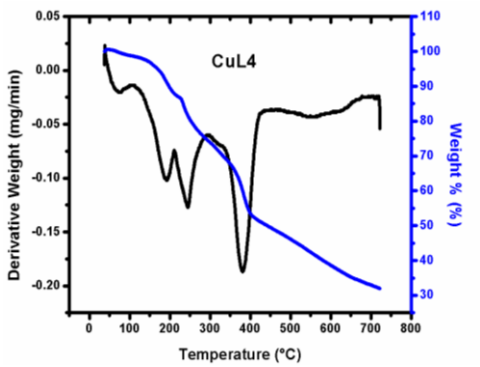

Fig.3.10(d):TG /DTG of CuL4

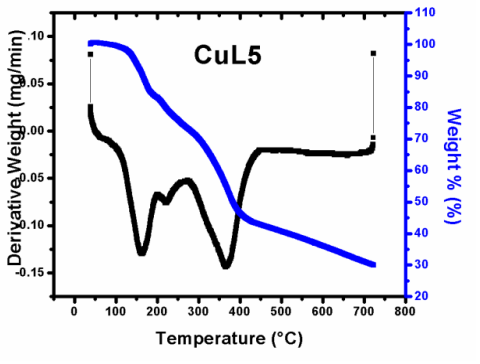

Fig. 3.10(e): TG /DTG of CuL5

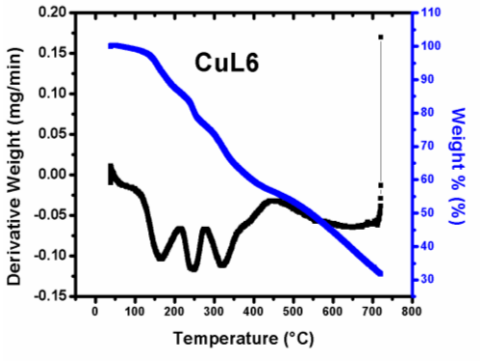

Fig.3.10(f):TG /DTG of CuL6

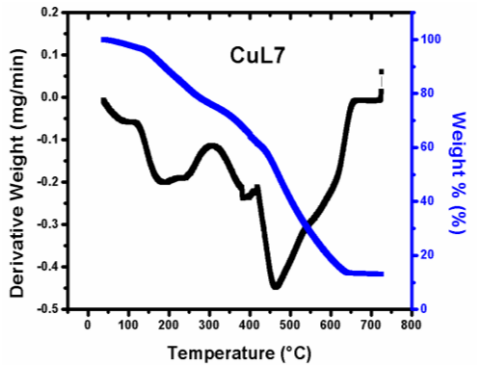

Fig. 3.10(g): TG /DTG of CuL7

3.3.6.3 TG/DTG analysis of zinc complexes

Among Zinc complexes, only ZnL2 decomposed completely to leave metal oxide as the residue. All complexes exhibited a weight loss at 80-120 °C which corresponds to lattice water and at 120-400 °C corresponds to the combined weight loss of acetate group, methoxy group and the coordinated water.Table3.15 gives the thermo gravimetric data of zinc complexes and fig. 3.11(a-h) show the TG/DTG curves of Zn (II) complexes.

Table 3.15: TG/DTG data of ZnL1, ZnL2, ZnL3, ZnL4, ZnL5, ZnL6, ZnL7 and ZnL8

Compound	Temperature (°C)	Fragment lost	Weight %loss Found(calc.)
ZnL1 [ZnL1(OAc)$(H_2O)_2$]. H_2O	80-200	$3H_2O$+ OMe	17.93(18.48)
	220-300	OAc	12.82(13.0)
	310-455	$C_8H_6N_2O$	29.3(29.23)
ZnL2**[**ZnL2(OAc)$(H_2O)_2$].H_2O.MeOH	100-150	MeOH	4.7(5.02)
	250-320	$3H_2O$+OMe+OAc	25.99(26.03)
	400-600	$C_{15}H_8N_3O_3$	51.6(51.9)
ZnL3[ZnL_3(OAc)$(H_2O)_2$].½H_2O	50-100	0.5 H_2O	1.6(1.9)
	110-170	$2H_2O$	6.95(6.8)
	170-265	OAc	12.9(13.0)
	270-450	$C_6H_6N_2$	23.2(22.9)
ZnL4 [ZnL4(OAc)$(H_2O)_2$]	120-200	$2H_2O$+OMe	15.19(15.61)
	200-300	OAc	13.3(13.0)
	320-492	$C_8H_6N_2$	28.57(28.4)
ZnL5[ZnL5(OAc)(H_2O)]. H_2O	80-120	H_2O	3.8(3.9)
	250-320	H_2O+OAc	16.82(16.66)
	320-382	OMe	7.2(7.9)
	400-515	$C_8H_6N_2$	27.1(28.1)
ZnL6**[**ZnL6(OAc)$(H_20)_2$]. H_2O	60-120	H_2O	3.2(3.2)
	120-200	$2H_2O$	6.5(6.5)
	200-385	OAc+ $C_9H_9N_2$	33.8(33.5)
	400-712	C_6H_4O	16.3(16.9)
ZnL7**[**ZnL7(OAc)$(H_2O)_2$]. H_2O	50-110	H_2O	3.2(3.5)
	125-280	$2H_2O$	7.3(7.99)
	375-650	OAc+$C_6H_6N_2$	33.2(33.6)
ZnL8**[**ZnL8(OAc)(H_2O)]. H_2O	90-140	H_2O	3.72(3.96)
	150-240	H_2O+OMe	14.3(14.9)
	250-540	OAc+$C_7H_5N_2$	40.9(40.2)

Fig. 3.11(a-h): TG/DTG curves of ZnL1, ZnL2, ZnL3, ZnL4, ZnL5, ZnL6, ZnL7 and ZnL8

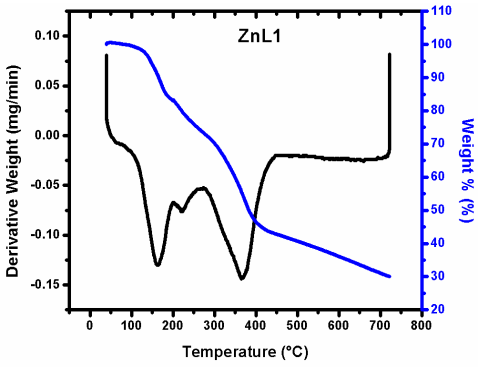

Fig.3.11(a): TG/DTG of ZnL1

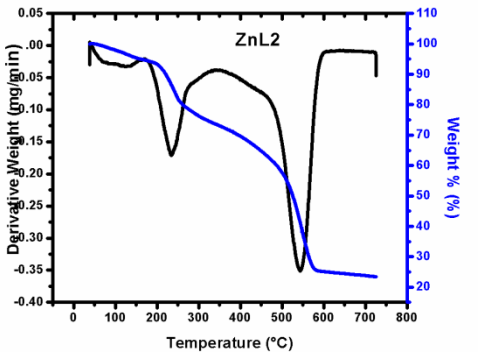

Fig.3.11(b): TG/DTG of ZnL2

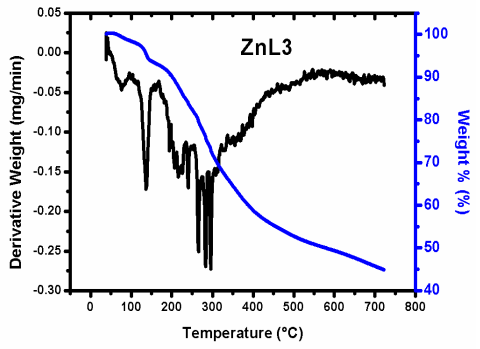

Fig. 3.11(c): TG/DTG of ZnL3

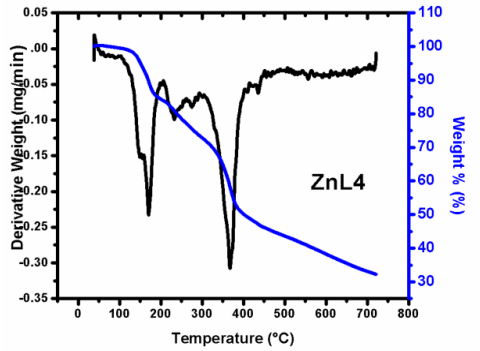

Fig. 3.11(d): TG/DTG of ZnL4

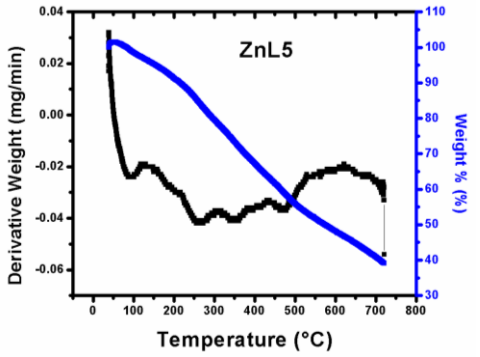

Fig. 3.11(e): TG/DTG of ZnL5

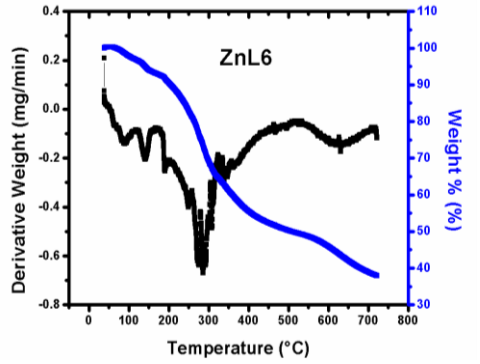

Fig. 3.11(f): TG/DTG of ZnL6

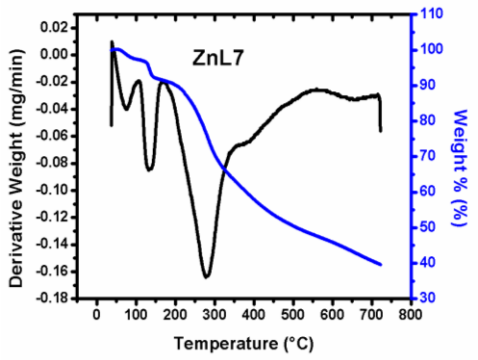

Fig. 3.11(g): TG/DTG of ZnL7

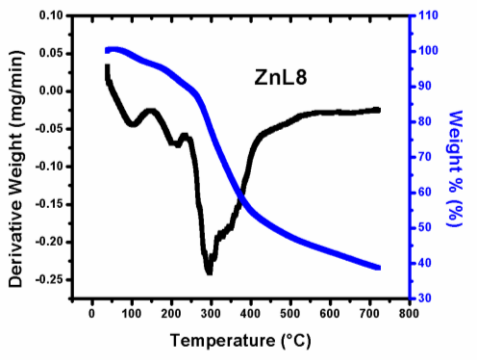

Fig. 3.11(h): TG/DTG of ZnL8

3.3.7 ^{1}H NMR measurement of zinc complexes

The ^{1}H NMR spectra of the Zn (II) complexes were recorded in DMSO d^{6} with reference to TMS. A singlet in the region of 1.8–2.0 ppm indicate acetyl methyl group. Singlet for methoxy protons was present in the region of δ 3.5–3.7 ppm. Presence of -OCH_3 in complexes can be confirmed by singlet at 5.6–5.8 δ values for proton at C-2. Absence of doublet discernible at δ 12 ppm in ligand was absent in spectra of complexes which indicate the coordination of NH proton. The remaining protons of chromanone and protons of pyridine moieties were present in the form of multiplets at δ 6.84–7.66. Proton NMR spectra of other paramagnetic complexes were not recorded.

Fig. 3.12(a-h) gives the proton NMR spectra of zinc complexes and table 3.16 gives the chemical shift assignments.

Table 3.16: ^{1}H NMR spectral data of ZnL1, ZnL2, ZnL3, ZnL4, ZnL5, ZnL6, ZnL7 and ZnL8

Complex	Chemical shift δ(ppm)	Assignments
ZnL1	1.829	C**H**$_3$,3H, s
	3.512	OC**H**$_3$,3H,s
	5.973	O-C**H**-O,1H,s
	6.4-8.9	Aromatic protons,8H,m
	7.78	C**H**, 1H, s

ZnL2	1.829	C**H**$_3$, 3H, s
	3.539	OC**H**$_3$, 3H, s
	5.44	O-C**H**-O,1H, s
	6.9 - 9.01	Aromatic protons,7H, m
	7.75	C**H**, 1H, s
ZnL3	1.829	C**H**$_3$, 3H, s
	2.07	C**H**$_3$, 3H, s
	3.53	OC**H**$_3$,3H, s
	5.7	O-C**H**-O, 1H, s
	6.9 – 9.1	Aromatic protons 7H, m
	8.25	C**H**, 1H, s
ZnL4	1.832	C**H**$_3$, 3H, s
	3.58	OC**H**$_3$,3H,s
	5.44	O-C**H**-O,1H,s
	6.8- 8.4	Aromatic protons, 8H,m
	8.3	C**H**, 1H, s
ZnL5	1.984	C**H**$_3$, 3H, s
	2.29	CH$_3$, 3H, s
	3.01	OC**H**$_3$,3H, s
	5.73	O-C**H**-O, 1H, s
	6.8-8.5	Aromatic protons 7H, m
	8.3	C**H** ,1H,s
ZnL6	1.832	C**H**$_3$, 3H, s
	2.29	C**H**$_3$, 3H, s
	3.51	OC**H**$_3$,3H, s
	5.9	O-C**H**-O, 1H, s
	6.7-8.2	Aromatic protons 6H, m
	8.26	C**H** ,1H,s
ZnL7	1.829	C**H**$_3$, 3H, s
	2.319,	C**H**$_3$, 3H, s
	2.379	C**H**$_3$, 3H,s
	3.512,	OC**H**$_3$,3H, s
	5.704	O-C**H**-O, 1H, s
	6.7-8.3	Aromatic protons 6H, m
	8.31	C**H** ,1H, s
ZnL8	1.84	C**H**$_3$, 3H,s
	2.29	C**H**$_3$, 3H, s
	3.44	OC**H**$_3$,3H, s
	5.58	O-C**H**-O, 1H, s
	6.8-8.3	Aromatic protons 7H, m
	8.29	C**H** ,1H,s

Fig.3.12(a-h): ^{1}H NMR spectra of ZnL1, ZnL2, ZnL3, ZnL4, ZnL5, ZnL6, ZnL7 and ZnL8

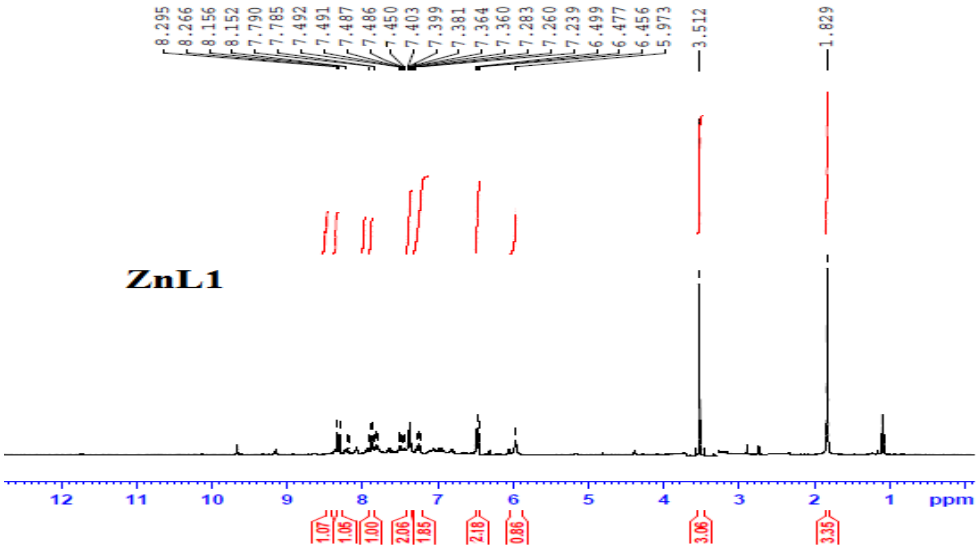

Fig. 3.12(a): ^{1}H NMR spectra of ZnL1

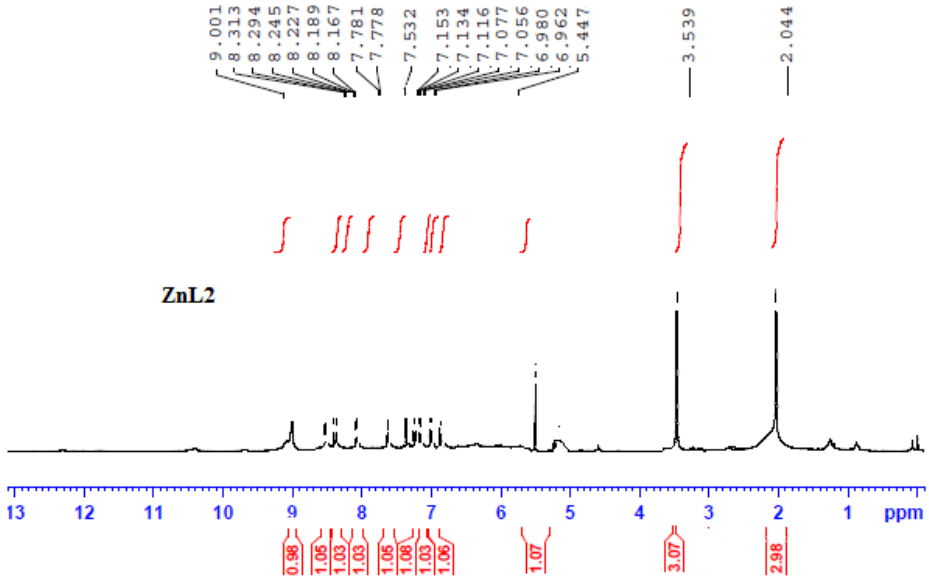

Fig. 3.12(b): ^{1}H NMR spectra of ZnL2

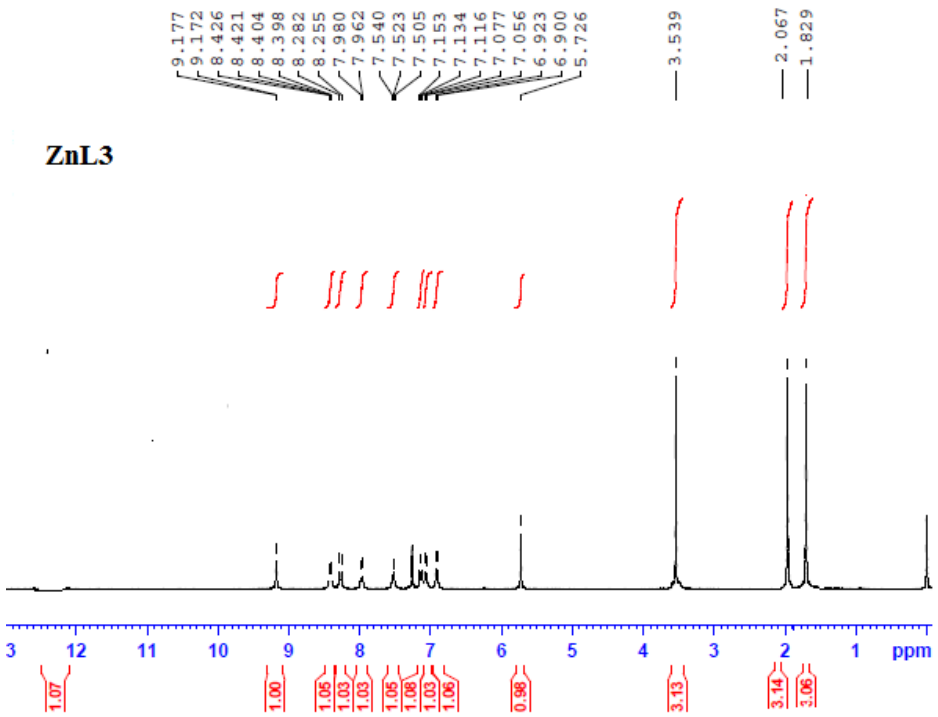

Fig. 3.12(c): ^{1}H NMR spectra of ZnL3

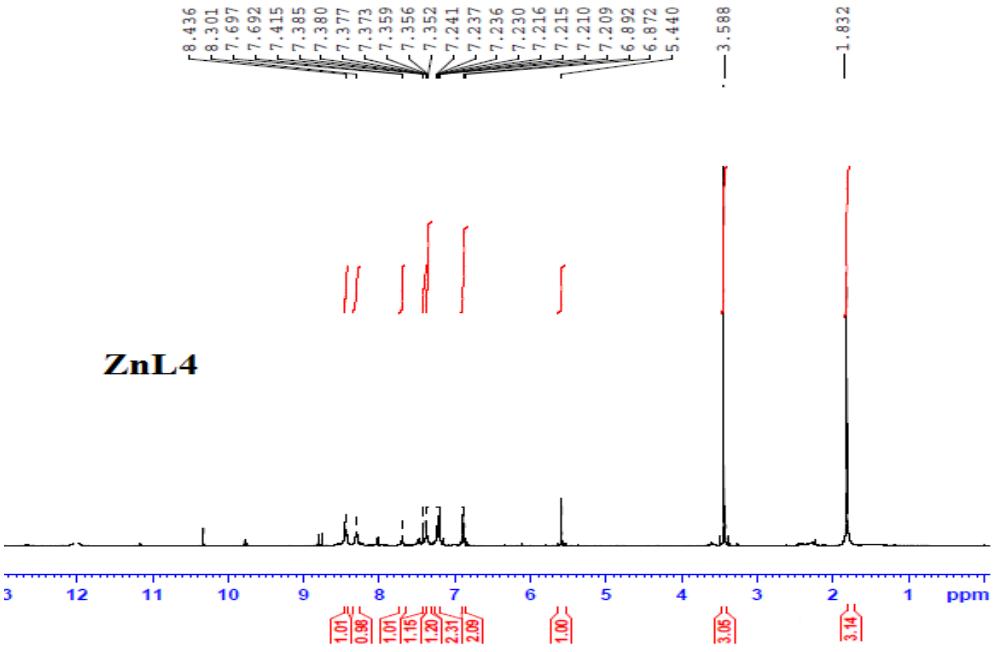

Fig. 3.12(d): ^{1}H NMR spectra of ZnL4

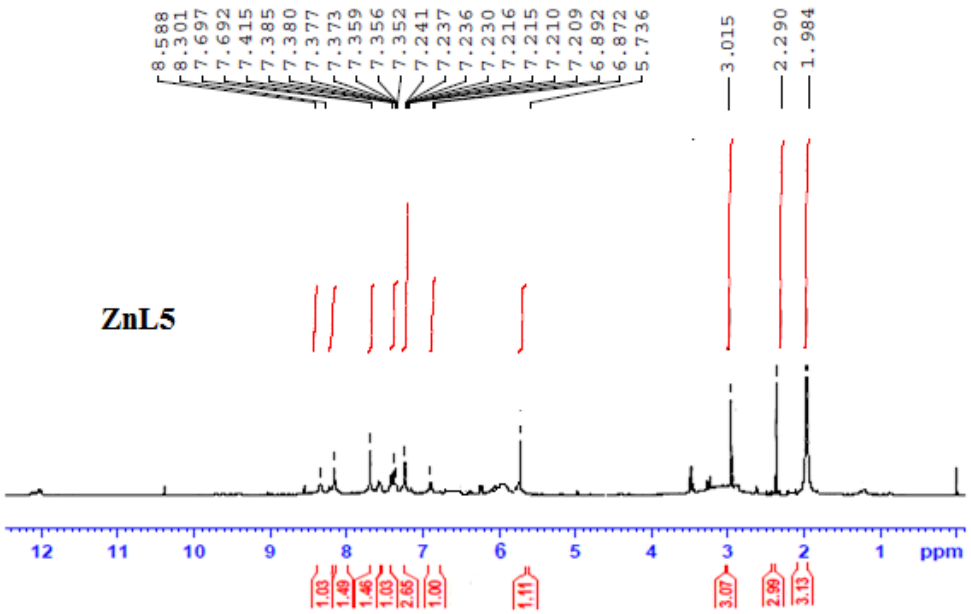

Fig. 3.12(e): ^{1}H NMR spectra of ZnL5

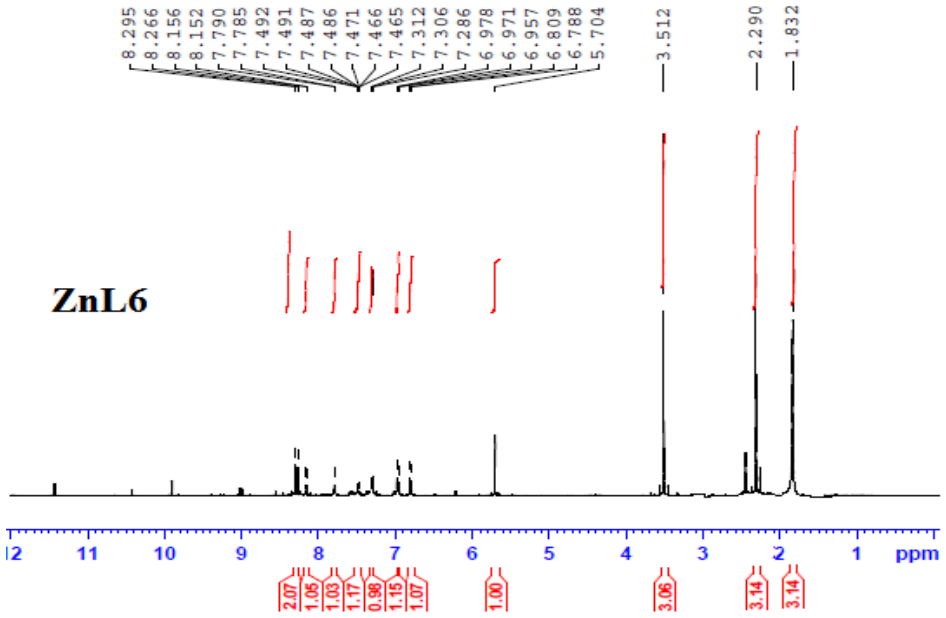

Fig. 3.12(f): ^{1}H NMR spectra of ZnL6

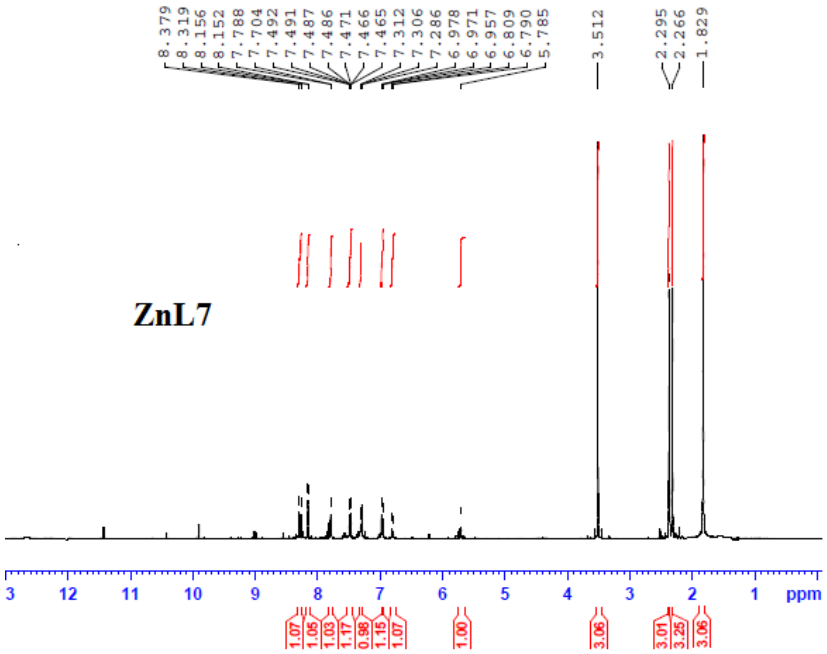

Fig. 3.12(g): ^{1}H NMR spectra of ZnL7

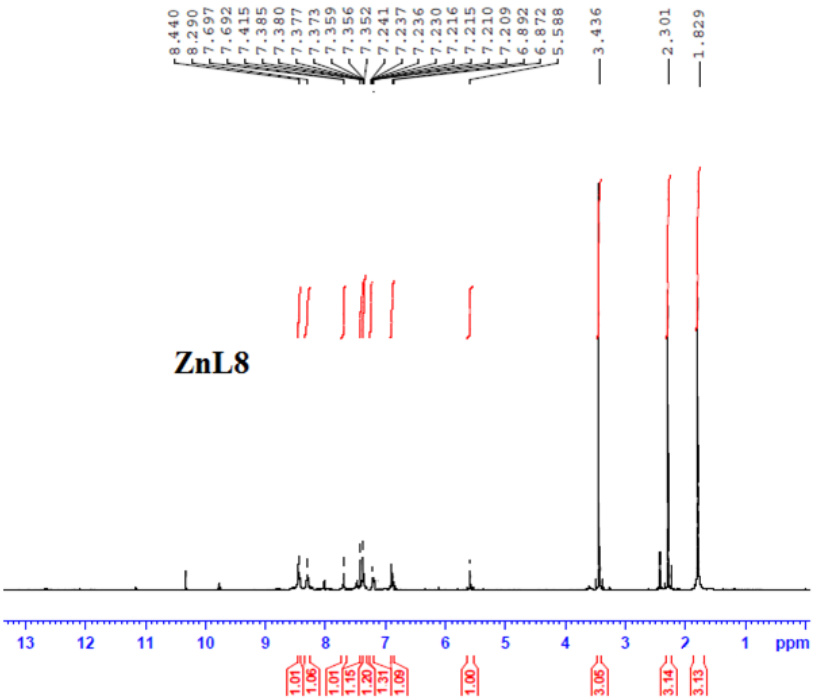

Fig. 3.12(h): ^{1}H NMR spectra of ZnL8

In the light of the above interpretation of elemental and thermal analyses in addition to spectral data as well as magnetic susceptibility measurements at room temperature and conductivity measurements, structures are proposed for the metal complexes. Fig.3.13 give the proposed structures of Ni (II) complexes, fig. 3.14 give the structures for Cu (II) complexes and fig.3.15 give the structures for Zn (II) complexes

Fig.3.13: Proposed structures of NiL1, NiL2, NiL3, NiL5, NiL6, NiL7

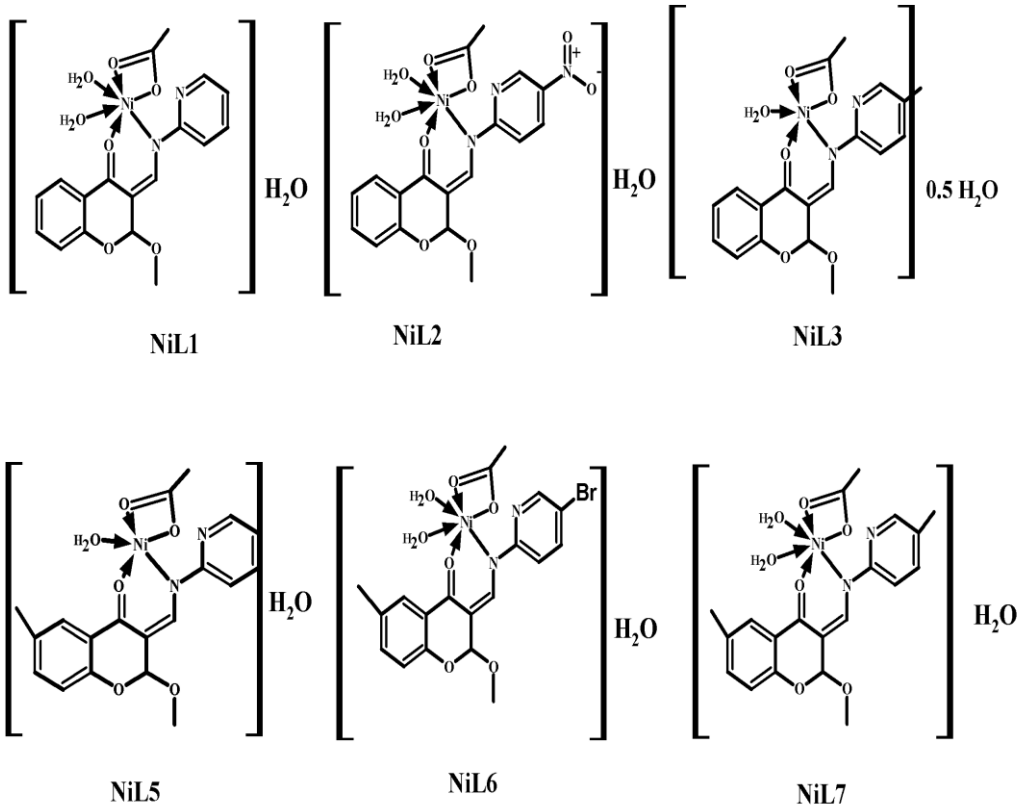

NiL1 NiL2 NiL3

NiL5 NiL6 NiL7

Fig.3.14: Proposed structures of CuL1, CuL2, CuL3, CuL4, CuL5, CuL6, CuL7

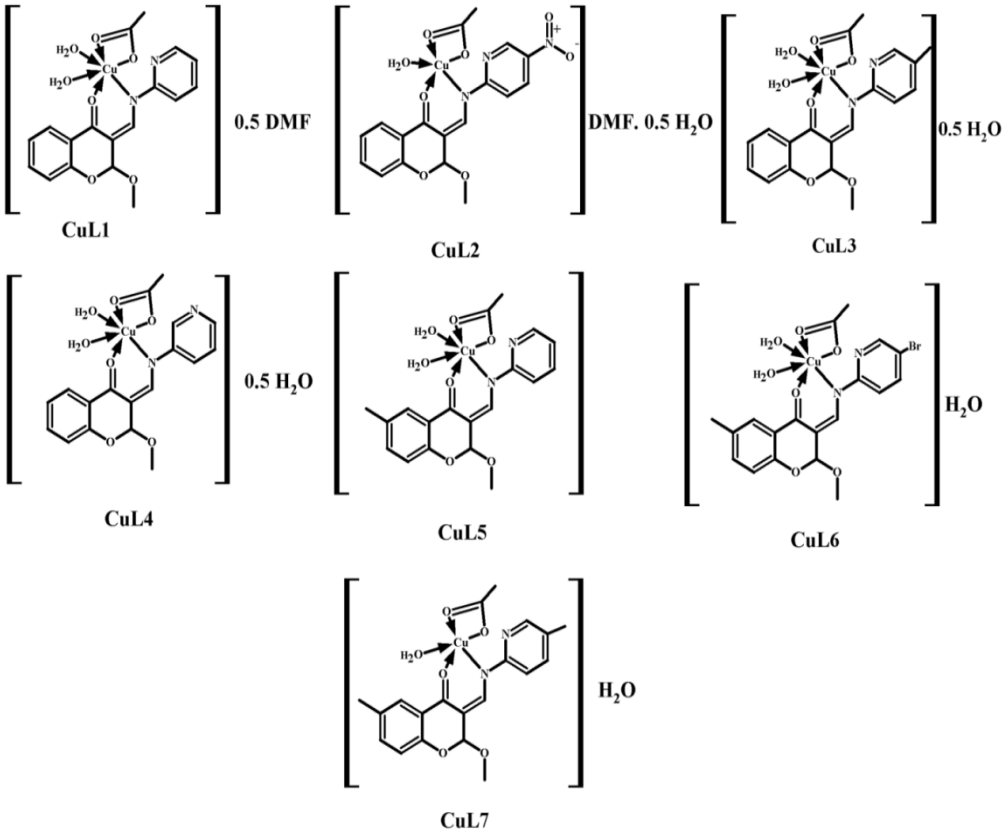

Fig.3.13: Proposed structures of ZnL1, ZnL2, ZnL3, ZnL4, ZnL5, ZnL6, ZnL7 and ZnL8

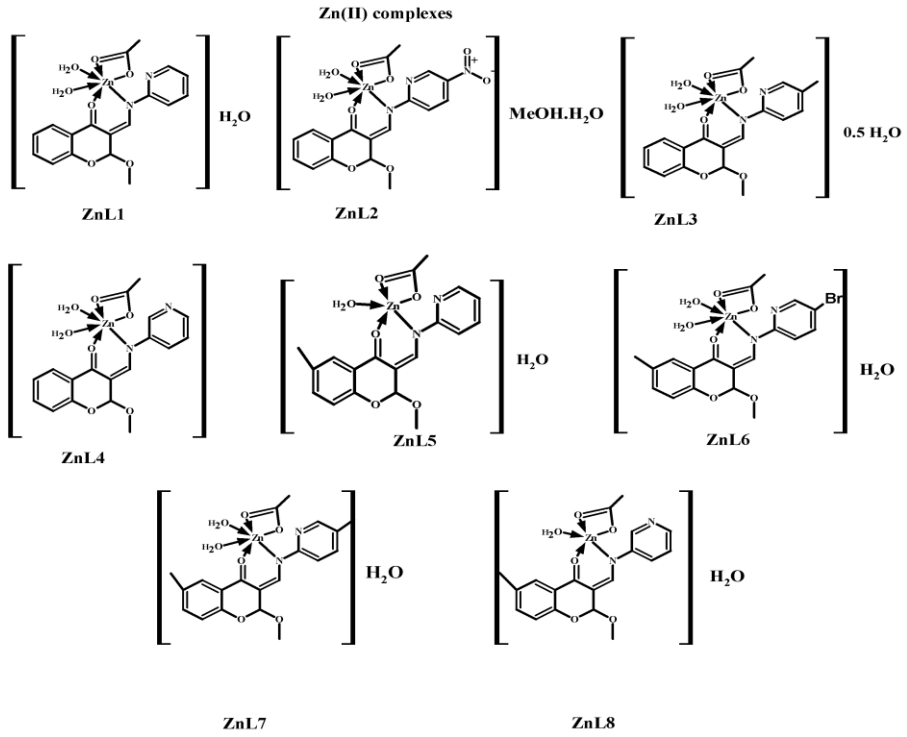

3.4 Conclusion

Twenty one new mononuclear transition metal complexes ligating 2-methoxy-4-chromanones are synthesized at room temperature and characterized using different analytical and spectral techniques. Seven copper complexes, eight zinc complexes and six nickel complexes were synthesized. Mononuclearity and purity of the samples were confirmed using elemental analysis. Low molar conductance values point to non electrolytic nature of complexes. IR spectral values and NMR spectral studies showed that ligands are monobasic and ligate bidendately. Thermal studies indicated thermal stability of complexes and also the mode of water coordination in the complex. Electronic studies together with magnetic moment and electron paramagnetic measurements gave proper idea about geometry and orientation of ligands in the complexes. Complexes NiL3, NiL5, CuL2, CuL7, ZnL5 and ZnL8 have

penta coordinate square pyramidal geometry which was confirmed from their magnetic moment and EPR data. Distorted octahedral geometries are proposed to the remaining complexes.

References

[1] Inorganic Aspects of Biological and Organic Chemistry, Academic Press, New York **1976**.

[2] D. Shier, J. Buttler, R. Lewis Hole's Human Anatomy & Physiology (eighth ed.), McGraw-Hill, Boston, **1996.**

[3] R. Mukherjee; In Comprehensive Coordination Chemistry II; Editors-in-Chief, J. A. M., Meyer, T. J., Eds.; Pergamon: Oxford, **2003**.

[4] C. Ramakrishnan; Y. S. Geetha;. J. Chem. Sci. **1990**, 102, 481.

[5] P. Kumar; A. Kalita; B. Mondal; Inorg. Chim. Act. **2013**, 404, 88.

[6] K. L. Haas; K. J. Franz; Chem. Rev. **2009**, 109, 4921.

[7] R. A. McCance; E. M. Widdowson. Biochem. J. **1942,** 36, 692.

[8] G. Parkin, Chem. Commun. **2000**, 1971.

[9] M. D. Pluth; E. Tomat; S. J. Lippard; Annu. Rev. Biochem. **2011**, 80, 333.

[10] R. Lancaster; 'The Bioinorganic Chemistry of Nickel', VCH Publishers, Inc.: New York, **1989**.

[11] E. R. Braithwaite; Chem. Ind. (London) **1979**, 23, 84.

[12] G. Kalaiaras; S. R. Jey; Rajkumar; S. Dharani; Nigam; P. Rath; R. Prabhakaran; J. Photochem. Photobio. B: Bio. **2018**, 180, 77.

[13] F. Rahman; S. Yu; S. K. Khalil; S. Koppireddi; Z. Li; H. Wang; D. Zhang; Sens. Actuators B Chem. Volume , **2018**, 263, 594.

[14] M. M. E. Shakdofa; H. A. Mousa; A. A. Labib; A. S. Abd-El-All; A. A. El-Beih; M. M. Abdalla; App. Organomet. Chem. **2018**, 32, 4345.

[15] F. Arjmand; A. Jamsheera, M. Afzal , S. Tabassum, Chirality, **2012**, 24, 977.

[16] N. Beyazit; D. Çakmak; C. Demetgül, Tetrahedron **2017**, 73, 2774.

[17] A. D.-Kułaczkowska; J. Therm. Anal. Calorim. **2012**, 109, 7.

[18] W. J. Geary; Coord. Chem. Rev. **1971**, 7, 81.

[19] A. D. Kułaczkowska; L. Mazur; J. Mol. Struc. **2011**, 985, 233.

[20] S. A. Galal; K. H. Hegab; A. S. Kassab; M. L. Rodriguez; S. M. Kerwin; A. A. El-Khamry; H. Diwani; Eur. J. Med. Chem. **2009,** 44, 1500.

[21] M. Shebl, J. Mol. Struct. **2017**, 1128, 79.

[22] M. Manjunath; A. D. Kulkarni; G. B. Bagihalli; S. Malladi; S. A. Patil; J. Mol.Struct. **2017**, 1127, 314.

[23] F. A. Cotton; G. Wilkinson; Advanced Inorganic chemistry, A Comprehensive Text book, third Ed., New Delhi, 1**985**, 449.

[24] H. Seleem; B. El-Shetar; M. Shebl; Heteroatom Chemistry, Wiley Online Library, **2007,** 18**,** 100.

[25] E. A. Boudreaux, Trans18. Faraday Soc. **1963**, 59, 1055.

[26] G. A. Bain; J. F. Berry; J. Chem. Educ. **2008,** 85, 532.

[27] Y. Wang; Z.-Y. Yang; J. Lumin; **2008**,128, 373.

[28] M. Singh; V. Agarwal; U. P. Singh; N. K. Singh; Polyhedron **2009**, 28,195.

[29] A. B. P. Lever, Inorganic Electronic Spectroscopy, 2nd Ed, Elsevier, Amsterdam, **1984**.

[30] P. Kavitha; K. Laxma Reddy; B. Selvakumar; V. Rajendira; P.U. Maheshwari; H. Stoeckli-Evans; M. Palaniandavar; Arabian J. Chem. **2016,** 9, 596.

[31] G. G. Mohamed, M. M. Omar, A. A. Ibrahim, Eur. J. Med. Chem. **2009**, 44, 4801.

[32] F. A. Cotton, G. Wilkinson, C.A. Murillo, M. Bochmann, Advanced Inorganic Chemistry, sixth ed. Wiley, New York, **1999**.

[33] E. Garribba, G. Micera, J. Chem. Educ. **2006**, 83, 1229.

[34] U. L. Kala; S. Suma; S. Krishnan; M. R. P. Kurup; R. P. John; Polyhedron **2007**, 26, 1427.

[35] I. M. Procter; B. J. Hathaway; P. Nicholis; J. Chem. Soc. A **1968**, 1678.

[36] N. Figgis; Introduction to Ligand fields, Interscience, New York, **1996**, 295.

[37] B. J. Hathaway; G. Wilkinson; R. D. Gillard; J. A. McCleverty (Eds.), Comprehensive Coordination Chemistry, Pergamon, Oxford, **1987**, 5, 533

[38] L. Latheef; M. R. P. Kurup; Spectrochim. Acta, Part A **2008**, 70, 86.

[39] S. Stoll; Spectral Simulations in Solid-State Electron Paramagnetic Resonance Ph.D. thesis, ETH, Zurich, **2003.**

[40] B. J. Hathaway; A. A. G. Tomilinson; Coord. Chem. Rev. **1970**, 5, 1.

[41] V. S. X. Anthonisamy; R. Murugesan; Chem. Phys. Lett. **1998**, 287, 353.

[42] V. L. Siji; M. R. SudarsanaKumar; S. Suma; M. R. P. Kurup; Spectrochim. Acta Mol. Biomol. Spectrosc. **2010**, 76, 22.

[43] R. Takjoo; A. Akbari; S. Y. Ebrahimipour; M. Kubicki; M. Mohamadi; Inorg. Chim. Act. **2017**, 455, 173.

******

Chapter 4

In vitro inhibitory studies of 2-methoxy-4 -chromanones and its Ni (II), Cu (II), Zn (II) complexes on alpha-amylase and alpha-glucosidase

Contents

Abstract

Enzyme inhibition is a fundamental concept underneath the design and application of several drug analogues and pharmaceuticals. Mechanism of enzyme actions and metabolic enzyme regulations are usually clarified by the study of enzyme inhibition kinetics and enzyme active site-inhibitor structure relationship studies. Alpha-amylase and alpha-glucosidase are the key enzymes which are involved in the dietary carbohydrate digestion in organisms. Inhibition of these two enzymes is regarded as significant measure for controlling postprandial hyperglycemia. In this chapter, we discuss the alpha-amylase and alpha-glucosidase inhibition ability of the synthesized ligands and their Ni (II), Cu (II), Zn (II) complexes and compared with the standard acarbose. Inhibition kinetics, which is helpful for understanding the underlying mechanism of inhibition, revealed the mode of inhibition and kinetic parameters. Among the synthesized compounds CuL1, CuL2, CuL5, ZnL5 and ZnL2 have IC_{50} values less than that of acarbose. Compounds inhibited either competitively or noncompetitively. Our findings are in line with the reports that, mild amylase inhibition and potent glucosidase inhibition can be considered as the effective way to decrease the carbohydrate metabolism in the intestine.

4.1 Introduction

Diabetes mellitus is a faction of diseases characterized by increased blood glucose level that is an upshot from flaw in the body's ability to generate and/or use the hormone, insulin. It is a situation principally defined by the level of hyperglycemia which increases the risk of various microvascular damages (nephropathy, retinopathy and neuropathy). It is allied with reduced life expectancy, major morbidity due to specific diabetes linked microvascular difficulty, high risk of macrovascular complications and lessened quality of life [1]. In the development of diabetes, several pathogenical processes are involved which destroy the beta cells of the pancreas with resultant insulin deficiency, others that result in resistance to insulin activity. The anomaly of carbohydrate, fat and protein metabolism are due to scarce action of insulin on target tissues consequential from insensitivity or lack of insulin [2]. A perceptive familiarity about the pathophysiology of diabetes rests upon idea of the basics of metabolism of carbohydrate and insulin action. Followed by the food consumption, carbohydrates get broken down into glucose in the gut. Glucose is then absorbed into the bloodstream which causes elevation in blood glucose levels. This rise in glycemia will stimulate the beta cells of the pancreas for insulin secretion. Insulin is required by most cells to permit glucose entry. Insulin combines to specific cellular receptors and will facilitate the cell entry of glucose, where glucose is used for energy production. The hike in insulin secretion from the pancreas and the succeeding cellular uptake of glucose results in lowering of blood glucose levels. Lower glucose levels then lead to in decreased insulin secretion [3].

DM can be classified as type I and type II. Both Type I and Type II diabetes share one vital feature: elevated blood sugar (glucose) levels. Type I diabetes is consequence of β-cell destruction or by an autoimmune process, typically leading to total insulin deficiency. It is frequently referred as insulin-

dependent, juvenile or childhood diabetes featured by insufficient or no insulin production by the β cells of pancreas. It is one of the common types of diabetes in children. Type I is typically characterized by the presence of anti–glutamic acid decarboxylase, islet cell or insulin antibodies which identify the autoimmune processes that lead to destruction of beta cells. As a result, raise in postprandial glucose levels is observed due to lack of insulin stimulated glucose loss, inadequately regulated hepatic glucose production, and increased or irregular gastric emptying following a meal. The cause for this diabetes is usually cured by administration of external insulin [4].

Type II diabetes, previously referred to as non-insulin-dependent diabetes, is characterized by insulin resistance and usually have relative (rather than absolute) insulin deficiency which in turn causes continuously deteriorated uptake of glucose into the cells. In the long term, glucose concentration in the blood rises substantially which result in glucose toxicity. It is prefigured that there will be at least 350 million people with type II diabetes by the year 2030 (World Health Organization, 2003) unless proper action is taken. Type II constitutes 80-90% of all cases of DM [5].

The reducing sugars can react with amino groups in proteins and eventually promote the irreversible formation of reactive advanced glycation end products (AGEs) [6]. This process is known as non-enzymatic glycation which has been reported to play a very important role in the long term complications of diabetes. If this condition is neither duly nor effectively medicated, it may lead to several diabetic complications [7]. Dietary intervention to manage hyperglycemia and diabetic dyslipidemia are the keystone of treatment for diabetic patient. For patients with insulin-dependent diabetes mellitus (IDDM), dietary management coupled with insulin treatment is prescribed to control early postprandial hyperglycemia and avoid late postprandial hypoglycemia. In patients with NIDDM, dietary management,

although regularly focused on weight reduction, is also directed specifically at the treatment of hyperglycemia [8].

At present, the fundamental mechanisms of anti-hyperglycemic activities are mainly regarded as the inhibition of carbohydrate digestive enzymes, such as alpha-glucosidase, and alpha-amylase, and anti-glycation activities [9]. Quickly digested and absorbed dietary carbohydrates causes a sharp increase in the postprandial blood glucose level. In diabetic patients, the prominent blood glucose level after a meal presents a challenge for controlling meal-associated hyperglycemia. Hence, the inhibition of alpha-amylase and alpha-glucosidase by pharmaceutical compound is a widely accepted clinical method for managing postprandial glycemia in diabetic patients [10].

In human body salivary and pancreatic alpha-amylase and four small intestine mucosal alpha-glucosidase subunits are engaged to produce dietary glucose from starchy foods. Pancreatic alpha-amylase is a key enzyme in the human digestive system which catalyses the initial step in hydrolysis of starch to a mixture of oligoglucans. These are then catalysed by alpha-glucosidase in the mucosal brush borders of the small intestine and further degraded to glucose sub units which on absorption enter in to blood stream [11].

Alpha-amylases or alpha-1, 4-glucan-4-glucanohydrolases (EC 3.2.1.1) are a type of endoglycosidases and are the members of glycosyl hydrolase family. It is the major variety of amylase found in humans and other mammals. It is also present in seeds containing starch as a food reserve, and is secreted by many fungi [12]. This class of proteins employs a double displacement catalytic mechanism which proceeds through a glycosyl enzyme intermediate and hydrolyzed by acid/base catalysis via an oxocarbenium ion-like transition

state. Alpha- amylases hydrolyze 1, 4 -glucosidic linkages with retention of alpha configuration at the C1 anomeric center of sugar [13].

Alpha-glucosidase is widespread in various organisms including bacteria, yeasts, archaea, fungi, plants, and animals. Alpha-glucosidases(alpha-D-glucoside glucohydrolase EC. 3.2.1.20) are membrane-bound enzymes found at the blush border epithelium of the small intestine [14] and are considered as the key enzymes of carbohydrate digestion. It specifically hydrolyzes the α-glucopyranoside bond, thereby releasing one unit of α-D-glucose from the non-reducing end of the substrate [15].

Inhibition of alpha-amylase will reduce the rate at which carbohydrates are metabolised. Drop in the production of secondary metabolites will ultimately reduce the amount of glucose produced, and thus may allow for more control of blood sugar levels. There are many naturally occurring alpha-amylase inhibitors like nojirimycin and lucomycin A. They are usually proteins, or oligosaccharide and polysaccharide compounds with structures similar to that of the natural substrate of the enzyme. Commonly used alpha-amylase inhibitors such as acarbose, miglitol, voglibose, nojirimycin and 1-deoxynojirimycin, also refered as carbo- blockers will prevent degradation of complex dietary carbohydrates to oligosaccharides and dissacharides. These inhibitors are indirectly helpful in weight loss due to ability to prevent sugar assimilation, through inhibition of starch hydrolysis [16]. Inhibitors of alpha-glucosidase are usually saccharides that behave as competitive inhibitors of enzymes (especially alpha-glucosidase) which are needed to digest carbohydrates.

These compounds have higher glycemic control over hyperglycemia in diabetes mellitus type II, predominantly with regard to postprandial hyperglycemia, by interfering with the rate of digestion of carbohydrate in diet. Therefore, less glucose is absorbed because the carbohydrates are not degraded into glucose molecules. In diabetic patients, the short-term effect of these drugs therapies is to decrease current blood glucose levels: the long-term effect is a small reduction in glycosylated hemoglobin (glycohemoglobin or hemoglobin A1C) level [17]. A pictorial representation of action of inhibitors is given in scheme 4.1

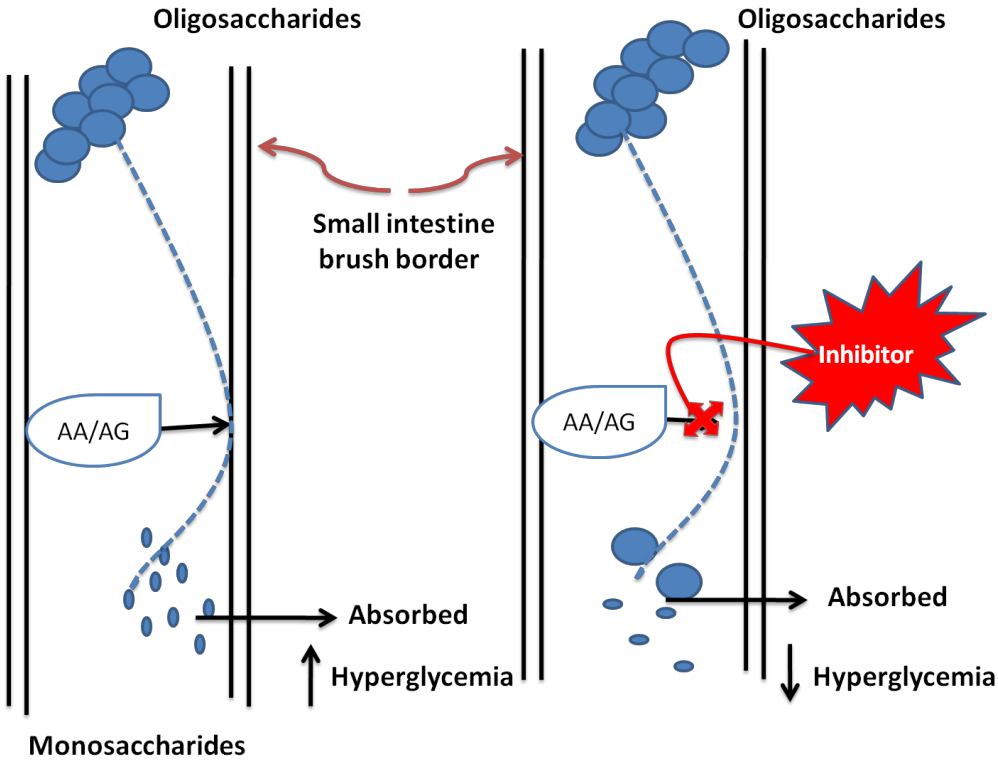

Scheme 4.1

Typical examples of alpha-amylase and alpha-glucosidase inhibitors are acarbose, miglitol, voglibose, rosiglitazone, metformin etc. They decrease

both postprandial hyperglycemia and hyperinsulinemia, and thus may develop sensitivity to insulin and decrease the stress on β-cells [18]. These compounds do not bring on hypoglycemia and have a good safety profile, although gastrointestinal adverse effects may limit long-term fulfillment to therapy. At present acarbose is the only oral anti-diabetes agent accepted for the treatment of both pre-diabetes and type II diabetes [19]. However, it has been seriously connected with side effects. Acarbose being a non-specific inhibitor inhibits both alpha-glucosidase and alpha-amylase. The inhibition of alpha-amylase produces severe gastrointestinal (GI) side effects, which alleviate complications. In the colon, bacteria digest the complex carbohydrates causing gastrointestinal side effects such as diarrhea, flatulence, abdominal discomfort, and bloating. The most common side effects seen with rosiglitazone alone or in combination with drug metformin are head ache, upper respiratory tract infection, back pain, fatigue, sinusitis, diarrhea, and hypoglycemia [20].

Many efforts have to be made to specify more effective and unique inhibitors for the treatment of diabetes. Chemistry of formylchromones and chromanones has aroused much interest in recent times, due to their broad array of biological properties and abundance as a core moiety of several natural products. Recently Maria *et al* reported a class of chromanones with superb inhibitory activities on alpha-glucosidase alkaline phosphatases [21] and ectonucleotidases [22]. On account of their inimitable chemical diversity and biological connectivity, metal complexes have been widely recognized as potential chemical resources in drug screening.

Metal based drugs to control diabetes was first investigated by Coulson *et al*. in 1980 and reported that $ZnCl_2$ can stimulate lipogenesis in rat adipocytes similarly to the insulin action [23]. Many metal complexes have been synthesized and evaluated to overcome the problems of painful insulin

injection and the side effects for type I or type II DM. So far chromium, manganese, molybdenum, copper, cobalt, zinc and vanadium ions have been reported to exhibit insulin-mimetic or enhancing insulin like properties under *in vitro* and *in vivo* condition.

Of great interest, several mechanisms were proposed for action for metal induced hypoglycemia. Probable mechanisms of antidiabetic activity include insulin-like effects (chromium, magnesium), antioxidant effect (cobalt, manganese, tungstate, zinc), inhibition of enzyme phosphatases (vanadium), stimulation of glucose uptake, glycogen and lipid synthesis in muscle, adipose and hepatic tissues and inhibition of gluconeogenesis (chromium, cobalt) or stimulation of the activities of the gluconeogenic enzymes: phosphoenol pyruvate carboxykinase and glucose-6 phosphatase (manganese)[24,25].

Yasumatsu *et al*. reported that by single intraperitoneal injection copper (II)-picolinate [Cu $(Pic)_2$] complexes have shown an increased hypoglycemic effect in selected animal models [26]. Zinc being the component of insulin, meet diabetes at several times during metabolism in a cell. Surprisingly, zinc was found to have significant physiological and pharmacological functions involving an insulin-mimetic activity. Hyperzincuria and impaired absorption of zinc in intestine may lead to diabetes. However, increased zinc intake has also been related with a slightly lower risk of type II diabetes in women [27]. Therefore, discovery of novel classes of metal complexes that act as alpha-amylase and alpha-glucosidase inhibitors for treatment of diabetes can be regarded as a potential topic for research.

With the consideration of above points, in this chapter we discuss the alpha-amylase and alpha-glucosidase inhibitory potential of the synthesized 2-methoxy-4-chromanones and their Cu (II), Ni (II) and Zn (II) complexes.

4.2 Experimental

4.2.1 Materials used

2-Methoxy-4-chromanones and their Ni (II), Cu (II), Zn (II) complexes used for the inhibition study were synthesized as per procedure described in Chapter 2 and 3 respectively. Alpha-amylase (15.8 U/mg solid) and alpha-glucosidase (15 U/ mL) were purchased from Himedia Chemicals and Sigma Aldrich respectively. Both the enzymes were stored at 0-4 °C.

4.2.2 Reagents used in alpha-amylase inhibition study

4.2.2.1 Sodium phosphate buffer (0.02M) with 0.006 M NaCl at pH = 6.9

The three solutions such as 284 mg of Na_2HPO_4 (MERCK) in 100 mL distilled water, 312 mg of NaH_2PO_4 (MERCK) in 100 mL distilled water and 175 mg of NaCl in 50 mL of distilled water were prepared separately and the mixed thoroughly followed by the addition of 200 mL distilled water to obtain the required pH of 6.9. Any deviation from pH of 6.9 was adjusted by adding either Na_2HPO_4 as base or NaH_2PO_4 as acid. Finally the solution was brought up to the final volume of 500 ml in the volumetric flask. The buffer thus prepared was stored at 25°C and was used within 2 weeks.

4.2.2.2 Dinitrosalicylic acid (DNSA) reagent

About 1 g of DNSA is dissolved in 50 mL of distilled water. To this solution add about 30g of potassium sodium tartrate tetrahydrate (Roschelle salt) in small lots. The solution turns milk yellow. Then add 20 mL of 2N NaOH, which turns the solution to transparent orange yellow colour. The final

volume is made up to an amber coloured bottle. The reagent was freshly prepared prior to assay.

4.2.2.3 Starch solution

Soluble starch (1g) was dissolved in 100 ml of 0.02 M sodium phosphate buffer. Constant stirring at 90°C helped the easy dissolution of starch in buffer. The starch solution was then cooled and stored at 4°C. The starch solution was incubated at 25°C for 5 minutes prior to assay.

4.2.3 Assay for alpha-amylase inhibition

Inhibition studies were performed as per the procedure reported by Rosa *et al*. with a minor modification [28]. 500 µL of sample solution in DMSO with different concentrations(0-0.5 mM) was allowed to react with 500 µL of enzyme solution with 0.5 mg/mL concentration and 0.02 M sodium phosphate buffer (pH=6.9). After preincubation at 37 °C for 10 min, 500 µL of 1 % starch solution is added. The mixture was incubated for 15 min at 37 °C followed by the addition of 1 mL of 3, 5-dinitrosalicylic acid for terminating the reaction. It is then incubated in boiling water for 5 min, cooled to room temperature, diluted and the absorbance was measured at 540 nm. Acarbose was used as the standard inhibitor and negative control was carried out in the same way devoid of sample. An alpha-amylase unit was defined as the amount of enzyme required to release 1 mM maltose/min at 37°C from the substrate under the given assay conditions. Percentage Inhibition was calculated by the expression:

$$\%\text{inhibition} = \frac{(Absorbance_{\ control} - Absorbance_{\ test})}{Absorbance_{\ control}} \times 100$$

50% inhibition concentration (IC_{50}) was determined graphically. All experiments were performed in triplicate and the results were expressed in mean ± SD.

4.2.4 Reagents used in alpha-glucosidase inhibition studies

4.2.4.1 0.1M potassium phosphate buffer (pH 6.9)

The two solutions such as 9.11 g K_2HPO_4 (MERCK) in 200 mL distilled water, 6.49 g KH_2PO_4 (MERCK) in 200 mL distilled water were prepared separately. Both solutions were then mixed thoroughly followed by the addition of 400 ml distilled water as to attain the desirable pH of 6.9. If the pH deviates from 6.9, the pH was adjusted by adding either K_2HPO_4 as base or KH_2PO4 as acid. Finally the solution was made to a final volume of 1000 ml in volumetric flask. The buffer prepared was stored at 25°C and used within 2 weeks.

4.2.4.2 20 mM p-nitrophenyl-alpha-D-glucopyranoside substrate solution

Potassium phosphate buffer (0.1M, pH 6.9) was slowly added into 5 mM p-nitrophenyl-alpha-D-glucopyranoside until it fully dissolved. This solution was freshly prepared prior to alpha-glucosidase assay.

4.2.5 Assay for alpha-glucosidase inhibition

50 µL of sample solution in DMSO with different dilutions (0.0 -0.125 mM) was allowed to react with 50 µL of enzyme solution (0.1mg/ mL) and 0.02 M sodium phosphate buffer (pH=6.9). After preincubation at 37°C for 10 min, 50 µL of 20 mM p-nitrophenyl-alpha-D-glucopyranoside solution was added. The mixture was incubated for 30 min at 37° C followed by the addition of 1 mL of 0.1 M sodium carbonate for stopping the reaction. The absorption of 4-nitrophenol formed as a result of hydrolysis of p-NPG by alpha-glucosidase was measured at 405 nm. Acarbose (Bayer Pharmaceuticals, Leverkusen, Germany) was used as the standard inhibitor and negative control was carried out as in the same way without sample. Percentage Inhibition was calculated by the equation:

$$\%\text{inhibition} = \frac{(Absorbance_{\ control} - Absorbance_{\ test})}{Absorbance_{\ control}} \times 100$$

50% inhibition concentration (IC_{50}) was determined graphically. All experiments were performed in triplicate and the results were expressed in mean ± SD [29].

4.2.6 Enzyme inhibition kinetics

The experiments were conducted according to the protocols as described above at a constant concentration of sample fraction with a variable concentration of substrate. For the alpha-glucosidase inhibition assay, 0.5-2.5 mmol of pNPG was used and 0.1- 0.5 % of starch was used for the alpha-amylase inhibition assay. Experiment was conducted in absence and presence of inhibitor. Inhibitor concentrations selected were IC_{50} (concentrations for 50%inhibition) and double of IC_{50}. All experiments were performed in triplicate and the results were expressed in mean ± SD. The initial rates of reactions were determined from calibration curves constructed using varying concentrations of p-nitro phenol and maltose for the alpha-glucosidase and alpha-amylase inhibition assays, respectively. The initial velocity data obtained were used to construct Michaelis-Menton plot. Lineweaver-Burk's plot was used to determine the K_m (Michaelis constant), V_{max} (maximum velocity) of the enzyme and the type of inhibition for both enzymes [30]. Inhibitor constant, K_i was determined from obtained K_m and V_m values using the following equations:

For competitive inhibition,

$$K_i = \frac{[I].K_m}{({K_m}^{+I} - K_m)}$$

Where, [I] is the inhibitor concentration, ${K_m}^{+I}$ and K_m are the Michaelis constant in presence and absence of inhibitor respectively.

For non-competitive inhibition,

$$K_i = \frac{[I].V_m{}^{+I}}{(V_m - V_m{}^{+I})}$$

Where, [I] is the inhibitor concentration, $V_m{}^{+I}$ and V_m are the V_{max} in presence and absence of inhibitor respectively [31].

4.3 Results and Discussion

4.3.1 Determination of IC_{50}

Hyperglycemia is a condition exemplified by an abnormal excess of blood sugar. Elevated postprandial blood glucose levels are widely accepted as one of the earliest disease markers in the prediction of subsequent microvascular and macrovascular complications, which can proceed to full symptomatic type II diabetes (T2DM). Inhibition of alpha-amylase and alpha-glucosidase delays the absorption of glucose following starch and sucrose conversion, moderates the postprandial blood glucose hike, and thus mimics the effects of dieting on hyperglycemia. However, increased alpha-amylase inhibition, resulting from certain alpha-glucosidase inhibitors (acarbose), has several side effects, such as abdominal distention, flatulence and possibly diarrhea [32]. Alpha-amylase and alpha-glucosidase inhibitors having lower inhibitory effect against alpha-amylase activity and a stronger inhibitory activity against alpha-glucosidase, which therefore can be used as effective therapy for postprandial hyperglycemia with reduced side effects [33]. The ability of the synthesized 2-methoxy-4-chromanones and their complexes to inhibit alpha-amylase and alpha-glucosidase was studied at different concentrations of the compounds. Table 4.1 gives concentration of the sample for giving 50% inhibition for enzyme activity (IC_{50}) of ligands and copper complexes. Table 4.2 gives IC_{50} of zinc complexes and nickel complexes. IC_{50}

values of the ligands and the complexes are compared with the values of standard acarbose. All the ligands and complexes inhibited alpha-amylase mildly and alpha-glucosidase strongly in concentration dependent manner.

Table 4.1: IC_{50} values of alpha-amylase and alpha-glucosidase inhibition by ligands and Ni (II) complexes

Sample	IC_{50} (mM)		Sample	IC_{50} (mM)	
	Alpha-amylase	Alpha-glucosidase		Alpha-amylase	Alpha-glucosidase
Acarbose	0.1516±0.1	0.068 ±0.3	NiL1	0.323 ±0.3	0.083 ± 0.1
L1	0.422 ±0.3	0.121 ± 0.3	NiL2	0.254± 0.4	0.081 ± 0.1
L2	0.402 ±0.1	0.094 ±0.5	NiL3	0.427 ± 0.1	0.070 ± 0.1
L3	0.441 ±0.1	0.112 ± 0.2	NiL5	0.381± 0.3	0.082 ±0.1
L4	0.455 ± 0.3	0.094 ± 0.2	NiL6	0.231± 0.4	0.084 ± 0.3
L5	0.372 ±0.1	0.104 ±0.3	NiL7	0.335 ± 0.2	0.079 ± 0.2
L6	0.358 ±0.1	0.116± 0.3			
L7	0.472 ± 0.3	0.113 ±0.5			
L8	0.460 ±0.3	0.117 ± 0.2			

Table 4.2: IC_{50} values of alpha-amylase and alpha-glucosidase inhibition by Cu (II) complexes and Zn (II) complexes

Sample	IC_{50} (mM)		Sample	IC_{50} (mM)	
	Alpha-amylase	Alpha-glucosidase		Alpha-amylase	Alpha-glucosidase
CuL1	0.276 ±0.3	0.060 ± 0.2	ZnL1	0.323 ±0.3	0.098 ± 0.3
CuL2	0.251± 0.3	0.064 ± 0.1	ZnL2	0.254± 0.4	0.081 ± 0.1
CuL3	0.375 ± 0.1	0.079 ± 0.1	ZnL3	0.338 ± 0.1	0.079 ± 0.1
CuL4	0.431 ± 0.2	0.068 ±0.1	ZnL4	0.367± 0.2	0.082 ±0.1
CuL5	0.4 ± 0.2	0.067 ± 0.3	ZnL5	0.361 ± 0.2	0.064 ± 0.1
CuL6	0.240 ± 0.4	0.058 ± 0.1	ZnL6	0.237 ± 0.2	0.058 ± 0.2
CuL7	0.42 ± 0.4	0.085 ±0.2	ZnL7	0.439± 0.1	0.071 ±0.2
			ZnL8	0.338 ± 0.1	0.082 ± 0.4

Among ligands, as shown by the IC_{50} values, in alpha-amylase inhibition ligand L6 inhibited more than the other ligands. It may be attributed to the presence of electron withdrawing bromo group. Among copper complexes, complexes CuL2 and CuL6 are having the most alpha-amylase

inhibition potential with IC_{50} in the range of 0.240- 0.247 mM. ZnL2 is having most inhibitory activity against alpha-amylase with IC_{50} of 0.237 mM among Zn (II) complexes. NiL6 inhibits most among nickel complexes and have IC_{50} value of 0.231 mM. Complexation has evidently increased the inhibitory potential of the synthesized compounds. Results clearly indicate the influence of electron withdrawing group in inhibitor moiety. Even though the inhibitory potential of ligands and complexes are still underneath the standard therapeutic drug acarbose, from the data it is clear that these compounds can promisingly take part in alpha-amylase inhibition.

Compounds have much less IC_{50} values for the inhibition of alpha-glucosidase than alpha-amylase inhibition is pointing to the stronger inhibition ability. Among ligands, L2 and L4 are the strongest inhibitors with IC_{50} of 0.094 mM. Among copper complexes CuL1, CuL2, CuL4 and CuL6 have IC_{50} less than that of standard acarbose out of which CuL6 is having the least value of 0.054 mM. Among zinc complexes, ZnL5 and ZnL6 inhibit strongly than acarbose. None of the Ni (II) complexes inhibit more than acarbose. But their IC_{50} values are comparable with that of standard acarbose.

Inhibition might be modulated by the electronic effects that depend upon the different substituent or groups in the inhibitor. It is perfectly established that the ability of inhibitor to form hydrogen bond with the catalytic residue of enzyme is significant feature for the inhibition action. Exhibited inhibition activity of all the synthesized ligands can be attributed to their ability to form hydrogen bonds and to induce conformational changes in the enzyme. The enzymatic hydrolysis of glucosidases probably proceeds via a glucosyl enzyme intermediate through oxocarbonium ion-like transition states. Therefore substitution of an electronegative atom should destabilize these transition states and decrease both the rates of glycosylation and

deglycosylation [34]. While in the case of complexes, the nature and position of substituent affect the electronic properties and causes diverse inhibitory activity against enzymes. Presence of electron withdrawing bromo group has evidently favoured inhibition than electron donating methyl group.

Inhibitors may get stabilized in enzyme active sites also by forming corporative hydrophobic contacts. For a protein, percentage of α-helix structure is related to its hydrophobic property. Higher percent of α-helix within the secondary structure of the protein, stronger hydrophobic property the molecule have. However, alpha-glucosidase must form somewhat hydrophobic domain (active center) to hydrolyze the substrate. Poor hydrophobic surroundings led to the formation of impaired active center. Presence of metal ions can increase the hydrophilic nature of a-glucosidase and weaken the hydrophobic property. Thus metal complexes can influence and decrease the activity [35]. It is possible that the inhibitors bind to the different sites of the enzyme by means of non-covalent bond, thus influence the hydrophilic and hydrophobic property of the enzyme molecule.

The percent of α-helix within the secondary structure of alpha-glucosidase declined during the enzyme inhibition by the metal ions, thus the hydrophilic character of alpha-glucosidase get augmented much. The inhibitor induced conformational changes of specific elements of the secondary structure in the molecule of enzyme may be part of the mechanism of the inhibition required to prevent the hydration of the substrate binding site and also essential to tempt the cleft closure to avoid substrate entrance. Thus failure of the formation of active centre occur due to poor hydrophobic surrounding, eventually leading to conformational changes and misfolding of polypeptide chain which causes strong inhibitory effect on enzyme [36].

While comparing the activity of complexes, it is clear that Cu (II) and Zn (II) complexes possess more anti diabetic activity than Ni (II) complexes. Oxidative stress, which is one of the major causative agents of diabetes, can be more tolerated by pancreatic β-cells in the presence of copper. Treatment with a copper chelating agent can decrease both serum copper ion and reactive oxygen species levels, and accordingly improved glucose and lipid metabolism. Copper ions and ROS are involved in the development of type II diabetes and that a copper chelating agent could be a novel therapeutic strategy for type II diabetes [37]. In addition, it has been reported that a copper chelating agent put forth favorable effects on the development of inflammation in the autoimmune model of type I diabetes as well as on the development of diabetic nephropathy including renal fibrosis and albuminuria [38]. Therefore, taken together, it is likely that a copper chelating agent exerts a variety of beneficial effects on the pathogenesis of both type I and type II diabetes and on the development of diabetic complication. It has been reported, that copper treats hyperglycemia by activating the phosphoinositide 3'kinase (PI3-K/Akt) pathway leading to GLUT 4 translocation [39].

Here from the results, it can be inferred as the compounds are mild inhibitors of alpha-amylase and strong inhibitors of alpha-glucosidase. These results can be tagged with the reports indicating the preference for mild alpha-amylase inhibitory activity, as excessive inhibitory activity will results in the irregular bacterial fermentation of undigested carbohydrates in the intestine [40]. Hence these compounds can be considered to be potential candidates for antidiabetic therapeutics.

4.3.2 Mode of enzyme inhibition

4.3.2.1 Michaelis–Menten Plots and Lineweaver-Burk plots

Enzyme inhibition turns out in numerous ways, for instance by competing with the substrate to bind to the active site of the enzyme or by disrupting irreversibly the catalytic process. It will result in the delay of starch and oligosaccharide degradation which in turn inhibit the increase of postprandial blood glucose level in human blood. A preliminary study about the possible mode of inhibition was done using Michaelis-Menten kinetics at their IC_{50} value against varying concentration of substrate. Lineweaver−Burk plots were employed to investigate the mechanism of inhibition kinetics of the inhibitors to the enzymes. The double reciprocal plots generated a series of lines which showed intersection either at Y-axis of first quadrant or X-axis of second quadrant. Lineweaver Burk plots were obtained by plotting reaction rates with different concentrations (0 mM, IC_{50}, Double IC_{50}) of the substrates. Fig 4.1 (a-h) and Fig 4.2 (a-h) show Michaelis–Menten plots of ligands and its complexes in the presence and absence of the alpha-amylase inhibitors and alpha-glucosidase inhibitors respectively. Fig. 4.3(a-h)LB plots of ligands in the presence and absence of the alpha-amylase inhibitors. Fig 4.4 (a-f) shows LB plots for Ni (II) complexes of ligands and Fig 4.5 (a-g) show LB plot in the presence and absence of the Cu (II) complexes and Fig. 4.6(a-h) give LB plots for Zn (II) complexes. Fig 4.7 (a-h) shows LB plots of ligands in the presence and absence of the alpha-glucosidase inhibitors. Fig 4.8 (a-f) shows LB plots for Ni (II) complexes of ligands and Fig 4.9 (a-g) show LB plot in the presence and absence of the Cu (II) complexes and Fig. 4.10 (a-h) give LB plots for Zn (II) complexes.

Fig. 4.1 (a-h): Michaelis-Menten plots (MM plots) for alpha-amylase inhibition of ligands and complexes

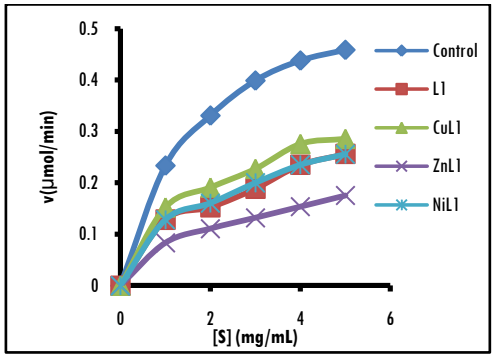

Fig. 4.1(a)

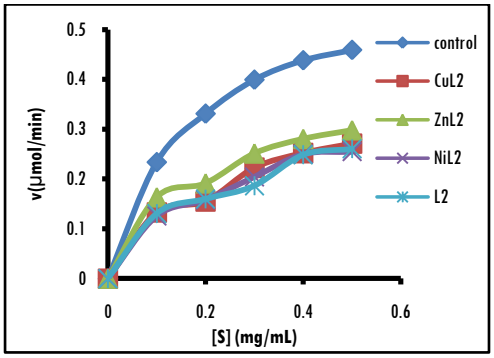

Fig. 4.1(b)

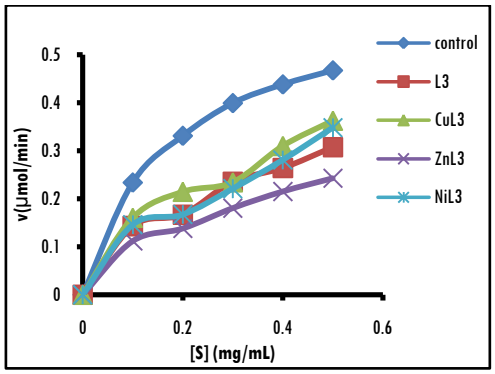

Fig. 4.1(c)

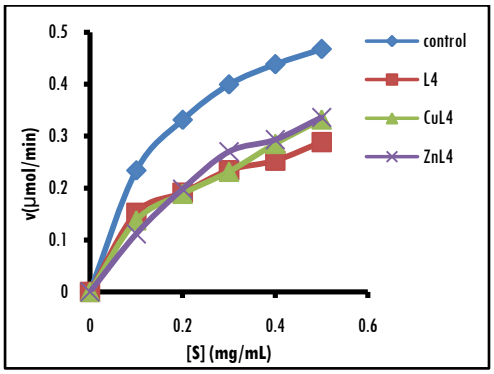

Fig. 4.1(d)

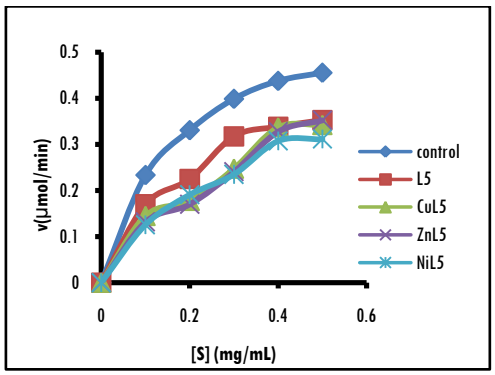

Fig. 4.1(e)

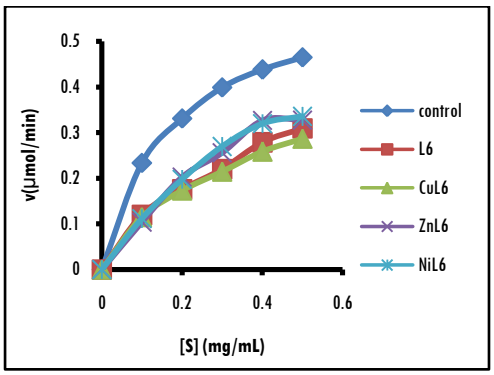

Fig. 4.1(f)

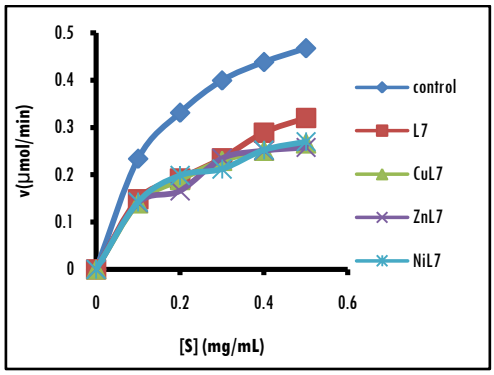

Fig. 4.1(g)

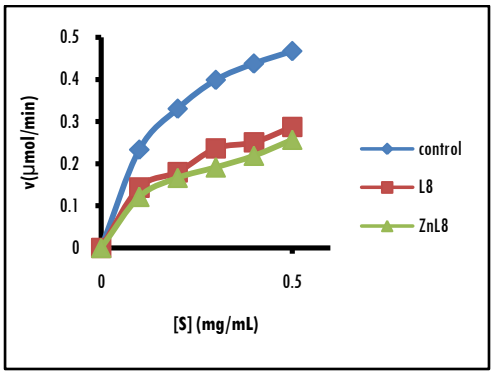

Fig. 4.1(h)

Fig. 4.2 (a-h): Michaelis Menton plots (MM plots) for alpha-glucosidase inhibition of ligands and complexes

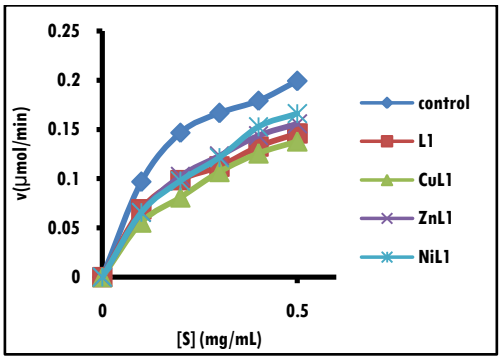

Fig.4.2 (a)

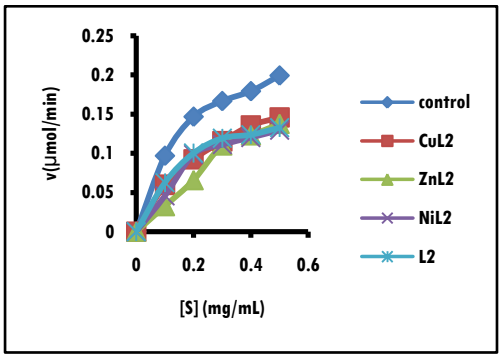

Fig.4.2 (b)

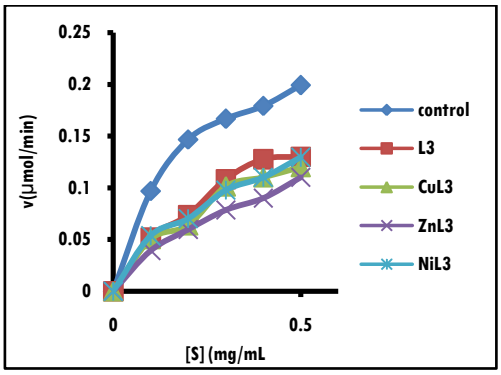

Fig.4.2 (c)

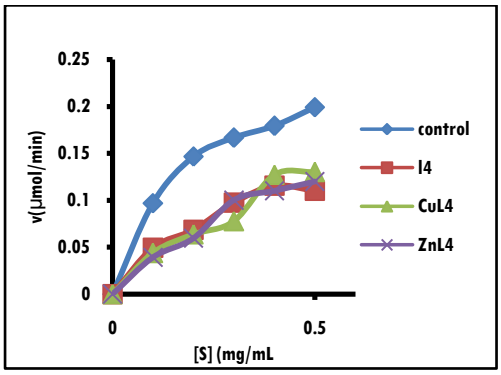

Fig.4.2 (d)

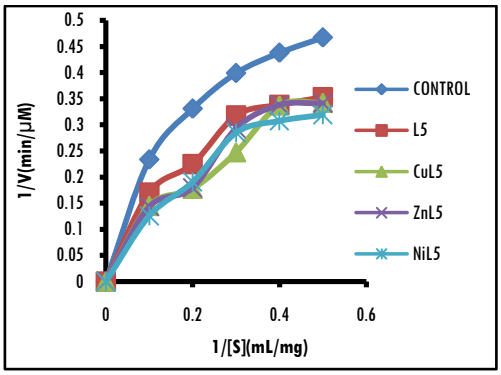

Fig.4.2 (e)

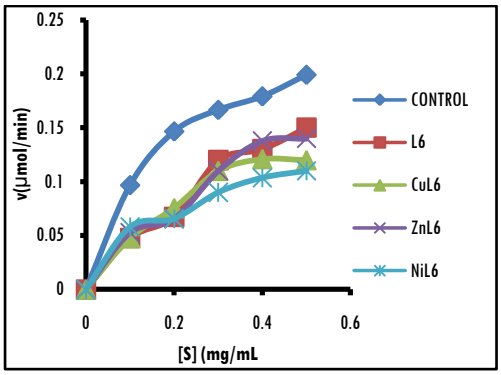

Fig.4.2 (f)

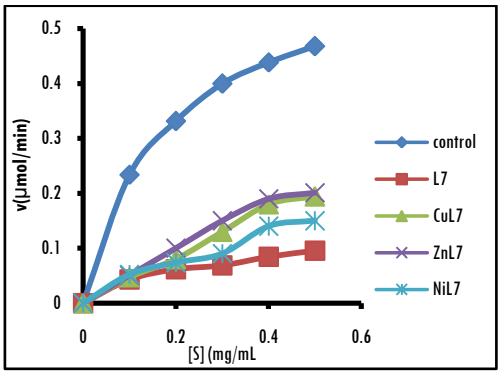

Fig.4.2 (g)

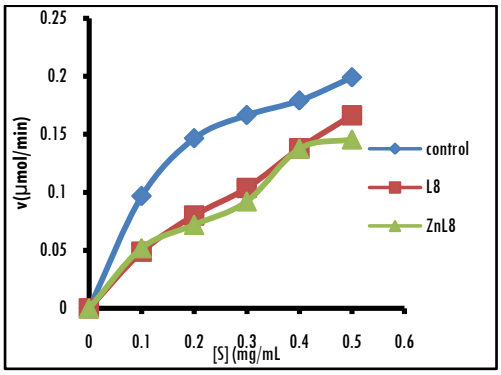

Fig.4.2 (h)

Fig 4.3 (a-h): LB plot for ligands against alpha-amylase at 0 mM, IC_{50}, double IC_{50} substrate concentrations

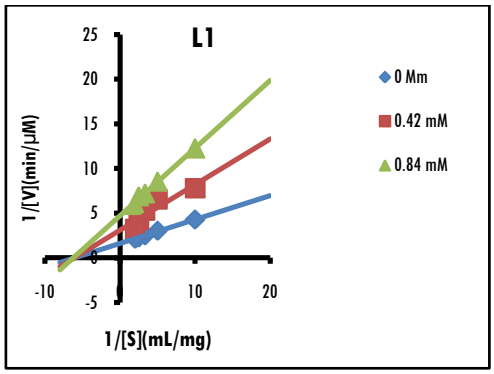

Fig 4.3 (a)

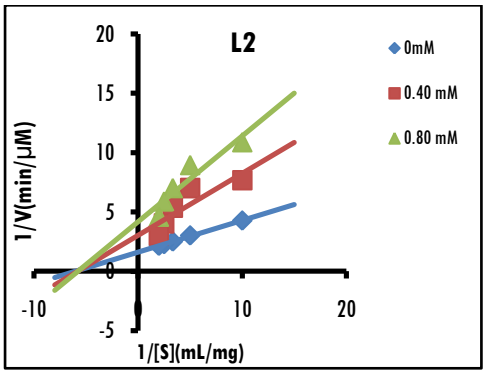

Fig 4.3 (b)

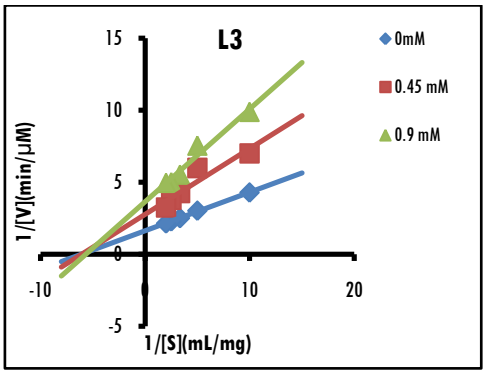

Fig 4.3 (c)

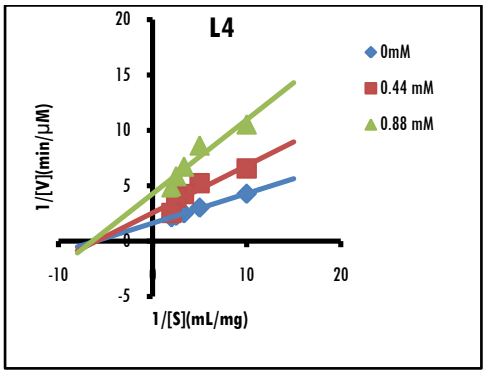

Fig 4.3 (d)

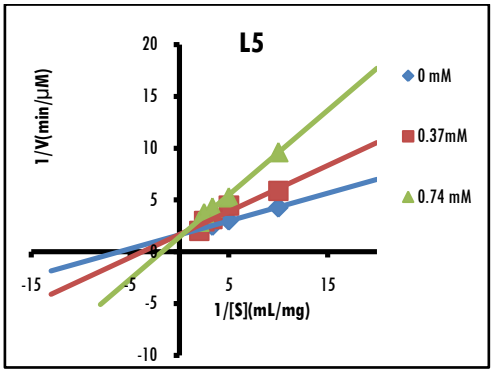

Fig 4.3 (e)

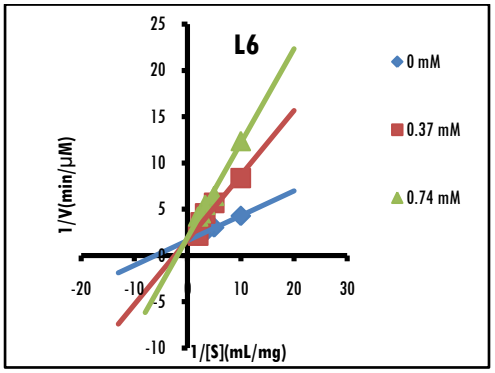

Fig 4.3 (f)

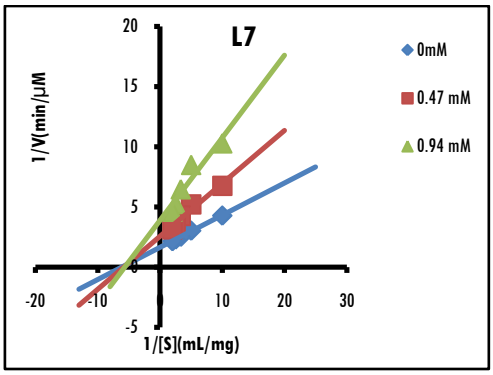

Fig 4.3 (g)

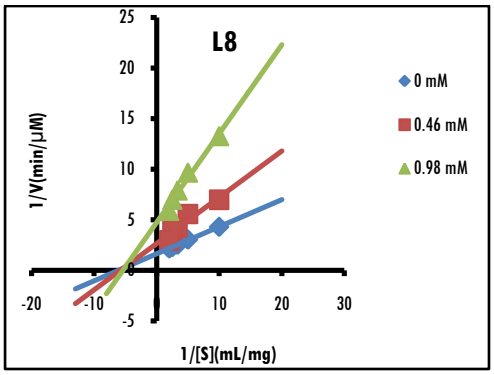

Fig 4.3 (h)

Fig 4.4 (a-f) : LB plots for NiL1, NiL2, NiL3, NiL5, NiL6, NiL6 at 0mM, IC_{50}, double IC_{50} substrate concentrations against alpha-amylase

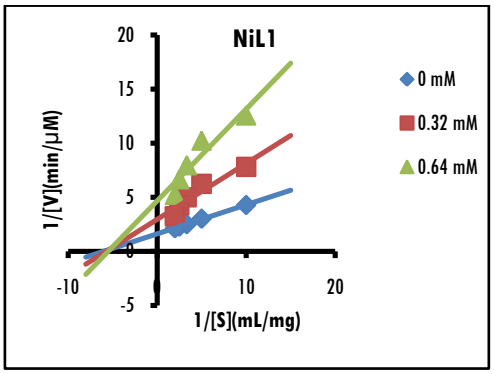

Fig. 4.4(a)

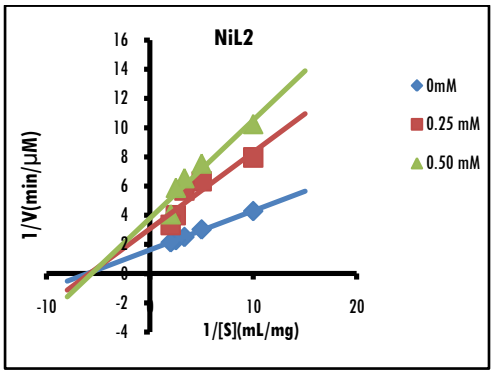

Fig. 4.4(b)

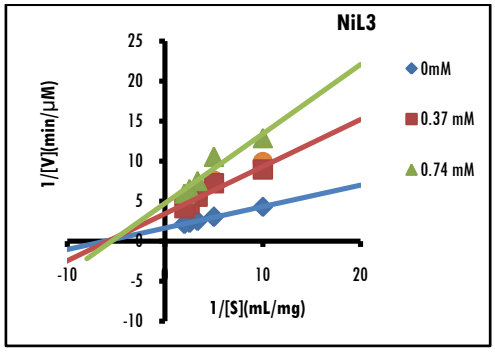

Fig. 4.4(c)

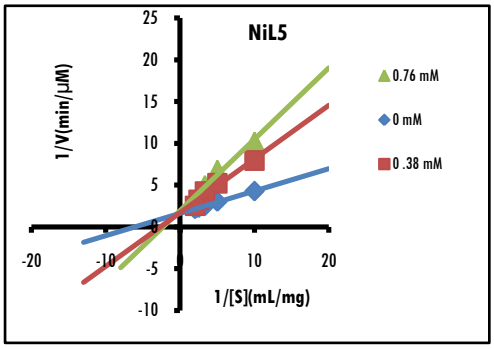

Fig. 4.4(d)

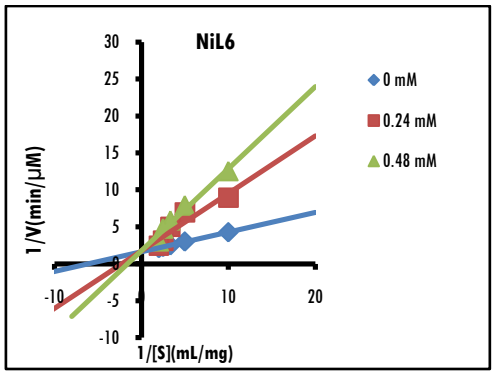

Fig. 4.4(e)

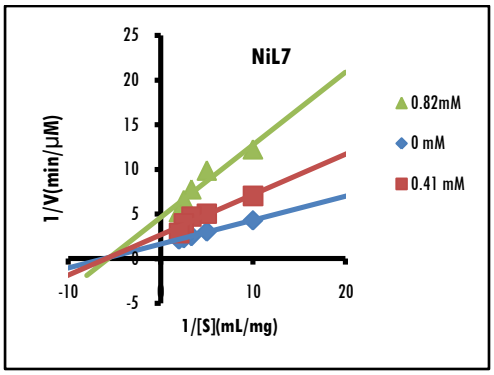

Fig. 4.4(f)

Fig 4.5 (a-g): LB plots CuL1, CuL2, CuL3, CuL4, CuL5, CuL6, CuL7 at 0mM, IC_{50}, double IC_{50} substrate concentrations against alpha-amylase

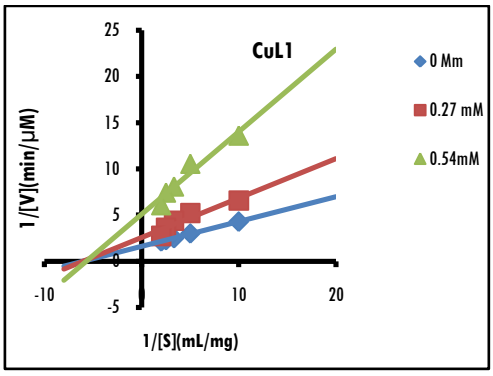

Fig. 4.5(a)

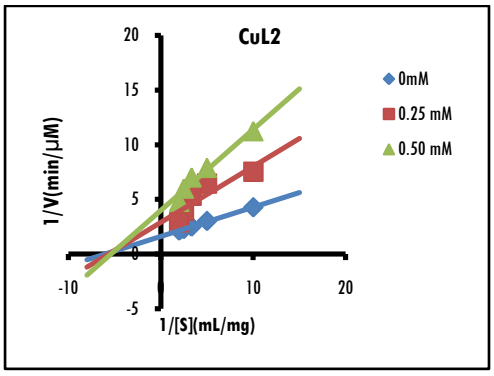

Fig. 4.5(b)

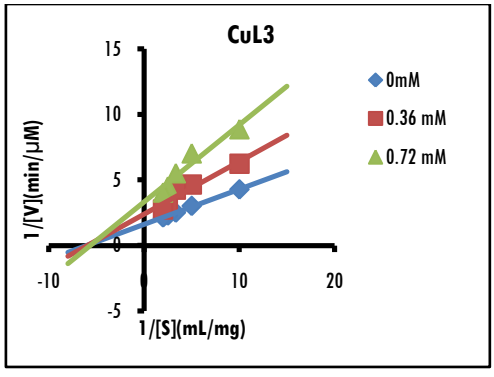

Fig. 4.5(c)

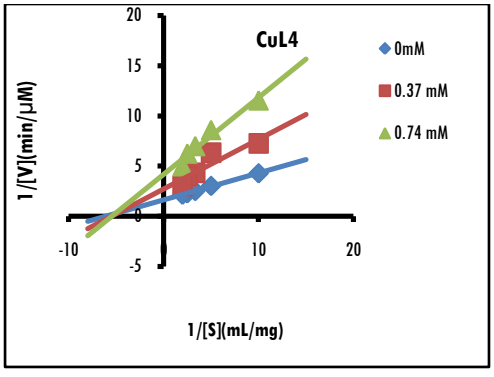

Fig. 4.5(d)

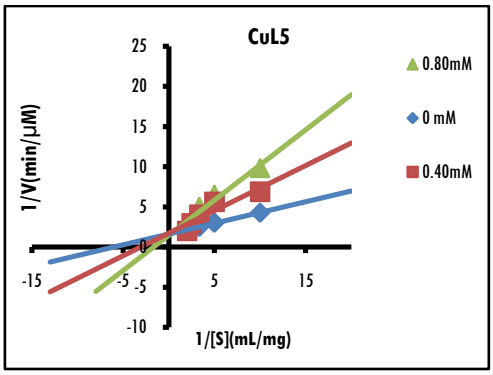

Fig. 4.5(e)

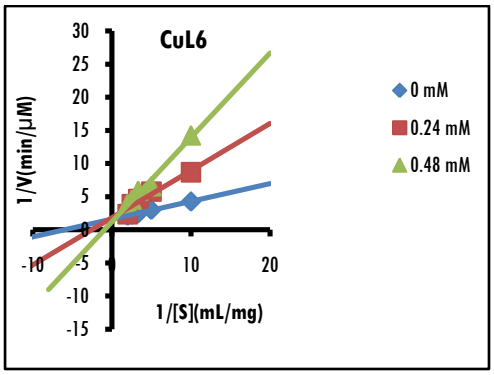

Fig. 4.5(f)

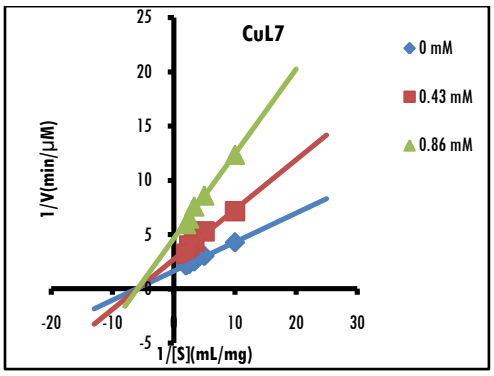

Fig. 4.5(g)

Fig.4.6 (a-h): LB plots ZnL1, ZnL2, ZnL3, ZnL4, ZnL5, ZnL6, ZnL7 and ZnL8 at 0mM, IC_{50}, double IC_{50} substrate concentrations against alpha-amylase.

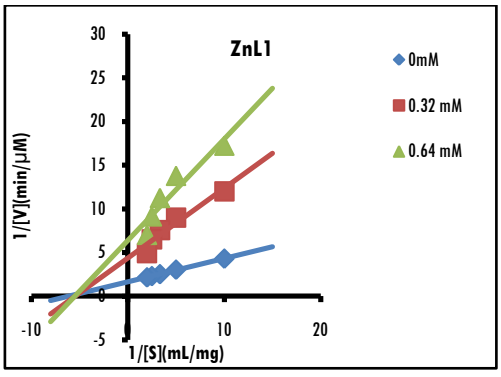

Fig. 4.6(a)

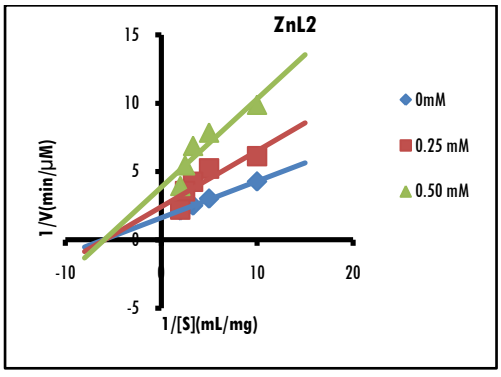

Fig. 4.6(b)

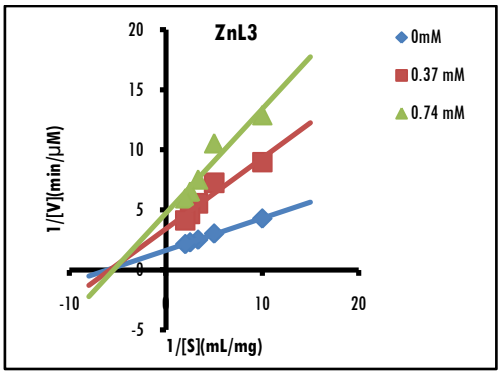

Fig. 4.6(c)

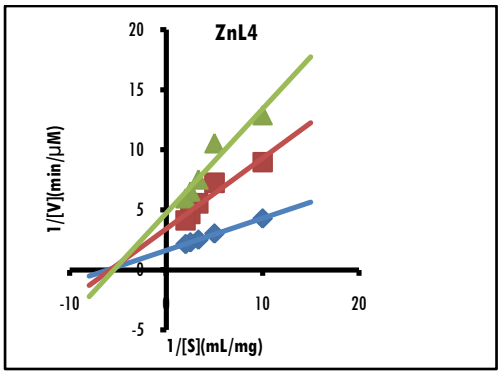

Fig. 4.6(d)

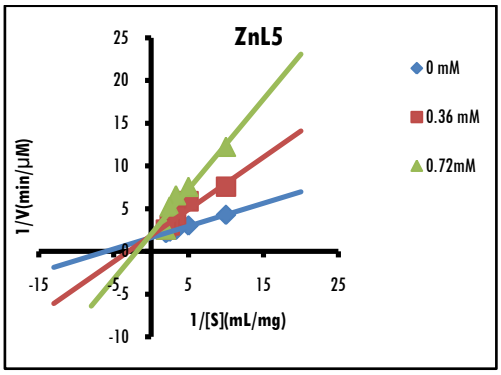

Fig. 4.6(e)

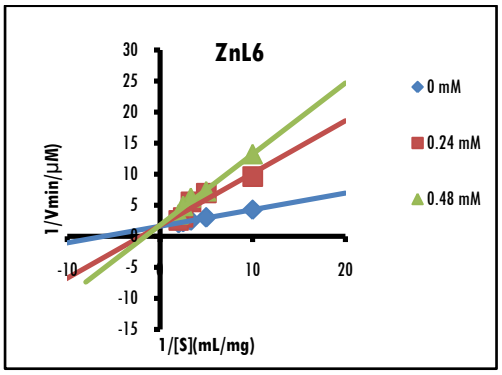

Fig. 4.6(f)

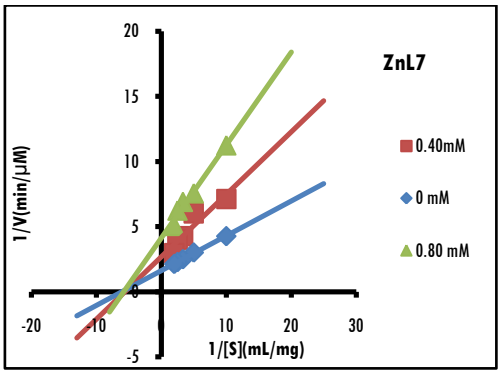

Fig. 4.6(g)

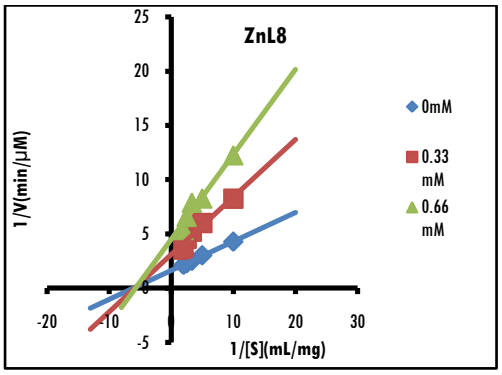

Fig. 4.6(h)

Fig.4.7 (a-h): LB plots of ligands against alpha- glucosidase at 0mM, IC_{50}, double IC_{50} substrate concentrations

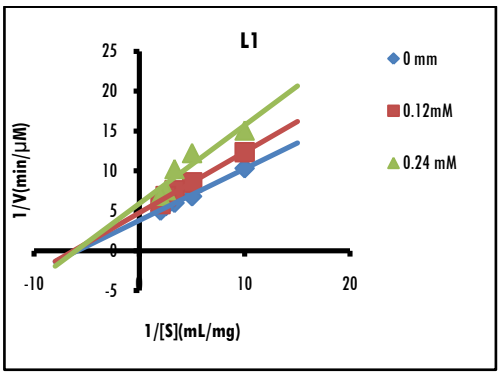

Fig. 4.7(a)

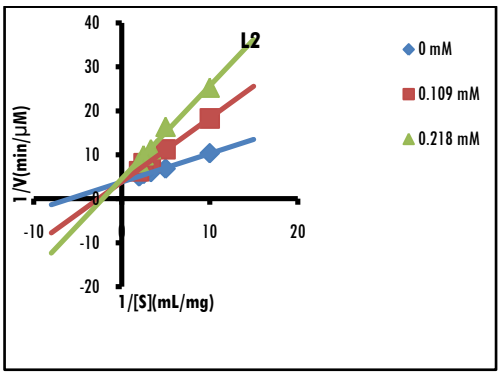

Fig. 4.7(b)

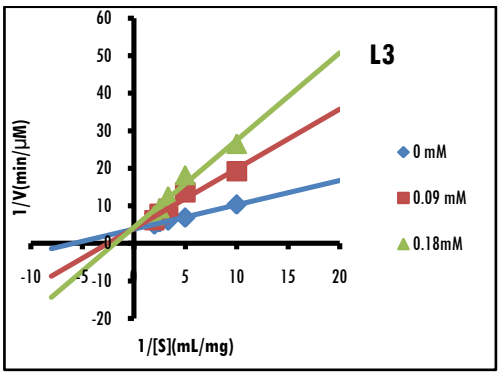

Fig. 4.7(c)

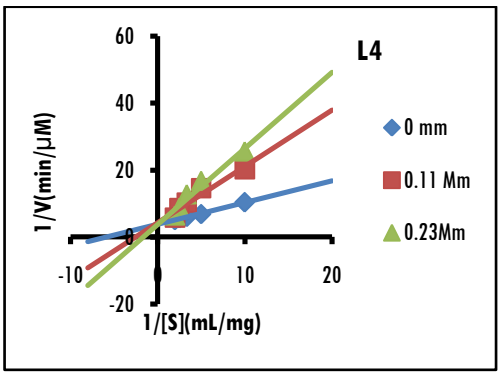

Fig. 4.7(d)

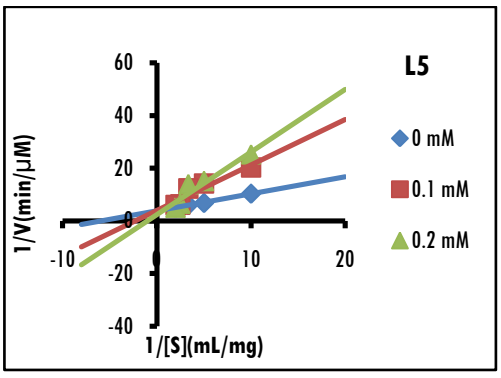

Fig. 4.7(e)

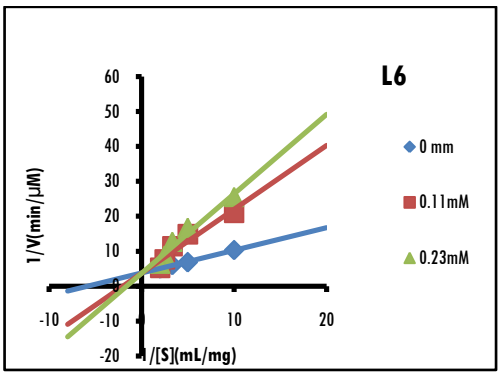

Fig. 4.7(f)

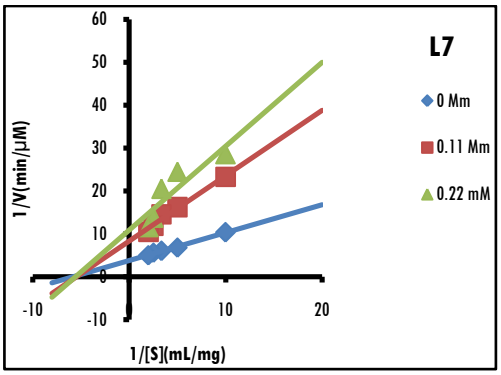

Fig. 4.7(g)

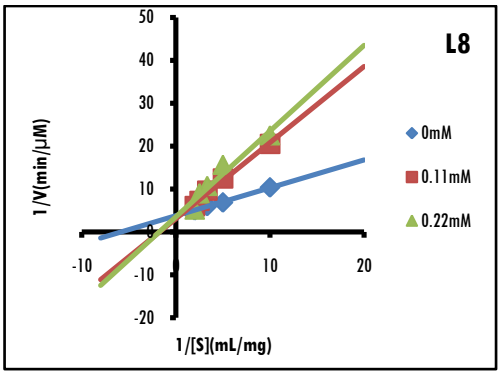

Fig. 4.7(h)

Fig. 4.8(a-f): LB plots of NiL1, NiL2, NiL3, NiL5, NiL6 and NiL7 against alpha-glucosidase at 0 mM, IC_{50}, double IC_{50} substrate concentrations against alpha-glucosidase

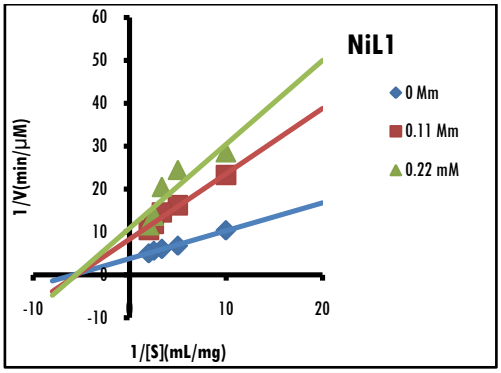

Fig. 4.8 (a)

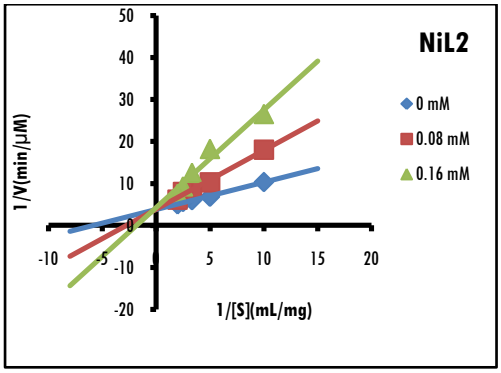

Fig. 4.8 (b)

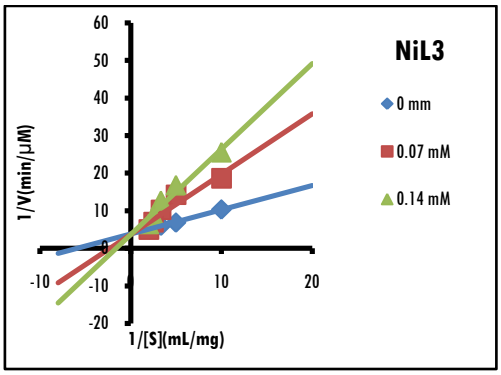

Fig. 4.8 (c)

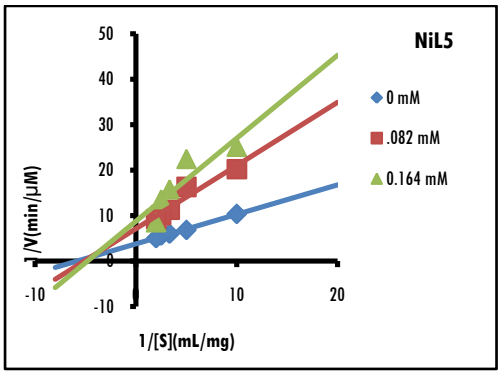

Fig. 4.8 (d)

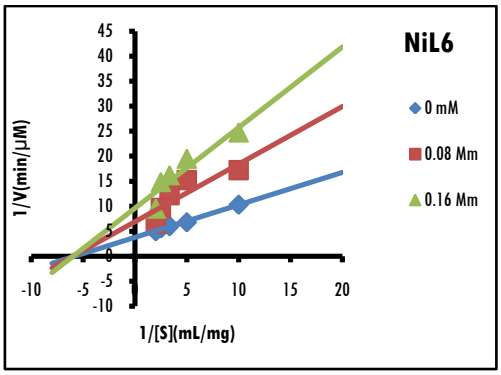

Fig. 4.8 (e)

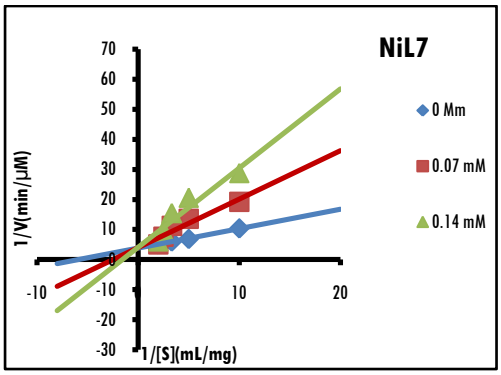

Fig. 4.8 (f)

Fig. 4.9(a-g): LB plots of CuL1, CuL2, CuL3, CuL4, CuL5, CuL6, and CuL7 against alpha-glucosidase at 0 mM, IC_{50}, double IC_{50} substrate concentrations.

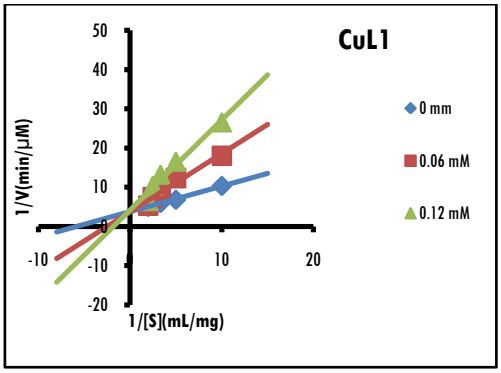

Fig. 4.9 (a)

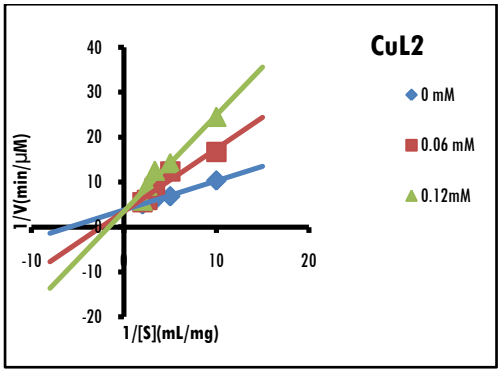

Fig. 4.9 (b)

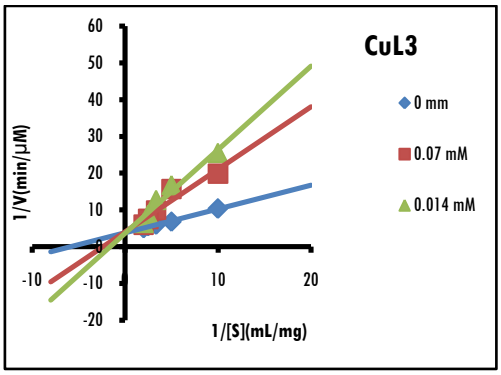

Fig. 4.9 (c)

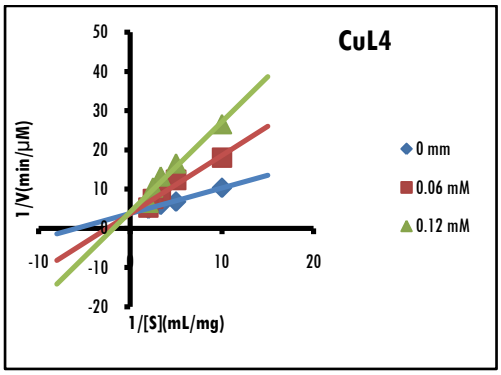

Fig. 4.9 (d)

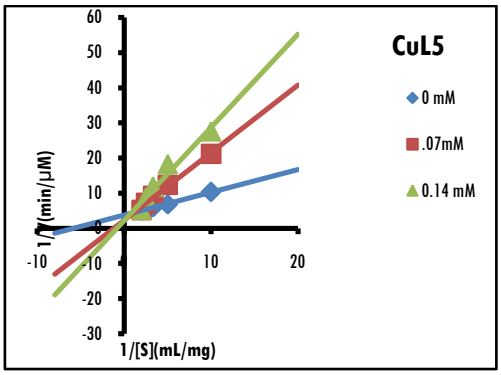

Fig. 4.9 (e)

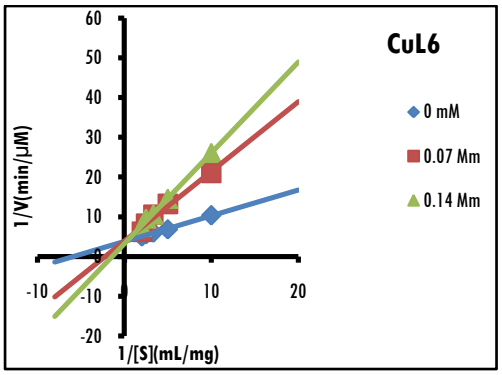

Fig. 4.9 (f)

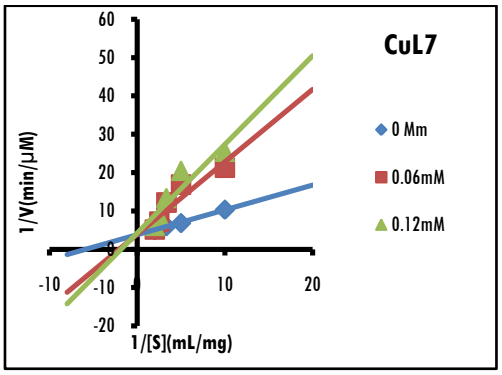

Fig. 4.9(g)

Fig. 4.10 (a-h): LB plots of ZnL1, ZnL2, ZnL3, ZnL4, ZnL5, ZnL6, ZnL7 and ZnL8 against alpha-glucosidase at 0 mM, IC_{50}, double IC_{50} substrate concentrations.

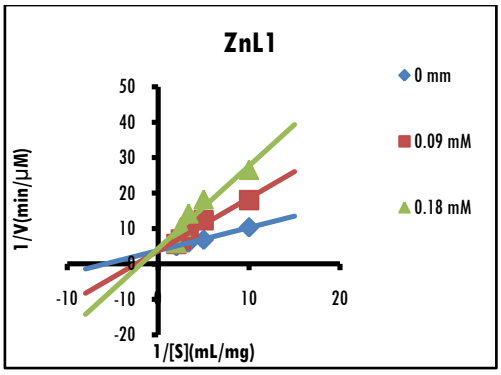

Fig. 4.10(a)

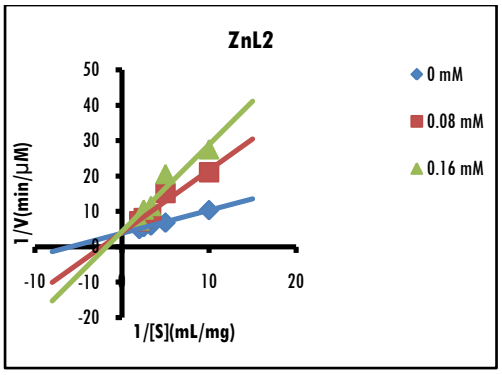

Fig. 4.10 (b)

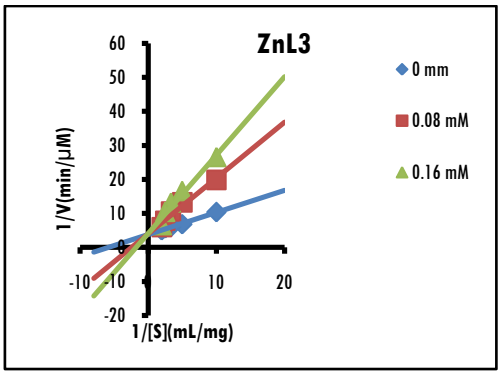

Fig. 4.10(c)

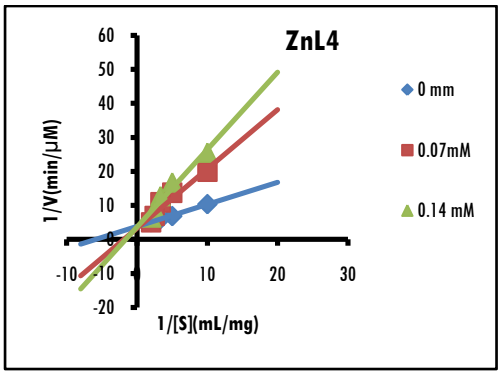

Fig.4.10 (d)

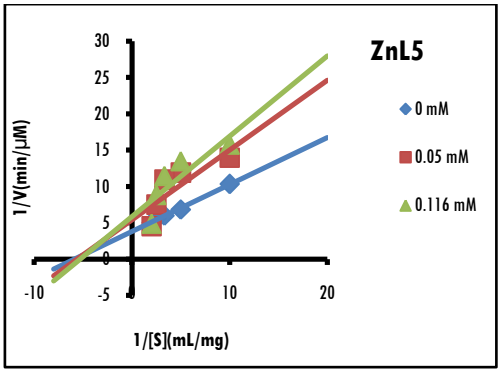

Fig. 4.10(e)

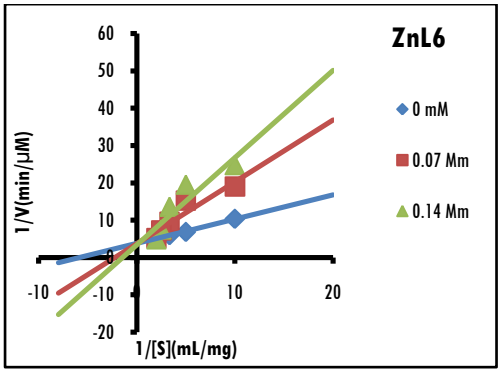

Fig. 4.10(f)

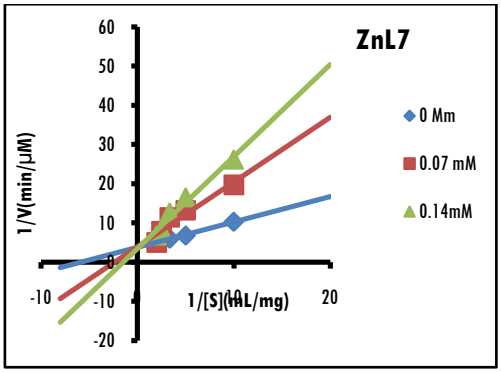

Fig. 4.10(g)

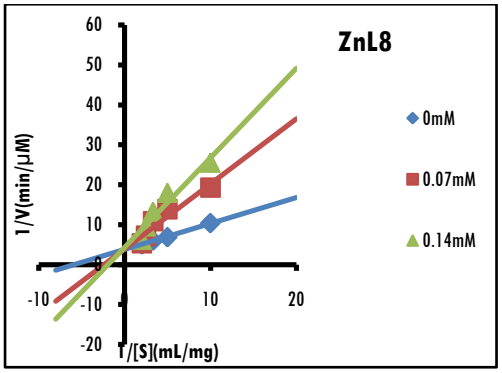

Fig.4.10 (h)

4.3.2.2 Determination of kinetic parameters and mode of inhibition

4.3.2.2.1 Kinetic parameters and mode of inhibition of ligands

Table 4.3: kinetic constants K_m,V_m, K_i and the type of inhibition of alpha-amylase and alpha-glucosidase by ligands

Sample	alpha-amylase				alpha-glucosidase			
	K_m(mM)	V_m(µM/ min)	K_i(mM)	Mode of inhibition	K_m (mM)	V_m	K_i(mM)	Mode of inhibition
Control	0.164	0.616			0.170	0.263		
L1	0.164	0.323	0.565	Non-Comp	0.155	0.209	0.590	Non-Comp
L2	0.177	0.330	0.466	Non-Comp	0.377	0.269	0.049	Comp
L3	0.164	0.360	0.646	Non-Comp	0.498	0.26	0.09	Comp
L4	0.166	0.389	0.759	Non-comp	0.391	0.237	0.080	Comp
L5	0.267	0.602	0.967	Comp	0.297	0.237	0.141	Comp
L6	0.416	0.596	0.426	Comp	0.491	0.269	0.061	Comp
L7	0.168	0.391	0.8286	Non-Comp	0.182	0.120	0.098	Non-Comp
L8	0.1706	0.384	0.764	Non-Comp	0.507	0.286	0.065	Comp

For amylase inhibition, L5 and L6 have an increase in their K_m value and almost same V_{max} value which indicates that they are competitors. All others inhibited non-competitively which can be confirmed from the unchanged K_m value on addition of inhibitor. Non-competitive inhibition indicate that the inhibitor bind to the enzyme at a site other than the active site which results in the conformational modification of the active site. As a result the substrate could not bind to the enzyme and consequently leading to the decrease in the reaction velocity and inhibition of enzyme activity. From alpha-glucosidase inhibition kinetic data, lower V_{max} and unchanged K_m values of L1 and L7 indicates non-competitive inhibition which means that inhibitors possibly do not bind to the active site of the enzyme, but instead diminish the catalytic activity by modulating the enzyme-substrate transition state. Rest of the ligands binds competitively. This pattern of inhibition suggests that active site of enzyme is directly involved in the inhibition process. K_i values for amylase and glucosidase inhibition are in micromolar range indicating strong binding of inhibitor. Still lower K_i values

compared to alpha- amylase inhibition points to the higher inhibitory activity against alpha-glucosidase by the synthesized compounds.

4.3.2.2.2 Kinetic parameters and mode of inhibition of NiL1, NiL2, NiL3, NiL5, NiL6 and NiL7

Table 4.4: kinetic constants K_m, V_m, K_i and the type of inhibition of alpha- amylase and alpha-glucosidase by Ni (II) complexes

Sample	alpha-amylase				alpha-glucosidase			
	K_m(mM)	V_m(µM/ min)	K_i(mM)	Mode of inhibition	K_m (mM)	V_m	K_i(mM)	Mode of inhibition
Control	0.164	0.616			0.170	0.263		
NiL1	0.173	0.338	0.398	Non-Comp	0.505	0.247	0.042	Comp
NiL2	0.169	0.326	0.287	Non-Comp	0.363	0.259	0.078	Comp
NiL3	0.157	0.339	0.525	Non-Comp	0.463	0.251	0.041	Comp
NiL5	0.382	0.583	0.668	Comp	0.195	0.141	0.094	Non-Comp
NiL6	0.445	0.572	0.386	Comp	0.165	0.144	0.056	Non-Comp
NiL7	0.174	0.388	0.802	Non-Comp	0.367	0.259	0.063	Comp

Among Ni (II) complexes NiL5 and NiL6 bind to amylase competitively while with glucosidase inhibition was in noncompetitive way. Strongest binder with amylase is NiL2 and with glucosidase was found to be NiL3.

4.3.2.2.3 Kinetic parameters and mode of inhibition of CuL1, CuL2, CuL3, CuL4, CuL5, CuL6 and CuL7

Table 4.5: kinetic constants K_m, V_m, K_i and the type of inhibition of alpha-amylase and alpha-glucosidase by Cu (II) complexes

Sample	alpha-amylase				alpha-glucosidase			
	K_m(mM)	V_m(µM/ min)	K_i(mM)	Mode of inhibition	K_m (mM)	V_m	K_i(mM)	Mode of inhibition
Control	0.164	0.616			0.170	0.263		
CuL1	0.165	0.389	0.475	Non-Comp	0.396	0.267	0.045	Comp
CuL2	0.169	0.344	0.318	Non-Comp	0.402	0.288	0.047	Comp
CuL3	0.127	0.318	0.393	Non-Comp	0.505	0.257	0.037	Comp
CuL4	0.175	0.368	0.556	Non-Comp	0.496	0.250	0.059	Comp
CuL5	0.323	0.575	0.813	Comp	0.371	0.244	0.066	Comp
CuL6	0.389	0.549	0.317	Comp	0.539	0.307	0.036	Comp
CuL7	0.169	0.370	0.657	Non-Comp	0.480	0.254	0.037	Comp

For copper complexes, CuL5 and CuL6 inhibit amylase competitively while the rest bind noncompetitively. All the copper complexes bind competitively to inhibit glucosidase. K_i value for amylase inhibition and glucosidase inhibition is least for complex CuL6. It clearly indicates stronger inhibition by CuL6 against both the enzymes.

4.3.2.2.4 Kinetic parameters and mode of inhibition of ZnL1, ZnL2, ZnL3, ZnL4, ZnL5, ZnL6, ZnL7 and ZnL8

Table 4.6: kinetic constants K_m, V_m, K_i and the type of inhibition of alpha-amylase and alpha-glucosidase by Zn (II) complexes

Sample	alpha-amylase				alpha-glucosidase			
	K_m(mM)	V_m(µM/ min)	K_i(mM)	Mode of inhibition	K_m (mM)	V_m	K_i(mM)	Mode of inhibition
Control	0.164	0.616			0.170	0.263		
ZnL1	0.183	0.229	0.292	Non-Comp	0.455	0.305	0.055	Comp
ZnL2	0.131	0.321	0.277	Non-Comp	0.431	0.244	0.053	Comp
ZnL3	0.171	0.292	0.342	Non-Comp	0.563	0.97	0.037	Comp
ZnL4	0.171	0.308	0.376	Non-Comp	0.418	0.281	0.047	Comp
ZnL5	0.330	0.540	0.718	Comp	0.150	0.156	0.085	Non-Comp
ZnL6	0.567	0.590	0.365	Comp	0.445	0.269	0.029	Non-Comp
Znl7	0.171	0.372	0.673	Non-Comp	0.418	0.253	0.048	Comp
ZnL8	0.171	0.322	0.376	Non-Comp	0.539	0.304	0.052	Comp

Among zinc complexes ZnL5 and ZnL6 inhibit amylase competitively and the rest inhibit noncompetitive manner. Least K_i value was obtained for ZnL2. But against alpha-glucosidase, ZnL5 and ZnL6 inhibited noncompetitive way.

The K_i values can also be a useful strategy to compare the activity of the compounds, being insightful of the binding affinity of the inhibitor for the enzyme. Lower K_i indicates higher binding affinity which leads to increased potential of inhibition. From K_i values, it is clear that on complexation binding affinity has increased evidently. On complexation electronic structure may be

modified so that they mimic substrate analogues and compete for active site. Still lower K_i values compared to alpha-amylase inhibition points to the higher inhibitory activity against alpha-glucosidase by all the synthesized compounds [41]. The strong hydrogen bond interactions with active site amino acids are consistent with a very favorable binding affinity to the active site, indicating a competitive type of inhibition [42].

Among all the ligands and complexes, ZnL2 is having the strongest inhibition against alpha-amylase. And against alpha-glucosidase the most potent inhibitor among the synthesized compounds is ZnL6 which is in accordance with IC_{50} determination studies.

4.4 Conclusion

Diabetes Mellitus is a metabolic dysfunction which develops due to impaired insulin production or insulin resistance in tissues. Diabetes is marked by postprandial hyperglycemia or elevated levels of fasting blood glucose. One of the most promising therapeutic strategies for the control of diabetes is the inhibition of the key enzymes which hydrolyses dietary carbohydrate. In this chapter we have screened inhibitory potential of synthesized 2-methoxy-4-chromanones and their Cu (II), Zn (II), Ni (II) complexes on alpha-amylase and alpha-glucosidase. All the results were compared with the standard acarbose. Complexes CuL1, CuL2, CuL5, ZnL5, ZnL2 have IC_{50} values less than that of acarbose. And all other compounds have comparable IC_{50} values even though they are less that of the standard acarbose. It is found that all the compounds could inhibit both the enzymes in concentration dependent manner. The inhibition kinetic studies revealed that inhibitors bind to enzymes either competitively or non-competitively. Among the complexes, Zn (II)

complexes were found to have more inhibitory potential on both the enzymes. Complexes containing electron withdrawing group were found to have higher activity than those present with electron donating methyl group. Our findings are in line with the reports that mild amylase inhibition and potent glucosidase inhibition can be considered as the effective way to decrease the carbohydrate metabolism in the intestine.

References

[1] A. M. Aalto; A. Uutela; A. R. Aro; Patient EducCouns. **1997**, 30, 215.

[2] T. D. Adams; R. E. Gress; S. C. Smith; R. C. Halverson; S. C. Simper; W. D. Rosamond; M. J. Lamonte; A. M. Stroup; S. C. Hunt; N. Eng; J. Med. Chem. **2007**, 357, 753.

[3] P. Mccue; Y. I. Kwon; K. Shetty; J. Food Biochem. **2005**, 3, 278.

[4] D. Devendra; E. Liu;G. S. Eisenbarth; BMJ **2004**, 328, 750.

[5] M. D. Gunawan-Puteri; J. Kawabata; Food Chem. **2010**, 123, 384.

[6] A. Szkudlarek; A. Sulkowska; M. Maciqzek-Jurczyk; M. Chudzik; J. Rownicka-Zubik; Spectrochim. Acta, Part A. **2016**, 152, 645.

[7] Z. Yu; Y. Yin; W. Zhao; Y. Yu; B. Liu; J. Liu; F. Chen; Food Chem. **2011**, 129, 1376.

[8] S. Harold; E. Lebovitz; Endocrinol. Metab. Clin. North Am. **1997**, 3, 539-551.

[9] S. Adisakwattana; P. Jiphimai; P. Prutanopajai; B. Chanathong; S. Sapwarobol; T. Ariyapitipan; Int. J. Food Sci. Nutr. **2010**, 61, 295.

[10] M. Al-Kazaz; V. Desseaux; G. Marchis-Mouren; E. Prodanov; M. Santimone; Eur. J. Biochem. **1998**, 252,100.

[11] S. Dhital; L. A. Hui-Mei; R. H. Bruce; J. G. Michael; M. Anbuhkani; **2013**, DOI:10.1371/journal.pone.0062546.

[12] B. Henrissat; Biochem. J. **1991**, 280, 309.

[13] G. D. Brayer; G. Sidhu; R. Maurus; E. H. Rydberg; C. Braun; Y. Wang; N. T. Nguyen; C. M. Overall; S. G. Withers; Biochem., **2000**, 39, 4778.

[14] A. J. Hirsh; S.Y. Yao; J. D. Young; C. I. Cheeseman; Gastroenterology. **1997**, 113, 205.

[15] W. F. Caspary; Lancet. **1978**, 1, 1231.

[16] J. S. Kim; C. S. Kwon; K. H. Son; Biotechnol. Biochem. **2000**, 64, 2458.

[17] J. Samantha; V. Aschenbrenner; S. Diane; Drug Therapy In Nursing. **2008**, ISBN 0-7817-4839-9.

[18] A. J. Scheen; Drugs. **2003**, 63, 933.

[19] M. Hanefeld; Cardiovas. Diabetol. **2007**, 14, 620.

[20] M. Barrett; J. Udani; Nutr. J. **2011**, 1024.

[21] M. al-Rashida; R. Raza; G.Abbas; M. Shakil Shah; G. E. Kostakis; J. Lecka; J. Sévigny; M. Muddassar; Eur. J. Med. Chem. **2013**, 66, 438.

[22] M. al-Rashida; G. Batool; A. Sattar; S. A. Ejaz; S. Khan; J. Lecka; J. Sévigny; A. Hameed; J. Iqbal; Eur. J. Med. Chem. **2016**, 115, 484.

[23] I. P. Tripathi; M. M. Kumar; K. Arti; M. Chinmayi; T. Ruchita; S. L. Kant; P. K. Bihari; Res. J. Chem. Sci. **2013**, 12, 54.

[24] S. K. Bharti; S. K. Singh; Der. Pharmacia. Lettre. **2009**, 2, 39.

[25] N.Wiernsperger; J. Rapin. Diabetol. Metab. Syndr. **2010**, 2, 70.

[26] H. Sakurai, A. Katoh, T. Kiss, T. Jakusch, M. Hattori; Metallomics. **2010**, 26, 70.

[27] S. Rafique; M. Idrees; A. Nasim; H. Akbar; A. Athar; Biotechnol. Mol. Biol. Rev. **2010**, 5, 38.

[28] S. Rosa; F. Nadjafi; M. Francesco; Nat. Prod. Res. **2006**, 20, 882.

[29] E. A. Mohamed; M. J. Ahmad Siddiqui; L. F. Ang; A. Sadikun; S. H. Chan; S. C. Tan; M. Z. Asmawi; M. F. Yam; Complemen. Altern. Med. **2012**, 12, 176.

[30] H. Sun; D. Wang; X. Song; Y. Zhang; W. Ding; X. Peng; X. Zhang; Y. Li; Y. Ma; R. Wang; P. Yu; J Agric Food Chem., **2017**, 65, 1574.

[31] H. Lineweaver; D. Burk; J. Am. Chem. Soc. **1934**, 56, 658.

[32] S. Horii; K. Fukasse; T. Matsua; K. Kameda; N. Asan; Y. Masui; J. Med. Chem. **1987**, 29, 1038.

[33] Y. I. Kwon; D. A.Vattem; K. Shetty; Asia Pac. J. Clin. Nutr. **2006**, 15, 107.

[34] G. W. Stephen; P. Ian Street; P. Bird; H. David; Dolphin; J. Am. Chem. Soc. **1987**, 109, 1531.

[35] W. Yufang; M. Lin; L. Zhong; D. Zhiyun; L. Zhong; Q. Jiangke; W. Xiaodong; H. Zhishu; G. Lianquan; S. C. Albert; FEBS Letters. **2004**, 576, 46.

[36] S. Qiong; S. Jialiang; P. Quan; Z. Wanjin; M. Lin; S. C. Albert; Chan; G. Lianquan; J. Med. Chem. **1986**, 53, 8252.

[37] T. Ayako; K. Hideaki; M. Takeshi; Y. Kaoru; Y. Kazutomi;Y. Yoshimitsu; S. Iichiro; M. Taka-aki ; M. Munehide; Endocr. J. **2009**, 56, 696.

[38] G. J. Brewer; R. Dick; C. Zeng; G. Hou; J. Inorg. Biochem. **2006**, 100, 927.

[39] E. A. Ostrakhovitch; M. G. Cherian, Arch. Biochem. Biophy. **2004**, 423, 351.

[40] M. A. Ibrahim; N. A. Koorbanally; M. S. Islam; Acta Pharm. **2014**, 64, 311.

[41] A. J. Krentz; C. J. Baily; Drugs. **2005**, 65, 385.

[42] A. A. Kumaran; R. J. Karunakaran; Lebens. Wiss. Tech. **2007,** 40, 344.

******

Chapter 5

DNA Binding studies of 2-methoxy-4-chromanones and its Ni (II), Cu (II), Zn (II) complexes

Contents

Abstract

Interaction of small molecules with DNA is always of considerable interest due to the functional importance as effective pharmaceutical agents, especially as anticancer drugs. Metal based pharmaceuticals are promising candidates as they can behave as models for several biological reactions. Chromone core is often treated as a valid scaffold for the development new drug libraries which is the fundamental to the new improved class of drugs. In this chapter we are reporting a novel class of DNA intercalators incorporating 2-methoxy-4-chromanones, which have comparable binding constants with the standard intercalators. Uv-visible absorption studies together with viscosity measurements were used to evaluate the effect of binding of the molecules to Herring Sperm DNA. Clear hypochromism shown in the absorption spectra and increase in the relative viscosity of DNA during the viscosity measurements lead to the conclusion of intercalative mode of binding.

5.1 Introduction

It was the year of 1960 which witnessed one of the milestones in the history of metal based therapeutics by the discovery of cisplatin by Barnett Rosenberg. Since then metal complexes that can interact with DNA have been widely explored by different research groups all around the globe [1-6].

DNA-metal ion interaction has been an interesting subject of research for many years. DNA is considered as a super coiled negatively charged polymer of nucleotide units and is found in living cells usually as right-handed double helix (B-DNA). The two chains have complementary sequences of sugar bases, with the phosphate groups on the outside and the base pairs bonded by hydrogen bonding in the interior [7]. The positively charged metal ions bind directly or indirectly with sites rich by high electron density or negatively charged residues of DNA. Such sites on DNA can be the negatively charged phosphates of the backbone of both strands and the electron donors of the bases, such as nitrogen and oxygen atoms. The predominant mode of metal binding takes place at the N7 and O6 of guanine and N7 and N1 of adenine bases and the N3 of pyrimidines [8].

Metal binding to the bases of DNA helix will more often results in hydrogen bonding within the base pairs and thus causes destabilization of the double helix [9]. But presence of metal ion can stabilize the helix by the neutralization of excess negatively charge phosphate groups. Confirmation of sugar is also seriously influenced by the metal-nucleotide binding [10]. Wang *et al.* reported the 1.1 Å resolution crystal structure of the platinum complex $[Pt(SEtOH)(terpy)]^{+}$ which was intercalated into the dinucleotide dimer deoxy CpG and the structure revealed that when intercalated the DNA unwinds to

accommodate the metal complex between bases and the pucker of the sugar rings will change the geometry. This alternate sugar puckering was recommended as the base for the "neighbour exclusion principle" associated with DNA intercalation, where at most intercalators bind in every other interbase-pair site [11]. Komor *et al* have reported that intercalation happens from the major groove, with the intercalating aromatic ligand π-stacking with the π-orbitals of the flanking base pairs, similar to the stacking of consecutive base pairs in duplex DNA. This structure also confirmed the conformational changes as evident from shorter intercalated oligonucleotides like buckling of the base pairs, flanking the intercalation site, and a minor unwinding of the DNA localized at the site of intercalation [12]. Complexes bind to DNA either covalently or non-covalently. Covalent binding happens when one of the labile ligands of the complex replaces one of the nitrogen bases of DNA. Noncovalent binding results from the intercalation or groove binding. Shift in λ_{max} values while adding DNA to the complex is the consequence of the structural damage of DNA due to the binding of complexes [13, 14]. Intercalative mode of binding may result in hypochromism and bathochromism involving a strong stacking interaction between aromatic chromophores and DNA base pairs. Intercalation may result in the coupling of π* orbital of inercalators with π orbitals of base pairs of DNA, resulting in the decrease of $\pi \rightarrow \pi^*$ transition energies. Hyperchromism can be credited to external contact or partial uncoiling of helical structure revealing more bases of DNA. Extent of hyperchromism is indicative of partial or non intercalative binding modes [15].

Several classes of metal complexes have been designed as excellent DNA binding agents. Out of these, complexes incorporating chromones and its derivatives constitute an important subgroup owing to its fascinating chemical

properties. Recently, Prabhakaran and his research group reported four new water soluble Cu (II) complexes from 3-formylchromone N-substituted thiosemicarbazones which can bind with CT-DNA intercalatively [16]. Reports are there in the literature regarding the DNA binding abilities of various 4-chromanone derivatives [17, 18]. But DNA binding properties of metal complexes from chromanones are not yet reported. So, in the present study, objective was to find out the DNA binding abilities of the synthesized ligands and its metal complexes. The techniques that were selected were Uv-visible absorption spectroscopy and viscometric measurements.

5.2 Experimental

5.2.1 Materials and methods

2-Methoxy-4-chromanones and their Ni (II), Cu (II) and Zn (II) complexes used for DNA binding studies were synthesized as per procedure described in Chapter 2 and Chapter 3 respectively.

Deoxyribonucleic acid, Tris (Hydroxymethyl)Aminomethane (Tris Buffer Tris Base) was purchased from Sisco Research Laboratories Pvt. Ltd.

5.2.2 Preparation of Tris-HCl Buffer

5 mM Tris HCl(5 mM, 151.42 mg) and 50 mM NaCl(50 mM, 292.2 mg) were accurately weighed and made up to mark in a 250 mL standard flask using distilled water. pH of the solution was adjusted to 7.2 using 1 mM NaOH solution with the help of pH meter before making up the solution. This buffer solution was used for DNA binding studies.

5.2.3 Preparation of DNA stock solution

DNA stock solution was prepared in 5 mM Tris-HCl buffer/50 mM NaCl (pH=7.2) and showed a ratio of UV absorbance at 260 nm and 280 nm (A_{260}/A_{280}) between 1.8 and 1.9 indicating DNA is free of protein. DNA concentration was calculated from its absorption intensity at 260 nm with molar extinction coefficient of 6600 $M^{-1}cm^{-1}$. Stock solution was stored at 4°C and used within a day.

5.2.4 Electronic absorption study - procedure

Spectrophotometric titration analysis of samples were recorded before and after addition of DNA in the presence of Tris- HCl buffer (pH 7.2). Appropriate concentration of sample solution in dimethyl sulphoxide (concentration of stock solution is 10^{-4} M) was titrated with incremental amounts of DNA over the range of 1-10 µM concentration to make constant total volume of 3 mL. Concentration of DNA was calculated from the absorbance measured at 260 nm with the known molar extinction coefficient of 6600 M^{-1} cm^{-1}.The difference in absorbance value with the increasing amount of HS-DNA could be observed as the function of DNA concentration. The extent of perturbation of absorbance value indicates the extent of DNA binding. The equilibrium binding constant (K_b) values were obtained from absorption spectral titration data using the following equation

$$([DNA]) \,/\, (\varepsilon a\text{-}\varepsilon f)=([DNA]) \,/\, (\varepsilon b\text{-}\varepsilon f)+ 1/K_b \, (\varepsilon b\text{-}\varepsilon f)$$

Where εa, εf and εb are the molar extinction coefficient observed for the charge transfer absorption at a given DNA concentration, the extinction coefficient at the complex free in solution and the extinction coefficient of the complex when fully bound to DNA respectively. K_b and [DNA] are the equilibrium binding constant

and the concentration in nucleotides respectively. A plot of [DNA] / (εa-εf) versus [DNA] gives K_b as the ratio of the slope to the intercept [19].

5.2.5 Viscosity measurements- procedure

Viscosity experiments were performed in Ostwald viscometer which was thermostated at 25 °C. Sample solutions with differing concentrations (50-300 µM) were added to give a specific mole-ratio r (r = [complex]/ [DNA]) while keeping the DNA concentration constant at (2.6×10^{-5} M). After thermal equilibration, the time of the solution's flowing through the capillary was determined by a digital stopwatch. Flow time was calculated three times for each concentration and mean flow time was calculated. The control was carried out using the standard intercalator Ethidium Bromide using the same above method. The data were founded as $(\eta/\eta_0)^{1/3}$ versus the mole-ratio values, where η and η_0 are the viscosity of DNA in the presence and absence of complex, respectively. Viscosity values were calculated from the observed flow time of DNA containing solutions (t) and corrected for buffer solution (t_0), $\eta = (t-t_0)/t_0$ [20].

5.3 Results and discussion

5.3.1 Electronic absorption studies

Electronic absorption spectroscopy is one of the best and essential tools for studying DNA binding ability of complexes. Complexes can bind to DNA covalently or non-covalently. Structural damage caused by the binding of DNA to the metal complex will results in the shift in the λ_{max} values while adding DNA to the complex is the consequence of the structural damage of DNA [21]. Intercalative mode of binding may result in hypochromism and bathochromism involving a strong stacking interaction between aromatic

chromophores and DNA base pairs. Intercalation may result in the coupling of π* orbital of intercalators with π orbitals of base pairs, resulting in the decrease of π→π * transition energies. Hyperchromism can be credited to external contact or partial uncoiling of helical structure exposing more bases of DNA. Extent of hyperchromism is indicative of partial or non-intercalative binding modes [22]. In the present study, absorption titrations were done to investigate the binding of synthesized compounds with DNA. Incremental addition of DNA to a constant concentration of sample in buffer medium showed hypochromicity assisted by shift (2–10 nm) of peak maxima and single isobestic point.

5.3.1.1 Electronic absorption studies of ligands

Fig. 5.1 (a-h) gives the absorption spectra for ligands in Tris–HCl buffer in absence and incremental addition upon of DNA; r = [DNA]/ [complex]). All ligands bind with DNA giving moderate hypochromicity. Due to C–H···O and C–H···π interactions in the planar aromatic rings of the chromanone molecules, synthesized chromanones bind to DNA helical structure in an intercalation mode via hydrogen bonding and π···π stacking interactions. Binding constant which is the indicative of the strength of binding is calculated and tabulated in table 5.1. K_b values, which give quantitative DNA binding, fall within the range 10^3 to 10^4. Ligand L1 is having the highest K_b value indicating the strongest binder among the group.

Fig. 5.1 (a-h): Absorption spectra for L1, L2, L3, L4, L5, L6, L7, L8 in Tris–HCl buffer in absence and incremental addition of DNA; r= [DNA]/ [complex]). Inset graph of [DNA]/ (εa-εf) vs. [DNA]

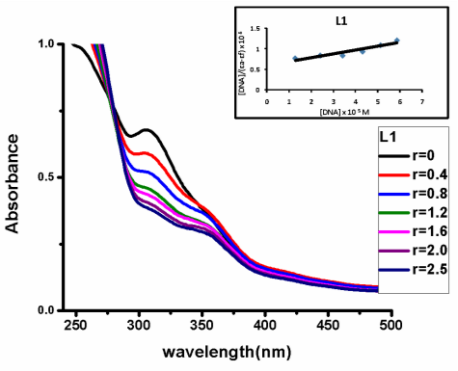

Fig. 5.1(a)

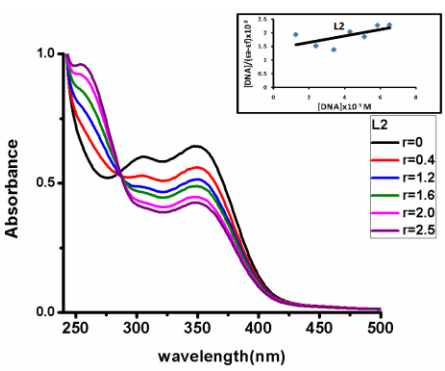

Fig. 5.1(b)

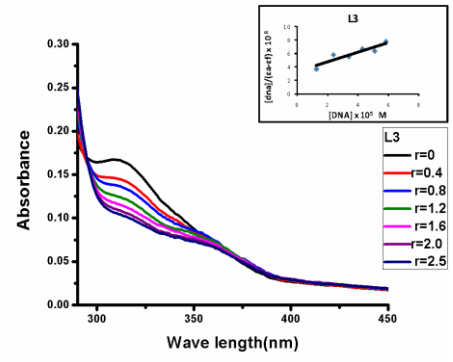

Fig. 5.1(c)

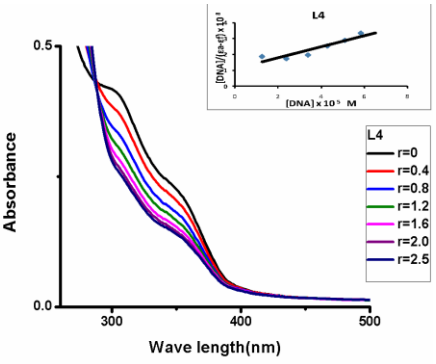

Fig. 5.1(d)

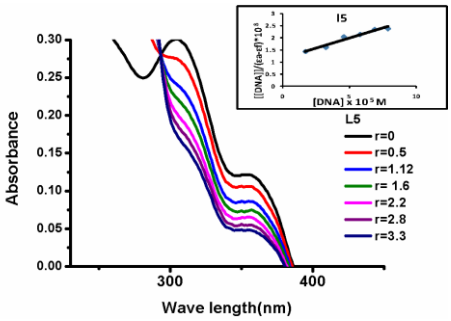

Fig. 5.1(e)

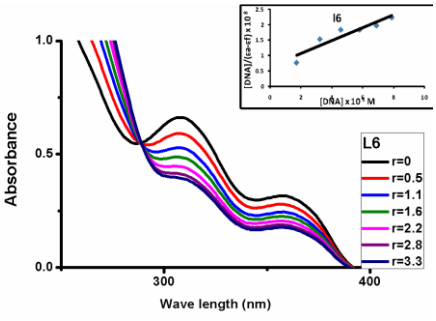

Fig. 5.1(f)

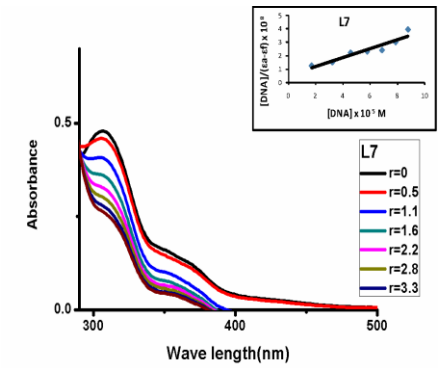

Fig. 5.1(g)

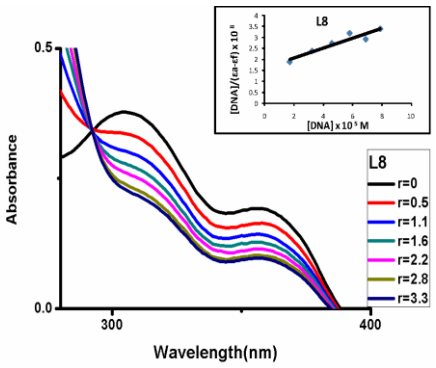

Fig. 5.1(h)

Table 5.1: Binding constant (M^{-1}) of ligands

Sample	$\lambda_{max(nm)}$		Δλ(nm)	H%[a]	Kb(M^{-1})
	Free	Bound			
L1	306	308	2	11	$1.8x10^{4}$
L2	349	351	2	12	$1.6x10^{4}$
L3	312	314	2	12	1.0×10^{4}
L4	304	305	1	4	$1.5x\ 10^{3}$
L5	306	309	3	12	1.5×10^{4}
L6	308	310	2	12	$1.1x\ 10^{4}$
L7	306	308	2	11	1.2×10^{4}
L8	306	308	2	11	1.3×10^{4}

5.3.1.2 Electronic absorption studies of Ni (II), Cu (II) and Zn (II) complexes

Complexation has evidently increased the metal binding affinity as metals play very crucial role in binding. Strong binding affinity of the metal complexes is due to further π-π interaction through the aromatic phenyl rings and central metal ions as compared with the ligands. Among Cu (II) complexes, CuL2 is having the strongest binding. NiL2 and ZnL8 are having stronger binding among the synthesized Ni (II) and Zn (II) complexes. Clear isobestic points in all ligands and complexes are indicative of the presence of two spectroscopically distinct chromophores (free and bound). Absence of isobestic point in some compounds may be due to the non alteration of chromophoric environment after interaction with DNA. The results clearly indicate that the samples actively interact with

DNA through intercalative mode. The extent of binding can be quantified using intrinsic binding constant K_b. Binding values obtained are less than the classical intercalators, but comparable to the reported chromone complexes [23]. Strong intercalation activity can be owed to the extensive aromatic plane and good conjugation for the ligands and the complexes [24]. Fig.5.2(a-f), Fig.5.3 (a-g), Fig. 5.4 (a-h) gives the absorption spectra for Ni(II) complexes, Cu(II) complexes and Zn (II) complexes respectively. Binding constants are also calculated and is tabulated in table 5.2.

Fig.5.2(a-f) : Absorption spectra for NiL1, NiL2, NiL3, NiL5, NiL6and NiL7 in Tris–HCl buffer in absence and incremental addition upon addition of DNA; r =[DNA]/[complex]). Inset graph of [DNA]/ (εa-εf) vs. [DNA]

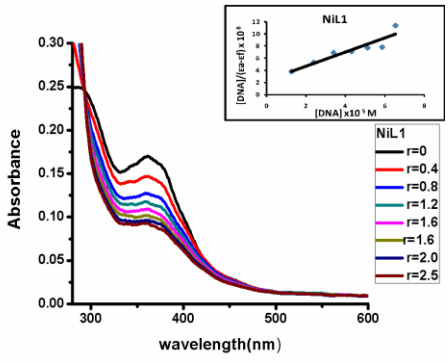

Fig. 5.2(a)

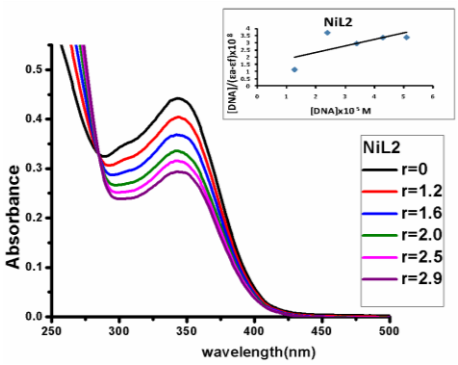

Fig. 5.2(b)

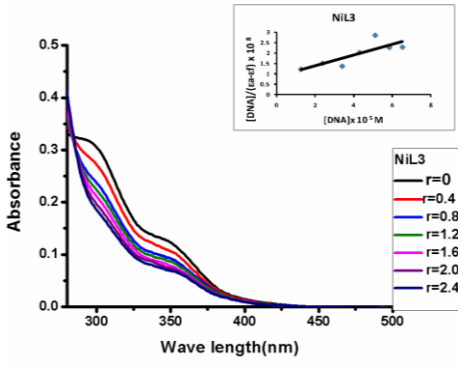

Fig.5.2(c)

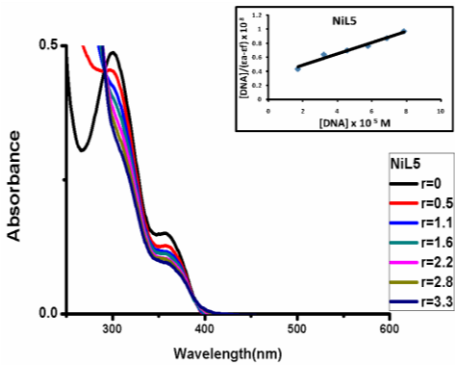

Fig.5.2 (d)

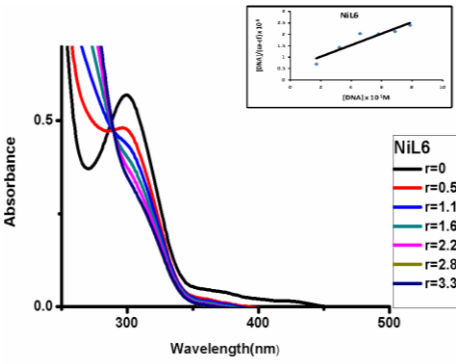

Fig. 5.2(e)

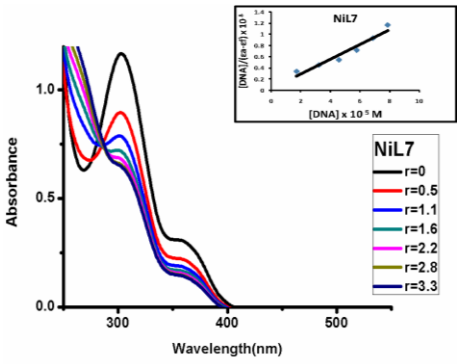

Fig. 5.2(f)

Fig. 5.3(a-g): Absorption spectra for CuL1, CuL2, CuL3, CuL4,Cu L5, CuL6 and CuL7 in Tris–HCl buffer in absence and incremental addition of DNA; r=[DNA]/[complex]). Inset graph of [DNA]/ (εa-εf) vs. [DNA]

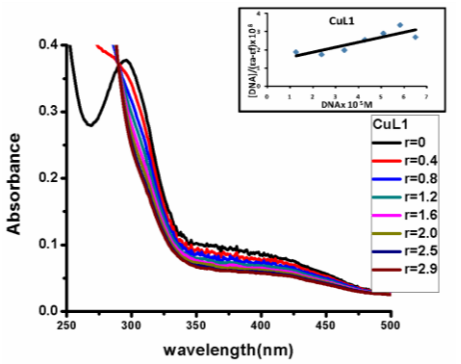

Fig. 5.3(a)

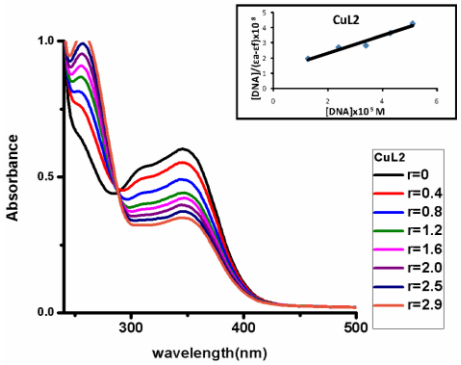

Fig. 5.3(b)

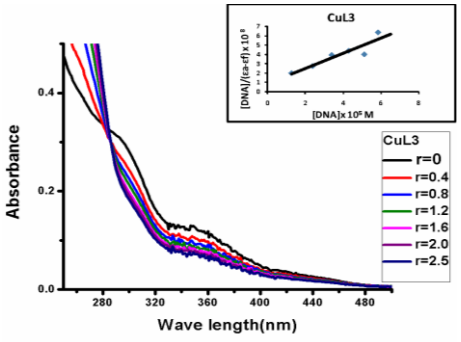

Fig. 5.3(c)

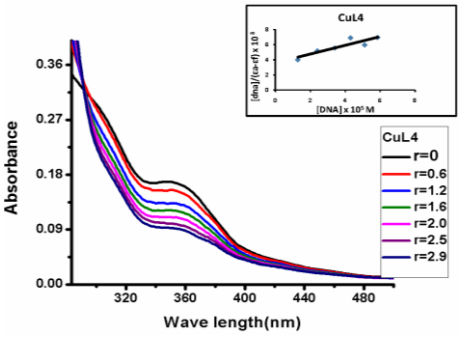

Fig. 5.3(d)

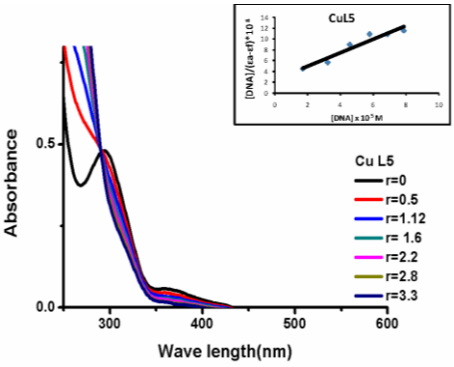

Fig. 5.3(e)

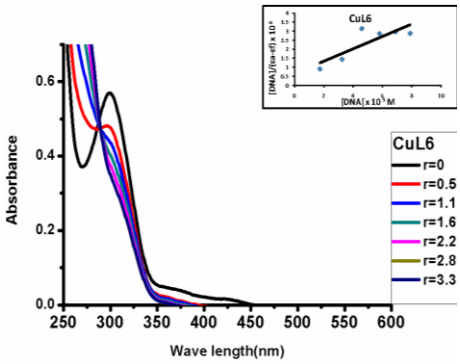

Fig. 5.3(f)

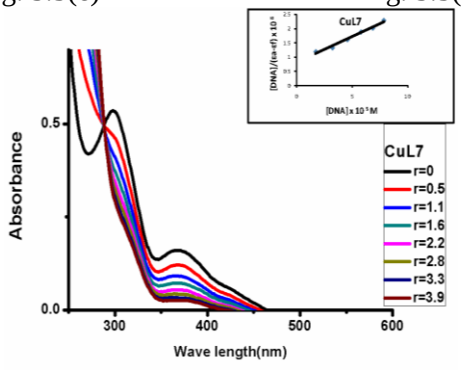

Fig. 5.3(g)

Fig.5.4 (a-h): Absorption spectra for ZnL1, ZnL2, ZnL3, ZnL4, ZnL5, ZnL6, ZnL7 and Zn L8 in Tris–HCl buffer in absence and incremental addition of DNA; r = [DNA]/[complex]). Inset graph of [DNA]/ (εa-εf) vs. [DNA].

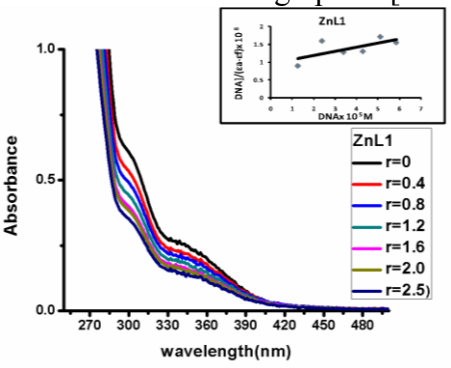

Fig. 5.4 (a)

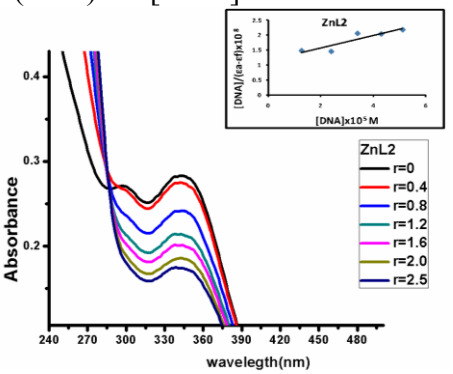

Fig. 5.4 (b)

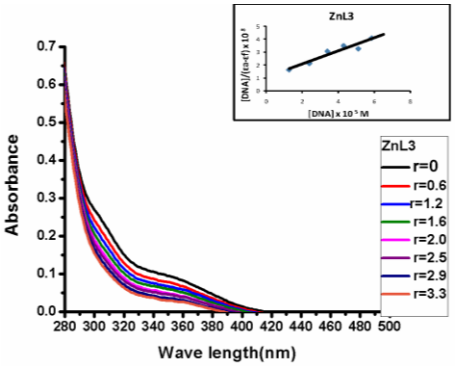

Fig. 5.4 (c)

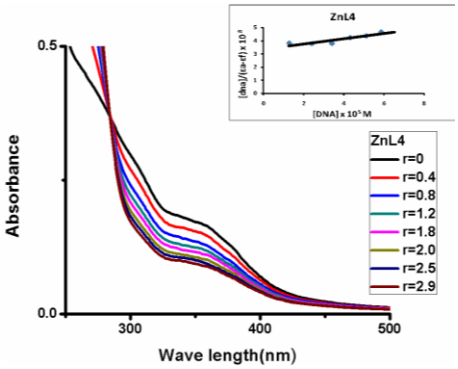

Fig. 5.4 (d)

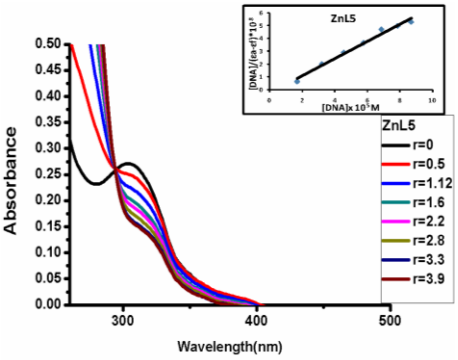

Fig. 5.4 (e)

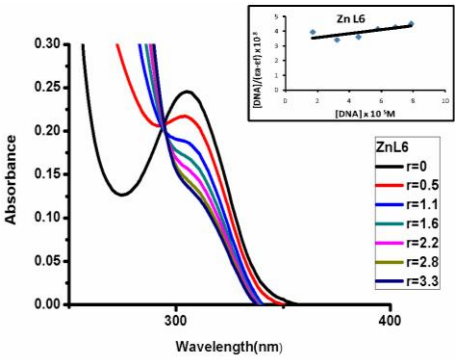

Fig. 5.4 (f)

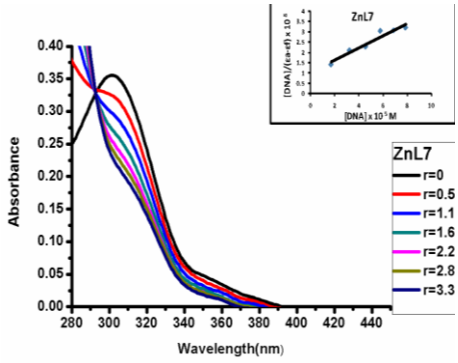

Fig. 5.4 (g)

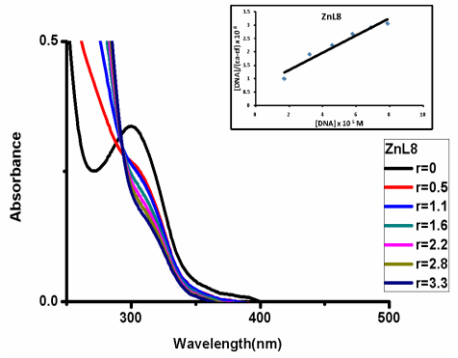

Fig. 5.4 (h)

Table 5.2: Binding constants of Ni (II), Cu (II), Zn (II) complexes

Sample	$\lambda_{max(nm)}$		Δλ(nm)	H%[a]	Kb(M^{-1})
	Free	Bound			
NiL1	360	364	4	21	1.1×10^5
NiL2	342	346	4	13	2.0×10^4
NiL3	296	304	5	18	9.8×10^4
NiL5	299	303	4	13	2.3×10^4
NiL6	298	305	7	23	1.2×10^5
NiL7	301	309	8	26	4.7×10^5
CuL1	297	300	3	13	1.9×10^4
CuL2	347	351	4	16	7.8×10^4
CuL3	293	296	3	14	3.1×10^4
CuL4	349	352	3	11	1.2×10^4
CuL5	299	302	3	14	5.0×10^4
CuL6	300	303	3	14	5.2×10^4
CuL7	299	304	4	17	7.6×10^4
ZnL1	303	307	4	15	5.1×10^4
ZnL2	343	347	5	17	7.7×10^4
ZnL3	305	309	4	13	2.2×10^4
ZnL4	339	343	4	11	1.6×10^4
ZnL5	305	310	5	13	2.4×10^4
ZnL6	305	310	5	13	2.7×10^4
ZnL7	309	314	5	14	2.8×10^4
ZnL8	301	308	7	21	1.2×10^5

5.3.2 Viscosity studies

Spectrophotometric probes generally provide essential, but not sufficient clues to prove how complex binds with DNA. Hydrodynamics studies(i.e. viscosity and sedimentation), which are sensitive to change of length, are considered as least confusing and more critical tests for investigating binding modes when crystallographic data is not present. So for further investigation of the binding abilities of the synthesized compounds with DNA, viscosity measurements were carried out on HS DNA by varying the concentrations of the sample and keeping constant DNA concentration. When a complex interacts with DNA, there will be changes in the relative viscosity of DNA. When the complex binds covalently, it causes bending and

unwinding of DNA double helix. For electrostatic binding there will be no effect on the relative viscosity of DNA solution. An increase in viscosity is a clear indication of intercalative DNA binding, because this binding mode causes elongation of DNA polymer by effecting separation of DNA base pairs. A partial or non-classical intercalation of the compounds can cause bend or kink in DNA followed by a decrease in its effective length with an associated decrease in its viscosity. Groove binding of DNA does not alter the viscosity of the DNA on addition to the DNA solution [25].

In order to make clear the binding mode and strength of samples with DNA, the relative viscosity is measured by the incremental addition of sample and is plotted against [sample]/ [DNA]. The plots show that relative viscosity of DNA has increased on the consecutive addition of sample. Results suggest that mode of binding of complexes and ligands with DNA follow base pair intercalation. This fact may be explained by the intercalation of the compounds in between the DNA base pairs, causing an increase in the separation of base pairs at intercalation sites and, thus, effectively an increase in overall length of DNA. It is clear from the figures that all these ligands and complexes show increase in the relative viscosity of HS DNA but is less when compared with the standard intercalator ethidium bromide. The values are comparable with the literature data [26, 27]. The viscosity results are graphically represented in Fig. 5.5-5.11 and may reflect the tendency of each ligand to intercalate into DNA base pairs. The increase in DNA viscosity observed in the complexes, suggests a classical intercalative mode. The observed viscosity results are in concomitant with the spectrophotometric titration results. Table 5.3-5.10 gives the viscosity data for ligands L1, L2, L3, L4, L5, L6, L7, L8 and its Ni (II), Cu (II) and Zn (II) complexes.

Table 5.3: Viscosity of data L1 and its Cu (II), Zn (II) and Ni (II) complexes

r=[complex]/ [dna]	$(\eta/\eta_0)^{1/3}$				
	L1	CuL1	ZnL1	NiL1	EB
0	1	1	1	1	1
0.07	1.66	2.26	2.16	2.06	3.2
0.14	1.93	2.90	2.31	2.39	4.3
0.22	2.12	3.30	2.51	2.67	5.6
0.29	2.28	3.80	2.66	2.87	6.3
0.37	2.38	4.00	2.87	3.06	7.2

Table 5.4: Viscosity of data L2 and its Cu (II), Zn (II) and Ni(II) complexes

r=[complex] /[dna]	$(\eta/\eta_0)^{1/3}$				
	L 2	**CuL2**	**ZnL2**	**NiL2**	**EB**
0	1	1	1	1	1
0.07	1.63	1.96	2.50	2.33	3.2
0.14	1.91	2.27	3.22	2.55	4.3
0.22	2.08	2.49	3.51	2.68	5.6
0.29	2.23	2.68	3.69	2.80	6.3
0.37	2.33	2.85	3.92	2.95	7.2

Table 5.5: Viscosity of data L3 and its Cu (II), Zn (II) and Ni(II) complexes

r=[complex] /[dna]	$(\eta/\eta_0)^{1/3}$				
	L3	**CuL3**	**ZnL3**	**NiL3**	**EB**
0	1.00	1.00	1.00	1.00	1
0.07	1.63	1.95	2.52	2.02	3.2
0.14	1.90	2.29	2.89	2.35	4.3
0.22	2.08	2.51	3.22	2.60	5.6
0.29	2.25	2.68	2.70	2.72	6.3
0.37	2.34	2.87	2.89	2.93	7.2

Table 5.6: Viscosity of data L4 and its Cu (II) and Zn (II) complexes

r=[complex]/ [dna]	$(\eta/\eta_0)^{1/3}$			
	L4	**CuL4**	**ZnL4**	**EB**
0	1.00	1.00	1.00	1
0.07	1.65	2.26	2.02	3.2
0.14	1.94	2.56	2.29	4.3
0.22	2.12	2.90	2.50	5.6
0.29	2.28	3.55	2.68	6.3
0.37	2.37	3.97	2.87	7.2

Table 5.7: Viscosity data of L5 and its Cu (II), Zn (II) and Ni(II) complexes

r=[complex]/[dna]	$(\eta/\eta 0)^{1/3}$				
	L5	**CuL5**	**ZnL5**	**NiL5**	**EB**
0	1	1	1	1	1
0.07	1.62	2.55	2.05	2.07	3.2
0.14	1.90	3.02	2.34	2.30	4.3
0.22	2.07	3.50	2.53	2.50	5.6
0.29	2.24	3.90	2.72	2.75	6.3
0.37	2.32	4.30	2.89	2.91	7.2

Table 5.8: Viscosity data of L6 and its Cu (II), Zn (II) and Ni (II) complexes

r=[complex] /[dna]	$(\eta/\eta_0)^{1/3}$				
	L6	**CuL6**	**ZnL6**	**NiL6**	**EB**
0	1.00	1.00	1.00	1.00	1
0.07	1.65	2.50	2.00	2.01	3.2
0.14	1.93	2.90	2.50	2.31	4.3
0.22	2.10	3.50	2.90	2.54	5.6
0.29	2.26	3.80	3.20	2.72	6.3
0.37	2.35	4.02	3.50	2.89	7.2

Table 5.9: Viscosity data of L7 and its Cu (II), Zn (II) and Ni (II) complexes

r=[complex] /[dna]	$(\eta/\eta_0)^{1/3}$				
	L7	**CuL7**	**ZnL7**	**NiL7**	**EB**
0	1.00	1.00	1.00	1.00	1
0.07	1.61	1.95	2.35	1.98	3.2
0.14	1.90	2.30	2.56	2.10	4.3
0.22	2.08	2.50	2.73	2.20	5.6
0.29	2.24	2.68	3.20	2.50	6.3
0.37	2.34	2.86	3.50	2.70	7.2

Table 5.10: Viscosity of data L8 and its Zn (II) complex

r=[complex] /[dna]	$(\eta/\eta_0)^{1/3}$		
	L8	**ZnL8**	**EB**
0	1.00	1.00	1
0.07	1.63	2.01	3.2
0.14	1.92	2.33	4.3
0.22	2.10	2.55	5.6
0.29	2.26	2.72	6.3
0.37	2.35	2.89	7.2

Fig. 5.5- 5.12: Plots of $[\eta/\eta_o]^{1/3}$ versus [Complex]/[DNA] for ligands and its Ni(II), Cu(II), Zn(II) complexes

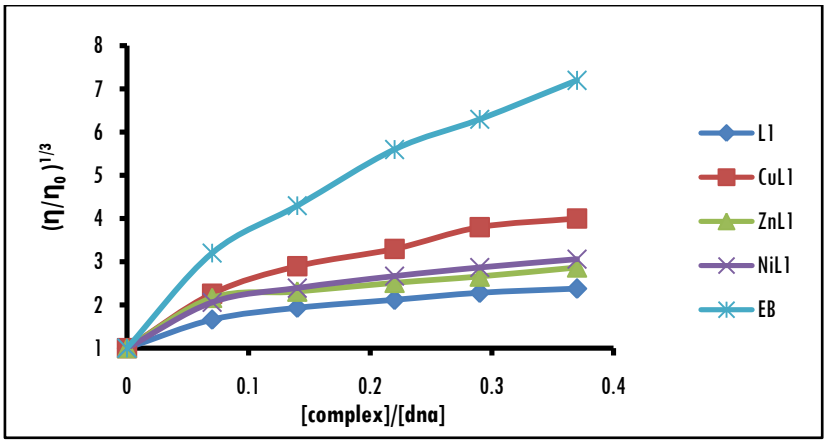

Fig.5.5: Plot of $[\eta/\eta_o]^{1/3}$versus [Complex]/[DNA] for L1 and its Ni(II), Cu(II), Zn(II) complexes

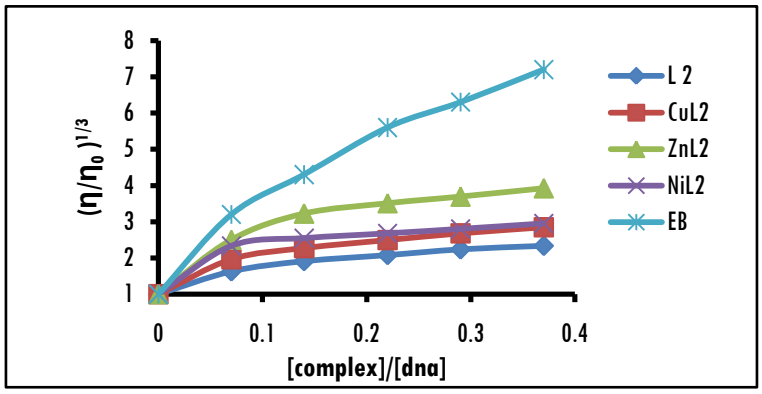

Fig. 5.6: Plot of $[\eta/\eta_o]^{1/3}$versus [Complex]/[DNA] for L2 and its Ni(II), Cu(II), Zn(II) complexes

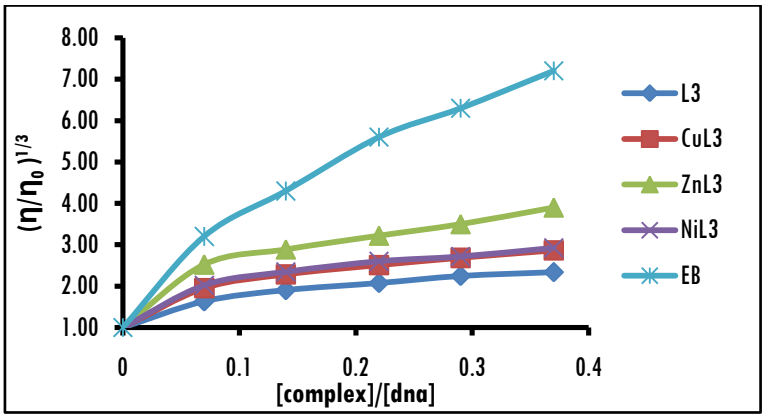

Fig.5.7: Plot of $[\eta/\eta_o]^{1/3}$versus [Complex]/[DNA] for L3 and its Ni(II), Cu(II), Zn(II) complexes

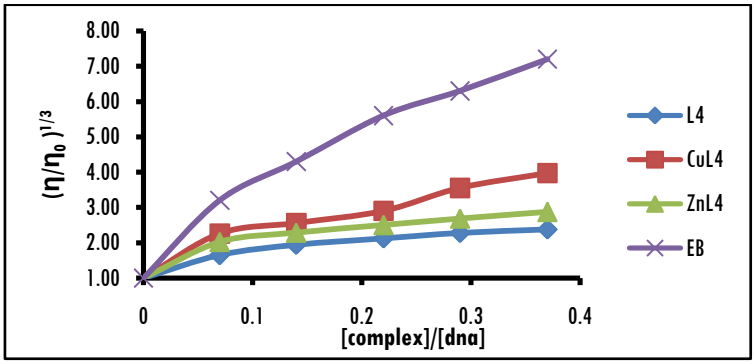

Fig.5.8: Plot of $[\eta/\eta_o]^{1/3}$versus [Complex]/[DNA] for L4 and its Cu(II), Zn(II) complexes

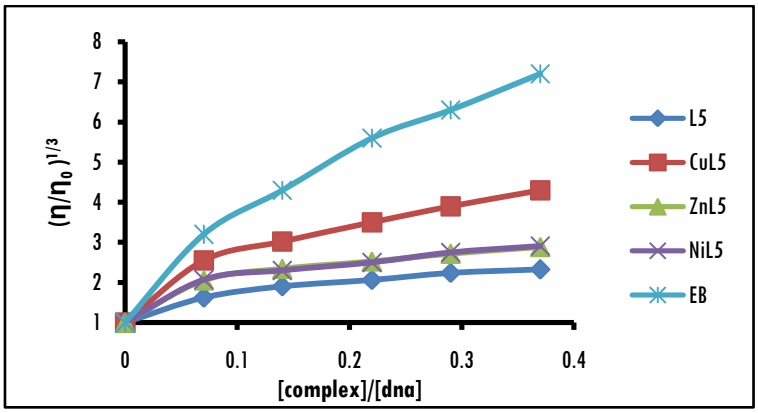

Fig.5.9: Plot of $[\eta/\eta_o]^{1/3}$versus [Complex]/[DNA] for L5 and its Ni(II), Cu(II), Zn(II) complexes

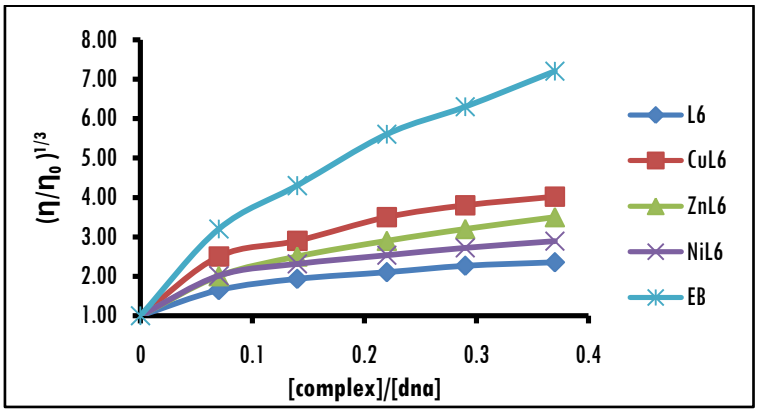

Fig.5.10: Plot of $[\eta/\eta_o]^{1/3}$versus [Complex]/[DNA] for L6 and its Ni(II), Cu(II), Zn(II) complexes

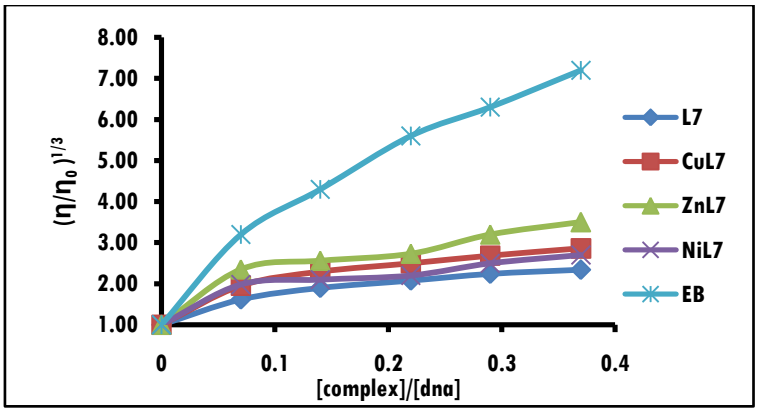

Fig.5.11: Plot of $[\eta/\eta_o]^{1/3}$versus [Complex]/[DNA] for L7 and its Ni(II), Cu(II), Zn(II) complexes

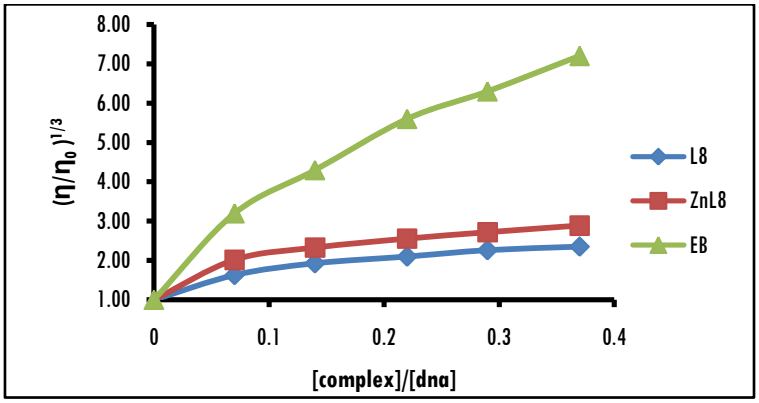

Fig.5.10: Plot of $[\eta/\eta_o]^{1/3}$versus [Complex]/[DNA] of L8 and its Zn(II) complexes

5.4 Conclusion

HS-DNA binding behavior with the synthesized ligands and complexes were performed. Uv-visible spectrophotometry together with viscosity measurements were selected for studying the binding behavior of DNA. Uv-visible studies showed clear hypochromism which indicate that DNA binds intercalatively. Intrinsic binding constant K_b values were also determined and were in the range of 10^4- 10^5 and is comparable with the standard intercalators. Results obtained from viscosity studies of DNA binding were also in accordance with the optical studies. Complexation has evidently increased the binding ability due to the crucial role of metal ions. Strong intercalation activity can be attributed to the extensive aromatic plane and good conjugation for the ligands and the complexes.

References

[1] T. Alessio; D. Cosimo; M. Louise; B. Giampaolo; J. H. Michael, Dalton Trans. **2013**, 42, 11220.

[2] J. Tan; B. C. Wang; L. C. Zhu; Bioorg. Med. Chem. **2009**, 17, 614.

[3] S. Shi; X. T. Geng; J. Zhao; T. M. Yao; C. R. Wang; D. J. Yang; L. F. Zheng; L. N. Ji; Biochimie. **2010**, 92, 370.

[4] A. Patra; B. Sen; S. Sarkar; A. Pandey; E. Zangrando; P. Chattopadhyay; Polyhedron. **2013**, 51, 156.

[5] S. Shobana; J. Dharmaraja; S. Selvaraj; Spectrochim. Acta A: Mol. Biomol. Spectrosc. **2013**, 107, 117.

[6] S. M. Hecht; J. Nat. Prod. **2000,** 63, 158.

[7] T. Theophanide; Appl. Spectrosc. **1981**, 35, 461.

[8] J. Anastassopoulou; J. Mol. Struc. **2003**, 19, 651

[9] D. Yang; A. H. Wang; Prog. Biophys. Mole. Biol. **1996**, 66, 81.

[10] H. A. Tajmir-Riahi; T. Theophanides; Can. J. Chem. **1984**, 62, 266.

[11] A. H. J. Wang, J. Nathans; G. van der Marel; J. H. van Boom, A. Rich; Nature. **1978**, 276, 471.

[12] A. C. Komor; J. K. Barton; Chem. Commun. (Camb). **2013**, 49, 3617.

[13] M. A. Ibrahim; N. A. Koorbanally; M. S. Islam; Acta. Pharm. **2014**, 64, 311.

[14] Q. Zhang; J. Liu; H. Chao; G. Xue; L. Ji; J. Inorg. Biochem. **2001**, 83, 49.

[15] T. Kiran; V. G. Prasant; M. M. Balamural; C. S. Vasavi; P. Munusami; K. I Sathiyanarayanan; M. Pathak; Inorg. Chim. Act. **2015**, 433, 26.

[16] G. Kalaiarasi; S. R. JeyaRajkumar; S. Dharani; V. M. Lynch; R. Prabhakaran; Inorg. Chim, Acta. **2018**, 471, 759.

[17] B. Mayuri; P. Kavitha; S. Basavoju; G. Bhargavi; K. L. Reddy; J. Mol. Struc. **2017**, 1145, 1.

[18] A. Dziewulska-Kułaczkowska; J. Therm. Anal. Calor**. 2012**,109, 7.

[19] N. Deepika; C. S. Devi; Y. P. Kumar; K. L. Reddy; P. V. Reddy; D. A. Kumar; S. S. Singh; S. Satyanarayana; J. Photochem. Photobiol. **2016,** 160, 142.

[20] E. S. Jose; J. E. Philip; A. A. Shanty; M. R. P. Kurup; P. V. Mohanan; Inorg. Chim. Acta. **2018**, 478, 155.

[21] M. E. Reichmann, S. A. Rice, C. A. Thomas, P. Doty, J. Am. Chem. Soc. **1954**, 763047.

[22] T. Ghosh; B. Mondal; T. Ghosh; M. Sutradhar; G. Mukherjee; Inorg. Chim. Acta. **2007**, 360. 1753.

[23] J. Ta; Y. Lu; Z. Huang; L. Gu; J. Wu; Eur. J. Med. Chem. **2007,** 42, 1169.

[24] Q. Wang; Z. Yang; G. Qi; D. Qin; Biomet. **2009**, 22, 927.

[25] F. Arjmand; I. Yousuf; J. Organomet. Chem. **2013**, 4, 355.

[26] N. Raman; R. Mahalakshmi; L. Mitu; Spectrochim. Acta A Mol. Biomol. Spectrosc. **2013,** 115, 399.

[27] M. Sunita; C. Anupama; Ushaiah; .GyanaKumari; Arab. J. Chem. **2017**, 10, S3367.

****

Chapter 6

Antimicrobial screening of 2-methoxy-4-chromanones and its Ni (II), Cu (II), Zn (II) complexes

Contents

Abstract

Resistance against antimicrobials by various infectious agents has emerged as a serious cause of public threat at an alarming rate. Continuous use and misuse of antimicrobial drugs and poor infection control practices is considered as the major reason for the resistance by the microbial species. There is an increased urge for new and better class of antimicrobial drugs that can better treat or manage the infections. This chapter discusses the antimicrobial efficacy of selected ligands and complexes against two gram positive bacterial strains (Staphylococcus aureus (MTCC 96) and Bacillus subtilis (MTCC 121)), two gram negative bacterial strains (Pseudomonas aeruginosa (MTCC 741) and Escherichia coli (MTCC 1652)) and one fungal species (Candida albicans (ATCC 10231)). Disc diffusion method was used for determining antimicrobial activity and resazurin reduction method for determining MIC. All the values were compared with the standard drugs. Complexation has evidently increased the antimicrobial efficiency which can be tagged with the reports that hike in the antimicrobial activity due to the presence of metal ions. ZnL6 was having the least MIC and is against the species B. subtilis.

6.1 Introduction

The management of contagious diseases still remains an important and challenging problem because of a blend of factors including emerging infectious ailments and the increasing number of multi-drug resistant microbial pathogenic strains. Due to manifestation of old and new antibiotic resistance created in the last decades, a substantial medical need for new classes of antimicrobial agents has emerged in spite of a large number of antibiotics and chemo medications available for therapeutic use [1]. There is a real perceived need for the discovery of new class of compounds capable with antimicrobial activity, possibly acting through mechanism of action, which is distinct from those of well-known classes of antimicrobial agents to which many clinically relevant pathogens are now found to be resistant. Once bacteria become resistant to any antibiotic, they pass on this trait to their descendants through horizontal or vertical transfer. Evolution of new resistant strains of bacteria that are somewhat more lethal compared to the parent strain is the major side effect of the indiscriminate and irrational use of antibiotics these days. Many health-related problems have aroused due to the plethora of cases of widespread occurrence of resistant bacteria [2]. Different antibiotics have different mode of action based on the bacterial target sites. Antibiotic potential depends on the nature of their structure and their affinity towards the target cells. Antibacterial mechanisms include

a) Protein dysfunction and loss of enzyme activity.
b) Production of reactive oxygen species (ROS) and depletion of antioxidants.
c) Impairing membrane function.
d) Interference with nutrient assimilation.
e) Genotoxicity [3].

The use of metals and metal based drugs for their antimicrobial potentials was prevalent for several years before the advent of antibiotics. The first successful application of metal complexes was in 1900s by the discovery of Salvarsan, an organo silicon compound. In order to discover benign and effectual metal based biologically active compounds as impending antimicrobial drugs intensive research programs are taking place all over the world. Among the diverse therapeutic approaches to wipe out microbial menace, the appraisal of using transition metal complexes, as metallodrugs is believed to have a vast and great potential [4, 5]. Metal complexes are supposed to exert their effect by various mechanisms which include inhibition of enzymes, intracellular biomolecular interaction, enhanced lipophilicity, alteration of cell membrane properties and arrest of cell cycle etc. [6]. Due to a wide variety of coordination spheres, ligand design, oxidation states and redox potential, metal complexes are believed to modify the kinetic and thermodynamic properties of the complexes towards biological receptors [7]. Thus, chelation brings out severe changes in biological properties of ligands as well as metal moiety [8].The total charge of the complex can influence antibacterial activity. Generally the antimicrobial efficiency increases in anionic complex to neutral complex to cationic complex. The nature of the counter ion in the case of ionic complexes can affect antimicrobial potential. Usually binuclear complexes are more active against bacterial strains than mononuclear metal complexes [9].

Many metal complexes of quinoline group of antibiotics such as ciprofloxacin, norfloxacin and tetracycline were evaluated and reported to have superior activity than antibiotic alone [10, 11]. Feng *et al*. reported antimicrobial activity of a series of chromanones against Mycobacterium tuberculosis and a wide range of clinically significant Gram positive and Gram

negative bacteria, namely, *E. faecalis*, *S. aureus*, *E. coli*, *K. pneumoniae*, and *P. aeruginosa*. Although the majority of the chromanone derivatives had weak antituberculosis activity, stimulating data were obtained for the other systems. The SAR study showed that C5- and C7-hydroxyl groups, the presence of hydrogen bond donor/acceptors at C4, and a lipophilic 2-alkyl moiety were essential for antibacterial activity [12]. Shaikh *et al.* reported that bismuth-norfloxacin complex possess enhanced antimicrobial activity than norfloxacin alone. Enhanced activity is due to increased bioavailability of the complex. Hence carrying of organic ligands into bacterial cells can be made possible by the complexation of metal [13].

Natural products are often considered as wealthy sources of bioactive molecules and chemical diversity. Thus provided invaluable chemical scaffolds as well as served as stimulation in the direction of antibacterial drug discovery and development. Chromanones constitute a class of compounds in the large family of flavanoids, the polyphenolic phytochemicals. Recently, a new class of chromanone acids isolated from the bark of Calophyllum brasiliense Cambess showed moderate to strong antibacterial activity against *Bacillus cereus* and *Staphylococcus epidermidis* [14]. Sarasije *et al.* reported new naphthospirochromanone scaffolds using ionic liquids as a green solvent under microwave irradiation with potent antimicrobial properties [15]. Although metal-based antimicrobials hold great promise, their ability for toxicity in humans confines their existing use. In many instances, the mechanisms of antimicrobial metal toxicity stay vague, and identifying the precise, physiologically relevant cellular injuries connected with metal toxicity is a matter of question confronting bacteriologists and toxicologists. The recognition of bacterial targets and the drug uptake pathways could lead to

new methods for targeting toxic metals specifically to bacteria and may help to surmount some of the barriers coupled with human toxicity.

This chapter discusses the antibacterial and antifungal properties of the synthesized ligands and complexes. Minimum inhibitory concentrations of bacterial species having significant activity are also determined.

6.1.1 Bacterial strains used for the study

6.1.1.1 *Bacillus subtilis*

Bacillus subtilis, a gram-positive, catalase-positive bacterium, is an amazingly diverse bacterial species– competent of growth within diverse environmental conditions including the animal gastrointestinal tracts and soil. Microarray-based comparative genomic analyses have exposed that strains of this species also exhibit considerable genome diversity. Bacteria have the widespread ability to form surface-associated multicellular aggregates, generally known as biofilms [16]. *Bacillus subtilis* has been a best studied model organism for the study of bacterial chromosomal replication, cell differentiation and biofilm formation [17]. It is one of the bacterial title holder in secreted enzyme production and used by biotechnology companies on industrial scale [18].

6.1.1.2 *Staphylococcus aureus*

Staphylococcus aureus (also known as golden staph) is a gram-positive, round-shaped bacterium that is a member strain of the Firmicutes, and is frequently found in the nose, respiratory tract, and on the skin. [19]. *S. aureus* is a

foremost source of bacteremia and infective endocarditis as well as osteoarticular, skin and soft tissue, pleuropulmonary and device-related infections. Pathogenic strains frequently endorse infections by creating virulence factors such as potent protein toxins, and the expression of a cell-surface protein that binds and thus inactivating antibodies. Clinical infections with *S. aureus* will possibly linger both common and serious. Not only have there been waves of increasing antimicrobial resistance, but the spectrum of clinical disease also continues to change [20].

6.1.1.3 *Pseudomonas aeruginosa*

P. aeruginosa, rod shaped gram negative bacterium, is a multidrug resistant pathogen familiar for its ubiquity and it's fundamentally advanced antibiotic resistance mechanisms. The species is notorious for its association with severe illnesses – hospital-acquired infections such as ventilator-associated pneumonia and various sepsis syndromes [21]. *P. aeruginosa* strains produce two types of soluble pigments, pyoverdin, the fluorescent pigment and pyocyanin, the blue pigment. The latter is produced abundantly in low-iron content media of and functions in iron metabolism in the bacterium. Pyocyanin refers to "blue pus", which is a characteristic of suppurative infections caused by *Pseudomonas aeruginosa*. The resistance of bacterium to many of the antibiotics is due to low permeability afforded by its gram-negative outer membrane. Also, its increased tendency in biofilm formation makes the cells unreceptive to therapeutic concentrations of various antibiotics. Since its natural habitat is the soil, it obviously has developed resistance to a variety of their naturally-occurring antibiotics. Moreover, maintains antibiotic resistance plasmids, both R-factors and RTFs, and moreover *Pseudomonas* can maintain and transfer antibiotic resistance plasmids by means of the bacterial mechanisms of horizontal gene transfer (HGT), mainly transduction and conjugation [22].

6.1.1.4 *Escherichia coli*

Escherichia coli are rod-shaped most ubiquitous infecting organisms in the family of gram-negative bacteria known as enterobacteriaceae that is usually found in the lower intestine of warm-blooded organisms. Most *E. coli* strains are harmless, but some strains can cause serious food contaminations often leading to the food poisoning in their hosts [23]. German bacteriologist Theodor Escherich discovered *E. coli* bacteria in the human colon in 1885. Dr. Escherich also pointed that certain members of the bacterium were accounted for infant diarrhea and gastroenteritis [24]. The *E. coli* those are liable for the various reports of contaminated foods and beverages are those that produce Shiga toxin. Such produced toxins are named so because the toxin is almost equal to that produced by *Shigella* dysenteria type 1 [25].

6.1.2 Fungal strain used in the study

6.1.2.1 *Candida Albicans*

C. albicans continues to be the most common among the species of the genus, Candida, that are involved in the major opportunistic yeast infection in the world, candidiasis. Even though, *C. albicans* is an inevitable element of the commensal flora of more than half of the healthy population, this yeast is conscientious for about 50–90 % of human candidiasis. *C. albicans* colonies promote the functioning of the immune system and also limit growth of other opportunistic pathogenic fungi [26, 27]. *Candida albicans* is a frequent strain found in genitourinary and gastrointestinal tracts of healthy people. Mouth and mucocutaneous infections are also caused by this microorganism. However, it has been often identified an evolution to chronic forms, creating convoluted infections, such as septicemia, endocarditis, meningitis and peritonitis, especially in patients with decreased immune function or taking serial

antibiotic therapies. Despite the other types of mucocutaneous candidiasis, still the most frequent is oral candidiasis [28].

Due to the increasing substantiations of antimicrobials and antifungals resistance, several studies have been developed toward the recognition and assessment of competent alternative therapeutics. In consideration of the call for fresh antimicrobials to address the multi-resistance bacteria, the transition metal complexes with antimicrobial activity are potential candidates to be used as an alternative or supplement to antibiotics. So in this chapter we report the antibacterial and antifungal screening of six ligands and their Cu (II), Ni (II), and Zn (II) complexes.

6.2 Experimental

6.2.1 Materials and methods

Six 2-methoxy-4-chromanone and their Cu (II), Ni (II) and Zn (II) complexes were prepared as per the procedure given in Chapter 2 and Chapter 3.

6.2.2 Test organisms selected

Bacterial and fungal strains were selected based on their effect on humans. In vitro anti- bacterial activity of the ligand and its complexes were tested against bacterial species *Staphylococcus aureus* (MTCC 96), *Bacillus subtilis* (MTCC121), *Pseudomonas aeruginosa* (MTCC 741) *Escherichia coli* (MTCC 1652). Fungal species selected was *Candida albicans* (ATCC 10231) for testing antifungal activity.

6.2.3 Screening method

Antimicrobial studies were performed using the standard disc diffusion method [29]. Nutrient plate was uniformly spread by using a sterile glass spreader. Fresh stock solutions (1 mg/mL) of the synthesized compounds were

prepared in redistilled dimethyl sulfoxide (DMSO) according to the required concentrations. Sterile antibiotic discs (6 mm in diameter, prepared using Whatman No. 1 paper) were placed over the medium. To determine the antimicrobial activity, 100 µg of the compounds (initially dissolved in DMSO) was transferred to each disc with the help of a micropipette, simultaneously maintaining standard ciprofloxacin (30 µg /disc) against bacteria and nystatine (10 µg/disc) for fungi. After overnight incubation at 37 °C for bacteria and 48 hours incubation at 25 °C for fungus, the zone of inhibition was measured in 'mm' and compared with standard antibiotics. Control measurements were carried out with DMSO without samples. All the experiments were performed in triplicates and the average zones of inhibition were recorded.

6.2.4 Determination of Minimum Inhibitory Concentration (MIC)

The compounds which showed substantial inhibition of bacteria were tested further for the minimum inhibitory concentration (MIC). Standard pathogenic bacterial strains, *Pseudomonas aeruginosa* and *Staphylococcus aureus* were used in the determination of MIC of bacteria. The resazurin reduction method was used for determining the MIC in 96well microlitre plates. All the compounds were dissolved in DMSO having a final stock concentration of 1 mg/mL. 50 µL of this stock solution was serially diluted to eight times and 50 µL of each serially diluted compound was added to microplate wells. All the microbial cultures were grown in nutrient agar to reach 0.5 McFarland concentrations and 50 µL of this culture was added to each well. Microplate contents were mixed well and incubated at room temperature for 12 hours.

After 12 hours of incubation, 10 µL of mixture from each well was spread on the agar plate and checked for the Colony Forming Units (CFU). Further 30 µL of 0.1% resazurin solution was added to each well and incubated up to another

24 hours. Microplate well contents were observed in the change in colour from blue to pink. Those wells that have microbes growing will change the blue resazurin into pink color. The well, which remains blue after 24 hours of incubation indicates there are no microorganisms survived in the well, the minimum concentration where no microbial growth found are considered as MIC value. Negative control was set without test material. Values were compared with the standard ciprofloxacin [30].

6.3 Results and Discussion

For antimicrobial study of the synthesized ligands and complexes, two gram positive and two gram negative bacteria and a fungal strain were selected. Mean zone diameter values of all the compounds were determined using disc diffusion method and MIC values of selected compounds were determined using resazurin reduction method.

Table 6.1: Codes for the samples in Zone of inhibition

Sample	code	sample	code	sample	code
L1	1	L2	9	L3	17
CuL1	2	CuL2	10	CuL3	18
ZnL1	3	ZnL2	11	ZnL3	19
NiL1	4	NiL2	12	NiL3	20
L5	5	L6	13	L7	21
CuL5	6	CuL6	14	CuL7	22
ZnL5	7	ZnL6	15	ZnL7	23
NiL5	8	NiL6	16	NiL7	24

6.3.1 Antimicrobial activity against *Bacillus subtilis*:

Mean zone diameter against the species was measured and tabulated in table 6.2 and graphically represented in Fig.6.1. Fig. 6.2 gives the photographs of the mean zone diameter of ligands and complexes against *B. subtilis*.

Table 6.2: Mean zone diameter of ligands and complexes against *B. subtilis*

Ligands	Mean zone diameter (mm)[a]			
	ligands	Cu(II)	Zn(II)	Ni(II)
L1	9.1±0.1	11.3±0.2	18.5±0.2	17.9±0.1
L2	0	0	15.6±0.1	20.3±0.2
L3	0	0	0	15.8±0.3
L5	9.0±0.1	10.3±0.2	12.9±0.1	14.0±0.1
L6	0	12.8±0.1	24.3±0.1	14.4±0.1
L7	0	0	0	14.5±0.1
Ciprofloxacin	24.0±0.4			

[a]Values, including diameter of the disc (6mm), are means of three replicates± SD.

Fig. 6.1: Graphical representation of mean zone diameter of ligands and complexes against *B. subtilis.*

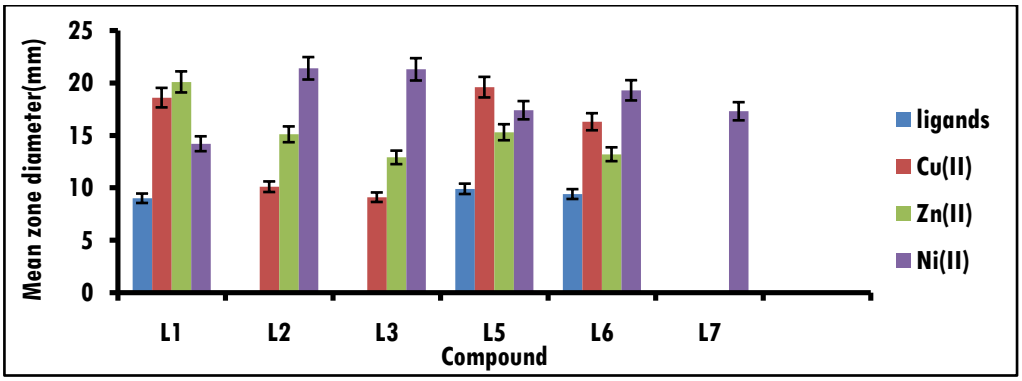

Against *B. subtlis*, ligands showed very weak activity. Complexes ZnL1, ZnL2, ZnL5, and NiL3 were moderately active with mean zone diameter above 15 mm. ZnL6 and NiL1 showed good activity against *B. subtilis*. All the copper complexes were found to have weak inhibitory potential against *B. subtilis*. Among all tested compounds ZnL6 was the most active against the bacterial strain. It can be attributed to the presence of electron withdrawing bromo group synergic with the presence of the metal centre. L3, L7 and their Cu (II) and Zn (II) complexes were inactive but their Ni (II) complexes were moderately active.

Fig. 6.2: Zone of inhibition of ligands and its Ni (II), Cu (II) and Zn (II) complexes against *B. subtilis*

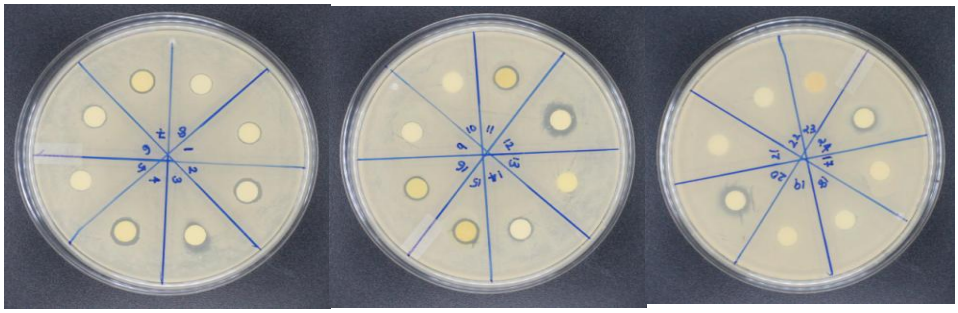

6.3.2 Antimicrobial activity against *Staphylococcus aureus*:

Mean zone diameter against the species was measured and tabulated in table 6.3 and graphically represented in Fig. 6.3. Fig. 6.4 gives the zone of inhibition of the mean zone diameter of ligands and complexes against *S. aureus*.

Table 6.3: Mean zone diameter of ligands and complexes against *S .aureus*

ligands	Mean zone diameter (mm)[a]			
	ligands	Cu(II)	Zn(II)	Ni(II)
L1	9.0±0.1	18.6±0.2	20.1±0.3	14.2±0.1
L2	0	10.1±0.1	15.1±0.1	21.4±0.1
L3	0	9.1±0.1	12.9±0.3	21.3±0.1
L5	9.9±0.2	19.6±0.1	15.3±0.4	17.4±0.1
L6	9.4±0.1	16.3±0.1	13.2±0.2	19.3±0.1
L7	-	-	-	17.3±0.1
Ciprofloxacin	26.0±0.4			

[a]Values, including diameter of the disc (6mm), are means of three replicates± SD.

Fig.6.3 Graphical representation of mean zone diameter of ligands and complexes against *S.aureus*

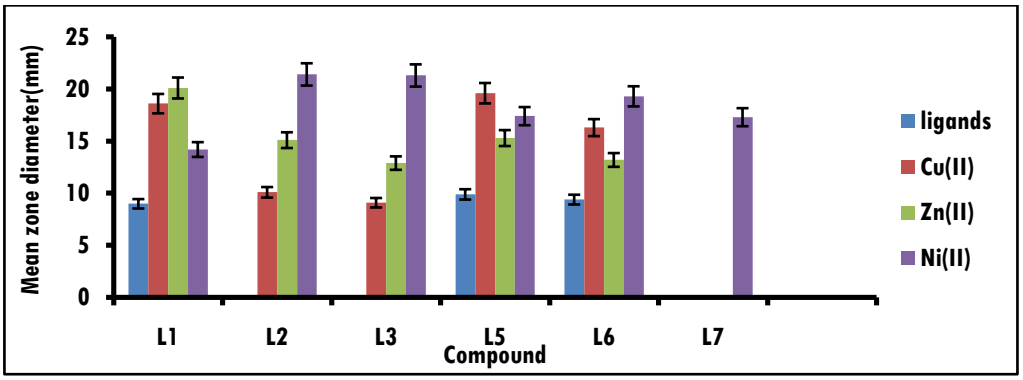

Against *S. aureus*, most active was NiL2 complex. CuL5, CuL1, CuL6, ZnL5, ZnL2, NiL7, NiL5, NiL6 were moderately active. Increasing order of the antibacterial activity of compounds showing good antibacterial activity is ZnL1<NiL3<NiL2. Here also the most active compound is having an electron withdrawing substitution. L7 and its copper and zinc complexes were inactive but its nickel complex was found to be active.

Fig. 6.4: Zone of inhibition exhibited by ligands and its Ni (II), Cu (II) and Zn (II) complexes against *S. aureus*

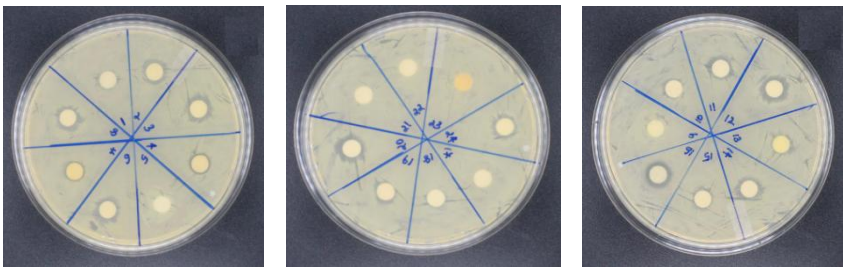

6.3.3 Antimicrobial activity against *Pseudomonas aeruginosa*

Mean zone diameter against the species was measured and tabulated in table 6.4 and graphically represented in Fig. 6.5. Fig. 6.6 gives the zone of inhibition of the mean zone diameter of ligands and complexes against *P. aeruginosa*.

Table 6.4: Mean zone diameter of ligands and complexes against *P. aeruginosa*

ligands	Mean zone diameter (mm)[a]			
	ligands	Cu(II)	Zn(II)	Ni(II)
L1	0	11.3±0.1	15.4±0.2	14.3±0.2
L2	11.3±0.2	14.3±0.2	16.3±0.2	21.4±0.1
L3	0	14.3±0.3	0	15.2±0.1
L5	9.1±0.2	11.2±0.1	18.3±0.1	13.2±0.1
L6	9.2±0.3	13.9±0.1	21.3±0.1	0
L7	-	13.7±0.1	0	0
Ciprofloxacin		22.0±0.1		

[a]Values, including diameter of the disc (6mm), are means of three replicates± SD.

Fig.6.5 Graphical representation of mean zone diameter of ligands and complexes against *P. aeruginosa*

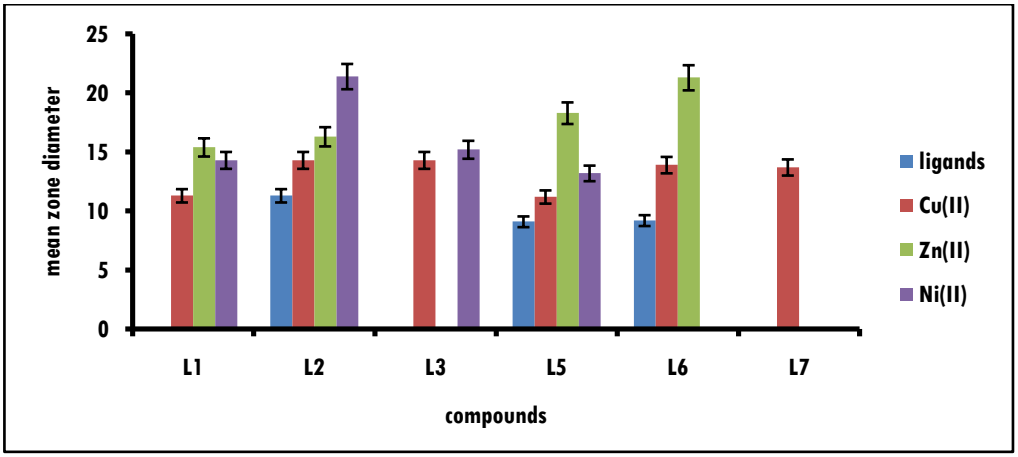

Ni (II) complex of ligand L2, i.e, NiL2 is the most active compound among the tested samples against *P. aeruginosa*. Only ZnL6 and NiL2 were good against the strain. L1, L3 and L7 were inactive against the strain. L2, L5 and L6 were weakly active. ZnL1, ZnL2, ZnL5 and NiL3 were moderately active against *P. aeruginosa*. Among the complexes of L7, only copper complex was mildly active and other two were inactive.

Fig. 6.6: Zone of inhibition of ligands and its Ni (II), Cu (II) and Zn (II) complexes against *P. aeruginosa*

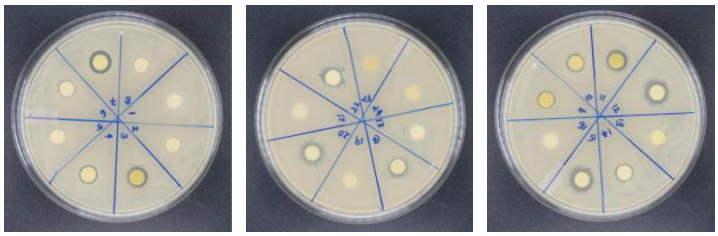

6.3.4 Antimicrobial activity against *Escherichia coli*

Mean zone diameter against the species was measured and tabulated in table 6.5 and graphically represented in Fig. 6.7. Fig. 6.8 gives the zone of inhibition of ligands and complexes against *E. coli*.

Table 6.5: Mean zone diameter of ligands and complexes against *E. coli*.

ligands	Mean zone diameter (mm)[a]			
	ligands	Cu(II)	Zn(II)	Ni(II)
L1	10.3±0.1	11.3±0.2	13.4±0.1	16.3±0.2
L2	0	0	21.2±0.1	0
L3	0	19.3±0.2	16.3±0.3	13.4±0.1
L5	0	16.2±0.2	15.3±0.2	13.2±0.2
L6	0	14.3±0.2	14.9±0.2	17.9±0.2
L7	-	-	-	13.5±0.3
Ciprofloxacin	25.0±0.2			

[a]Values, including diameter of the disc (6mm), are means of three replicates± SD.

Fig.6.7. Graphical representation of mean zone diameter of ligands and complexes against *E. coli*

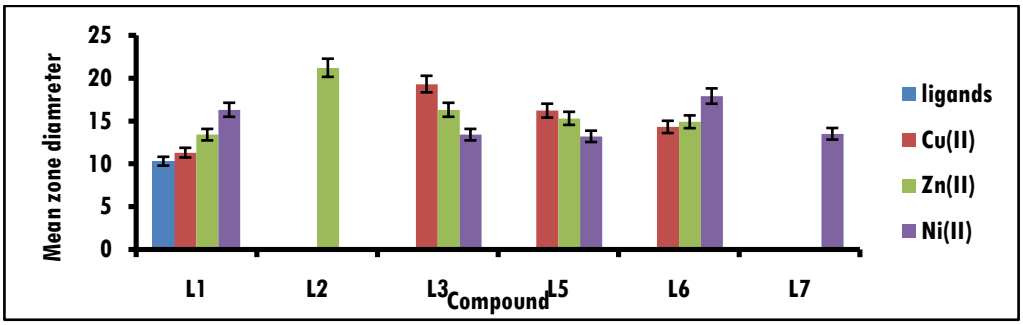

Against *E. coli*, only L1 was active among the tested ligands. Complexation has evidently increased the activity against *E. coli*. ZnL2 was the most potent against the strain. CuL3, CuL5, ZnL3, ZnL5, NiL1and NiL6 were found to be moderately active.

Fig. 6.8: Zone of inhibition of ligands and its Ni (II), Cu (II) and Zn (II) complexes against *E. coli*.

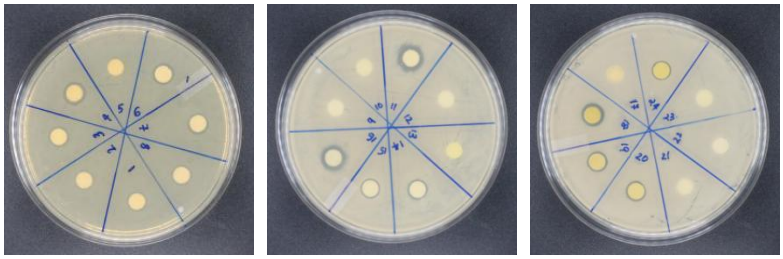

6.3.5 Antimicrobial activity against *Candida albicans*

Mean zone diameter against the species was measured and tabulated in table 6.6 and graphically represented in Fig. 6.9. Fig. 6.10 gives the zone of inhibition of the mean zone diameter of ligands and complexes against *C. albicans.*

Table 6.6: Mean zone diameter of ligands and complexes against *C. albicans*

ligands	**Mean zone diameter (mm)[a]**			
	ligands	Cu(II)	Zn(II)	Ni(II)
L1	14.3±0.2	0	19.3±0.2	11.3±0.1
L2	15.5±0.1	10.8±0.2	12.3±0.3	21.0±0.1
L3	19.3±0.1	21.3±0.2	24.4±0.2	22.9±0.1
L5	11.3±0.1	13.4±0.1	12.4±0.2	10.0±0.2
L6	0	14.8±0.1	0	18.5±0.2
L7	15.4±0.1	0	17.4±0.3	16.3±0.2
Nystatin 100 Units (10_g/disc).		19±0.1		

[a]Values, including diameter of the disc (6mm), are means of three replicates± SD.

Fig. 6.9 Graphical representation of mean zone diameter of ligands and complexes against *C. albicans*

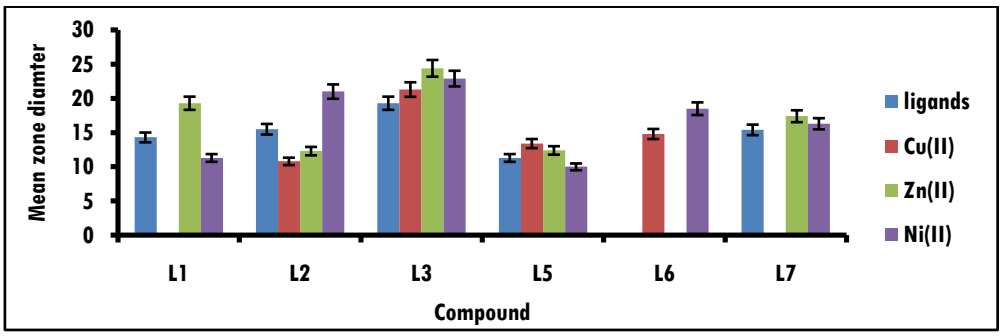

Almost all samples were active against the fungal species *Candida albicans*. L6 was inactive among the ligands. Complex ZnL3 was the most active against fungal species among the tested samples.

Fig.6.10: Zone of inhibition of ligands and its Ni (II), Cu (II) and Zn (II) complexes against *C. albicans.*

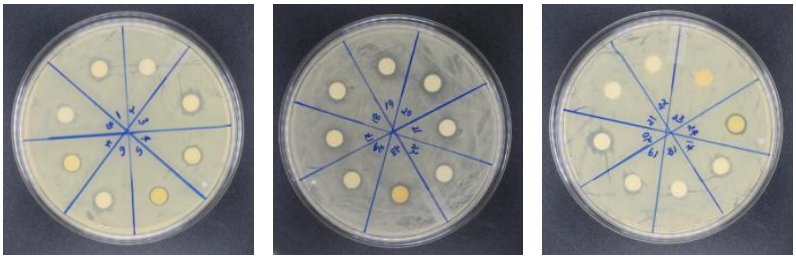

6.3.6 Determination of Minimum Inhibitory Concentration (MIC)

Compounds which showed good antibacterial activity (above 20 mm of mean zone diameter) selected for the determination of MIC. Values were compared with that of the standard ciprofloxacin. ZnL6 has the least MIC and is against *B. subtilis* among the selected compounds. Table 6.7 gives the minimum inhibitory concentration values of selected compounds against bacterial strains.

Table 6.7: MIC values for ZnL2, ZnL1, NiL2, NiL3 and ZnL6

Compound	MIC (µg/mL)			
	S. aureus **(MTCC 96).**	***B. subtilis*** **(MTCC 121).**	***P. aeruginosa*** **(MTCC 741).**	***E.coli*** **(MTCC 1652).**
ZnL2	-	-	-	15.2
ZnL1	15.3	-	-	-
NiL2	61.2	15.3	31.3	-
NiL3	31.2			-
ZnL6		15.0	61.4	-
Ciprofloxacin	>5	>5	>5	>5

Synthesized compounds were found to be more active against gram positive bacteria than gram negative pathogens. It may be due to the difference in the bacterial structure features. Gram negative bacteria are having a highly impermeable extra outer layer on the top of peptidoglycan. But, a negatively charged polysaccharide, teichoic acid present in the outer cell wall of gram positive bacteria facilitates the penetration of positively charged metal ions into the cell. This accounts for the high antibacterial activity of the complexes against gram positive strains.

Antibacterial activity can be increased by the phenomenon of chelation. According to Overtone's concept of cell permeability and Tweedy's chelation theory, π electron cloud delocalizes over the whole molecule as a result of the sharing of the positive charge of the metal with the ligands. Thus, delocalisation decreases lipophobic character of the compound which helps in enhanced penetration into the bacterial membranes and blocking of metal binding sites of enzymes of microorganism [30]. Formation of hydrogen bonds between the complexes and the cell constituents may interrupt the normal cell process which results in the bacterial cell death more aggressively .There are several other factors like nature of metal ion, nature of ligand, coordinating sites, geometry, hydrophilicity, lipophilicity and presence of co-ligands which

influence activity of compounds [31]. Some complexes are found to be less active. High bonding capacity of ligands makes the metal ions less available for the activity. Low lipid solubility is also a major reason for the low activity of complexes [32].

6.4 Conclusions

Six ligands and their Ni (II), Cu (II) and Zn (II) complexes are screened for their antibacterial and antifungal efficiency. Disc diffusion method was used for determining antibacterial activity and resazurin reduction method was used for minimum inhibitory concentration determination. Bacterial species selected were gram positive *Staphylococcus aureus* (MTCC 96), gram positive *Bacillus subtilis* (MTCC 121), gram negative *Pseudomonas aeruginosa* (MTCC 741) gram negative *Escherichia coli* (MTCC 1652). Fungal species selected was *Candida albicans* (ATCC 10231) for testing antifungal activity. Antimicrobial activity exhibited by the synthesized compounds was compared with standard antibiotics. All ligands were weakly active or inactive against bacterial strains. Complexation has evidently increased the antibacterial activity. Compound ZnL6 showed the least MIC value against *B. subtilis*. Presence of electron withdrawing groups has marked effect on antibacterial activity. Almost all samples showed moderately or good antifungal activity against *Candida albicans*.

References

1) World Health Organization (WHO), Antimicrobial Resistance; Fact Sheet No. 194; WHO: Geneva, Switzerland, **2002**.

2) K. Bush; Clin. Microbiol. Inf. **2004**, 10, 10.

3) J. A. Lemire; J. J. Harrison; R. J. Turner; Nat. Rev. Microbiol. **2013,** 11, 371.

4) P. Krishnamoorthy; P. Sathyadevi; A. H. Cowley; R. R. Butorac; N. Dharmaraj; Eur. J. Med. Chem. **2011**, 46, 3376.

5) F. Arjmand; A. Jamsheera; D. K. Mohapatr; J. Photochem. Photobiol. B **2013**, 121, 75.

6) S. K. Bharti; S. K. Singh; Der Pharmacia Lettre, **2009**, 1(2), 39.

7) B. Xing; C. Yu; P. Ho; K. Chow; T. Cheung; H. Gu; Z. Cai; B. Xu; J. Med. Chem., **2003**, 46 (23), 4904.

8) L.Yesilel; O. Z. G. Kastas; C. Darcan; I. Ilker; H. Pasaoglu; O. Büyükgüngör; Inorg. Chim. Act. **2010**, 363, 1849.

9) V. H. Naik; A. D. Kulkarni; P. S. Badami; Spectrochim. Act. A: Mol. Biomol. Spec., **2010**, 75, 347.

10) V. Uivarosi; Molecules **2013**, 11153.

11) M. Imran; J. Iqbal; S. Iqbal; N. Ijaz; Turk. J. Bio. **2007**, 31, 67.

12) L. Feng; M. M. Maddox; M. Z. Alam; L. S. Tsutsumi; G. Narula; , D. F. Bruhn; X. Wu; S. Sandhaus; R. B. Lee; C. J. Simmons; Y. -C. Tse-Dinh; J. G. Hurdle; R. E. Lee; D. Sun; J. Med. Chem. **2014**, 57, 8398.

13) A. R. Shaikh; R. Giridhar; M. R. Yadav; Int. J. Pharm. **2007**, 6, 24.

14) F. Cottiglia; B. Dhanapal; O. Sticher; J. Heilmann; *J. Nat. Prod.* **2004**, 67, 537.

15) M. Sarasija; K. Sudershan; D. A. Shivaraj; Russ. J. Gen. Chem. **2014**, 84, 1622.

16) M. Otto; Curr. Top. Microbiol. Immunol. **2006**, 306, 252.

17) M. A Hamon; B. A Lazazzera; Mol. Microbiol. **2001**, 42, 1199.

18) R. Jaenicke; Science (New York, NY) **2005**, 308, 73.

19) M. Masalha; I. Borovok; R. Schreiber; Y. Aharonowitz; G. Cohen; J. Bacteriol. **2001**, 183 (24), 7260.

20) S. Y. C. Tong; J. S. Davis; E. Eichenberger; T. L. Holland, V. G. Fowler, Jr.· Clin Microbiol Rev. **2015**, 28, 603.

21) M. Cooper, G. R. Tavankar, H. D. Williams; Microbiol. **200**3, 149, 1275.

22) F. Harrison; L. E. Brownin; M. Vos; A. Buckling; **2006**, BMC Biology. 4, 21.

23) P. Singleton; Bacteria in Biology, Biotechnology and Medicine (5th ed.). Wiley. **1999**.

24) B. Eisenstein; D. Zaleznik; "Enterobacteriiaceae," in Mandell, Douglas, & Bennett's PRINCIPLES AND PRACTICE OF INFECTIOUS DISEASES, Fifth Edition, **2000**, Chap. 206, 2294

25) P. Griffin; R. Tauxe; Epidemiol. Rev. **1991**, 13, 60.

26) D. Vázquez-González; A. M. Perusquía-Orti; M. Hundeiker; A. Bonifaz; J. Ger. Soc. Dermatol. **2013**, 11, 381.

27) B. Wächtler; F. Citiulo, N. Jablonowski; S. Förster; F. Dalle; M. Schaller; PLoS One. **2012**, 7, 1.

28) S. Silva; M. Henriques; A. Haye; R. Oliveira; J. Azeredo; D.W. Williams; J. Oral Pathol. Med. **2011**, 40, 421.

29) C. Nagel; S. McLean; R. K. Poole; H. Braunschweig; T. Kramera; U. Schatzschneider; Dalton Trans. **2014**, 43, 9986.

30) N. Harikrishna; A. M. Isloor; K. Ananda; A. Obaid; H. Funde; RSC Adv. **2015**, 5, 43648.

31) M. Patil; R. Hunoor; K. Gudasi; Eur. J. Med. Chem. **2010**, 45, 2981.

32) K. Mohanan; S. Nirmala Devi; B. Murukan; Synth. React. Inorg. Met.Org. Chem. **2006**, 36, 441.

******

Chapter 7

Cytotoxicity studies of 2-methoxy-4-chromanones and its Ni (II), Cu (II), Zn (II) complexes

Contents

Abstract

Metal based therapeutics has raised much attention for several decades due to the relevance of metal ions in biological reactions. Significant side effects and drug resistance by metal based drugs limits their clinical applications. Low toxicity against normal cell lines is the preliminary criteria for successful development of metal based drugs. Better DNA binding, enzyme inhibitory and antibacterial properties of the synthesized complexes prompted us to check toxicity level of selected compounds against normal 3T3-L1 cells. Assay selected for the cell viability study is the sensitive, quantitative and reliable MTT colorimetric assay. Compounds were found to be nontoxic to the normal cells which make them better candidates for its development as good therapeutic agents.

7.1 Introduction

Cytotoxicity studies are considered as a constructive preliminary step in deciding the potential toxicity of a sample, including plant extracts or biologically active synthetic compounds. Minimal to no toxicity is main criteria for the successful development of a therapeutic or pharmaceutical preparation. In this regard cellular toxicity studies play a key role [1]. The cytotoxicity test uses tissue cells *in vitro* to monitor the cell growth, reproduction and morphological effects. Additionally, cytotoxicity testing can be considered for quality control purposes for release testing of raw materials or of manufactured drug products [2].The cytotoxicity assays evaluating the cell viability can be classified as methods assessing decreased membrane integrity, membrane metabolic activity, loss of monolayer adherence and arrest of cells in various stages of cell cycle. These assays which govern the *in vitro* methods of toxicological analysis recognize the cytotoxic or cytostatic prospective of the nanoparticles and spot of tissue injury by utilizing commercial test kits that are simple to work with [3].

Cell viability is the number of healthy cells in a sample and is a vital indicator for understanding the mechanisms in action of certain genes, proteins and pathways concerned with cell survival or death after exposure to toxic agents. In spite of the type of cell-based assay being used, it is key feature to know how many viable cells are left behind at the end of the experiment [4].

Various assay methods are available which are based on various cell functions such as enzyme activity, cell adherence, ATP production, cell membrane permeability, co-enzyme production and nucleotide uptake activity. These methods belong to different categories: (I) dye exclusion methods such as trypan blue dye exclusion assay, (II) methods based on metabolic activity, (III) ATP assay, (IV) sulforhodamine B assay, (V) protease viability marker

assay, (VI) clonogenic cell survival assay, (VII) DNA synthesis cell proliferation assays and (V) Raman micro-spectroscopy. In order to prefer the optimal viability assay, the cell type, applied culture conditions, and the specific questions being asked should be considered in detail [5].

Among them 3-(4, 5-dimethylthiazol-2-yl)-2, 5-diphenyltetrazolium bromide (MTT) is one of the most recurrently used methods. This method uses colorimeter to resolve on the cell viability and gives low background absorbance values in the absence of cells [6]. An accurate quantification of variation in the rate of cell death or proliferation is possible due to the establishment of linear relationship between metabolically active cells and the color produced. The MTT assay depends upon cellular metabolic activities due to NAD(P)H-dependent cellular oxidoreductase enzymes (Figure 7.1) in mitochondria of living cells. The healthy and rapidly growing cells display high rates of reduction of yellow water soluble MTT to purple coloured water insoluble formazan while the dead or inactive cells fail to do so. Purple colored formazan which is the final product is quantitatively read at 540 nm. Decreased purple colour denotes reduced cell number while high cell viability is indicated by deep purple colour [7].

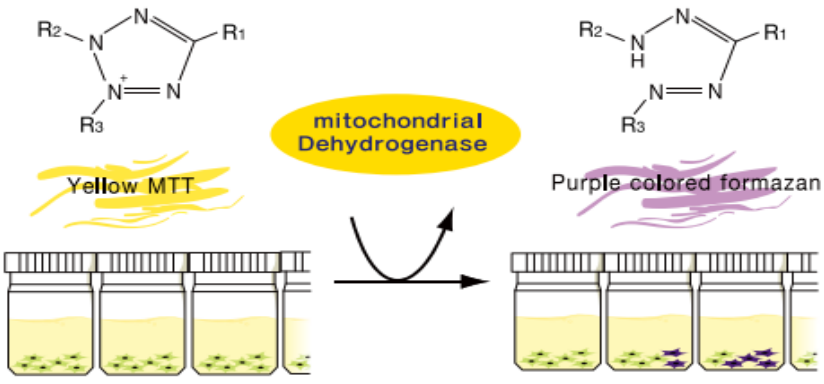

Fig. 7.1: Action of MTT assay

Chromones and its derivatives have been extensively explored and screened against several relevant biological targets [8]. Chromone and its analogs are considered as a valid scaffold and important pharmacophores in medicinal chemistry and chromone core is an inevitable part of various clinically relevant drugs. Kanagalakshmi *et al* reported a series of 2, 3 diarylchromanones under microwave irradiation and checked their cytotoxicity by the MTT assay using HL60 cells and PBMC (Peripheral blood mononuclear cells) and antioxidant activity by using lipid peroxidation. Compound diarylchromanone 2a exhibited highest cytotoxicity with 73.16 mM and for anti-oxidant activity; the chromanone 2b possesses highest activity with EC_{50} value of 129.86 mM. From their study diarylchromanone derivative with a nitrogroup at meta position 2b showed the highest radical modulation activity compared to other tested compounds [9]. Kupcewicz *et al* reported derivatives of *E*, *Z*-isomers of 3-arylidene substituted flavanone, chromanone and 3-aryl substituted flavone and screened for their in vitro cytotoxic activity against three cancer cell lines (HL-60, NALM-6, WM-115) and normal cell line (HUVEC). They observed that substitution at C3 position and isomeric configuration of 3-arylideneflavanones had a marked influence on the cytotoxic potential of the synthesized compounds [10]. Cottiglia and his coworkers isolated six new chromanone acids from the bark of *Calophyllumbrasiliense* Cambess which were cytotoxic against KB, Jurkat T, and myosarcoma cancer cells up to a concentration of 20 μg/mL [11]. A. Vanangamudi *et al* synthesized four different 2, 3-disubstituted chromanones and screened for cytotoxicity against a panel of 29 human cancer cell lines in five different concentrations. They found out that presence of methoxy group has increased the impact of compounds on cancer cell lines [12]. Inmitiaz Yusuff and his coworkers reported a novel chromone appended Cu (II) drug

entity which has potential anticancer chemotherapeutic activity. In vitro cytotoxicity studies of the complex via the MTT assay was carried out and IC_{50} values were found to be in the range of 5–10 μg mL^{-1}in HepG2 and MCF-7 cancer cell lines, which were found to be much lower than the IC_{50} values of previously reported similar Cu (II) complexes [13]. New four nickel (II) complexes containing 4-chromone-N-(4)-substituted thiosemicarbazone ligands were synthesized which have good cytotoxic activity against MCF-7 cancer cell line due to the terminal substituted thiosemicarbazones [14]. A series of Mn (II), Co (II), Ni (II), Cu (II) and Zn (II) Schiff base complexes were synthesized *via* condensation of salicylaldehyde and 3-hydroxypyridin-2-yliminomethyl-4H-chromen-4-one. Cytotoixcity studies were carried out against human liver Carcinoma (HepG2) cell lines and found to have excellent antitumor properties [15].

Silver (II) complexes of chromone derived hydrazones are synthesized by Lenka *et al.* which are having low toxicity against B16F10 (metastatic melanoma) and Melan-a (non-tumorigenic melanocyte) cells, reducing only about 20% of cell viability of B16F10 cells and at the concentration of 10 μM. These complexes cause less damage to normal non-malignant Melan-a-cells [16].

Obesity is due to the accumulation of adipose tissue in the body. In adipose tissue approximately one third is mature adipocytes and the remaining is a combination of preadipocytes, endothelial cells, macrophages, fibroblasts, and adipose derived stem cells (ADSC) in various stages of development. Preadipocytes which determine the number of fat cells throughout their entire lifespan [17] are capable to propagate and differentiate into mature adipocytes. Accumulation of adipose tissue mass can be reduced by the inhibition of adipogenesis from preadipocytes to mature adipocytes, prevention of lipid accumulation in adipocytes, and induction of apoptosis in adipose cells, which can

also contribute to the treatment of obesity [18]. In this chapter, cytotoxic effect of some synthesized compounds on 3T3-L1 preadipoytic cells is investigated.

Extended literature regarding the cytotoxic nature of chromone complexes and its derivatives and the biological properties of the synthesized compounds aroused our curiosity to check the cytotoxic potential of synthesized 2-methoxy-4-chromanones incorporated metal complexes. Eight complexes were selected for the study and the selection was random. Cell lines selected were normal 3T3-L1 cells.

7.2 Experimental

7.2.1 Materials and methods

Mice 3T3-L1 preadipocytic cells grown in Dulbecco's Modified Eagle's Medium (DMEM) from American Type Culture Collection, USA, were (DMEM) supplemented with 10% FCS and antibiotics (100 U/ml of penicillin and 100 µg/mL of streptomycin) under a humidified atmosphere with 5% CO_2 at 37°C. MTT [3-(4, 5-dimethyl-2-thia-zolyl)-2,5-diphenyl-2H-tetrazolium bromide)], and dimethyl sulfoxide (DMSO) were purchased from Sigma, St. Louis, MO, USA.

Compounds selected CuL1, CuL5, CuL6, ZnL2, ZnL3, ZnL5, NiL6 and NiL7were prepared as per the procedure given in Chapter 3, Section 3.2.

7.2.2 MTT assay

3T3-L1 cells were grown in Dulbecco's Modified Eagle's Medium (DME) and seeded in 96 well plates at a density of 5000 cells/well and incubated at 37°C, 5% CO_2 for 24 hours prior to addition of complexes. The cells were then treated with different concentrations (20, 40, 60, 80 and 100µM) of compounds dissolved in DMSO and incubated at 37°C, 5% CO_2 for 24 hours. Triplicate was maintained. After 24 hours, MTT was added (after

removal of media from the wells) at a concentration of 50 µg/well and incubated with CO_2. The working solution of MTT was prepared in Hank's balanced salt solution (HBSS) without phenol red. After 2.5-3 hours, the formazan crystals formed were viewed under the phase contrast microscope. The crystals were then solubilised by adding DMSO (after removal of MTT) and further incubated for 20 min at 37 ºC in the dark. After solubilisation, the plate was read at an absorbance of 570 nm. Control samples were cells without any treatment. The percentage cell viability of control cells were kept as 100%. The relative cell toxicity in percent was calculated as:

$$\text{Percentage Toxicity} = 100 - \frac{\text{Absorbanceof treated}}{\text{Absorbanceof control}} X\ 100$$

7.3 Results and discussion

In order to predict the possible toxic effect of the synthesized compounds, it is recommended to check viability of the cells grown in culture [19]. As per United States Food and Drug Administration (FDA), desirable pharmacological activity by newly synthesized compounds should be achieved in the absence of acute toxicity. Since toxicity studies include human cell lines, the results have a prognostic significance for humans [20]. In vitro toxicity studies of selected compounds at four different concentrations (10 µM, 30µM, 60µM and 100µM) were performed against normal 3T3-L1 cell lines by MTT assay. Cell viability was determined by the formation of purple coloured formazan crystals which was spectrophotometrically read at 570 nm. Deep purple colour is due to the formation of formazan by the action of mitochondrial dehydrogenase enzyme present in the living cells. All the tested compounds gave 100 % cell viability upto 100 µM concentration. Table 7.1 gives the percentage cell viability of the tested compounds.

Table 7.1 Percentage cell viability of CuL1, CuL5, CuL6, ZnL2, ZnL3, ZnL5, NiL6 and NiL7

Compounds	Cells	10 µM	30 µM	60 µM	100µM
CuL1	3T3-L1	100	100	100	100
CuL5	3T3-L1	100	100	100	100
CuL6	3T3-L1	100	100	100	100
ZnL2	3T3-L1	100	100	100	100
ZnL3	3T3-L1	100	100	100	100
ZnL5	3T3-L1	100	100	100	100
NiL6	3T3-L1	100	100	100	100
NiL7	3T3-L1	100	100	100	100

100 percent cell viability indicated the non toxicity of the tested compounds. Nontoxic profile of these compounds makes them promising candidates for the drug development process as they are causing no damage to the normal cells.

7.4 Conclusion

Toxicity of CuL1, CuL5, CuL6, ZnL2, ZnL3, ZnL5, NiL6 and NiL7 has been evaluated by MTT assay against normal 3T3-L1 cells. All selected compounds exhibited 100% viability up to 100 µM concentrations. Results prove the excellent nontoxic nature of the compounds which is essential for the further drug development studies. The study provides platform to pursue the biological properties to develop the compounds as effective pharmacological entities.

References

[1] S. J. Soenen; B. Manshian; J. M. Montenegro; F. Amin; B. Meermann; T. Thiron; M. Cornelissen; F. Vanhaecke; S. Doak; W. J. Parak; ACS Nano **2012**, 6, 5767.

[2] L. Weijia; Z. Jing; X. Yuyin; Biomed. Rep. **2015**, 3, 617.

[3] M. J. Stoddart; Methods Mol. Biol. **2011**, 740, 1.

[4] T. Mossman; J. Immunol. Meth. **1983**, 65, 55.

[5] A. Adan; Y. Kiraz; Y. Baran; Curr. Pharm. Biotechnol. **2016**, 17, 1213.

[6] G. Fotakis; J. A. Timbrell; Toxicol. Lett. **2006**, 160, 171.

[7] D. T. Vistica; P. Skehan; D. Scudiero; A. Monks; A. Pittman; M. R. Boyd; Cancer. Res. **1991**, 51, 2515.

[8] A .Gaspar; M. J. Matos; J. Garrido; E. Uriarte; F. Borges; Chem. Rev. **2014**, 114, 4960.

[9] K. Kanagalakshmi; M. Premanathan; R. Priyanka; B. Hemalatha; A. Vanangamudi; Eur. J. Med. Chem. **2010,** 45, 2447.

[10] B. Kupcewicz; G. Balcerowska-Czerniak; M. Małecka; P. Paneth; U. Krajewska; M. Rozalski; Bioorg. Med. Chem. Lett. **2013**, 23, 4102.

[11] G. Cottiglia; B. Dhanapal; O. Sticher; J. Heilmann; J. Nat. Prod .**2004**, 67, 537.

[12] A. Vanangamudi, S. Sudhakar; R. Gandhidasan; Ind. J. Exp. Biol. **1999**, 37, 173.

[13] I. Yousuf; F. Arjmand; S. Tabassum, L. Toupet, R. A. Khan; M. A. Siddiqui; Dalton Trans. **2015,** 44**,** 10330.

[14] S. Selvamurugan; R. Ramachandran; P. Vijayan; R. Manikandan; G. Prakash, P. Viswanathamurthi; K. Velmurugan; R. Nandhakumar; A. Endo; Polyhedron **2016**, 10757.

[15] R. A. Ammar; Abdel-Nasser; M. A. Alaghaz; M. E. Zayed; L. A. Al-Bedair; J. Mol. Struc. **2017**, 1141, 368.

[16] L. V. Tamayo; A. F. Santo; I. P. Ferreira; V. G. Santos; M. T. P. Lopes; H. Beraldo; BioMetals **2017**, 30, 379.

[17] J. K. Sethi; A. J Vidal-Puig; J. Lipid Res. **2007**, 48, 1253.

[18] A. Armani; C. Mammi; V. Marzolla; M. Calanchini; A. Antelmi; J. Cell Biochem. **2010**, 110, 564.

[19] M. Wind; Scientific workshop on Acute Chemical Safety Testing: Advancing In Vitro Approaches and Humane Endpoints for Systemic Toxicity Evaluations, **2008**, 1.

[20] World Health Organization: The WHO recommended classification of pesticides by hazard and guidelines to classification; **2009.**

****

Chapter 8

Summary of the work and future outlook

8.1 Summary of the work

Chromone ring systems was recognized as effective bioactive compounds by the chemists due to its natural wealth in flavonoid family and chemistry of these γ-pyrone ring and benzo annulated γ-pyrone ring has been explored extensively. Low toxic nature and wide array of pharmaceutical properties make these compounds more attractive for utilizing them for the synthesis of higher heterocyclic compounds. Among the different functionalized chromones, 3-formylchromone enjoys unique position due to its ability to behave as a successful scaffold for higher heterocycles with profound biological activities. Transition metal ion complexes of chromones have aroused much attention for the reason that presence of metal ions often augments the biological effectiveness of these compounds.

The thesis entitled **"2-Methoxy-4-chromanone ligated transition metal complexes: A novel class of effectual bioactive compounds"** is divided into various chapters. Chapter 1 gives the introduction, Chapter 2 is the synthesis and characterization of eight new 2-methoxy-4-chromanones, Chapter 3 is the synthesis and characterization of Ni (II), Cu (II) and Zn (II) metal complexes incorporating these ligands. Chapters 4, 5, 6 and 7 give the biological evaluation studies of the synthesized ligands and complexes. Bibliographical references are compiled at the end of each chapter.

Chapter 1: Gives the general introduction to the relevance and chemical reactivity of chromones and 3-formylchromone. It also discusses the

significance and application of transition metal complexes with chromone derivatives. A brief discussion about the structure and function of DNA, its interaction with molecules, chemistry of enzyme and enzyme inhibition, importance of antimicrobial studies and several methods use for antimicrobial study and importance of cytotoxicity tests are also included in this chapter. Scope and objectives of the study are summarized in this chapter. Details regarding various analytical methods used for the structural characterization of synthesized compounds are also included.

Chapter 2: Synthesis and characterization details of eight new 2-methoxy-4-chromanones are discussed in chapter 2. 3-formylchromone/ 3-formyl-6-methylchromone were reacted with different aminopyridines in methanolic media at room temperature to obtain the products. Aldehyde and amine groups underwent condensation reactions followed by the addition of methoxy group at C2 carbon to yield 2-methoxy-4-chromanones. Elemental analyses, mass spectrometry, FTIR, Uv-visible absorption studies, ^{1}H NMR and ^{13}C NMR spectra were used for the characterization of synthesized compounds. Synthesized ligands were expected to have good chelating ability and biological properties.

Chapter 3: Discusses the synthesis and characterizations of twenty one metal complexes incorporating the synthesized ligands. All complexes were synthesized by stirring equimolar quantity of ligands and metal salts dissolved in minimum amount of DMF at room temperature. Elemental analyses, FTIR, Uv-visible absorption studies, TG-DTG, EPR analysis, AAS, conductance and magnetic susceptibility measurements were used for the characterization of synthesized compounds. Proton NMR was used for characterization of diamagnetic Zn (II) complexes. Mononuclearity and purity of the samples were confirmed using elemental analysis. Low molar conductance values point

to non electrolytic nature of complexes. IR spectral values and NMR spectral studies showed that ligands are monobasic and ligate bidendately. Thermal studies indicated thermal stability of complexes and also the mode of water coordination in the complex. Electronic studies together with magnetic moment and electron paramagnetic measurements gave proper idea about geometry and orientation of ligands in the complexes. Complexes NiL3, NiL5, CuL2, CuL7, ZnL5, ZnL8 have penta coordinate square pyramidal geometry which was confirmed from their magnetic moment and EPR data. Distorted octahedral geometries are proposed to the remaining complexes.

Chapter 4: Alpha-amylase and alpha-glucosidase inhibitory properties of the synthesized compounds are described in chapter 4. DNS method was adopted for the determination of alpha-amylase inhibition and p-NPG method for alpha-glucosidase inhibition study. IC_{50} was determined in all cases and compared with the standard acarbose. Complexes CuL1, CuL2, CuL5, ZnL5, ZnL2 have IC_{50} values less than that of acarbose. And all other compounds have comparable IC_{50} values even though they are less that of the standard acarbose. It is found that all the compounds could inhibit both the enzymes in concentration dependent manner. The inhibition kinetic studies revealed that inhibitors bind to enzymes either competitively or non-competitively. Among the complexes, Zn (II) complexes were found to have more inhibitory potential on both the enzymes. Complexes containing electron withdrawing group were found to have higher activity than those present with electron donating methyl group. Our findings are in line with the reports that mild amylase inhibition and potent glucosidase inhibition can be considered as the effective way to decrease the carbohydrate metabolism in the intestine.

Chapter 5: Studies on DNA-small molecule interaction are always of considerable interest due to its functional importance as pharmaceutical

agents. Determination of HS-DNA binding behavior with the synthesized ligands and complexes were performed. Uv-visible spectrophotometry together with viscosity studies were selected for studying the binding behavior of DNA. Uv-visible studies showed clear hypochromism which indicate that DNA binds intercalatively. Intrinsic binding constant K_b values were also determined and were in the range of 10^4-10^5 and are comparable with the standard intercalators. Results obtained from viscosity studies of DNA binding were also in accordance with the optical studies. Complexation has evidently increased the binding ability due to the crucial role of metal ions. Strong intercalation activity can be attributed to the extensive aromatic plane and good conjugation for the ligands and the complexes.

Chapter 6: Increased demand for new class of antimicrobial compounds due to the increased levels of antimicrobial resistance prompted to check the antimicrobial efficacy of synthesized ligands and its complexes. Chapter 6 discusses the antibacterial and antifungal screening of L1, L2, L3, L5, L6, L7 and their Ni (II), Cu (II) and Zn (II) complexes. Disc diffusion method was used for determining antibacterial activity and resazurin reduction method was used for minimum inhibitory concentration determination. Bacterial species selected were gram positive *Staphylococcus aureus* (MTCC 96), gram positive *Bacillus subtilis* (MTCC 121), gram negative *Pseudomonas aeruginosa* (MTCC 741) gram negative *Escherichia coli* (MTCC 1652). Fungal species selected was *Candida albicans* (ATCC 10231) for testing antifungal activity. All the activities were compared with standard antibiotics. All ligands were weakly active or inactive against bacterial strains. Complexation has evidently increased the antibacterial activity. Compound ZnL6 showed the least MIC value against *B.subtilis*. Presence of electron withdrawing groups has marked effect on antibacterial activity. Almost all

samples showed moderately or good antifungal activity against *Candida albicans*.

Chapter 7: describes the cytotoxicity studies of selected compounds. Selection was random. Toxicity of CuL1, CuL5, CuL6, ZnL2, ZnL3, ZnL5, NiL6 and NiL7 has been evaluated by MTT assay against normal 3T3-L1 cells. All selected compounds exhibited 100% cell viability cells up to 100μM concentrations. Results prove the excellent nontoxic nature of the compounds against normal cell line which is essential for the further drug development studies. The study provides platform to pursue the biological properties to develop the compounds as effective pharmacological entities.

8.2 Future outlook

- Optimisation studies

  Influence of the amine nucleophilicity, solvent effects and environmental conditions should be optimized so that it will help to make the picture clear regarding the prevailing ambiguity about the reactions of primary aromatic amine with the 3-formylchromone.

- Theoretical studies

  Computational sketch of synthesized compounds will give us a precise picture about the molecular orbitals – HOMO & LUMO. Docking studies will help to explore the possible binding sites of the substrate to a given enzyme, DNA or any other protein and hence analyze the mechanism of the biochemical process.

- Extension of the compound library

  More interesting systems can be designed by changing substituent groups and metal ions. Development of heterometalic systems

including transition and inner transition metals will append more physical and biological properties. Employment of metal salts with different anionic counterpart will help to synthesize superior supramolecular architectures and MOFs.

- In vivo studies of the synthesized compounds

  Confirming pharmacological effects of the compounds can be done by performing in vivo studies on a living subject. It helps to develop the synthesized compounds as effective drugs.

******

Abbreviations

µg	micrograms
2-AP	2-Aminopyridine
3-AP	3-Aminopyridine
AAS	Atomic Absorption Spectroscopy
Anal.	Analytically
ATCC	American Type Culture Collection
Calc.	Calculated
Co	Cobalt
CT-DNA	Calf-Thymus Deoxyribonucleic acid
Cu	Copper
DM	Diabetes Melletus
DMF	Dimethylformamide
DMSO	Dimethylsulphoxide
DNA	Deoxyribo nucleic acid
DTG	Differential thermo gravimetry
EC	Enzyme Commision
EcoG	Electrocorticography
Eg	Example
EPSP	Excitatory postsynaptic potential
E-S	Enzyme-substrate
et al	et alia
FDA	Food and Drug Administration
Fig	Figure
FT IR	Fourier Transform Infrared
HIV	Human Immunodefeciency Virus
HS-DNA	Herring Sperm Deoxyribonucleic acid
IDDM	Insulin Dependent Diabetes Melletus
IPSP	Inhibitory postsynaptic potentia
L1	2-Methoxy-3-((pyridin-2-ylamino)methylenechroman-4-one
L2	2-Methoxy-3-(((5-nitropyridin-2-yl)amino)methylene)chroman-4-one
L3	2-Methoxy-3-(((5-methylpyridin-2-yl)amino)methylene)chroman-4-one
L4	2-Methoxy-3-((pyridin-2-ylamino)methylene)chroman-4-one
L5	2-Methoxy-6-methyl-3-((pyridin-2-ylamino)methylene)chroman-4-one
L6	3-(((5-Bromopyridin-2-yl)amino)methylene)-2-methoxy-6-methylchroman-4-one

L7	2-Methoxy-6-methyl-3-(((5-methylpyridin-2-yl)amino)methylene)chroman-4-one
L8	2-Methoxy-6-methyl-3-((pyridin-3-ylamino)methylene)chroman-4-one
LB	Lineweaver-Burk
M	Molar
MM	MichaelisMenten
mL	millilitre
mm	millimetre
mM	millimolar
Mn	Manganese
MTCC	Microbial Type Culture Collection
NADH	Nicotinamide adenine dinucleotide
Ni	Nickel
NIDDM	Non Insulin Dependent Diabetes Melletus
nm	nanometre
PC	Paper chromatgraphy
Pd	Palladium
PDS	Paroxysmal depolarization shifts
pH	Potent hydrogen
PM3	Parameterized Model number 3
RTF	Resistance Transfer Factor
SD	Standard Deviation
SIV	Simian Immunodeficiency virus
TB	Tuberculosis
TGA	Thermogravimetric analysis
TLC	Thin-layer chromatography
TMS	Trimethylsilane
Uv-vis	Ultra violet-Visible
WHO	World Health Organization
XRD	X-ray diffraction
Zn	Zinc
ε	Molar absorptivity
λ_{max}	Maximum wavelength
ν	Frequency

******

List of publications

- Novel class of mononuclear 2-methoxy-4-chromanones ligated Cu (II), Zn (II), Ni (II) complexes: synthesis, characterization and biological studies, **E. Sneha Jose**, Jessica Elizabeth Philip, A. A. Shanty, M. R. P. Kurup, P. V. Mohanan, Inorg. Chim. Acta 478 (2018) 155–165.
- Synthesis, characterization and biological studies of Schiff bases derived from heterocyclic moiety, A. A. Shanty , J. E. Philip , **E. J. Sneha** , M. R. P. Kurup , S. Balachandran , P. V. Mohanan , Bioorg. Chem. 70 (2017) 67–73.
- Design, synthesis, antimicrobial and antioxidant activity of 3-formyl chromone hydrazone and their metal (II) complexes , J. E. Philip, A. A. Shanty, **E. J. Sneha**, M. R. P. Kurup, P. V. Mohanan, Inorg. Chim. Acta,469 (2018) 87-97.
- Synthesis and characterisation of novel 2- methoxy-4-chromanone derivatives, Sneha Jose E, P. V. Mohanan, Proceedings of Prof K. V. Thomas Endowment National Seminar - Molecular Approach to Current Advances in Chemistry, Sacred Heart College, Thevara, 2015, ISBN: 978-81-930558.
- Spectral Characterisation Of Newly Synthesized 4-Chromanone Derivatives From 3-Formyl Chromone , Sneha Jose E, P. V. Mohanan, Proceedings of International Conference on Materials for the Millennium, MATCON-2016,ISBN:978-93-80095-738.

Participation / Presentations at Conferences / Seminars:

- National Seminar on Current Trends in Chemistry CTriC 2013, Department of Applied Chemistry, Cochin University of Science and Technology.
- National Seminar on Current Trends in Chemistry CTriC 2014, Department of Applied Chemistry, Cochin University of Science and Technology.
- Two day seminar on Recent Trends in Inorganic Organic Hybrid Metal Frameworks, January 2015, School of Chemical Science, M.G University, Kottayam.
- Poster presentation at Two day National seminar on Chemistry in Cancer Research CCR-2015,St.Alberts College, Ernakulam, October 8 & 9, 2015.
- Oral Presentation on 'Synthesis & Characterization of Chromanones', Prof K. V. Thomas Endowment National Seminar - Molecular Approach to Current Advances in Chemistry, Sacred Heart College, Thevara (Won Special Prize for best paper), 7-8 December 2015.
- Poster presentation at International Conference on Materials for the Millennium, MATCON-2016, January 14 -16, 2016, Department Of Applied Chemistry, CUSAT.
- Poster presentation on Antimicrobial Studies of Zn (II) complexes Incorporating 2-Methoxy- 4-Chromanones, Sneha Jose E and P. V. Mohanan, National seminar on Current Trends in Chemistry (Ctric 2017),Cochin University of Science and Technology, Cochin

- Poster presentation on Alpha amylase inhibition and antimicrobial studies of 2-Methoxy- 4- Chromanones , Sneha Jose Eettinilkunnathil and Puzhavoorparambil Velayudhan Mohanan, Prof. K V Thomas Endowment International Symposium On New Trends In Applied Chemistry (NTAC - 2017), 09 – 11 February 2017, Sacred Heart College (Autonomous), Thevara, Kochi.

******